AD-A102 377 JOHNS HOPKINS UNIV LAUREL MD APPLIED PHYSICS LAB F/G 13/1
THE APL SATELLITE REFRIGERATOR PROGRAM.(U)
JUL 81 C S LEFFEL, R VON BRIESEN N00017-72-C-4401
UNCLASSIFIED JHU/APL/TG-1332 NL

1 OF 3
AD A
102377

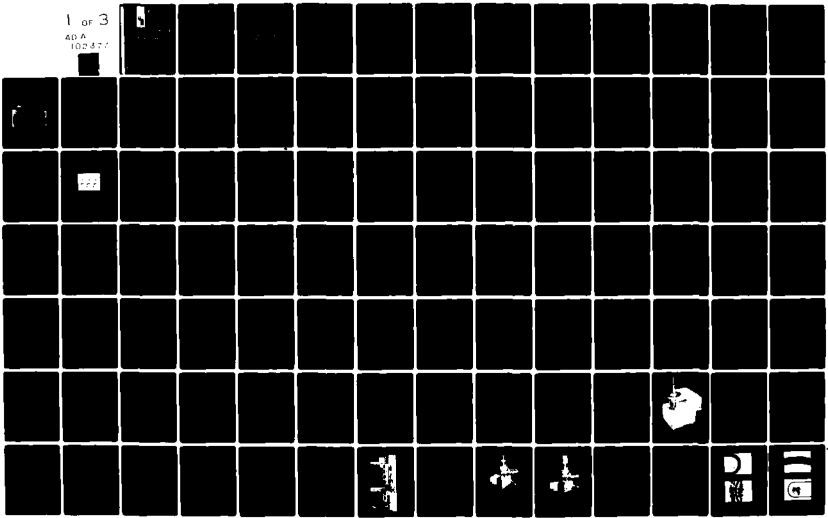

LEVEL II

19

12

JHU/APL
TG 1332
(QM-80-178)
JULY 1981

AD A102377

Technical Memorandum

THE APL SATELLITE REFRIGERATOR PROGRAM
FINAL REPORT

C. S. LEFFEL, JR, AND R. VONBRIESEN

THE JOHNS HOPKINS UNIVERSITY ■ APPLIED PHYSICS LABORATORY

JHU/APL/9R-89-1992

Unclassified

SECURITY CLASSIFICATION OF THIS PAGE

PLEASE FOLD BACK IF NOT NEEDED FOR BIBLIOGRAPHIC PURPOSES

REPORT DOCUMENTATION PAGE

1. REPORT NUMBER JHU/APL/TG-1332	2. GOVT ACCESSION NO. AD-A102 377	3. RECIPIENT'S CATALOG NUMBER
4. TITLE (and Subtitle) THE APL SATELLITE REFRIGERATOR PROGRAM, ~~FINAL~~ REPORT		5. TYPE OF REPORT & PERIOD COVERED Technical Memorandum
		6. PERFORMING ORG. REPORT NUMBER JHU/APL TG 1332
7. AUTHOR(s) C. S. Leffel, Jr. ~~and~~ R. von Briesen		8. CONTRACT OR GRANT NUMBER(s) ARPA Order 2037 Contract No. N1772C-4401
9. PERFORMING ORGANIZATION NAME & ADDRESS The Johns Hopkins University Applied Physics Laboratory Johns Hopkins Road Laurel, MD 20810		10. PROGRAM ELEMENT, PROJECT, TASK AREA & WORK UNIT NUMBERS Q4S0/CQO
11. CONTROLLING OFFICE NAME & ADDRESS Naval Plant Representative Office Johns Hopkins Road Laurel, MD 20810		12. REPORT DATE July 1981
		13. NUMBER OF PAGES 256
14. MONITORING AGENCY NAME & ADDRESS Naval Plant Representative Office Johns Hopkins Road Laurel, MD 20810		15. SECURITY CLASS. (of this report) UNCLASSIFIED
		15a. DECLASSIFICATION/DOWNGRADING SCHEDULE
16. DISTRIBUTION STATEMENT (of this Report) Approved for public release; distribution unlimited.		
17. DISTRIBUTION STATEMENT (of the abstract entered in Block 20, if different from Report)		
18. SUPPLEMENTARY NOTES		

19. KEY WORDS (Continue on reverse side if necessary and identify by block number)

cryogenics
gamma ray spectroscopy
mechanical refrigerators
satellite
stirling cycle

20. ABSTRACT (Continue on reverse side if necessary and identify by block number)

Four APL satellite refrigerators were built and installed on a satellite to cool gamma ray spectrometers. The spectrometers were constructed by Lockheed Palo Alto Laboratories. The P-78-1 satellite, launched on February 24, 1979, was the first satellite to carry gamma ray detectors that were cooled by mechanical refrigerators. Still operating successfully after over 18 months in orbit, this is the first satellite experiment of any kind on which mechanical refrigerators have been operated for longer than a few weeks. This report describes the selection and specifications of the refrigerators as determined by APL and Lockheed, the design and construction of the refrigerators by Philips Laboratories, the design and construction of the motor drive and instrumentation electronics by APL, the APL qualification and acceptance test programs, and the APL laboratory life test program. The orbital performance of the refrigerators is discussed.

DD FORM 1 JAN 73 1473

Unclassified

SECURITY CLASSIFICATION OF THIS PAGE

JHU/APL
TG 1332
(QM-80-178)
JULY 1981

THE APL SATELLITE REFRIGERATOR PROGRAM

FINAL REPORT

C. S. LEFFEL, JR, AND R. VONBRIESEN

THE JOHNS HOPKINS UNIVERSITY ■ APPLIED PHYSICS LABORATORY
Johns Hopkins Road, Laurel, Maryland 20810
Operating under Contract N00024 81 C 5301 with the Department of the Navy

ABSTRACT

Four APL satellite refrigerators were built and installed on a satellite to cool gamma ray spectrometers. The spectrometers were constructed by Lockheed Palo Alto Laboratories. The P-78-1 satellite, launched on February 24, 1979, was the first satellite to carry gamma ray detectors that were cooled by mechanical refrigerators. Still operating successfully after over 18 months in orbit, this is the first satellite experiment of any kind on which mechanical refrigerators have been operated for longer than a few weeks. This report describes the selection and specifications of the refrigerators as determined by APL and Lockheed, the design and construction of the refrigerators by Philips Laboratories, the design and construction of the motor drive and instrumentation electronics by APL, the APL qualification and acceptance test programs, and the APL laboratory life test program. The orbital performance of the refrigerators is discussed.

CONTENTS

ILLUSTRATIONS

TABLES

1. INTRODUCTION

Cryogenic cooling of radiation detectors used in orbital missions is often desirable and sometimes necessary to achieve the performance required for the mission. The advantages and limitations of the types of sensor cooling that have been tried in space are discussed in Ref. 1. The requirements for the cooling system depend upon the sensor used and the objectives of the mission.

High resolution gamma ray spectroscopy requires the use of solid state germanium detectors that are usually cooled to liquid nitrogen temperatures (77K) in the laboratory. This convenient laboratory temperature is not required for the detector; cooling to 130 to 140K suffices for detector performances. The first attempt to obtain high resolution spectra in space was made in October 1972 on a satellite experiment fielded by the Lockheed Palo Alto Research Laboratory (LPARL). This experiment used a lithium-drifted germanium detector cooled by a solid carbon dioxide cryogen and maintained a detector temperature of about 128K for eight months. However, because of problems not associated with the cooling system, high resolution data were collected for only a few weeks (Ref. 2).

A solid cryogen cooler, vented to space vacuum, maintains a constant temperature throughout its useful life even though the heat load may vary over a considerable range. For drifted germanium gamma ray detectors this is a desirable feature since the detectors are destroyed if warmed above a specified temperature (typically about 140K). However, the development of the intrinsic germanium gamma ray detector significantly changes the cooling requirements. For maximum resolution, this detector must be operated below a temperature of 140K, but can be warmed to ambient temperature without destruction. This feature permits greater flexibility in the use of the detector in space; it need only be cooled when data collection is desired and it may be warmed to the satellite ambient temperature to free contaminants that have frozen on the detector surface.

Mechanical refrigerators, which can be turned on and off by ground command and which, with respect to weight and launch survivability, are competitive with solid cryogen systems, appeared to offer some advantages for cooling intrinsic germanium detectors in orbital flight. The Applied Physics Laboratory (APL), under

the auspices of the Defense Advanced Research Projects Agency (DARPA), began the development and construction of satellite cryogenic refrigerators in 1973. The refrigerators were to be used on a high resolution gamma ray spectrometer designed and constructed by LPARL. In 1973, APL contracted with Philips Laboratories in Briacliff Manor, N.Y., for the design and construction of six Stirling cycle mechanical refrigerators for satellite applications. Philips delivered the first refrigerator in 1975 and after modifications dictated by APL performance and environmental testing, subsequently delivered five flight model refrigerators. The LPARL gamma ray experiment, which consisted of two intrinsic germanium detectors cooled by four refrigerators, was launched on 24 February 1979. After over 18 months in orbit, the refrigerators were adequately cooling the detectors. This experiment is the first application of the cooling of gamma ray detectors by mechanical refrigerators and the first satellite experiment of any kind on which mechanical refrigerators have successfully operated for more than a few hundred hours.

2. DESIGN OF THE REFRIGERATOR AND REFRIGERATOR ELECTRONIC CIRCUIT

At the beginning of this program, the choices for mechanical refrigeration were the Vuilleumier (VM) cycle and Stirling cycle. The VM cycle used both heat and mechanical energy as inputs to perform the work of refrigeration and is attractive if a non-electrical source of heat is available. However, if electrical energy must be converted to heat, the state-of-the-art VM cycle in 1973 did not appear as promising as did the all-mechanical (that is, electrically powered) Stirling cycle. Requests for bids for the development and manufacture of a satellite refrigerator resulted in a subcontract by APL to Philips Laboratories in 1973. Philips Laboratories had long been the acknowledged leader in the development of the Stirling cycle machines (both as heat engines and as refrigerators) and was the only respondent with the engineering and manufacturing resource that promised successful completion of the project.

The original specifications for the refrigerators, as set by APL in consultation with LPARL, are listed in Table 1. Throughout the design, manufacture, and testing of the refrigerators, some modifications of these specifications were necessary. The flight models, delivered to APL over the period from December 1975 to December 1976, met the specifications as listed in the second column of Table 1.

The evolution of the refrigerator design by Philips Laboratories is given in Appendix I of this report. Appendixes A and B to Appendix I give the basic theory of the Stirling cycle refrigerator and the advantages of the two-state construction. Section 1 of Appendix I describes the mechanical testing program that resulted in the final mechanical design of the refrigerator.

The final design that Philips Laboratories adopted was a two-stage Stirling cycle using a helium charge of about 70 psia. Figure 1 shows the flight model refrigerator as it was delivered to LPARL, a design of the refrigerator and its associated electronics that was not its final form until January 1976. In the LPARL experiment, the refrigerators were supported by the heat exchange flange, which is screwed to a heavy aluminum plate that acts as the heat sink. The first stage flange is connected to a heat shield that surrounds the detector and its thermal link to the

Table 1

Satellite refrigerator specifications.

Item	Original specification	Delivered specification
Cooling capacity		
First stage	<170K at 1.5 W	140K at 1.5 W
Second stage	<90K at 0.30 W	65-75K at 0.30 W
Power Consumption	<30 W, 24 to 30 VDC	30-35 W
Speed	3, selectable	1000 rpm ± 150
Weight	4.6 kg, without electronics	5.36 kg, without electronics
		7.18 kg, with electronics
Size	16.5 × 16.5 × 32.0 cm	15.37 × 18.03 × 30.68 cm
Heat sink temperature	0 to 45°C	0 to 45°C
Vibration	<0.001 cm in any direction	0.00033 cm
Starting torques	0.0007 dyn-cm	<<0.0007 dyn-cm
Launch environment	18.9 g rms for 2 min, each axis	Met specification
EMI	Minimize	Acceptable to payload contractors
Lifetime	8000 hours, continuous or intermittent	8100 hours, at least 400 hours continuous

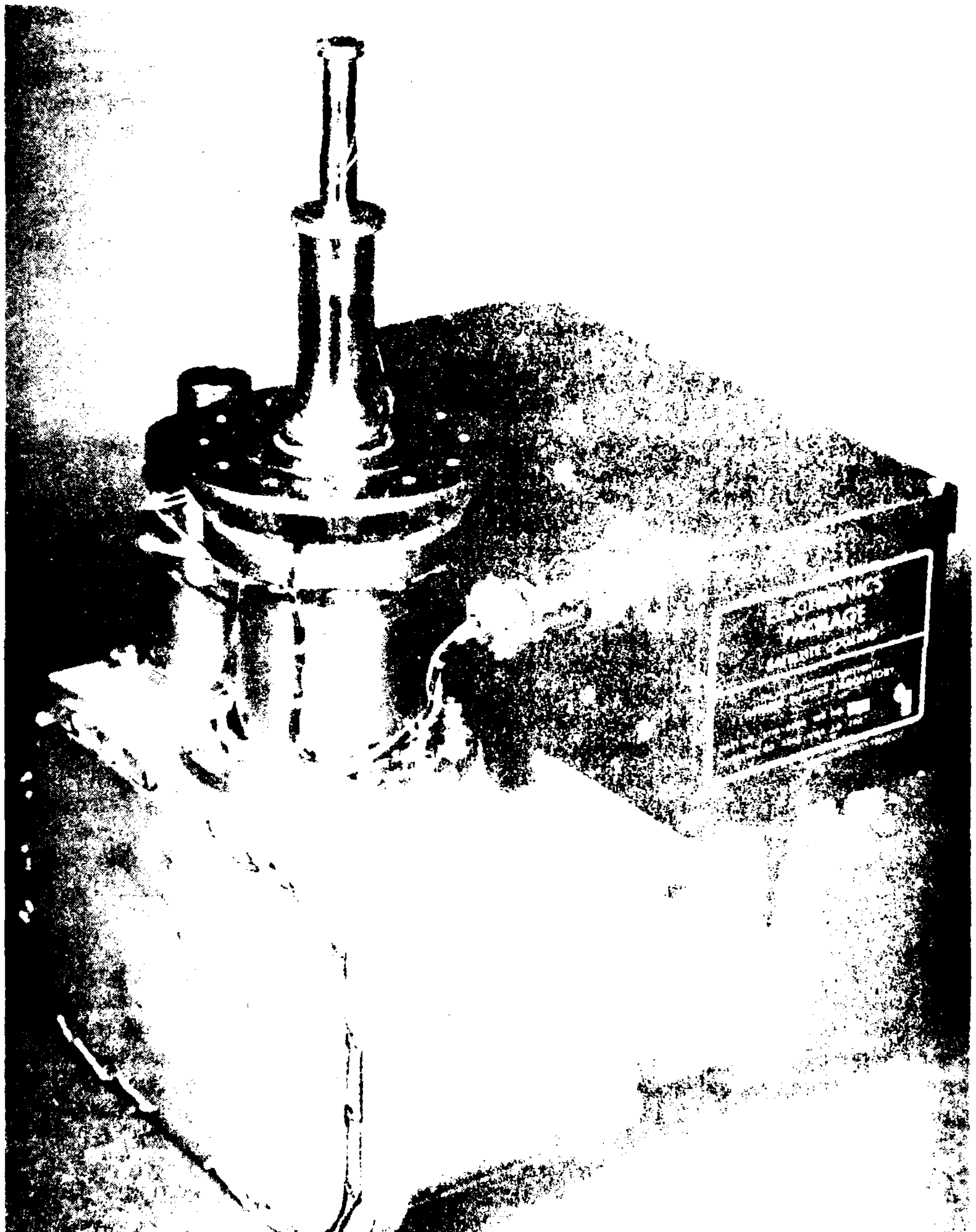

Fig. 1 Flight

refrigerator, and the second stage flange is connected by a thermal link to the intrinsic germanium detector. The flight model refrigerator (Fig. 1) differed from the engineering model (S/N 1) refrigerator as first delivered in April 1975 in that the first and second stage heat exchange flanges had been reduced in diameter and the electronics box had been slightly increased in size.

As explained in Appendix I, the Philips design evolved from their experience in laboratory model Stirling refrigerators and was directed at adapting their previous experience to the requirements of orbital flight. Tests were conducted to assure a year's lifetime for the piston and displacer seals and for the lubricated bearings. The problem of eliminating starting torques was solved by using two counterrotating motors. Appendix C of Appendix I describes the rhombic drive mechanism that Philips perfected to eliminate vibration on the refrigerator first and second stages.

The internal mechanism of the refrigerator is shown in Fig. 2 of Appendix I. This figure shows the crankcase separated from the working volume of the refrigerator (the piston and displacers within the cold finger) by a pair of metal bellows. These metal bellows (electroplated nickel) were chosen because the rubber rolling diaphram seal that Philips had used in laboratory models was dissipative and leaky and it imposed a large starting load on the refrigerator motors. These bellows were designed to isolate the working volume of the refrigerator (charged with helium) from the gas charge of the crankcase, which could be nitrogen. This isolation had two advantages: (1) it would prevent impurities (which were an inevitable consequence of the lubricants and wiring used in the crankcase) from being cold-trapped in the refrigerator regenerators, and (2) it would permit the crankcase to be charged with a gas such as nitrogen, which is much easier to contain in the crankcase than is helium.

Unfortunately, it became evident by mid-1974 that the nickel bellows would present a serious reliability problem. Preliminary designs had failed in the Philips life test and after an extensive fatigue-failure analysis by APL, the bellows were redesigned and remanufactured. Theoretically, the bellows had an infinite life, but Philips tests in the spring of 1975 again revealed cases of infant mortality. Because of the time constraints existing at that time in the program (launch was scheduled for mid-1977), it was decided to manufacture the first two refrigerators without bellows, while continuing the bellows test program at Philips. Furthermore, APL analysis of the diffusion rate of the low vapor pressure grease used in the bearing into the working volume indicated that it might be possible to achieve a year's operation without significant cold-trapping of grease vapors in the regenerators. By early 1976, Philips had demonstrated a one year lifetime for one set of

bellows, but infant mortality was still occurring in other samples. As a consequence, all six satellite refrigerators were delivered to APL without bellows installed (in this respect, Fig. 2 of Appendix I is in error). The decision to eliminate the bellows and charge the entire refrigerator with helium was made with the realization that a price might be paid in performance, but a failure of the bellows produced fragments that would have been mechanically disastrous in orbit.

The electronics box shown in Fig. 1 contained the motor drive electronics and the signal processing electronics for the instrumentation installed on the refrigerator. Two counterrotating motors, locked together by the two gears of the rhombic drive mechanism (Fig. 13 of Appendix I and Fig. 1 of Appendix C of Appendix I) were installed in each refrigerator. The motor design is described in Appendix II.

The motors were designed for high efficiency operation from a nominal 28 VDC power supply and were constructed with permanent magnet armatures. Switching of the field coils (described in Appendix II) was accomplished by sensing the position of the armature by Hall effect switches. The circuitry to start, operate, and provide speed regulation for the drive motors was designed and constructed by APL and is described in Appendix II. Besides providing the necessary current switching to properly phase the motor field coils for operation at the desired speed, the APL circuitry also provided for limiting the current drawn by the refrigerator to about 3 A starting current and 1.5 A after speed regulation becomes effective (2 seconds after the refrigerator starts). The motor drive circuit provided three speeds (which in orbit can be selected by the ground control station): 850 rpm, 1000 rpm, and free-running. In the free-running speed position, the motor speed was determined by the voltage applied to the drive circuit and by the load presented by the refrigerator, and was 1100 to 1150 rpm under the usual operating conditions.

Provision was made to measure five parameters indicative of refrigerator performance while in orbit. These were:

1. Second stage temperature, measured with a Lake Shore Cryogenic Model DT-500FP-HRC-7 silicon diode, encapsulated in Epibond 123 epoxy (a custom made sensor for this application).

2. Crankcase pressure, measured with a Kulite Semiconductor Products model VQM-1-250-100 pressure transducer (a custom made unit with a stainless steel diaphram).

3. Plenum pressure, measured with a four arm bridge constructed of Kulite Model DGP-1000-500 strain guages and cemented to the helium plenium with Epibond 123 epoxy.

4. Motor speed, measured by integrating the output of a Hall effect switch (described in Appendix II).

5. Total current, measured by the voltage across a 0.1 Ω resistor (described in Appendix II).

Signals from the above sensors are all processed in the electronics box to cover the range of 0 to 5 V; in the satellite, this voltage signal is telemetered back to earth by means of an 8 bit telemetery system. As shown on circuit diagram 5114-2051 in Appendix II, additional test signals are available at J1 and J2 for laboratory test purposes. The output of a Hall effect switch is available at pin E of J2; that signal provides an absolute measurement of motor rpm when fed into a low speed counter.

Some flexibility in the arrangement of the return ground circuits is provided in the electronics box. In practice, it was found both in the laboratory and on the satellite that minimum noise was achieved by returning all -28 V return lines to the -28 V supply bus. Because of the field coil switching and the reciprocating load of the Sterling cycle refrigerator, current noise is inherently large for these machines. The input filter shown on circuit diagram 5114-2301 of Appendix II was chosen as being the most effective that could be mounted in the space available.

3. APL LABORATORY TEST PROGRAM

GENERAL PROCEDURES

The APL laboratory test program had two primary objectives: (1) to conduct performance and environmental tests to qualify the refrigerators for space operation, and (2) to conduct a test program that gave a reasonable expectation of a year's operation in orbit. This later objective was particularly important because in the scientific community, mechanical cryogenic refrigerators had a dubious reputation for reliability. The necessity for establishing a creditable lifetime as early as possible, while at the same time meeting the delivery schedule for the flight model refrigerators, determined the sequence of events in the APL laboratory test program. In che following discussion, the test program is presented in historical order.

Prior to the final assembly of the refrigerators at Philips Laboratories, it was necessary for APL to test and calibrate the crankcase pressure transducers and to install and calibrate the strain guage pressure-measuring bridge on the helium plenum tank. The Kulite pressure transducer was a custom unit because the usual quartz diaphram (which works against a vacuum reference chamber) is not impervious to helium. Therefore, the APL transducers were faced with a thin steel diaphram. The units were tested in a pressure chamber filled with helium over the pressure range of 0 to 70 psia. It was found that the transducer output (typically 60 mV at 70 psia) was linear, temperature independent, and reproducible to better than 0.5 psi. However, the transducers showed a tendency to leak helium into the evacuated reference chamber, which decreased the stress on the diaphram and lowered the output reading. As a consequence, it was necessary to test each transducer by leaving it in the high pressure helium atmosphere for at least a month and observe the degradation in output before delivery to Philips. About half the transducers were rejected and had to be remanufactured. This testing program was carried out from January 1975 to August 1977 and no transducer that showed an error of more than 0.5 psi per month in laboratory test was installed in a flight model refrigerator. Philips installed the transducers within the crankcase. That form of mounting has the advantage that only wires are fed into the crankcase to obtain the pressure reading; the disadvantage that the refrigerator crankcase must be opened to replace a transducer.

Once the decision to omit the bellows from the refrigerator was made, the strain guage pressure-measuring bridge installed on the helium plenum tank was redundant. However, it was decided to retain this additional pressure indicator. After fabrication at Philips, the tanks were delivered to APL, where the strain guages were attached to the tank using the epoxy cement recommended by the manufacturer (Kulite). The maximum strain on the thin portion of the tank was only about 150×10^{-6}. Therefore, in order to obtain an output from a four armed bridge of about 50 mV, a semiconductor strain guage was used. This installation proved to be sensitive enough and reproducible, but was temperature independent only if no temperature gradient existed across the stainless steel plenum. Because the installation and curing of the epoxy cement produced various stains on the strain guage elements, it was necessary to provide for trimming the four arm bridge by external resistors as shown on drawing 5114-2001 of Appendix II.

The engineering model refrigerator S/N 1 was delivered to APL on 30 April 1975. The unit was fitted with the APL electronics box, which was electrically identical with that described in Appendix II, except that it was not constructed with space-qualified electronic components and it was slightly smaller in physical size. As supplied by Philips, the internal wiring of the refrigerators was completed to crankcase feedthroughs 1 and 2 shown on drawing 5114-2001; all the remaining wiring, including the installation of the second stage temperature diode, was completed at APL.

All operating and testing of the refrigerators at APL was done using the APL refrigerator electronics box and connections to connectors J1 and J2 of drawing 5114-2051 was made by the circuit shown in Fig. 2. That circuit was mounted in a small chassis and, when connected to a 28 V power supply capable of supplying several amperes, provided the voltages to operate the refrigerator and the refrigerator instrumentation. When connected to a digital voltmeter, the circuit provided measurements of the instrumentation voltages as processed for the satellite telemetry inputs. In addition to the five refrigerator parameters discussed in Section 2, outputs were provided for the 5 and 10 V sensor voltages generated within the electronics, the 5 V converter voltages generated for the motor drive logic circuits, and a Hall effect switch voltage to apply to a counter to obtain an absolute measure of refrigerator drive motor speed. Two of the test chassis as shown in Fig. 2 were built; one contained its own 28 V power supply and digital voltmeter.

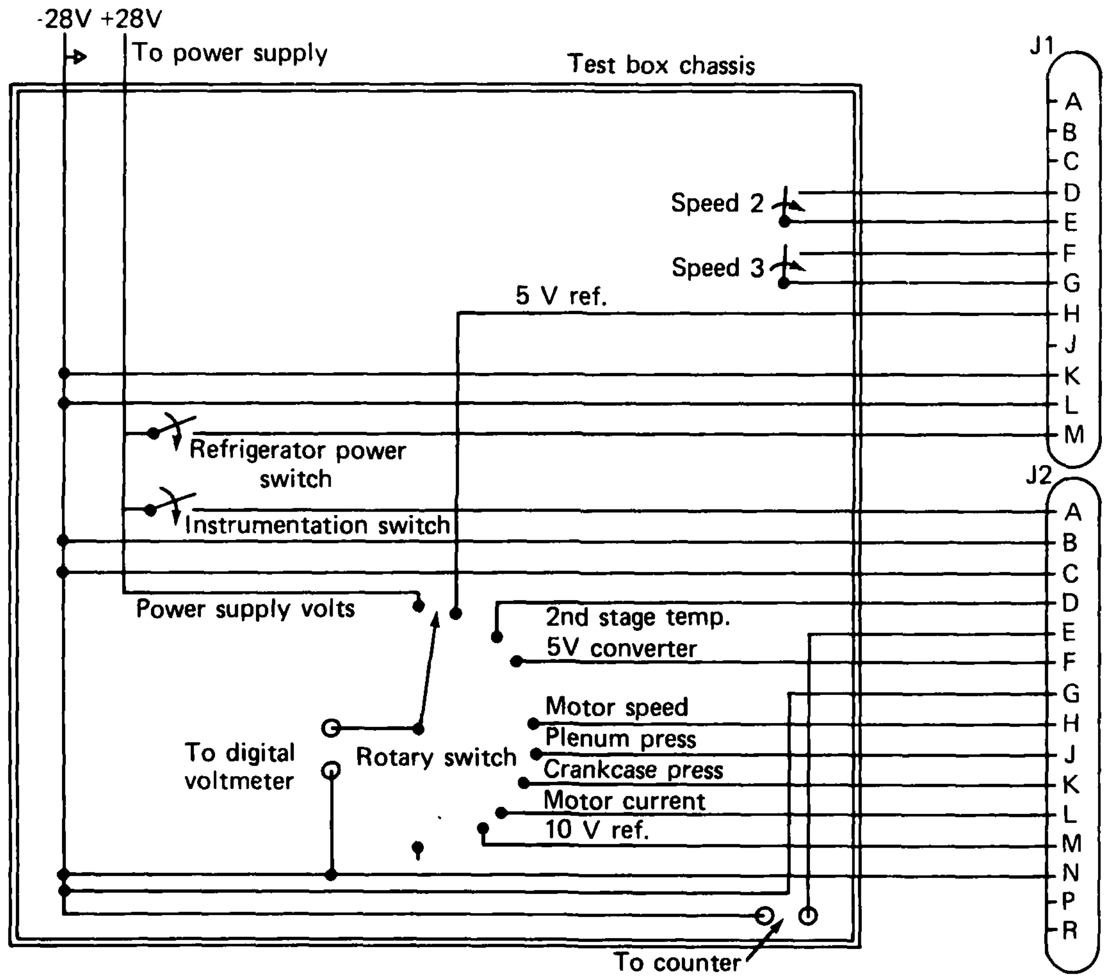

Fig. 2 Small chassis refrigerator test box circuit.

After installing and checking the APL electronics box on the refrigerator and trimming the telemetry operational amplifier outputs to cover the 0 to 5 V range, the refrigerator was installed on the test stand (Fig. 3). This test stand was mounted in a bell jar pumped by a 6 in. diffusion pump and capable of maintaining a vacuum of 10^{-6} torr. The base and heat exchange flange of the refrigerator were tightly screwed to platens that could be maintained at any temperature between -20 and +45°C by cool nitrogen gas and resistive heating elements. Plates were clamped to the first and second stage flanges on the refrigerator which contained resistors to provide the heat loads and thermocouples to measure the temperatures. The voltages of the first and second stage chromel-constantan thermocouples, referenced to an ice bath, were read on a Leeds and Northrup potentiometer. a pair of thermocouples were mounted on each of the platens and these and other thermocouples mounted on the cool N_2 gas entering and leaving the platens were measured on a Brown digital printing recorder. This Brown recorder was referenced to a thermocouple placed in a deep pit under the laboratory floor that maintained a constant temperature to ±0.25°C throughout the year. Readings of the platen temperatures were accurate to within ±0.5°C, and readings of the first and second stage refrigerators temperatures were accurate to within ±0.25°C.

The heat loads were measured by using an accurate (0.01%) digital voltmeter to measure the voltage drop across a calibrated resistor (as a measure of the current) and by measuring the voltage across the load resistor (at the point where the load resistors wires are clamped to the platens 1 ft from the resistors). Although some heat is produced in the 1 ft lead wire and some heat is conducted to the first and second stages by conduction along the lead wires to the load resistor, the product of the current and voltage as measured by the digital voltmeters was used as the stated head load. Calculating the errors (for a nominal 0.300 W load on the second stage and a 1.50 W load on the first stage), the results, for temperatures of 70 and 140K are as follows:

	Power in load resistor (W)	Power produced in lead wire (W)	Power conducted into heat load (W)
Second stage	0.294	0.006	0.0073
First stage	1.44	0.06	0.0052

Since most of the heat generated in the lead wires must flow into the cold first and second stage flanges, the heat loads are, if anything, slightly greater than stated. The thermocouple leads, which

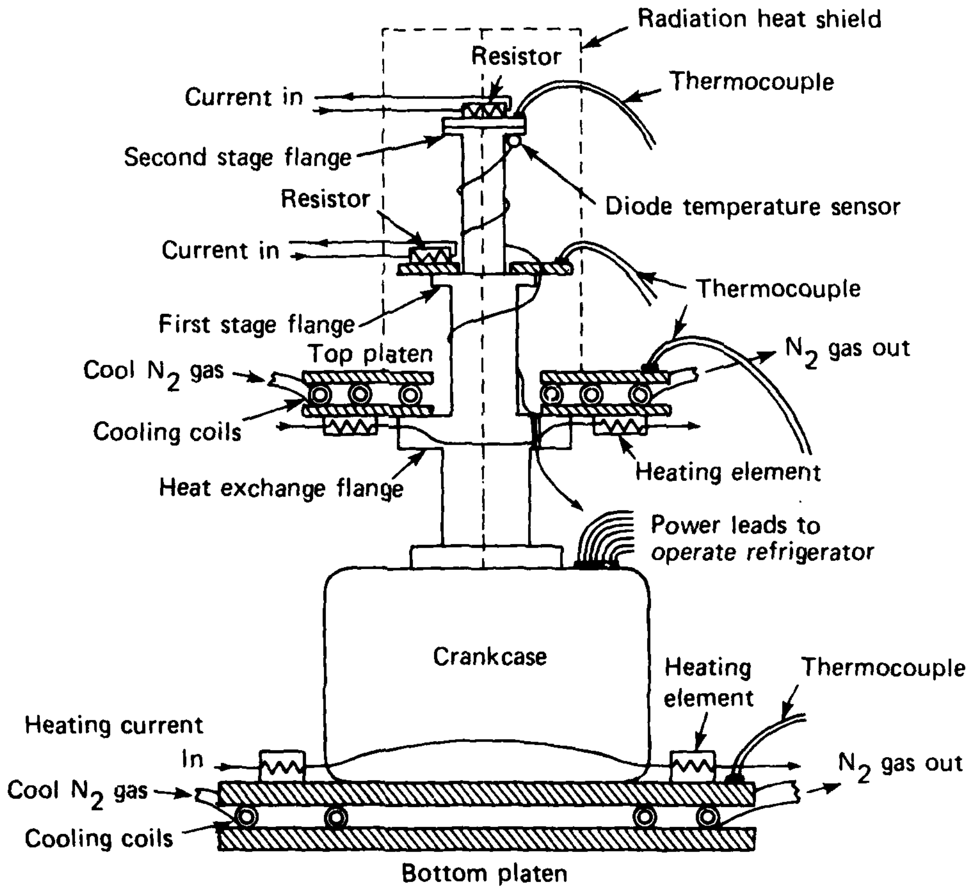

Schematic diagram of refrigerator as mounted in vacuum chamber. All electrical leads, thermocouple leads, and nitrogen gas tubes are connected to vacuum feedthroughs.

Fig. 3 Refrigerator test stand.

are 0.005 in. diameter chromel and constantan wires, have such small thermal conductivity compared to copper that their contribution to the heat load can be ignored.

Thermal testing of the S/N 1 refrigerator was begun in August 1975. The results of these initial tests are of little interest in view of subsequent events. On September 3, 1975, the refrigerator was removed from the bell jar and mounted on a shake table for the random vibration tests. The titanium cold finger failed in this test at the acceptance test level (see Appendix I, Section 7.1). It was decided to reduce the sizes of the first and second stage refrigerator flanges from those shown in Fig. 30 of Appendix I to those shown in Fig. 1 (that is, from diameters of 2.00 to 0.875 in. for the first stage, and from 1.0 to 0.500 in. for the second stages.

A stress analysis using the NASTRAN structural analysis computer program was made by APL on the titanium cold finger. This analysis showed that for the qualification test level, the principal stress on the cold finger would be 67,000 psi for the original large disk configuration and 20,000 psi for the reduced disk configuration. Since the allowable stress for the titanium alloy used for the cold finger was 115,000 psi, the original configuration should have survived with a margin of safety of 0.75; with the reduced flange, the margin of safety was 4.7. This margin of safety was judged to be adequate and the S/N 1 refrigerator was returned to Philips, fitted with a new cold finger with the reduced flanges, and returned to APL on October 3, 1975.

On November 3, 1975, the S/N 1 refrigerator survived the random vibration tests at full qualification levels and thermal performance testing was resumed. On November 18, a start of the refrigerator produced the anomalous result that the second stage temperature increased to 75°C within a few minutes. When the anomalous behavior was observed, the refrigerator was turned off. After cooling to about 45°C, the refrigerator was restarted and both the first and second stages cooled normally. Since the Stirling cycle refrigerators operate with the piston (compressor) and regenerators phased about 90° apart, if the direction of rotation is reversed, the refrigerator pumps heat in the direction to heat the first and second stages rather than cool them.

The possibility of a motor reversal had ominous implications for orbital flight and APL reviewed the motor drive electronic logic circuit and conducted numerous laboratory tests to assess the probability of this event occurring. No such failure mode could be found, either in theory or practice. Since the limited data available for the November 18 event indicated that no heating had occurred on the first stage, APL concluded that

the heating had been caused by a temporary high friction situation probably caused by loose debris on the second stage regenerator. This hypothesis was supported by the fact that the refrigerator performance had significantly improved after the November 3 event. By September 1976, APL had decided that to protect the motor drive against reversal by additional electronic circuitry presented a greater risk than the benefit would be.

In November and December of 1975, performance maps of the S/N 1 refrigerator were run. Figure 4 shows the temperature of the second and first stage flanges, as the heat load on the second stage is varied, for two values of the first stage heat load and a fixed refrigerator speed of 1000 rpm. Figure 5 shows the temperatures for fixed heat loads as the temperature of the heat exchange flange is varied from 0 to 50°C. It is observed that the variation on the first and second stage flanges is relatively insensitive to the heat exchange flange, as is expected both from the consideration of Carnot efficiency and from the variation in power consumption. The performance map for fixed heat loads and heat exchange temperature but varying motor speeds is shown in Fig. 6.

After the S/N 1 refrigerator had met the thermal performance specifications, it was placed on life test on January 6, 1976. This life test continued (with interruption caused by difficulties revealed by the test procedures and the acceptance testing program for the flight model refrigerators) until March 8, 1978. One of the consequences of the life test was that the necessity for an improved method of charging the refrigerators was revealed; this complicated the delivery schedule of the flight model refrigerators to LPARL.

The first flight model refrigerator (S/N 2) was delivered to APL on September 5, 1975, equipped with the large first and second stage flanges. It was also found that the cast magnesium crankcase end plates leaked excessively. The unit was returned to Philips Laboratories, the first and second flanges reduced in size, and new crankcase end plates were installed. On December 24, 1975, the S/N 2 refrigerator was returned to APL. By that time, Philips and APL had decided that machined (rather than cast) crankcase end plates would be required and Philips began the manufacture of the new end plates. However, S/N 2 and 3 were delivered to APL with cast magnesium end plates and, after acceptance testing, delivered to LPARL with the understanding that before launch, the crankcase end plates would be replaced with the new design.

The S/N 2 refrigerator was the first unit equipped with the flight model electronics box. Since the Stirling cycle refrigerator uses a simple piston compressor at the nominal motor speed of 1000 rpm, current fluctuations will occur at 16-2/3 Hertz due to

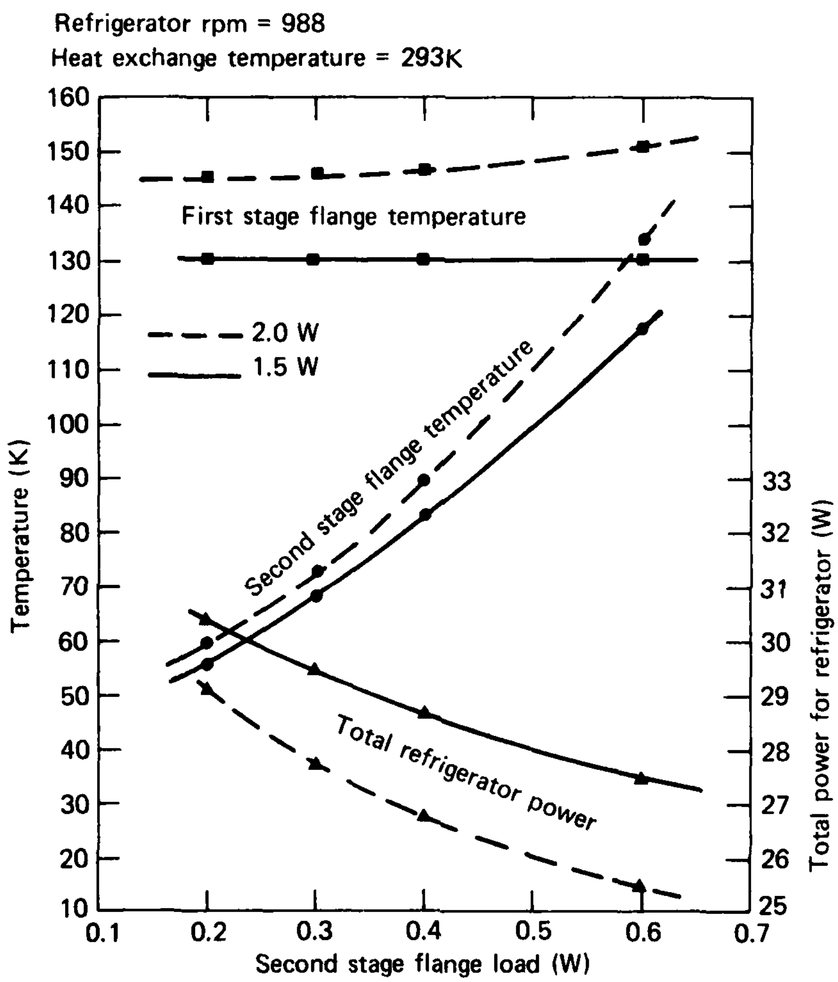

Intermediate and cold finger flange temperatures and power consumptions versus heat load on cold finger for first stage heat loads of 1.5 and 2.0 W.

Fig. 4 Refrigerator S/N 1 temperature versus second stage flange load.

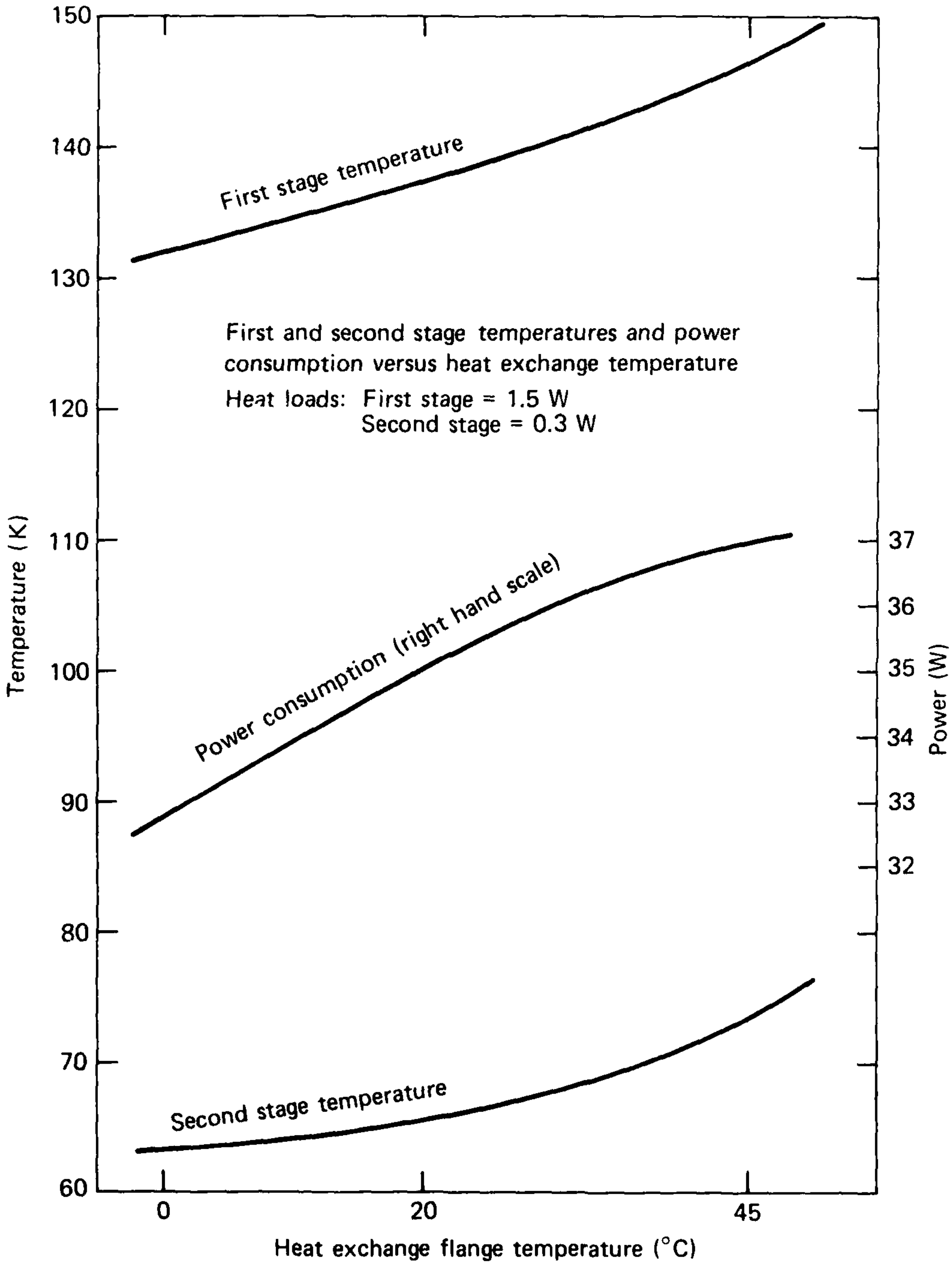

Fig. 5 Refrigerator S/N 1 temperature versus heat exchange flange temperature.

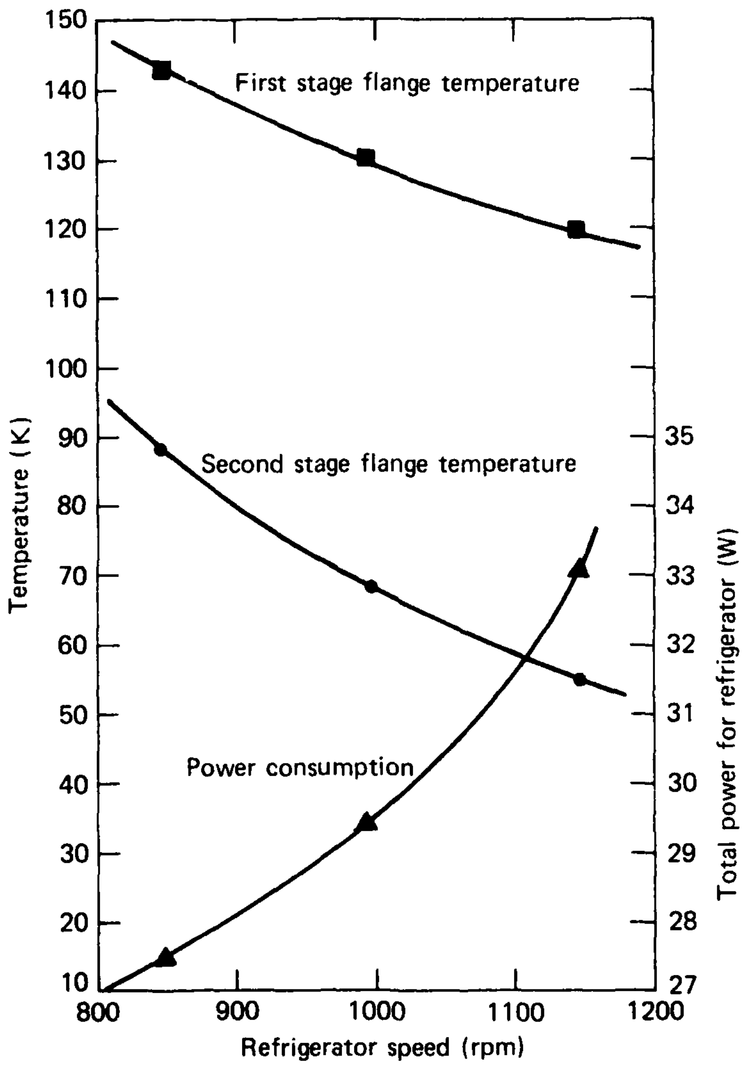

First stage and second stage temperatures and power *consumptions versus motor speed* for 1.5 W heat load on intermediate flange and 0.30 W on cold finger flange; heat exchange temperature = 293K.

Fig. 6 Refrigerator S/N 1 temperature versus speed.

the compression stroke alone. From the description of the motor drive coil switching circuits and the motor speed regulation circuits in Appendix II, switching noise will occur at 300 Hz and 10 kHz. Within the space available in the electronics box, there was no possibility of appreciably smoothing the lowest frequency current fluctuation. Several inductors were designed and built and with the capacitor values shown in Appendix II, the optimum choke value was chosen by experiment. For the final filter design, the input current waveform is shown on Fig. 7. The spectral analysis of the current waveform is shown in Figs. 8 and 9. It is observed that in the free-running (unregulated) speed position (about 1150 rpm) the current fluctuations are significantly reduced.

After completion of thermal and environmental testing, the S/N 2 refrigerator was delivered to LPARL on February 2, 1976. LPARL used this unit for tests in their experiment in 1976, returning it to APL for installation of the new crankcase end plates in January 1977.

ACCEPTANCE TESTING OF FLIGHT MODEL REFRIGERATORS

As stated above, the acceptance testing program of the flight model refrigerators was interactive with the life-test results on the S/N 1 refrigerator. Thus S/N 2 and 3 refrigerators were delivered to LPARL with the realization that they would have to be recalled for the installation of improved (machined) crankcase end plates and recharged with helium of higher purity. S/N 4, 5, and 6 were delivered (beginning in October 1976) with end plates of the new design and with crankcase pressure transducers that had undergone more careful and rigorous testing before installation.

The schedule for the acceptance testing and delivery of the flight model refrigerators to LPARL is given in Table 2. At LPARL, starting problems were experienced on two occasions with S/N 2, but these were not reproduced at APL, nor was any fault in the electronics drive circuit ever found that explained the starting problem. From the refrigerator log book starting difficulties always occurred after the refrigerator had been out of operation for six months or so and were apparently caused by a "set" or "sticking" of the piston or regenerator seals. Exhaustive testing of the starting circuits at APL always showed that they operated as designed (see Appendix II), and provided the required protection for the satellite power supply (Ref. 3). The several instances of the failure of the refrigerator to start experienced at LPARL (and at APL) are probably related to the use of current-limited power supplies in the laboratory. These power supplies, usually

(Current) voltage across 0.1 Ω resistor

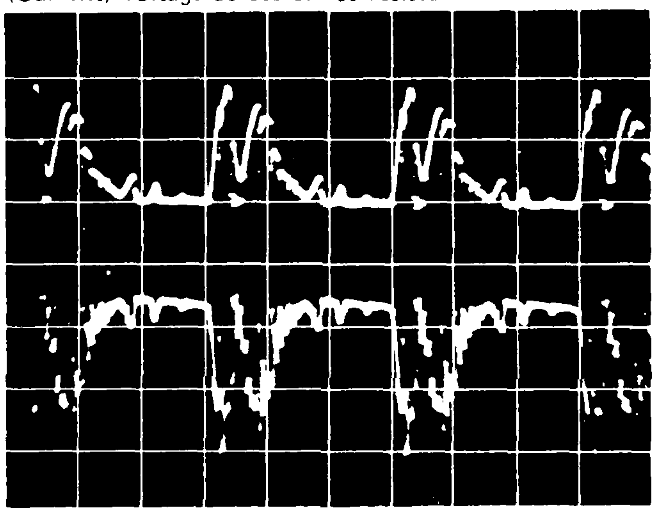

DC coupled

AC coupled

Voltage across power supply with 0.1 Ω impedance

Sweep: 20 ms/cm
Amplitude 0.2 V/cm
Refrigerator running at 1000 rpm

Fig. 7 Refrigerator input current waveform.

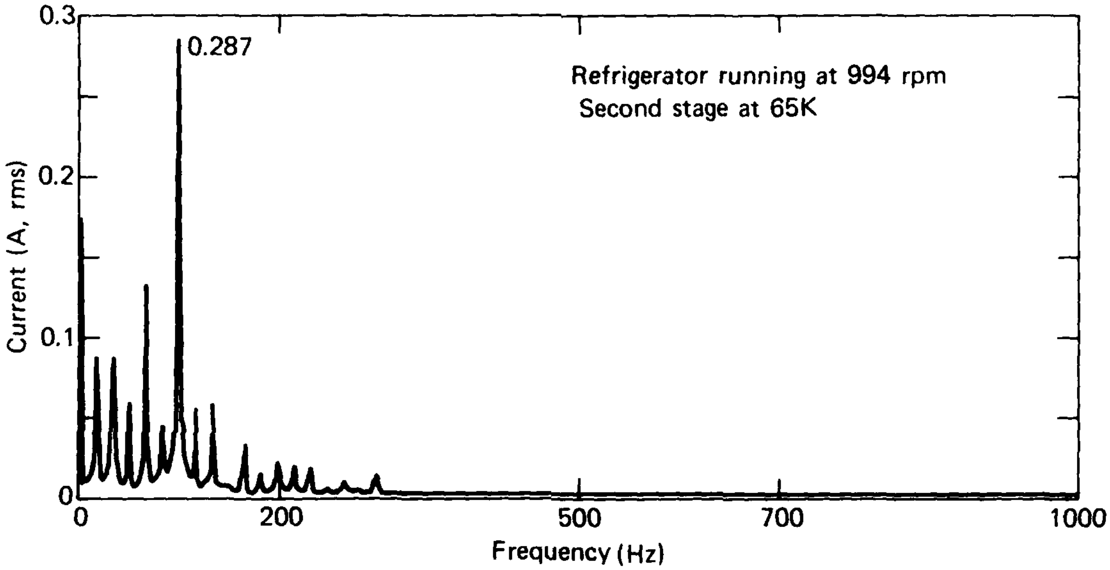

Fig. 8 Typical refrigerator current spectrum, 1000 rpm.

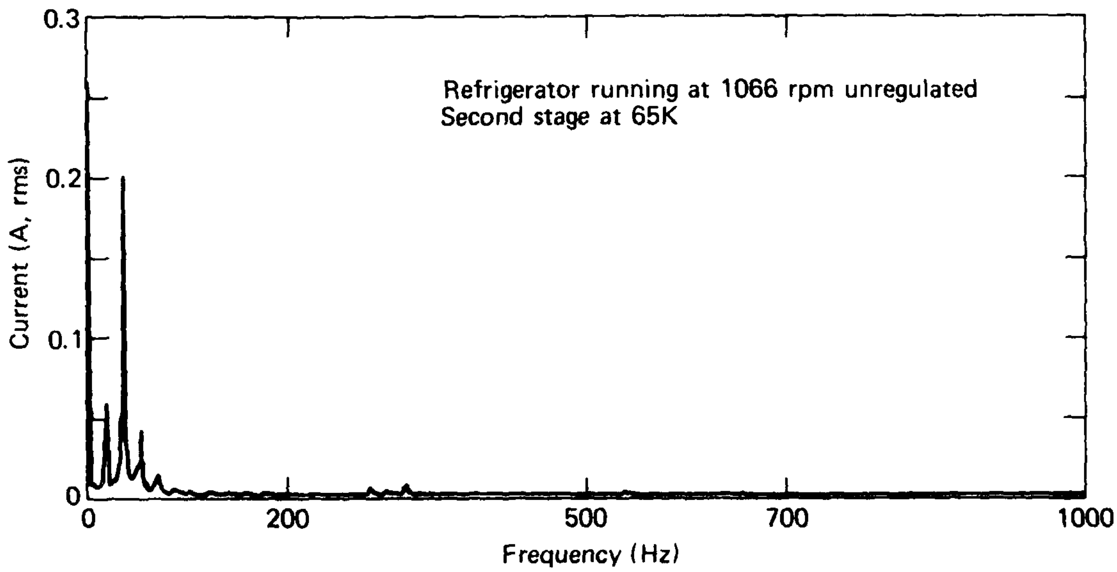

Fig. 9 Typical refrigerator current spectrum, speed unregulated.

Table 2

Acceptance test history, flight model refrigerators.

S/N	Received at APL	Acceptance test completed delivered to LPARL	Return to APL; Reason for return	Action taken	Returned to LPARL
2	5 Sep 1975	2 Feb 1976	18 Jan 1977 — starting problem	Strain gauge replaced, new end plates, pressure transducer replaced improved helium recharge	1 Jun 1977
			11 Jan 1978 — starting problem, pressure transducer failure	5 V converter replaced, new transducer	27 Apr 1978
3	13 Feb 1976	23 Apr 1976	26 Feb 1977 — pressure transducer failure	Transducer replaced new end plates, improved, helium recharge, strain gauge retrimmed	1 Jun 1977
4	13 Oct 1976	14 Dec 1976	6 Jan 1979 — starting problem, leak in cold finger	New cold finger and new 5 V converter installed	12 Feb 1979 (became flight spare)
5	14 Jul 1976	7 Oct 1976			
6	2 Dec 1976	27 Sep 1977			

limited to 2 to 2.5 A, do not duplicate the low impedance power source of the satellite; failure to start under laboratory conditions does not necessarily imply that this difficulty will be experienced in space.

Before delivery to LPARL, the flight model refrigerators were tested for thermal performance, subjected to the acceptance level vibration tests, and a spectrum analyzer run made for the current noise at the three operating speeds. Thermal performance tests were made in a vacuum bell jar at a pressure of 10^{-6} torr or less. Before shipment, calibration graphs were made for the telemetry outputs (0 to 5 V) of the crankcase pressure transducer, the pressure strain gauges, refrigerator current consumption, motor speed, and second stage temperature; they were forwarded to LPARL with the refrigerators.

The results of the thermal performance tests are given in Table 3. Results of the tests were essentially the same for the tests performed before and after the vibration tests. Starting tests were performed at each temperature of the heat exchange flange. After the final delivery of the refrigerators to LPARL as listed in Table 2, APL had no further experimental experience with them until the pre-launch tests conducted in November 1978 (discussed in Chapter 4).

LIFE TEST OF THE S/N 1 REFRIGERATOR

As stated earlier in this chapter, the life test of the S/N 1 refrigerator (the engineering model) was interactive with the delivery schedule and design changes of the flight model refrigerators. The initial performance testing and mapping of the S/N 1 refrigerator was carried out in November and December 1975 in the vacuum bell jar test set stand (Fig. 3). For the life test, a separate test chamber was constructed (Fig. 10). The vacuum region was limited to the region above the heat exchange flange and was pumped through a tube and valve connected to the bell jar vacuum system. Temperatures of the first and second stages were measured by thermocouples referenced to an ice bath, using a Leeds and Northrup potentiometer. The thermocouples were also read on a set of temperature controllers that shut off the refrigerator if the first or second temperatures exceeded a preset valve. A conventional locking relay was used to prevent restarting the refrigerators and test apparatus in the event of a failure of the laboratory AC power supply. The heat exchange flange was cooled by the

Table 3

Acceptance test results for flight model refrigerators.

S/N	*Heat exchange* flange temp. (°C)	Second stage temp. (K)	First stage temp. (K)	Power Consumption (W)	Speed (rpm)
2	0	70.1	121	30.2	988
	24	68.9	128	33.9	1000
	45	68.9	132	36.1	1012
3	1	73.0	123	31.9	992
	20	70.1	127	34.4	1002
	45	76.1	136	37.8	1018
4	0	63.3	126	33.6	988
	19	71.3	130	35.8	1008
	45	78.0	140	38.1	1030
5	0	74.1	126	29.1	982
	21	76.5	135	35.8	995
	44	83.5	139	37.8	1016
6	3	61.0	110	35.6	998
	20	68.9	118	36.7	1011
	44	71.3	122	37.2	1015

Notes:
Second stage heat load, 0.300 W
First stage heat load, 1.50 W
Refrigerator nominal motor speed, 1000 rpm

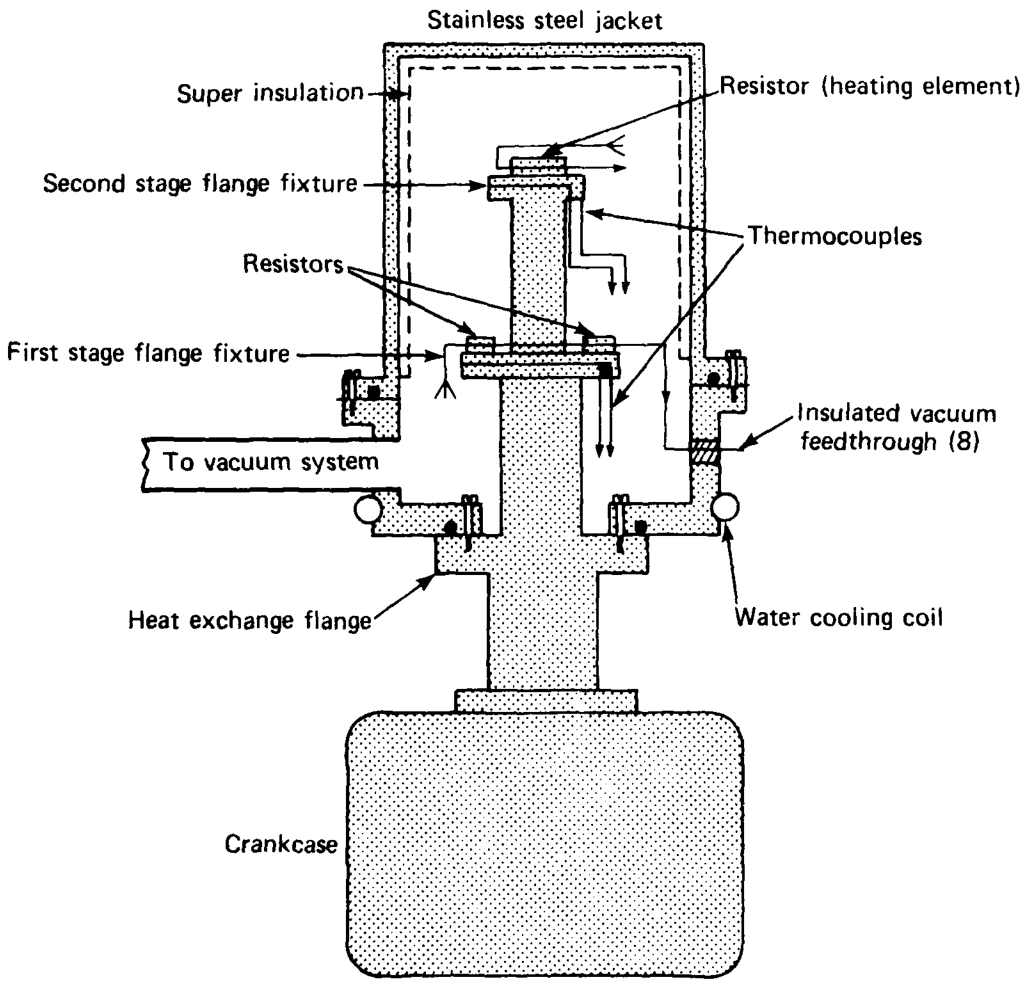

Fig. 10 Schematic diagram of refrigerator mounted in life test chamber.

laboratory chilled water supply to 18 to 22°C. Temperature controllers on both the heat exchange flange and refrigerator electronics box were set to turn off the experiment if temperatures exceeded normal values. The conventional automatic vacuum system that pumped both the bell jar and life test chamber had the usual interlocks against power failure and a pneumatic valve that isolated the evacuated volume in case of vacuum pump failures. Power supply voltages, refrigerator currents, and the telemetry outputs of the refrigerator instrumentation were read as described earlier in this chapter.

The life test began on February 8, 1976 and was completed on March 3, 1978. References 4, 5, and 6 contain a detailed history of the tests and the results obtained; here a brief resume is given with emphasis on the effects that the life test had on the completion of the flight model refrigerators.

An example of the refrigerator performance during the early part of the lift test is given in Fig. 11. During a continuous run of 145 hours, the temperatures of both the first and second stages were observed to continuously rise, the first stage at about 2.6K per day and the second stage at 4.1K per day. If the refrigerator was turned off and allowed to warm to ambient temperature, on restart the temperature returned or nearly returned to its value at the beginning of the test. Since the refrigerator cold finger acts as a cold trap and collects frost while in the vacuum chamber, it was thought (Ref. 4) that all or part of this temperature rise could be due to changes in the emissivity of the cold finger caused by the freezing of water vapor. Later events were to prove that all of this temperature rise could not be due to this effect.

About February 15, 1978, a significant change occurred in the S/N 1 refrigerator performance. The first stage temperature decreased, but the second stage temperature increased by about 10K and began a rapid rate of rise. This rather abrupt change in performance was confirmed in the bell jar test stand and on March 18, 1976 (after 868 hours of accumulated operation) the unit was returned to Philips Laboratories for examination.

When the S/N 1 refrigerator was disassembled at Philips (Ref. 5), it was found that the Roulon seal on the second stage displacer was excessively worn and that the second stage refrigerator was clogged with debris. The cause of this excessive wear could not be determined, but the second stage had been overheated on November 18, 1975 (as described earlier in this chapter), and the displacer connecting rod was slightly misaligned. After realigning the connecting rod and replacing the second stage displacer and regenerator, the unit was returned to APL.

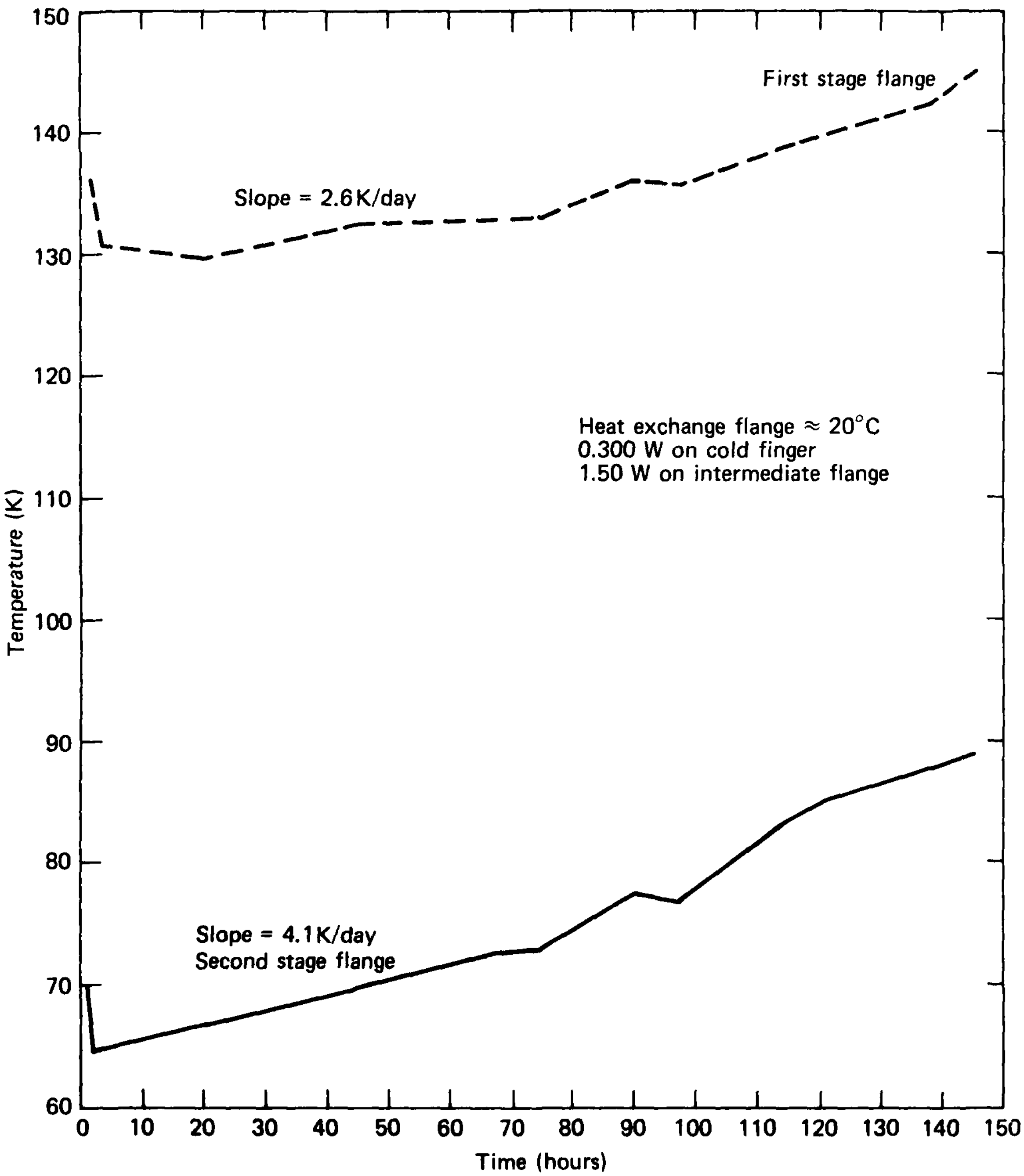

Fig. 11 Refrigerator S/N 1 life test beginning January 30, 1976.

Placed on life test on May 24, 1976, the unit operated satisfactorily for several days but then suffered a repeated series of stoppages after 8 to 18 hours of operation. These stoppages were caused by a rapid rise in the first stage temperature, which opened the safety interlock on the refrigerator power supply. An impurity, possibly water vapor trapped within the refrigerator, was suspected to be the cause of the problem. This was verified on July 14, 1976, when Philips disassembled the refrigerator at APL and found visible drops of water within the working volume of the cold finger.

Philips Laboratories now perfected an imporved method of recharging the refrigerators with helium. This method is described in detail in Section 5.1 of Appendix I, but essentially consisted of a bake-out of the refrigerator in vacuum at 140°F and a careful purging and recharge of the refrigerator with helium fed through a liquid nitrogen cold trap. Returned to APL on August 19, 1976, the electronics box was checked for possible motor reversal. No electronic failure was found that could cause reversal. On September 2, 1976, the unit was returned to life test.

Performance of the S/N 1 refrigerator as measured during the life-test was the best that had been observed under laboratory conditions. Figure 12 shows the temperatures of the first and second stages as measured during a 360 hour run made in October, 1976. The temperature rise of the first stage was about 0.66K per day; and for the second stage was about 0.93K per day. This slow temperature rise was acceptable for any experiment contemplated by LPARL in space. The S/N 1 refrigerator life test continued until March 3, 1978, at which time it was terminated because the lifetime specifications had been met. During that period, no failures or difficulties were experienced in the refrigerator operation, the helium gas charge in the refrigerator was unperturbed, and (except for interruptions caused by acceptance tests of flight model refrigerators, holidays, vacations, power outages and maintenance of the test facility) the life test was run continually until its completion. Tle longest uninterrupted runs were about 400 hours.

Again it was observed that following a long run, the temperatures of the first and second stages returned almost to their values before the run if the refrigerator was allowed to warm to ambient temperatures and restarted. Superimposed on the daily temperature rise observed during continuous operation was a slower degradation of performance observed following restart of the refrigerator. Figure 13 shows the refrigerator performance, measured about 24 hours after it was started, throughout the 8140 hours of the life test. For this figure, the heat load and refrigerator speed were held constant. The first stage temperature increased

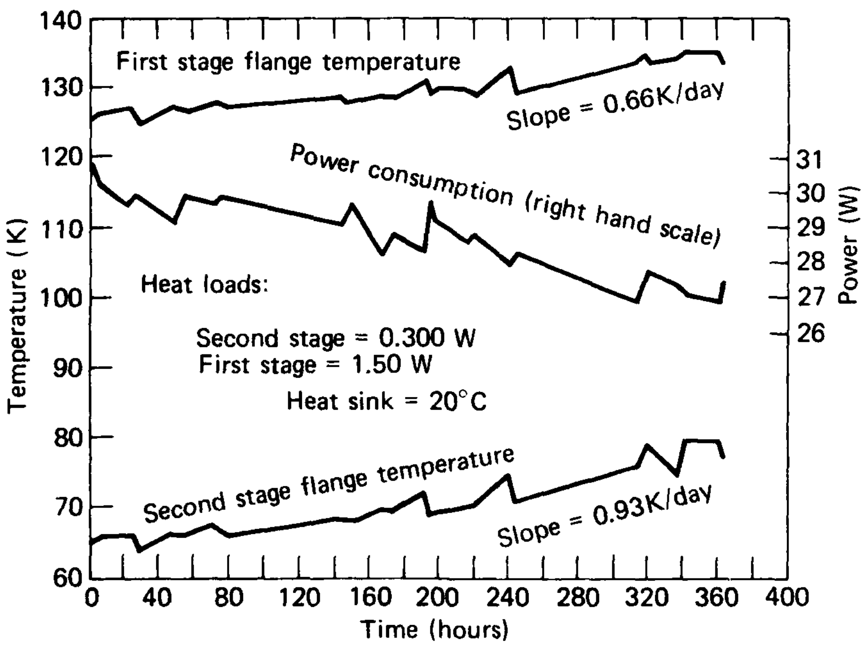

Fig. 12 Refrigerator S/N 1 life test beginning October 19, 1976.

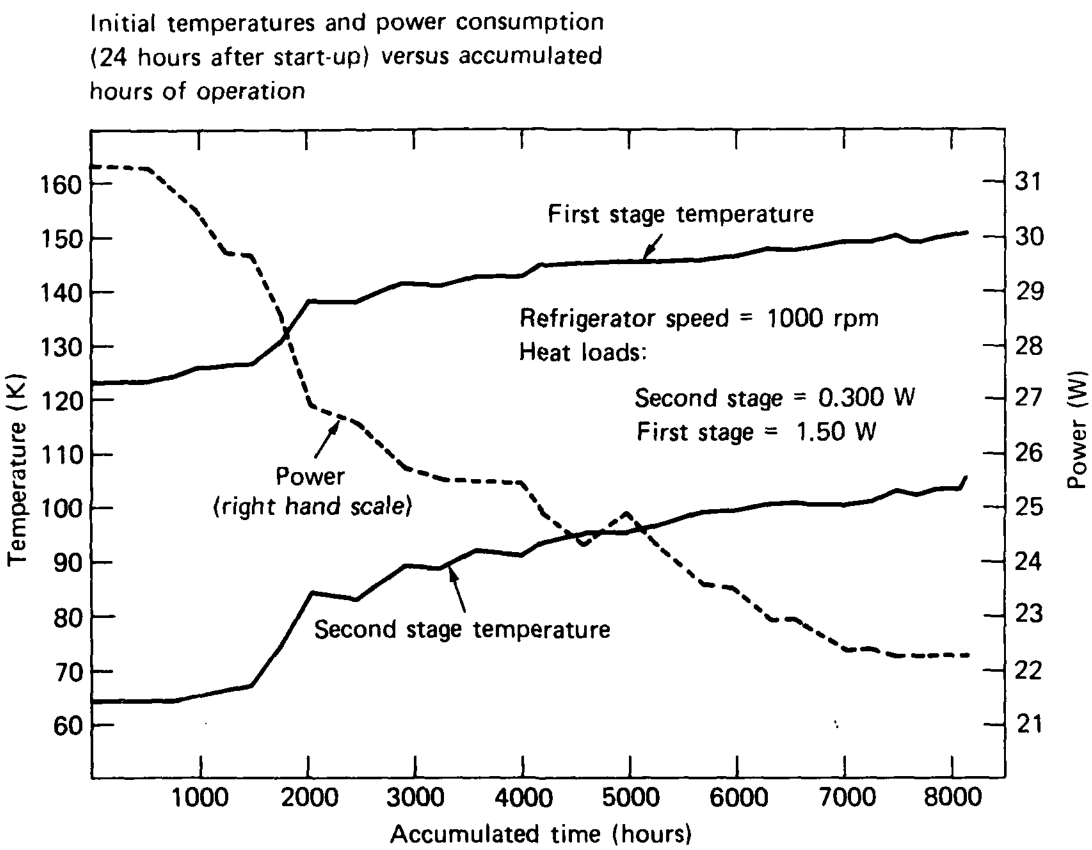

Fig. 13 Refrigerator S/N 1 initial temperatures and power consumption.

at a rate of 2.36K per month and the second stage temperature at a rate of 3.62K per month (where time is measured in units of accumulated operating time). At the end of the life test, the performance of the refrigerator versus motor speed was measured. The results are shown on Fig. 14. The second stage temperature was 82.4K and the power consumption was 24.4 W, well within the original specifications for the refrigerator ($\simeq$ 90K on the second stage for a 0.30 W heat load).

It should be noted that the laboratory chilled water supply used to cool the heat exchange flange fluctuated from 16°C to 24°C within a period of about 25 minutes. This regular fluctuation produced periodic fluctuations in the refrigerator first and second stage temperatures as well as in the current consumption. Figure 15 shows these fluctuations as recorded on strip chart recorders. While not of interest in themselves, these fluctuations cause a noticeable scatter in the plotted results of Figs. 12 and 13, which were taken at random times in the cooling water cycle.

The long time degradation of refrigerator performance and decrease in power consumption shown on Fig. 13 could have been caused by a loss of helium pressure, contamination of the regenerators by impurities in the helium charge, or by wear. The pressure within the refrigerator was monitored by the Kulite pressure transducer throughout the life test, but this transducer was known to be subject to long-time errors caused by leakage of helium into the evacuated reference volume, which appeared on the transducer output as a lower signal or lower pressure. To determine what the pressure in the refrigerator was at the end of life test and the effect of helium loss alone on refrigerator performance, the S/N 1 refrigerator was recharged on March 8, 1978. The pressure was read on an accurate diaphram absolute pressure guage with a specified accuracy of 0.25 psi. The results are shown on Table 4.

Table 4

Refrigerator helium pressure and performance at beginning and end of life test and after helium recharge.

	Sep 3, 1976	Mar 3, 1978	Mar 8, 1978
Helium pressure (psia)	71	60.5	71
First stage temperature (K)	64	105	77
Second stage temperature (K)	123	151	132
Power consumption (W)	30.5	22.7	28.7

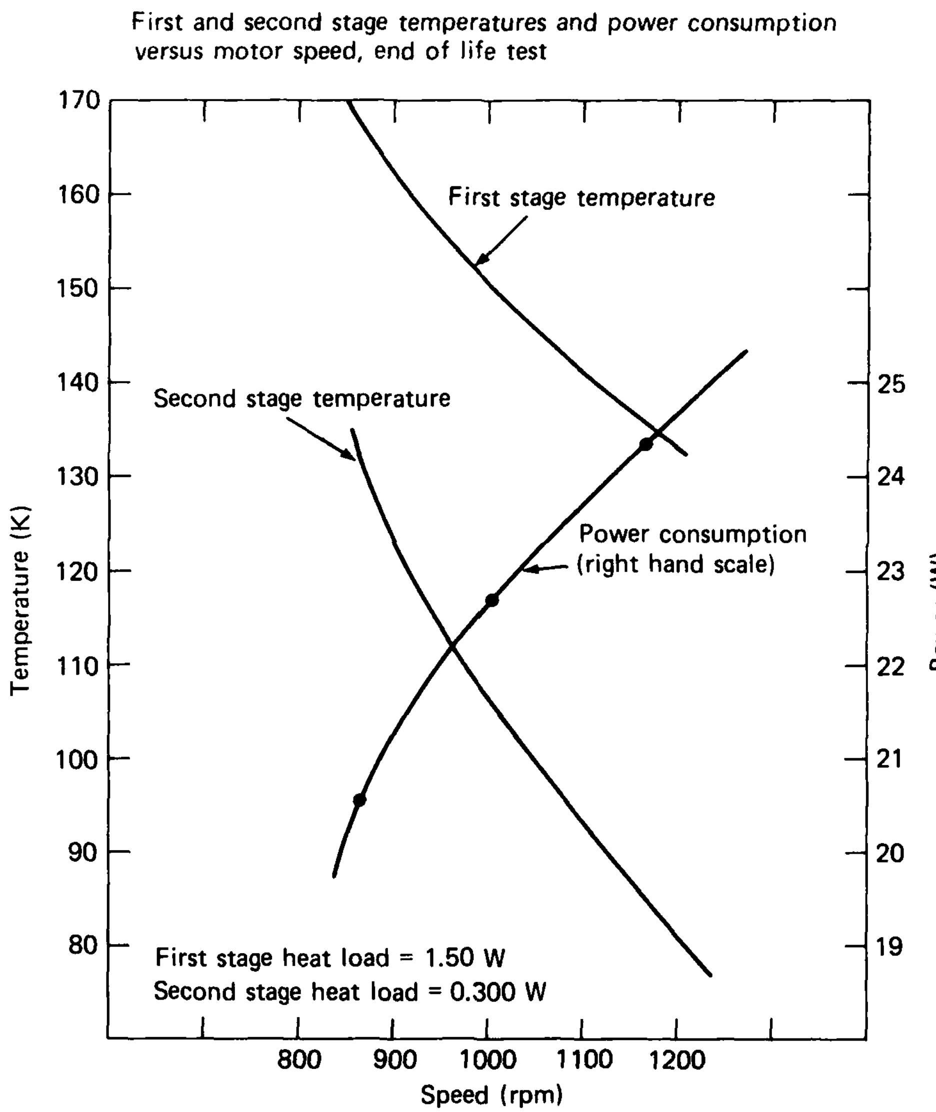

Fig. 14 Refrigerator S/N 1 performance map at end of life test.

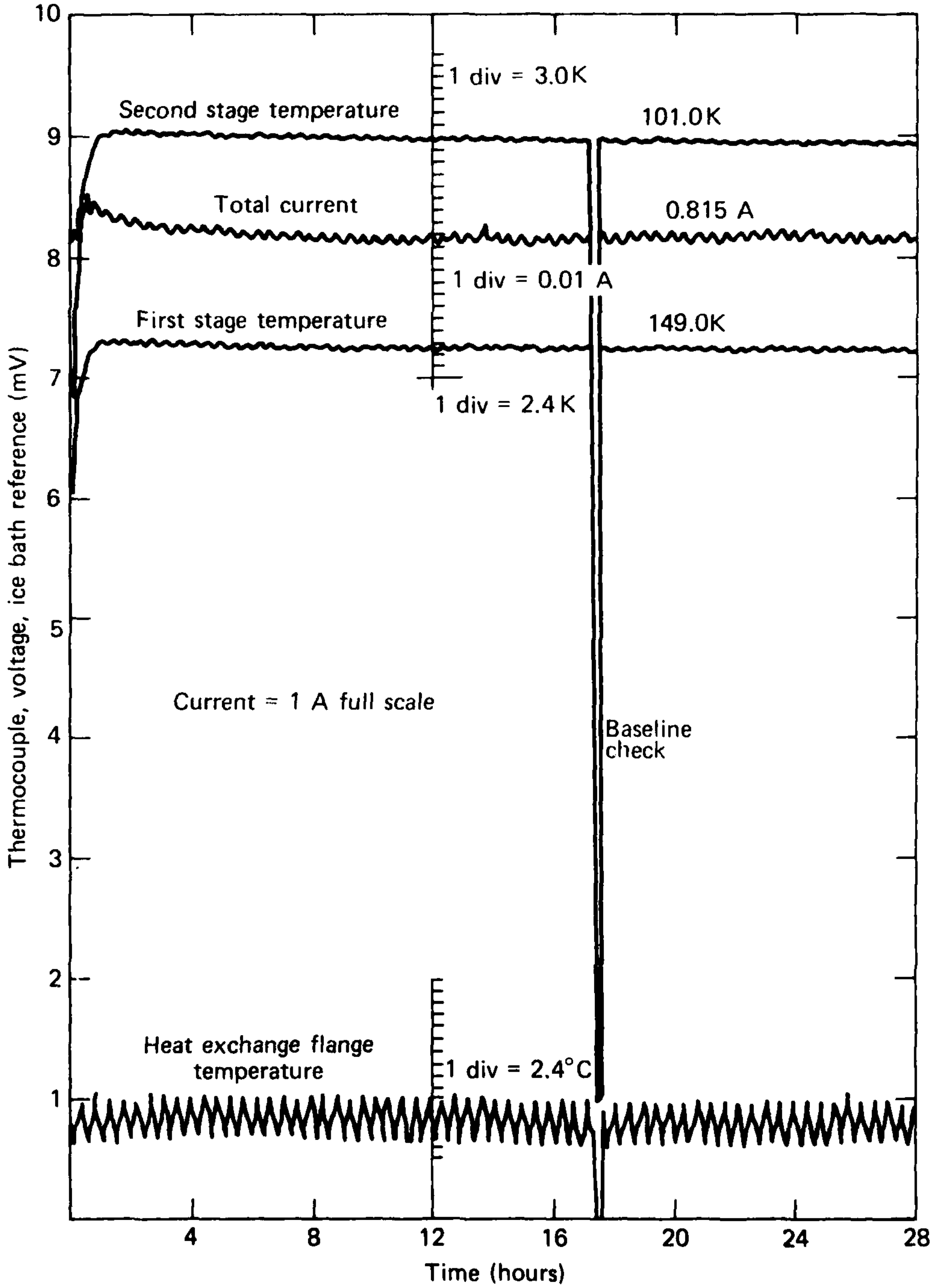

Fig. 15 Refrigerator S/N 1 strip chart record of temperatures and current.

It is observed upon repressurization that the first stage returns to within 9K and the second stage to within 13K of their initial temperatures. Thus the temperature degradation throughout the life test was largely (68%) due to the loss of helium pressure alone; the remaining 32% must have been caused by contamination of the regenerators and wear on piston and displacer seals. Figure 16 shows the calibration curve for the crankcase transducer at the beginning and end of the life test. For a given voltage out, the transducer error was -5.5 psi at the end of the life test.

On March 17, 1978, the unit was returned to Philips Laboratories for disassembly and inspection. The results of the inspection are given in Ref. 7. Philips found the interior of the refrigerator in very good condition. The regenerators were visibly clean and flow tests to measure the resistance to gas flow before and after cleaning the regenerators revealed no appreciable effects of debris collection. Chemical analysis of the fluids used to clean the regenerators revealed no crankcase lubricant, even though the bearings in the crankcase had lost a portion of their Krytox grease. The upper displacer had lost about 0.0004 in. of diameter, and the cylinder in which the upper displacer moved had increased in size about 0.0008 in. No other significant wear that would affect performance was observed. Mass spectroscopy analysis of the helium charge revealed that the gas was over 98% helium, about 1% nitrogen and oxygen, and 0.34% other gases. The water vapor concentration (which could not have exceeded about 0.5%), could not be measured with sufficient accuracy for a significant result because of limitations in the mass spectrographic and infrared scan techniques. Philips estimates that the mechanical part of the refrigerator would certainly have continued to operate for 3000 to 4000 additional hours. After disassembly and inspection, Philips replaced the piston, first stage displacer seals, and crankcase end plates, but did not distrub the second stage displacer. After recharge and check for proper operation, the unit was returned to APL on July 14, 1978.

Several tests of the S/N 1 refrigerator were then made at APL. Typical performance when it was first returned are given in Table 5 along with the results obtained before the Philips inspection.

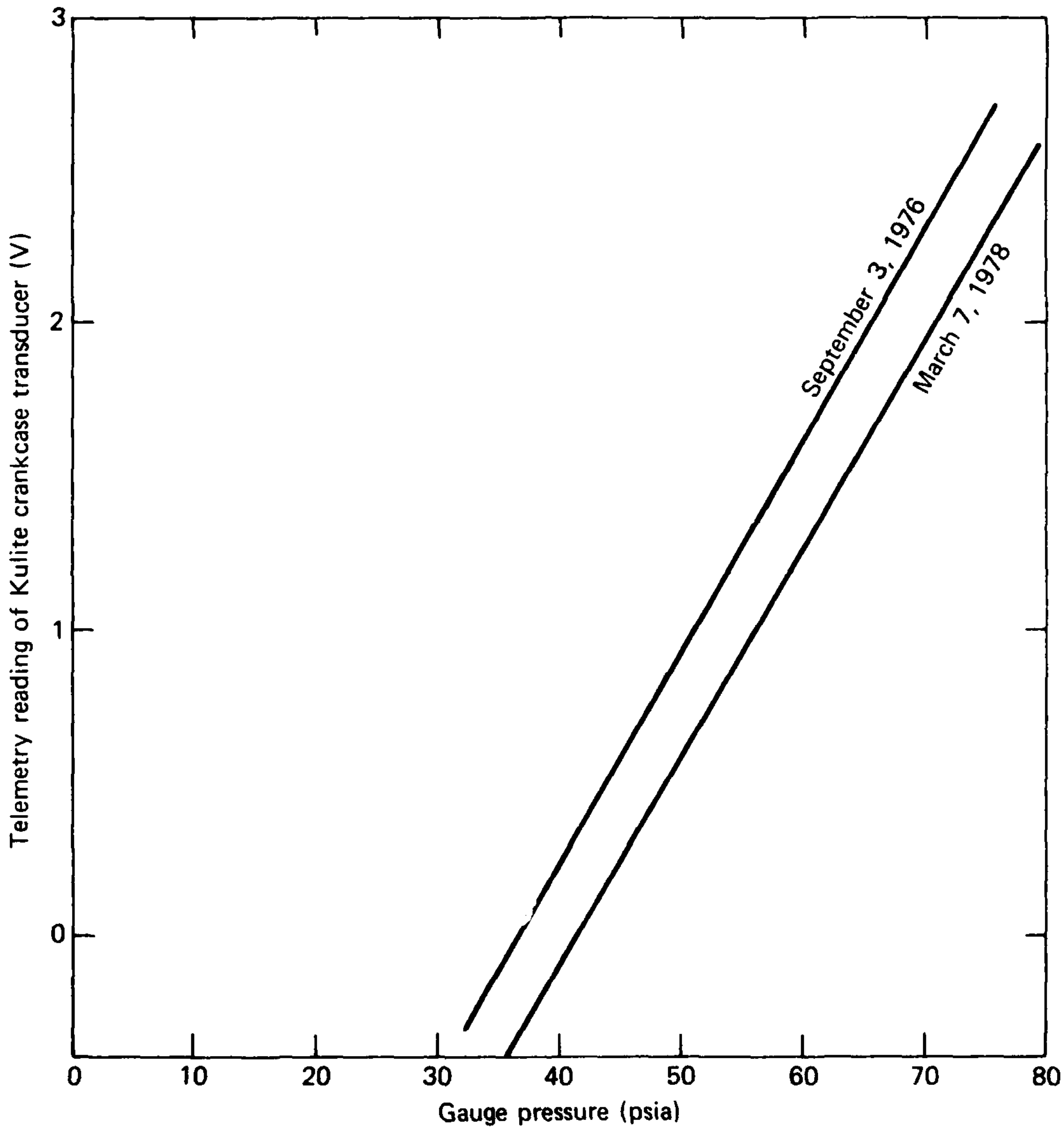

Fig. 16 **Refrigerator S/N 1 crankcase pressure transducer calibration at beginning and end of life test.**

Table 5

Refrigerator performance before and after Philips inspection and reassembly.

	March 8, 1978	July 21, 1978
Helium pressure (psia)	71	71
Second stage temperature (K)	77	70
First stage temperature (K)	132	131
Power consumption (W)	28.7	40.8

Comparing Tables 4 and 5, it is observed that the S/N 1 refrigerator did not return to its original performance, but showed an improvement over the results obtained immediately after conclusion of the life test. The high power consumption on July 21 was caused by the installation of the piston and first stage displacer seals at Philips, neither of which has been run-in for a sufficient length of time.

During August 1978, several runs, about a week's duration each, were made. Power consumption decreased to about 35 W, but the rate of temperature on the second stage remained at about 1K per day, as it had been throughout the life tests. At the request of LPARL, tests were performed in the vacuum bell jar to determine the low ambient temperature at which the refrigerator would fail to start. It was found that starts were uncertain or erratic but ultimately successful at -30°C for the crankcase and heat exchange flange. At -20°C, starts were smooth for all three motor speeds.

The reason for the daily rise of the first and second stage temperatures has never been quantitatively explained by any experiment performed at APL. It is clear that the refrigerator cold finger acts as a cold trap when in vacuum; the trapping effect is easily observed on an ionization guage after the refrigerator is started. Since the predominant gaseous constituent in conventional vacuum systems is water vapor, frosting of the cold finger will occur and the resulting change in emissivity will change the radiative heat transfer into the cold finger. When in the life test chamber (or the bell jar), the refrigerator cold finger is a relatively small surface at a temperature T_2 surrounded by a large surface at a temperature T_1, and the heat load supplied

to the cold finger by radiation is given by

$$H/cm^2 = e\,(5.67 \times 10^{-12})\,(T_1^{\,4} - T_2^{\,4})\ W/cm^2, \qquad (1)$$

where e = emissivity.

The temperature of the cold finger between the first stage flange and second stage flange varies from about 135K to 70K; the result of Eq. 1 is not very sensitive to the value of T_2; taking T_2 as 77K and T_1 as 300K, Eq. 1 gives

$$H/cm^2 = e\,(4.57 \times 10^{-2})\ W/cm^2. \qquad (2)$$

Assuming that the emissivity of a gold plated surface is 0.02, for the 15 cm^2 area of the cold finger the heat input is

$$H = (0.02)(4.57 \times 10^{-2})(15) = 0.0137\ W. \qquad (3)$$

Thus, the measured heat load on the second stage of 0.300 W is really 0.3137 W, and if the effect of frosting increases the emissivity to 0.1, the heat load becomes 0.3685 W. From the performance map of Fig. 4, this change of second stage heat load would produce a temperature increase of 9K.

For water vapor, the pumping speed for a surface near liquid nitrogen temperature is (Ref. 8):

$$\text{pumping speed}/cm^2 = 14.7\ \ell/s. \qquad (4)$$

The measured pressure in the vacuum chamber surrounding the cold finger is from 5×10^{-7} to 1×10^{-6} torr; assuming that the vapor pressure of water is 5×10^{-7} torr, then the number of molecules pumped per second per cm^2 surface is 2.49×10^{14} (or the mass of water vapor frozen out on a 1 cm^2 surface is 7.76×10^{-9} g/s). Thus each square cm of surface collects 6.7×10^{-4} g/day or the surface of the cold finger accumulates almost 0.001 cm/day of frost. THe effects of frosting on the emissivity (or absorptance) of a gold surface is unknown, but from Ref. 9, the absorptance of a polished aluminum surface increased from 0.07 to 0.60 for a cyro deposit of 0.001 cm exposed to black body radiation at 300K. Such a change in absorptance would result in a heat load increase that is many times that required to explain the daily temperature increase observed on the refrigerator life tests.

Nonetheless, in spite of the lack of quantitative agreement with experimental results, it was thought in January 1976 that the observed temperature increases of about 4K/day (Fig. 11) were probably caused by the freezing of contaminates on the exterior of the cold finger. Following the results of the October 1976 performance test (which are described above and given in Fig. 12) it was realized that the improved helium charging technique developed by Philips in the summer of that year had significantly reduced the rates of temperature rise measured on the second and first stages. It was clear that the greater part of the 4K/day temperature increase had been caused by the effects of internal contamination of the helium charge (probably freezing out in the regenerators), and not external frosting on the cold finger. Since the temperature rise observed after the improved method of gas charging was perfected was acceptable to LPARL for its projected experiments in space, the problem became ignorable. However, the 1K/day temperature rise that persisted throughout the life test remained unexplained; the bake-out procedure used by Philips would not have removed all the water vapor in the refrigerator and no method was available during the life test to evaluate the effects of the additional thermal loading caused by external frosting.

An attempt was made in October 1979 to determine if the rate of temperature rise of the second stage could be increased by increasing the pressure in the life chamber by an order of magnitude (from 1×10^{-6} to 1×10^{-5} torr, as read on the ionization guage). The pressure increase was obtained by throttling the tubing connecting the life test chamber to the main vacuum chamber. Since, when fully open, the pumping speed for this connection was only about 0.15 ℓ/s (which is very small compared to the cryogenic pumping speed of the cold finger for water vapor), this throttling process would have very little effect on the partial pressure of water vapor within the life test chamber. Thus, if the temperature increase was caused by the frosting from water vapor, this experiment would show little or no effect. No effect was observed. This result is consistent with the hypothesis that the frosting of water vapor increases the heat load on the cold finger but does not prove it. This problem will be further discussed in the following chapter, where the results of refrigerator performance in orbit are given.

4. PREFLIGHT PREPARATION, LAUNCH, AND IN-ORBIT PERFORMANCE

HELIUM RECHARGE OF REFRIGERATORS

As discussed earlier, all refrigerators showed helium leak rates that resulted in a pressure loss of about 0.5 psi/month. Since the refrigerators had been delivered to LPARL over a wide interval of time (see Table 2), it was necessary to recharge the refrigerators as close to the launch date as possible. This recharging procedure also provided the only opportunity to measure, over time periods of a year or more, the helium leak rates of the flight model refrigerators and the long-time accuracy of the crankcase pressure transducers and the strain guage pressure measurements.

The method of recharging and the design of the necessary recharging apparatus was a cooperative effort of APL and LPARL (Refs. 10 and 11). LPARL provided the in-house part of the apparatus that could not be easily transported by air (i.e., the vacuum system, cold traps, and helium cylinder). APL constructed the recharging tubing line with its valves, gauges, and interfacing connections. Figure 17 shows the recharging apparatus configuration.

On September 22, 1978, APL assembled the recharging apparatus at LPARL and tested it by recharging the S/N 2 refrigerator, which at that time was the flight spare (Ref. 12). In November 1978, the LPARL experiment, containing the S/N 3, 4, 5, and 6 refrigerators, was returned to LPARL from Ball Brothers (the satellite contractor) for pre-launch rework and final adjustments. On November 28 and 29, APL recharged the refrigerators mounted in the LPARL experiment. The telemetry voltages from the crankcase pressure transducers and strain gauges were measured both before and after recharging the refrigerator. A precision diaphram absolute pressure gauge was used as the reference gauge for all pressure measurements during the recharging process. Tables 6 and 7 show the results of measurements made during the recharging process.

From Table 6, it is seen that the helium leak rate for the refrigerators varied between 0.43 and 0.67 psi/month. Only the crankcase pressure transducer on S/N 3 showed an appreciable error as a function of time. For this unit, a new pressure calibration curve was prepared and left with LPARL. As shown on Table 7 the strain gauge mounted on the helium plenum volume shows an appreci-

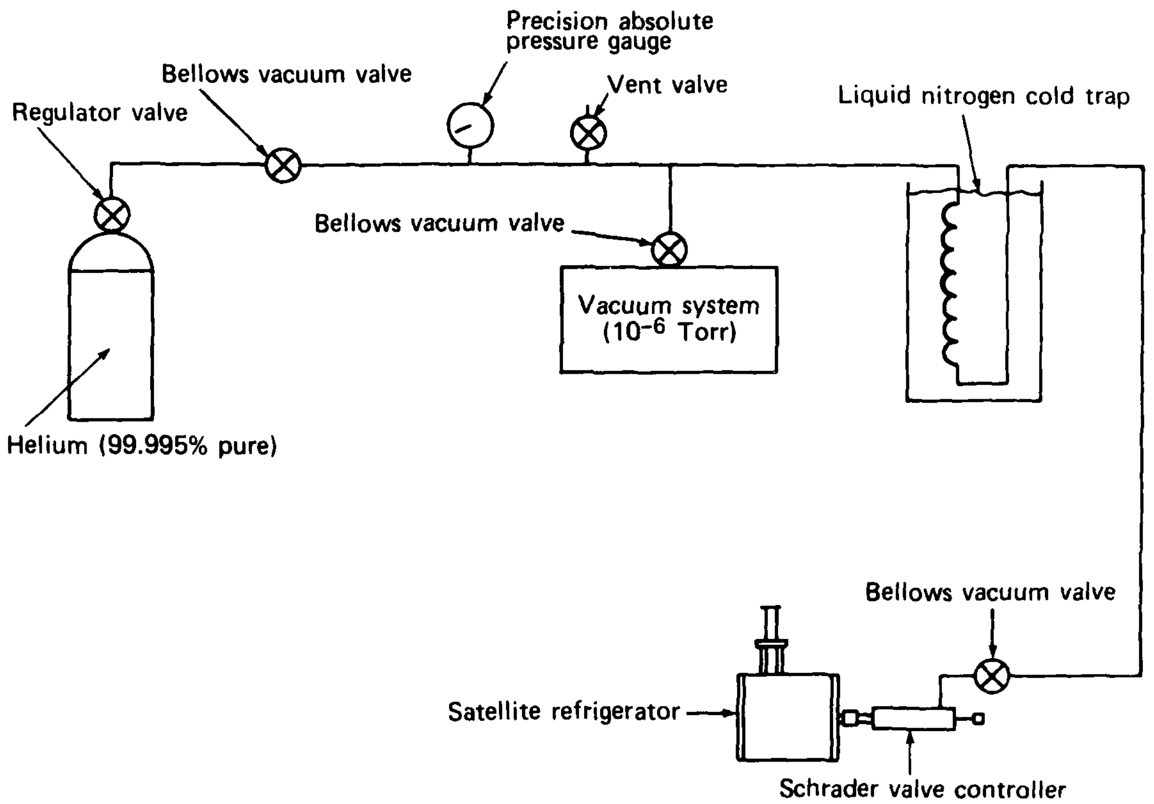

Fig. 17 Satellite refrigerator recharging configuration.

Table 6

Pressures, telemetry voltages, leak rates, and crankcase transducer errors, as measured when refrigerators were recharged.

S/N	Crankcase telemetry (V)	Crankcase pressure* (psia)	Leak Rate psi/month (V/month)	Transducer Error psi/month (V/month)
2	3.79 4.02	68 (C) 71	0.43 (0.032)	0.0 (0.0)
3	1.99 2.30 2.72	60 (C) 64.5 71.5	0.605 (0.036)	0.684 (0.039)
4	3.05 3.33 3.72	58 (C) 64 71.5	0.54 (0.027)	0.00 (0.00)
5	3.37 3.68 4.12	55 (C) 61 71.5	0.59 (0.025)	0.00 (0.00)
6	3.11 3.34 3.65	61 (C) 65.5 71.5	0.67 (0.032)	0.00 (0.00)

*As read on diaphram gauge except (C), which is the computed pre-recharge value.

Table 7

Buffer tank strain gauge errors.

S/N	Telemetry output (V)	Pressure, calibration curve* (psi)	Pressure, actual Nov. 28-29, 1978*	Error (psi)
2	2.40	47	53	6.0
	2.47	49.5	56	6.5
3	2.66	37.5	45	7.5
	2.93	45.5	56.5	11.0
4	1.68	39	43	4.0
	2.31	54.5	56.5	2.5
5	2.64	48.5	40	-8.5
	3.25	64.5	56.5	-8.0
6	3.12	44.5	46	1.5
	3.40	54.5	56.5	2.0

*The strain gauge pressure readings are given in psig since the recharging was performed at atmospheric pressure.

able error when the readings were compared with the original calibration curves. This error could have been caused by the long-time creep of the epoxy bond holding the strain gauge bridge to the steel plenum tank. In any case, this bridge was very sensitive to thermal gradients across the height of the plenum chamber. Since the strain gauges provided a redundant measurement that was difficult to reproduce within 5 to 10%, no attempt was made to generate new calibration curves for this instrumentation. It was adequate to indicate a catastrophic or unusual leak in space.

REPLACEMENT OF S/N 4 REFRIGERATOR WITH S/N 2

On January 2, 1979, APL was informed by LPARL that on the Gamma 003 spectrometer, a sharp rise in pressure had been indicated by the Vacion pump when refrigerator S/N 4 was started at the Ball Brothers facilities. All available information from the test installation at Ball Brothers indicated that the pressure rise in the pumped region of the Gamma 003 spectrometer was caused by a helium leak located above the heat exchange flange on either refrigerator S/N 4 or 5.

On January 6, 1979, Gamma 003 was returned to LPARL. The S/N 4 refrigerator was removed from the spectrometer and the leak tested by LPARL and APL with a Veeco MS helium leak detector. A helium leak was located at the brazed joint between the titanium cold finger and the copper second stage heat exchange flange (Ref. 13).

The flight spare refrigerator S/N 2, had been given a thorough telemetry and starting test by APL the previous day. It was installed in Gamma 003, tested for operation and LPARL started the final vacuum bake-out of Gamma 003 on January 7, 1979, prior to returning the spectrometer to Ball Brothers for final assembly and testing in the satellite.

On January 10, 1979, APL returned the S/N 4 refrigerator to Philips Laboratories for examination and rework. Philips Laboratories located the suspected helium leak in the brazed joint at the top of the cold finger (second stage flange). Phillips disassembled the refrigerator and attempted to rebraze the joint between the cold finger and the second stage flange, at the same time starting the machining of a new cold finger in the event that the brazing was unsuccessful or distorted the original titanium cold finger. The rebrazing was successfully performed and the unit was returned to APL for performance checking. On February 12, 1979, the S/N 4 refrigerator was returned to LPARL to become the flight spare for the launch of the payload, scheduled for the first favorable date after February 18, 1980.

REFRIGERATOR PERFORMANCE IN ORBIT

The P-78-1 satellite containing the DARPA 301 payload was successfully launched into a sun-synchronous polar orbit on February 24, 1979. Two LPARL gamma ray spectrometers were mounted in the DARPA 301 payload; a spectrometer detector connected to two refrigerators is shown in Fig. 18. The second stage of each refrigerator was connected to the thermal conductors leading to the germanium detector by flexible copper braid to minimize the transmission of vibration to the detector. On the LPARL spectrometer, the space above the heat rejection flange was actively pumped by a 2 ℓ/s Vacion pump. A heat shroud thermally connected to the first stage of the refrigerator surrounded the second stage and its thermal connection to the detector. The thermal shroud was designed with a large thermal capacity to retard the warming of the detector when the refrigerator was turned off.

The instrumentation available to measure thermal performance consisted of:

1. The thermal diode mounted in the second stage heat exchange flange by APL.

2. A thermal diode mounted on the base of the first stage heat shroud by LPARL.

3. Two platinum resistance thermometers mounted across the braid connecting the second stage to the detector heat conductors; the difference in temperature of this pair of thermometers was calibrated to read the heat flow across the braid.

4. Current to the Vacion pump was measured to give a measure of pressure within the pumped space above the heat exchange flange.

As Fig. 18 shows, there is no thermal isolation between the paired refrigerators; thus, if one refrigerator is operating the other refrigerator presents an additional heat load. LPARL designates the spectrometers as Gamma 003 and Gamma 004 and numbers the refrigerators as shown in Table 8, which relates the LPARL designation with the APL serial numbers.

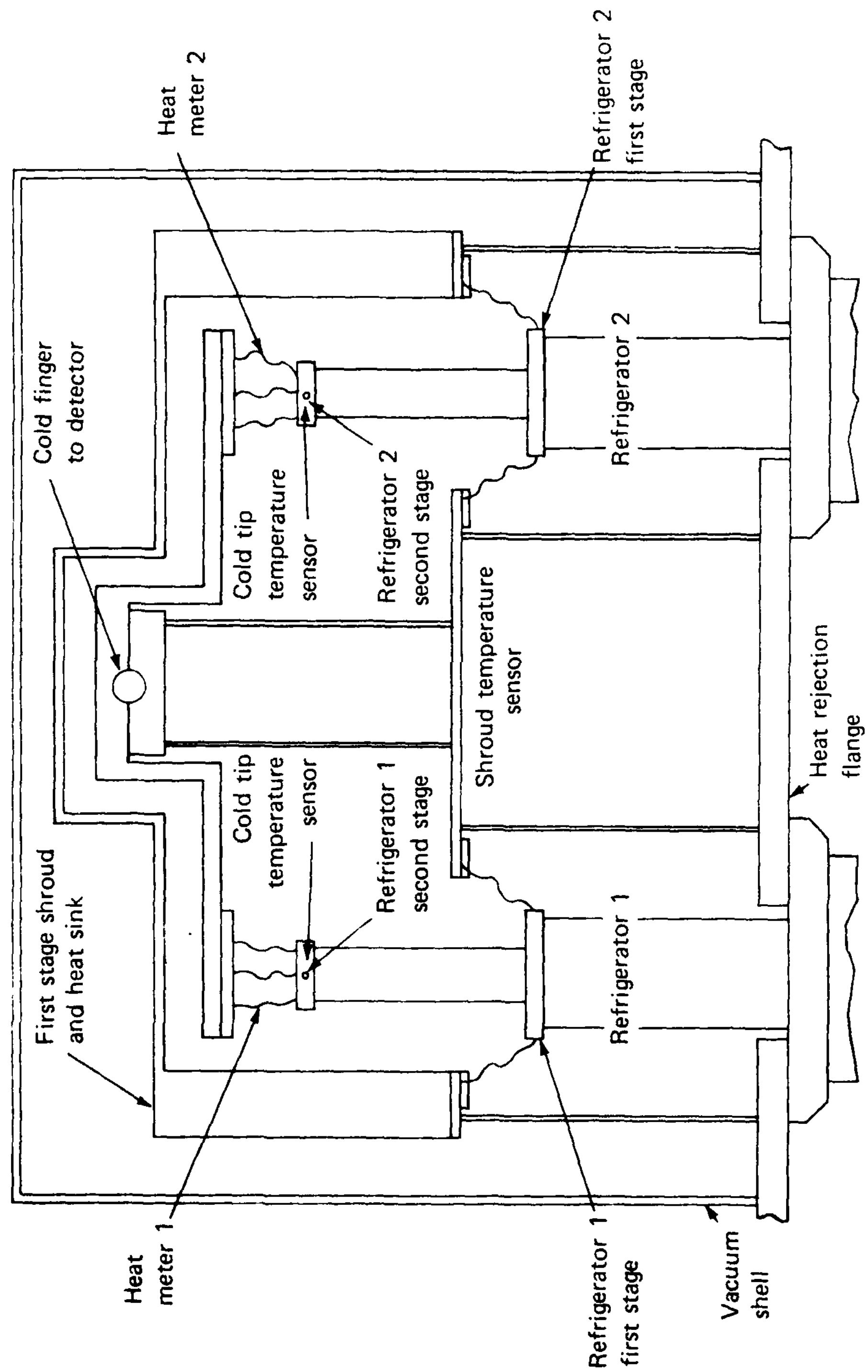

Fig. 18 Thermal connections and sensors in the LPARL gamma ray experiment.

Table 8

LPARL spectrometers and refrigerator numbers.

Spectrometer No.	Refrigerators APL S/N	Refrigerators LPARL No.
Gamma 003	5 2	1 2
Gamma 004	3 6	3 4

Within a few hours after launch, LPARL had started the refrigerators and determined that they operated satisfactorily. The following information on orbit performance has been supplied by LPARL, which has access to the telemetry information as it is acquired by the Air Force (Refs. 14 and 15).

Following launch, it was found that refrigerator telemetry signals were as expected with the following exceptions (all refrigerator numbers are APL S/N).

1. The crankcase pressure transducer and plenum chamber pressure strain gauge both read low on refrigerator S/N 6. On February 26, the telemetry reading indicated a pressure of about 42 psia in this unit. From the agreement of the pressure transducer and strain gauge data and the performance of the unit as determined later, the helium loss was real. Since the loss of helium in this unit was normal (about 0.7 lb/month) when the refrigerators were recharged in late November 1979, the logical explanation for this greatly increased rate of helium loss is that either the crankcase refill valve was not properly sealed following refill or that some leak developed in the crankcase between refill and launch. LPARL telemetry data on the launch pad revealed that the helium pressure in this unit was low before launch.

2. The second stage temperature diode telemetry readout on refrigerator S/N 3 was inoperative for unknown reasons. Thus, all second stage temperature on Gamma 004 must be inferred from the telemetry readout of the refrigerator S/N 6 temperature diode.

3. The LPARL heat load measurement on Gamma 004 was inoperative.

There was no way to directly measure the temperature of the germanium detector; from LPARL laboratory tests in a mockup, it was estimated that the detector temperature was about 8K higher than the measured temperature of the second stage diode.

The method of refrigerator operation in space was dictated by the requirements of the LPARL experiment and the power budget of the satellite (which included many other experiments). After satisfactory performance of the gamma ray experiment had been determined, LPARL began a long run on Gamma 003 cooled by refrigerator S/N 2 and Gamma 004 cooled by refrigerator S/N 3. Because of the power limitations of the satellite, initial operation consisted of operating the refrigerators for about seven orbits (about 11 hours) and turning them off for one orbit. Typical second stage refrigerator temperatures as a funtion of time after nine days in orbit are shown in Fig. 19. The temperature rise when the refrigerators were turned off is evident and it is observed that the temperature on Gamma 004 is lower than on Gamma 003. Irregularities on the time scale are caused by the location or availability of injection stations as the satellite circled the earth.

For spectrometer Gamma 003, this method of operation was continued for 78 days (1198 orbits). At that time, LPARL began a series of tests in which they allowed the experiment to warm to temperatures of about 170K and finally, after 98 days in orbit, to 276K (satellite ambient temperature). This warming resulted in so large an increase in pressure within the spectrometer pumped vacuum space that it was necessary to blow the squib, which exposed this volume to space vacuum. Thereafter, this unit was operated exposed to space vacuum through the venting port and with the Vacion pump operating.

The operation of the refrigerator on Gamma 003 for the first 250 days in orbit is shown in Fig. 20, where the periods of operation of the refrigerator (in the manner of Fig. 19), the shroud temperature (which is cooled by the first stage of the refrigerators), and the second stage temperature of refrigerator S/N 2 are plotted. Figure 20 is somewhat simplified in that some starts and turn-offs that LPARL conducted for experimental reasons are omitted in order to more clearly present the general trends in performance.

From the data, refrigerator S/N 2 had warmed from 85 to 121K in 98 days of operation, a rate of rise of about 0.38K/day (about 1/3 of that observed under laboratory conditions). Warming the refrigerator cold finger to the satellite ambient temperature for a period of days did not significantly improve performance when

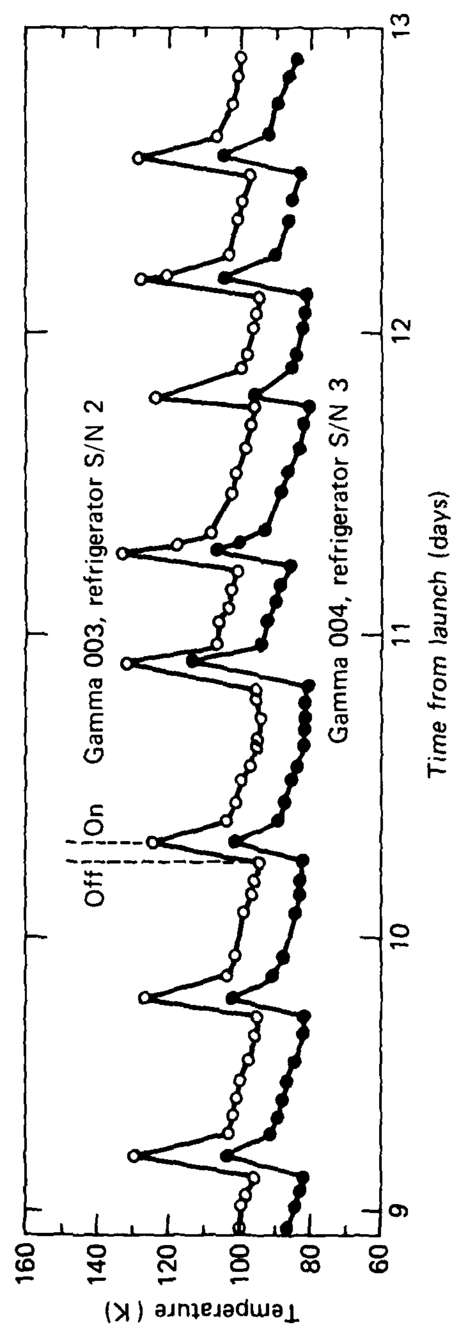

Fig. 19 Flight refrigerator second stage temperature versus time.

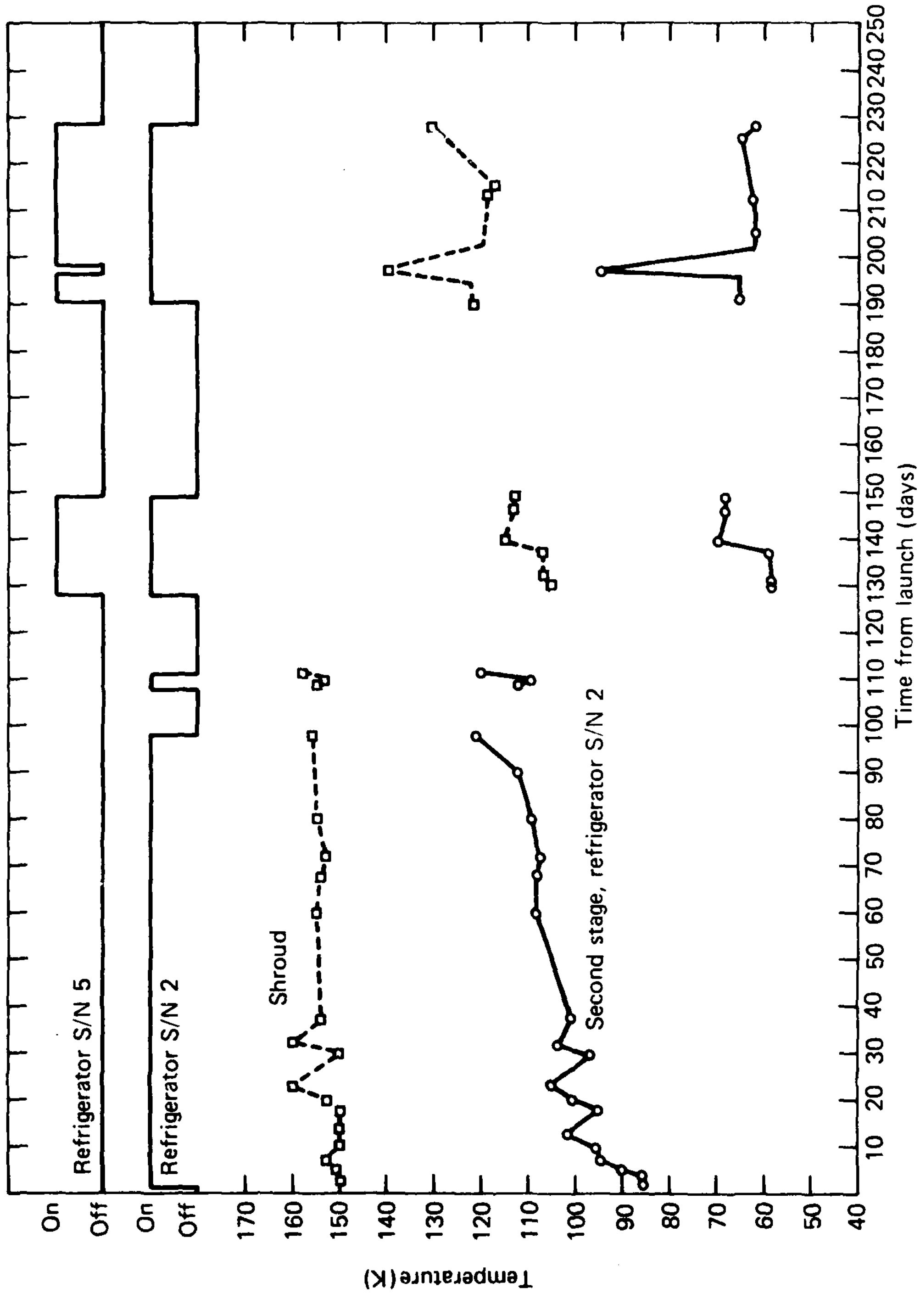

Fig. 20 Gamma 003 experiment temperature versus time.

the refrigerator was restarted, which is contrary to laboratory experience. When both refrigerators S/N 2 and 5 were started after 129 days in orbit, the second stage temperature dropped to between 60 and 70K (the data for refrigerator S/N 5 are not shown, but are essentially identical). This temperature was low enough to assure LPARL that any degradation of detector resolution was caused by factors other than a sufficiently low temperature on the detector.

The performance of the refrigerator on Gamma 004 are plotted in Fig. 21 for the first 220 days in orbit. On the refrigerator second stage, the temperature rose from 67K to 118K in 119 days (a rate of increase of about 0.42K/day). When refrigerator S/N 6 was turned on after 119 days, some decrease was observed, but since this latter unit was rapidly losing helium, the effect was not great. After the cold finger was warmed to ambient temperature, significant improvement was observed with both refrigerators operating. For Gamma 004, it was not necessary to blow the squib venting the pumped vacuum region to outer space when the refrigerators were warmed to ambient satellite temperature; this difference is consistent with LPARL pre-launch data, which always indicated a better vacuum on Gamma 004.

Ground measurements by LPARL measured the total heat on the second stage of one operating refrigerator to be 0.345 W, of which 0.114 W was the germanium detector and 0.231 W was the parasitic load provided by the idle refrigerator. In orbit, the heat load measured by the LPARL heat meter on Gamma 003 (no measurements were available for Gamma 004) were initially 0.6 W, of which about 0.4 W was provided by the detector. From the performance map of Fig. 4 and similar data taken by LPARL (Ref. 15) this increase in heat load would more than explain the high initial temperature observed in Gamma 003 at the beginning of its operation in space. Following the warm-up after 98 days of operation, the measured heat was somewhat reduced (at times as low as 0.5 W), but all heat load measurements on Gamma 003 have been well in excess of the 0.345 W of the pre-launch ground measurements.

Prior to launch, LPARL maintained the first stage of the refrigerators at near liquid nitrogen temperature (77K) and since this cooling continued for over a week, there is no question that both Gamma 003 and Gamma 004 entered space with contaminants frozen-out on the cold finger-detector assemblies. The history in orbit supports the belief that Gamma 003, with the inferior vacuum region, shows the effects of greater contamination.

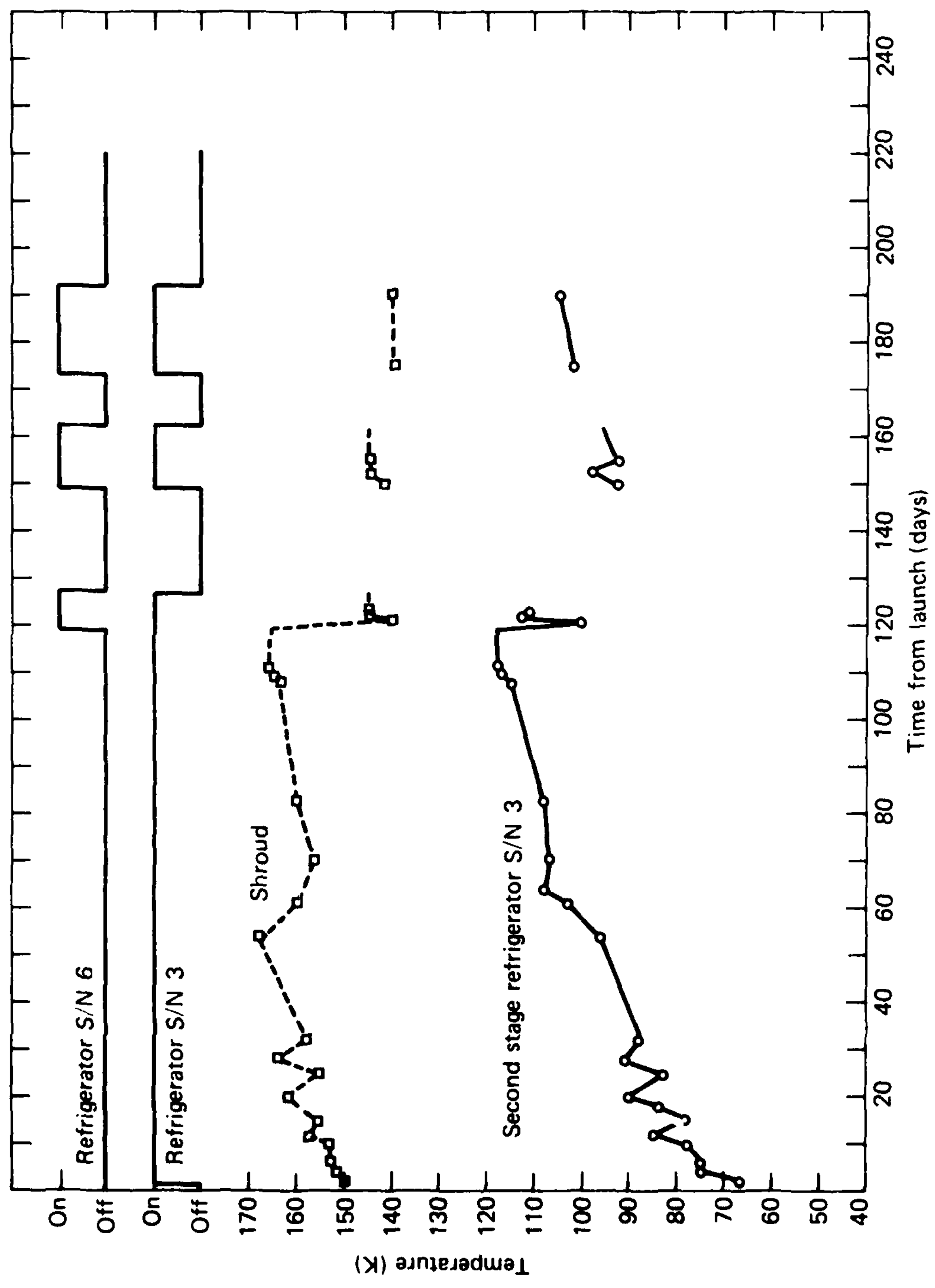

Fig. 21 Gamma 004 experiment temperature versus time.

Reference 15 reports the results of refrigerator performance for the first 400 days in orbit. At the end of this period, the accumulated hours of operation for the refrigerators were as follows:

Gamma 003	S/N 5	2657 hours
	S/N 2	5134 hours
Gamma 004	S/N 3	7442 hours
	S/N 6	4458 hours

As Figs. 20 and 21 indicate, after the first 150 days of operation only one spectrometer (using both its refrigerators) was operated at any given time. For example, on the 360th day in orbit, Gamma 003 was operating with both S/N 5 and 2 running, with a second stage temperature of about 120°K.

In March 1980, LPARL began operating refrigerators S/N 3 and 6 on Gamma 004 continuously; i.e., the refrigerators were not stopped and restarted as shown in Fig. 19. This method of operation was continued satisfactorily through August 1980, and as of that date, LPARL intended to continue the experiment (Ref. 16). As of August 27, 1980, the second stage temperature was still low enough (120K) to insure maximum resolution of the germanium gamma ray detector. Thus, after 551 days in orbit, LPARL was still obtaining useful gamma ray spectral data. The rate of temperature rise, with the refrigerators operating continuously is apparently significantly less than for the intermittent operation of the refrigerators during the first year in orbit. However, LPARL has not made available detailed performance data of the type available in Ref. 15 for the period after March 1980.

The choice of Gamma 004 for the continuous operation experiment was made because it draws slightly less power than does Gamma 003. This lower power consumption is caused by the low helium pressure in refrigerator S/N 6. At the end of the 400 days of operation, the pressure in refrigerator S/N 6 was about 15 psia. At this pressure, the refrigerator can provide little cooling capacity, but when operating it (to some extent) reduces the heat load on the S/N 3 refrigerator. The remaining three refrigerators maintained pressure, after 400 days in orbit, of 61 psia or more, in reasonable agreement with the results expected from Table 6. This pressure decrease would result in a second stage temperature increase of about 25K for the standard load conditions of Table 4. As mentioned above, no heat load information is available for Gamma 004 in orbit, but there is no reason to suppose it differs from ground test results. As Ref. 15 states, the long-time

degradation in refrigerator performance can, for the most part, be attributed to the loss of helium pressure within the refrigerators.

Gamma 003, whose two refrigerators have maintained their helium pressures as expected, may possess useful life after Gamma 004 becomes inoperative. However, because of the lower power consumption of Gamma 004 and because it is a spectrometer with better resolution, as of late August 1980 LPARL planned to continue operation of that spectrometer as long as possible.

5. CONCLUSIONS

The data from measurements of the refrigerator performance in orbital flight and the laboratory life test confirm the conclusion that the objectives of the Satellite Refrigerator Program have been met. The evolution of the final design of the flight model units was a tedious process, but as of late September 1980, over 18 months of successful operation has been achieved and the only known factor that will limit the time of operation is the loss of helium pressure. While mechanical refrigerators have not enjoyed a good reputation for reliablility (prior to the launch of the LPARL experiment on the P-78-1 satellite no record of successful operation for periods longer than a few weeks is known), the APL refrigerators clearly demonstrate that the mechanical design of these units (discussed in detail in Appendix I) is satisfactory.

Reference 17 discussed several uncertainties in the factors affecting refrigerator performances and suggested several possible design improvements. Results of orbital flight experience suggest slight modifications in the pre-flight conclusions of Ref. 17 and those are included in the enumerated conclusions and recommendations below:

1. No problem has been experienced in starting the refrigerators in space. Hundreds of starts have been made in the LPARL space experiment. The only precaution that has been taken is that no given refrigerator is allowed to stand idle for periods exceeding one month.

2. Thermal performance has been as expected within the uncertainties of the thermal load on the refrigerators.

3. The flexibility of operation possible with refrigerators has permitted LPARL to warm the intrinsic germanium detectors and free them of any substances cold-trapped on the surface. This flexibility is only of use for detectors that can be warmed, but for such detectors and surfaces, the mechanical refrigerator, in contrast to liquid or solid cryogens, permits the removal of materials that freeze-out on cryogenic surfaces.

4. The use of two refrigerators on each detector has made it possible to cool the detectors, when desired, to a

temperature well below that which would cause degradation in performance. Thus, for gamma ray detectors, the possibility exists for determining the effects of radiation damage and surface contamination.

5. The relative importance of the internal and external cold trapping of impurities has not been clearly established. In the APL life test of S/N 1, it was established that the rate of performance degradation was dependent on the purity of the refrigerator helium charge. But it is not clear to what extent the Philips improved charging procedures eliminated the problem. The long-time temperature degradation in orbit is less than measured on the APL laboratory tests. This improvement in performance could be a consequence of a better vacuum about the cold finger and detector achieved by the LPARL experiment in space. As Ref. 17 points out, the obvious method for maintaining a high purity of helium gas in the cold-producing region of the refrigerator is to isolate that region by bellows as originally designed into these refrigerators. The fact that Philips never obtained bellows without a high probability of early failure and that the orbital performance has satisfied the requirements of the experiment justify the decision to omit the bellows from the flight model refrigerators. The possibility exists that refrigerator performance would be improved if reliable bellows could be obtained.

6. Both the laboratory life tests and the orbital performance show that the principal contribution to the degradation in performance is the loss of helium pressure. This rate of helium loss (about 0.5 psi/month) could be eliminated by a redesign of the crankcase and the end plate gas seals. Replacing the Viton seals with metal gaskets, the magnesium crankcase housing with stainless steel, or (for a proven design that did not require disassembly during the testing and acceptance period) welding the end plates to the crankcase would eliminate the helium loss problem.

The results of the LPARL gamma ray experiment are not the subject of this paper. However, as Ref. 14 reports, at the beginning of the orbital experiements, the resolution of Gamma 004 and Gamma 003 was 2.7 and 4 keV, respectively, at the 511 keV annihilation line. After several months of orbital operation, the

resolution degraded but LPARL was able to cool the detectors sufficiently to assure that the degradation was not caused by temperature increases of the detector. Resolution was still much better than that obtained from a conventional cesium iodide crystal. It is reasonable to assume that LPARL has collected an amount of gamma ray data with high resolution that is unprecedented.

ACKNOWLEDGMENTS

The APL satellite refrigerator program was funded by the Nuclear Monitoring Research Office of the Defense Advanced Research Projects Agency. The cooperation, support, and understanding of COL G. V. Bulin of that office was always helpful. Many persons in several groups at APL contributed to this program, of whom only a few are mentioned here. Dr. J. W. Follin gave guidance on many difficult technical problems; C. A. Wingate performed the original thermal studies that led to the choice and design features of the Stirling cycle refrigerator, and designed and actively contributed to the APL test program; Gary Keys designed the electronics and Henry Lee performed the bench testing and trimming of the APL electronics box. The Environmental Test Laboratory provided and maintained much of the laboratory test equipment. The excellent cooperation of Philips Laboratories and the Lockheed Palo Alto Research Laboratory throughout all phases of the program is gratefully acknowledged.

REFERENCES

1. T. C. Nast and D. O. Murry, "Orbital Cryogenic Cooling of Sensor Systems," AIAA Paper No. 76-979, American Institute of Aeronautics and Astronautics, New York, NY.

2. G. H. Nakano, W. L. Imhof, and R. G. Johnson, "A Satellite-Borne High Resolution Ge (Li) Gamma-Ray Spectrometer System," IEEE Trans. Nucl. Sci , Vol. NS-21, 1974.

3. C. S. Leffel, Jr., "Starting Current of the Cryogenic Refrigerator Under Stalled Conditions," JHU/APL QM-79-014, 25 Jan 1979.

4. C. S. Leffel, Jr., "Performance of the Serial No. 1 Cryogenic Refrigerator, April 30, 1975 to March 12, 1976," JHU/APL QM-76-041, 14 Apr 1976.

5. C. S. Leffel, Jr., "Performance of the Serial No. 1 Cyrogenic Refrigerator, March 18, 1976 to November 3, 1976," JHU/APL QM-76-144, 22 Nov 1976.

6. C. S. Leffel, Jr., "Completion of the Life Test of the Serial No. 1 Satellite Refrigerator," JHU/APL QM-78-172, 9 Aug 1978.

7. E. Lindale, "Results of Examination of Engineering-Model Refrigerator (S/N 1) After One Year of Maintenance-Free Operation," PL-45-GR78-0725, Philips Laboratories, Briarcliff Manor, NY.

8. A. Guthrie, Vacuum Technology, John Wiley and Sons, New York, 1963.

9. R. P. Caren, A. S. Gilcrest, and C. A. Zierman, "Thermal Absorptances of Cryodeposits for Solar and 290°K Blackbody Sources," Advances in Cryogenic Engineering, Vol. 9, Plenum Press, 1963.

10. "Trip to LPARL on September 28 and 29, 1977," JHU/APL, QM-77-127, 6 Oct 1977.

11. "Discussing Recharging," JHU/APL CQO 2152, 24 Feb 1978.

12. "Recharging the Flight Model Satellite Refrigerators at LPARL, Nov. 27-Nov. 30, 1978," JHU/APL QM-78-256, 11 Dec 1978.

13. "Visit to LPARL from January 5 through January 8, 1979," JHU/APL QM-79-006, 18 Jan 1979.

14. "DARPA 301 Program Review, August 1, 1979 at Lockheed Palo Alto Research Laboratory," JHU/APL QM-79-199, 17 Aug 1979.

15. L. G. Naes and T. C. Nast, "Long Life Orbital Performance of Stirling Cycle Mechanical Refrigerators," Eighth International Cryogenic Engineering Conference, 3-6 June 1980, Genova, Italy.

16. Dr. William Imhof, Private Communication, Lockheed Palo Alto Research Laboratory, Palo Alto, Calif.

17. C. A. Wingate and C. S. Leffel, "An Ultra Reliable Miniature Cryogenic Refrigerator," Seventh International Cryogenic Engineering Conference, London, England, 1978.

APPENDIX I

Appendix I, on the following pages, is a reproduction of the final report on the Stirling cycle refrigerators that was prepared by Philips Laboratories.

PL-42-CR78-0713

Appendix

FINAL REPORT

STIRLING CYCLE REFRIGERATORS FOR GAMMA-RAY DETECTOR

by

Eric Lindale

Prepared for

The Johns Hopkins University
Applied Physics Laboratory
Laurel, Maryland 20810

APL Contract No. 372284

Prepared by

PHILIPS LABORATORIES
A Division of North American Philips Corporation
Briarcliff Manor, New York 10510

July 1978

FINAL REPORT

STIRLING CYCLE REFRIGERATORS FOR GAMMA-RAY DETECTOR

by

Eric Lindale

Prepared for

The Johns Hopkins University
Applied Physics Laboratory
Laurel, Maryland 20810

APL Contract No. 372284

Prepared by

PHILIPS LABORATORIES
A Division of North American Philips Corporation
Briarcliff Manor, New York 10510

July 1978

SUMMARY

Six long-life, low-power, miniature Stirling cycle cryogenic refrigerators for cooling a gamma-ray detector in a satellite experiment were designed, fabricated, tested, and delivered. Each refrigerator is capable of simultaneously producing two temperatures of 140° —> 170°K on the 1st stage and 77 —> 90°K on the 2nd stage, with heat loads of 1.5 W and 0.3 W, respectively. Total input electrical power for each refrigerator is less than 30 W. The bodily displacement of the cold finger with the refrigerator running was restricted to a maximum of 0.0004" in any direction. This result was achieved by the unique balancing capabilities of the rhombic drive. The control circuitry provides three operating speeds. The total weight of the refrigerator is 15.8 lbs, which includes 4 lbs of electronic hardware. The dimensions of the refrigerator are 12.08" x 7.1" x 6.05". Flexible metal bellows intended for separating the buffer and working volumes proved to be of questionable reliability and were therefore not used. Based on over 7000 hours of maintenance-free testing of the engineering model, a life expectancy of 8000 hours is anticipated.

FOREWORD

The cryogenic refrigerators described in this final report were designed and fabricated at Philips Laboratories, a Division of North American Philips Corporation, Briarcliff Manor, New York under the supervision of Mr. Alexander Daniels, Director, Mechanical Research Systems Research Group. The Project Leader was Mr. Charles Balas; Mr. Balas also contributed to the writing of this report. Dr. Richard C. Sweet, Supervisor, Heat Processing Laboratory, was instrumental in fabrication of the cold finger and piston-rod assembly. Mr. Bruno Smits, Chief Designer, aided in the hardware design. Fabrication was supervised by Mr. George Potanovic, Assistant Foreman, Instrument Shop. Mr. Eric Lindale performed the refrigerator testing and assisted in the development.

This contract from The Johns Hopkins University, Applied Physics Laboratory, was for cryogenic refrigerators for a satellite experiment to be conducted by Lockheed Palo Alto Research Laboratories and sponsored by the Defense Advanced Research Projects Agency (DARPA). Lt. Col. George V. Bulin was the DARPA Program Manager.

This final report covers the work performed between April 1, 1973 and September 30, 1977.

TABLE OF CONTENTS

TABLE OF CONTENTS (Cont'd)

LIST OF ILLUSTRATIONS

LIST OF ILLUSTRATIONS (Cont'd)

1. INTRODUCTION

The Stirling cycle is well known as a means of providing refrigeration at cryogenic temperatures. The high thermodynamic efficiencies attained with this cycle have made it desirable for many applications. Efforts to significantly improve the operating characteristics of the Stirling refrigerator without forfeiting its high efficiency were initiated with this program, i.e., extend life expectancy, increase reliability, and reduce vibration.

The goal of this program was to design, fabricate, test and deliver, six long-life, low-power, miniature rhombic-drive Stirling-cycle cryogenic refrigerators. Four of the refrigerators will be used for cooling a gamma ray detector in a satellite experiment; one will be a spare; the other was life-tested at Johns Hopkins University, Applied Physics Laboratory, Maryland.

Final design parameters were derived by the use of an existing rhombic-drive Stirling refrigerator. Evaluation of individual components was made using both the existing rhombic-drive refrigerator and a conventional crank-throw refrigerator.

The basic theory of the Stirling cycle refrigerator is given in Appendix A. Other Philips advances incorporated in the refrigerator, viz., the efficient double-expansion process and the vibration-free rhombic drive, are described in Appendices B and C, respectively.

2. DESCRIPTION OF REFRIGERATOR

The refrigerator (see Fig. 1) is a two-stage Stirling cycle machine charged with helium to 70 lb/in^2 abs. Two temperatures are simultaneously produced - one for cooling a gamma-ray detector (not shown) mounted on the second stage flange of the cold finger, and one for cooling a radiation shield (not shown) coupled to the first stage (see Fig. 2).

The radiation shield extends from the first stage flange to a point above the detector location. A heat exchanger flange at the base of the cold finger provides location for a heat conduction plate (not shown). Heat is rejected from the flange at a temperature of 30° -> 113°F during operation. The refrigerator is designed to operate maintenance-free for a minimum of one year, running continually or intermittently. Three operating speeds are available: 800 rpm for standby, 1000 rpm for normal operation, and 1180 rpm for a more rapid cooldown and a lower temperature output.

The refrigerator is driven by two permanent-magnet, brushless dc motors mounted in parallel and counter rotating within the crankcase. Both motors are synchronized to deliver equal power to the dual crankshafts of a Philips rhombic drive (see App. C). This drive is designed to allow a theoretically perfect dynamic balance of the reciprocating parts. The actual dynamic balance is restricted only by the limits of the dynamic balancing equipment used.

The total power input is less than 30 W with two outputs of refrigeration of 0.3 W at 77° -> 90°K and 1.5 W at 140° -> 170°K. The net vibration at the top of the cold finger in any direction is less than 0.00032". The refrigerator weighs 15.8 lbs; this includes 4 lbs for an electronic control package mounted on the crankcase. The overall dimensions of the refrigerator are 6.05" x 7.1" x 12.08".

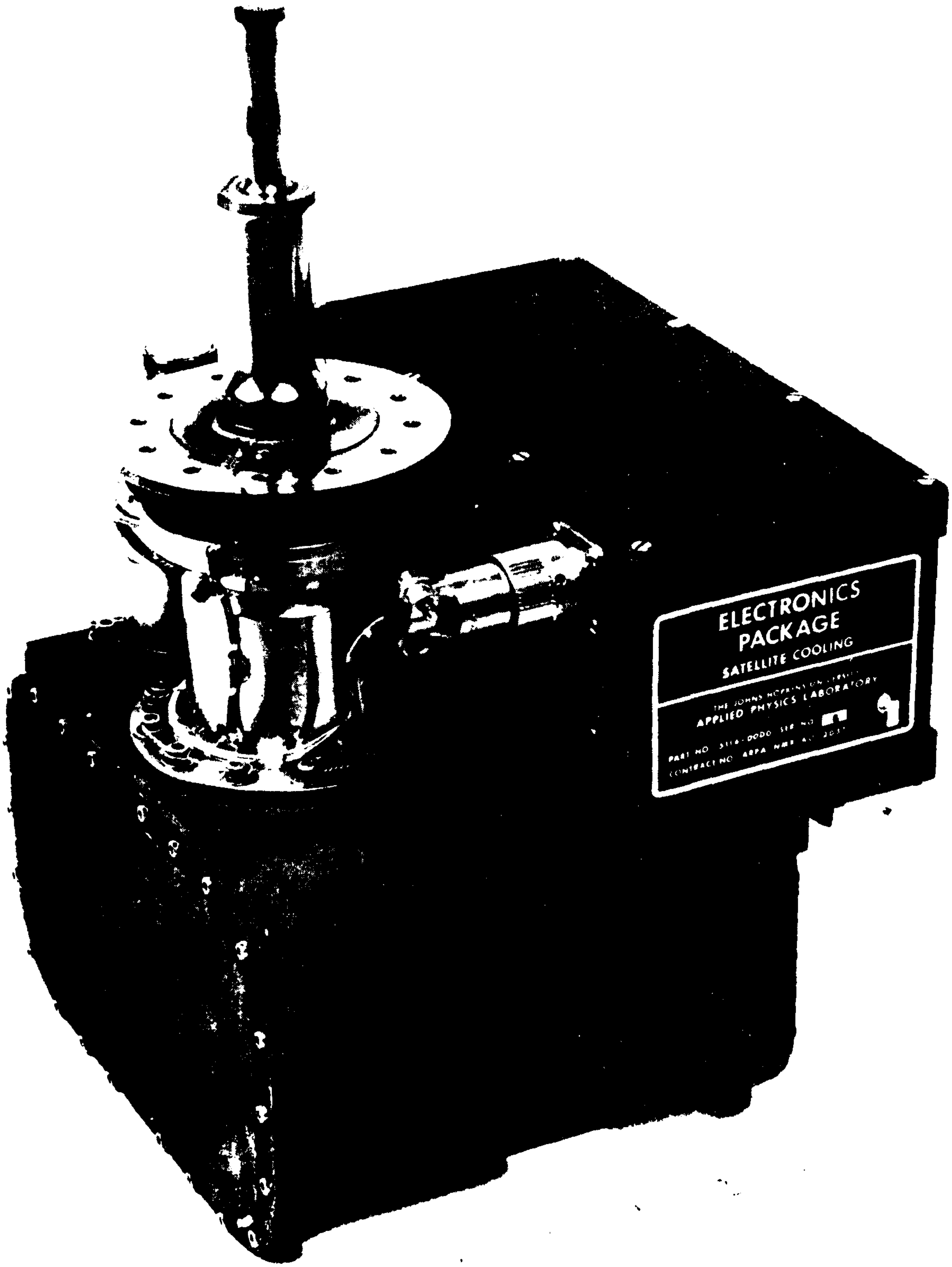
ELECTRONICS
PACKAGE
SATELLITE COOLING
APPLIED PHYSICS LABORATORY

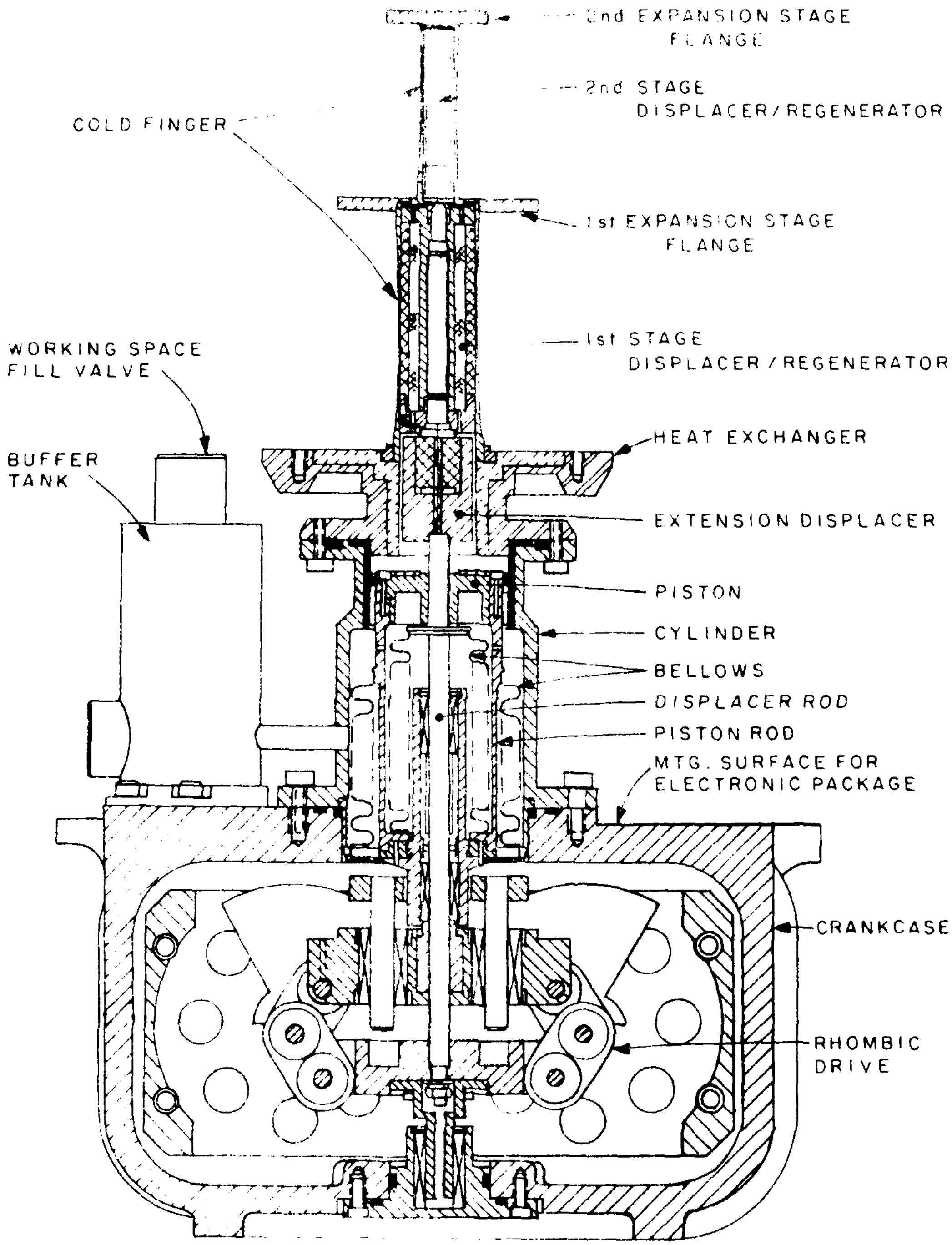

Figure 2: Sectional view of refrigerator.

3. DESIGN APPROACH

3.1 General

The basic approach to the design of this refrigerator was to conduct thermodynamic and mechanical analytical studies to optimize all parameters. An existing rhombic-drive Stirling-cycle refrigerator was modified and used as a test machine for evaluating design changes. A second Stirling cycle refrigerator with a conventional crank-throw drive was used to evaluate those component parts that would have to be optimized.

The major design trade-offs considered were:

- Refrigeration produced versus design variables such as: charge pressure, pressure ratio, displacer stroke, mass and specific heat of cold parts, overall structure of the regenerators and cold finger, and overall efficiency of the refrigerator.
- Vibration of the cold finger due to cyclic pressure variations of the working gas versus heat transfer losses due to conduction along the cold finger and versus charge pressure which influences both cycle efficiency and bearing life.
- Size and weight versus efficiency.

In addition, the following design areas were investigated:

- Efficiency. All components of the test refrigerator were analyzed to optimize overall efficiency.
- Life and Reliability. Performance and component failure data from the existing refrigerators were reviewed. Existing refrigerator components that had failed or contributed towards failures were either redesigned or replaced, i.e., bearings, seals, piston rings, drive motors.
- Refrigeration. Increase the thermodynamic efficiency by reducing friction losses; minimize the heat capacity of the cold parts without allowing pressure-induced vibration of the cold finger; reduce gas pressure losses past working seals to increase compression.
- Contamination. Evaluate flexible metal bellows to isolate contamination from the working volume.

3.2 Prototype Investigation

3.2.1 Test Effort

The in-house rhombic-drive refrigerator was originally constructed for analytical studies. By modifying the cold finger and regenerators to simulate the flight model cooler, an indication of component reliability was established.

Testing was conducted to determine as many ways as possible of increasing efficiency and subsequently extending life expectancy. The focal points of the tests were the evaluation of piston and displacer seals, low vapor-pressure grease, low heat-conducting materials, flexible metal bellows, and performance.

Obviously the time required to test all these items using a single unit would be extensive; therefore, various tests were conducted simultaneously. By combining the performance testing with the grease evaluation and the displacer seal test (using the in-house cooler), some freedom was gained to permit testing of other components by other means.

The piston ring test was performed with an existing compressor unit having a conventional crank-throw drive. A duplicate of the flight-model drive mechanism was constructed to act as a bellows tester. An experimental setup was constructed to determine the thermal conductance between the heat rejection flange and the two expansion stages of the finger. Tests were performed to verify the analytical prediction of the effective thermal conductivity of the 1st and 2nd stages of the cooler cold section. The tests were terminated after it was shown that the predicted and true conductance values both lay in a band less than ± 20% wide.

3.2.2 Performance of In-house Cooler

[illegible] the first flight model was still being fabricated during [illegible]nt testing, some estimates were used where specific

values were unknown. The size and weight of the flight model is slightly greater than the design goal, but, as a result, the efficiency is considerably higher.

The higher speed of 1000 rpm was selected over the original 600 rpm because the cooler performance is less sensitive to small variations in the quality of the dynamic sealing. Therefore, at 1000 rpm a more reliable cooler and a more stable performance is obtained.

The characteristics of the in-house cooler and the specifications of the flight model are given in Table 1. The thermal performance results given in Table 2 are for bench operation of the in-house cooler. Table 1 shows the temperature range of the in-house cooler for the heat rejection temperatures shown. The performance temperature range is also influenced by wear of the dynamic seals of the piston and displacers and possibly by the effect of debris collecting on the seals (causing improper seating). Further variation in performance includes the effects of small pertubations in charge pressure and the addition of a radiation shield coupled to the 1st expansion stage and partially covering the 2nd expansion stage.

Table 2 shows the best room-temperature, bench performance of the in-house cooler. The dynamic seals were optimized and properly seated. With no degradation, this is the best performance to be expected from the flight-model cooler. Performance at two off-design points are also shown, and there is close correlation with the off-design performance previously predicted in the performance maps for 500 and 700 rpm (600 rpm being the previous design speed). It should be noted that with the radiation shield coupled to the 1st expansion stage, the heat load on that stage is slightly greater than that indicated. The additional loading on both stages due to thermocouple and heater leads, although quite low, is also not included in the tables. Neither the cold end nor the vacuum dewar around it are gold plated, and both emissivities are considerably greater

TABLE 1: COMPARISON OF FLIGHT MODEL SPECIFICATIONS AND IN-HOUSE COOLER CHARACTERISTICS.

Item	Flight Model Specifications	In-House Cooler Characteristics
Size	12.6" x 6.5" x 6.5"	12.08" x 7.10" x 6.05"
Weight	Minimize with a goal of 10 lbs.	Est. 12 lbs.
Operating Speed	--	1000 RPM design speed with the option to operate in the range of approx. ± 300 RPM
Working Gas	Helium	Helium
Charge Pressure	--	4.7 - 5.2 atm abs depending upon performance desired
Thermal Performance	2nd expansion stage <90°K with 0.3W heat load and simultaneously the 1st expansion stage @ 140→170°K with 1.5W heat load	2nd stage 60→88°K 1st stage 138→156°K
Input Power	Minimized but <30W with a voltage variation between 24→30 V DC	approx. 19.5→24.6W
Life	8,000 hrs.	Designed to meet spec.
Ambient Pressure	Atmospheric to vac of 10^{-5} torr or less	Designed to meet spec.
Ambient Temperature	30°F→113°F with storage at -22°F→113°F	Designed to meet spec.

TABLE 1: COMPARISON OF FLIGHT MODEL SPECIFICATIONS AND IN-HOUSE COOLER CHARACTERISTICS. (Cont'd)

Item	Flight Model Specifications	In-House Cooler Characteristics
Heat rejection	Conduction to two structural mounts at $30 \rightarrow 113^{o}F$	Designed to meet spec.
Expansion cylinder emissivity	$< .03$	Designed to meet spec.
Vibration environment	As per APL Spec. 545-73-008	Designed to meet spec.
EMI	No spec., but reduce to as low a value as practical	APL will measure. Cooler design allows for shielding.
Residual torque	$< .01$ in.oz.	Expect $<< .01$ in.oz.
Cooler Vibration	$< .0064$ in.peak to peak in any direction with cooler freely floating	Expect to better. APL will measure.

TABLE 2: OPTIMUM ROOM-TEMPERATURE PERFORMANCE OF IN-HOUSE COOLER AT THREE OPERATING SPEEDS, WITH DESIGN AND REDUCED CHARGE PRESSURE, AND WITH AND WITHOUT A RADIATION SHIELD COUPLED TO THE 1ST EXPANSION STAGE.

Speed RPM	Charge Pressure psig	2nd Expansion Stage Temp °K	2nd Expansion Stage Load W	1st Expansion Stage Temp °K	1st Expansion Stage Load W	Estimated power for flight model W	Radiation Shield
1000	54	73	.3	145	1.5	20	No
"	62	71	.3	138	1.5	23	No
"	55	73	.3	150	1.5	19.5	Yes
"	62	60	.3	140	1.5	22.5	Yes
800	55	83	.3	121	.45	18	No
"	62	77	.3	118	.45	19	No
"	55	76	.3	130	.45	17	Yes
"	62	73	.3	128	.45	18.5	Yes
1200	54	67	.3	126	1.0	26.5	No
"	62	64	.3	119	1.0	30	No
"	54	61	.3	130	1.0	26	Yes
"	62	59	.3	131	1.0	28	Yes

than those expected for the flight-model cooler. The resulting radiation heat-load on the cold end of the cooler is also not included. Since these additional loads are not included in Tables 1 and 2, the reported thermal performance values are conservative.

3.2.3 Bench Tests

Figure 3 illustrates the bench setup for the in-house cooler tests. The instrumentation and equipment used were:

- dc ammeter and voltmeter to measure voltage and current to drive motors.
- Semiconductor pressure transducer to monitor working gas pressure.
- dc power supply with ammeter and voltmeter for transducer bridge excitation.
- Storage oscilloscope to observe working-gas pressure wave from transducer.
- Stroboscope-tachometer to measure speed.
- Two sets of dc power supplies, voltmeters and ammeters to measure voltage and current to the two electric heaters on the expansion stages of the cold end.
- Two chromel alumel thermocouples soldered to the two expansion stages of the cold end.
- Ice point reference to create a fixed-temperature, reference junction for the thermocouples.
- Millivolt potentiometer to measure thermocouple emf.
- Vacuum station to evacuate dewar surrounding cold finger.
- Fan to cool heat exchanger when temperature of heat exchanger exceeds 113°F.

Figure 3: Bench setup for testing in-house cooler.

3.2.4 Test Procedure

The test procedure for the in-house cooler is described in the following paragraphs:

The thermocouples were calibrated at 77°K by removing the cold finger from the cooler and filling the finger with liquid nitrogen (the dewar covering the outside of the finger is evacuated to about 10^{-6} mm Hg). When the potentiometer indicated a stable reading, the emf value was compared with that expected at 77°F and any discrepancy noted so it could be applied to the data to be taken.

With the crankcase charged with helium to 35 psig, the working-gas side was purged about 30 times, from maximum pressure to about 10 psig. At this time, the pressure transducer-oscilloscope system was calibrated with a standard test gauge. After purging was completed, the crankcase pressure was increased to the same value as the working gas pressure.

With the cooler operating, the oscilloscope was used to observe the pressure transient of the working gas. Speed was accurately measured by synchronizing the stroboscope-tachometer with the drive mechanism which is visible through the plexiglass cover-plate on the front of the crankcase. Speed changes were made by adjusting the voltage applied to the drive motors. Motor power was calculated using the voltage and current values obtained for the drive motors. Cooler shaft power was obtained by using the motor efficiency data available from the motor calibration data. This data was generated in-house by using precision miniature dynamometers.

The vacuum station was maintained at about 10^{-6} mm Hg to insure that the vacuum around the cold finger was at least 10^{-4} mm Hg. If the heat exchanger temperature exceeded 113°F, a fan was used to reduce the temperature to 113°F or lower.

A potentiometer with a reference junction was used to measure the expansion-stage temperatures. Heat loads were applied to the two expansion stages by electric heaters soldered to them. The magnitudes of these loads were accurately measured with the voltmeters and ammeters in the heater circuits. The heaters, heater leads and thermocouple leads are shown in Figure 4. The thin, polished-brass, radiation shield used in some tests is shown in Figure 5 coupled to the 1st expansion stage.

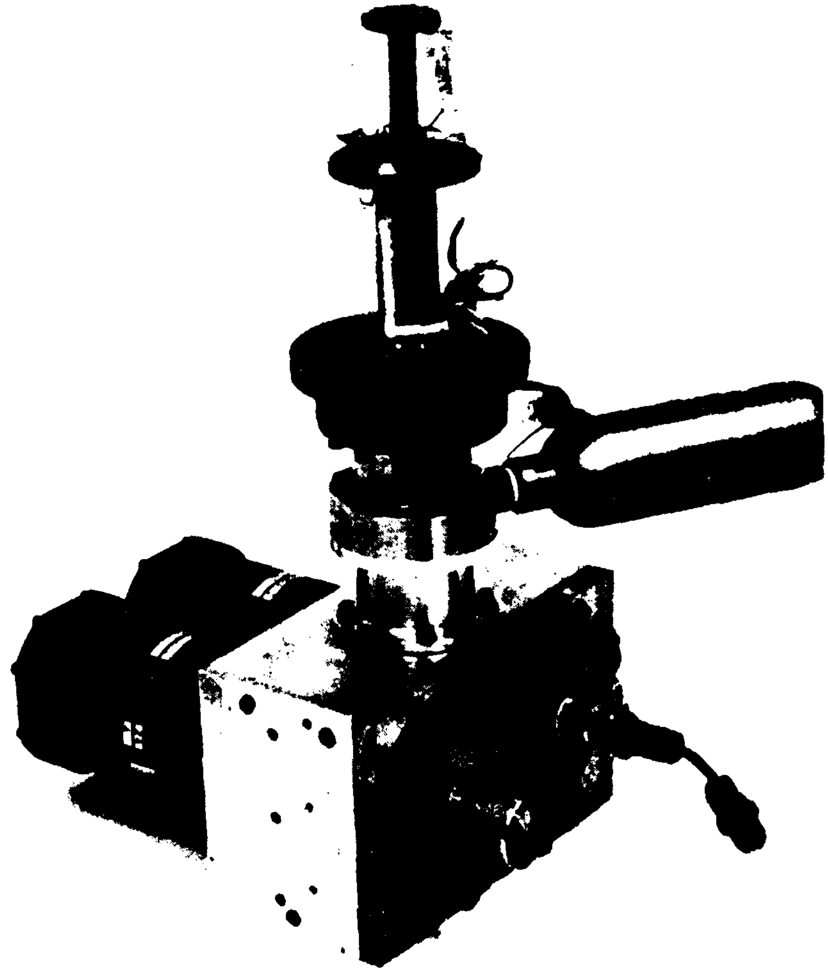

Figure 4: In-house cooler with dewar removed and instrumented cold finger.

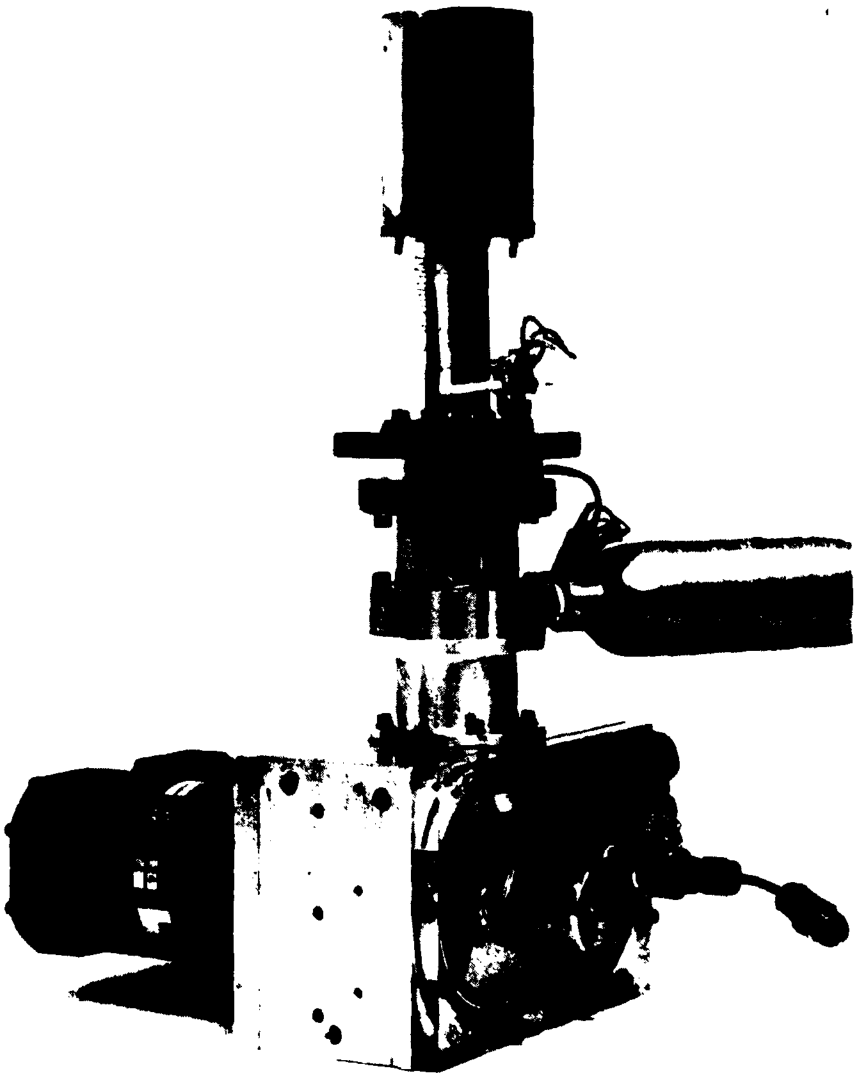

Figure 5: In-house cooler showing radiation shield coupled to 1st expansion stage.

3.2.5 Metal Bellows

Contamination of the working gas in the cold finger region is a major obstacle in all types of cryogenic coolers. Various methods have been employed to eliminate or at least reduce the contamination, e.g., dry lubrication on bearing surfaces; rolling diaphragms between the working volume and the buffer volume; and low vapor pressure lubrication.

Dry lubrication was rejected because particles could migrate up into the regenerators and create a blockage, or adhere to critical surfaces and increase heat leakage.

Rolling diaphragms were not practical for a space application since the oil system could not be guaranteed to maintain pressure. Another disadvantge of the rolling diaphragm is the permeability of the material which would permit a loss of helium pressure and, therefore, require an additional replenishing supply tank.

An alternative to the diaphragm was to use flexible metal bellows. To evaluate their potential, a duplicate of the in-flight cooler was constructed with two metal bellows installed one inside the other beneath the piston. The inner bellows was connected to the displacer rod; the other end was connected to the inside of the piston rod. The large bellows were soldered at one end to the piston rod, and the other end was coupled to the lower section of the cylinder wall.

Testing of the first pair of bellows began March 6, 1975 with a starting speed of 1200 rpm which was increased to 3750 rpm after 3 hours. A total of 4.8×10^7 cycles were completed before the small inner bellows failed.

Servometer Corp. supplied new bellows for evaluation. To determine the uniformity of the nickel deposition of the bellows, they were potted and sectioned for metallographic examination.

With reference to the photomicrographs, the results were:

- The thickness of the outer convolution is nearly twice that of the inner (Fig. 6).
- Machine tool marks on the mandrel resulted in considerable roughness on one side of the inner convolution (Fig. 7a).
- There is an offset between the radius curvature of the inner convolution and the web. This seems to be a common point of failure in service (Fig. 7b).
- The copper deposit is well centered.

Microscopic examination of the failed area indicated serious structural flaws in the deposition material. To combat this, production techniques were altered to produce a more uniform deposition of material with less stress points.

The new modified bellows were installed in the test unit and testing re-started on August 16, 1975 at a speed of 2250 rpm and gradually increased to 3000 rpm with a charge pressure above the bellows of 25 psi. This test continued until February 2, 1976 when 5.256×10^8 cycles were completed.

At this point, the unit was dismantled and examined for wear. The longer crankshaft was worn 0.004" on the diameter of the main bearing location, indicating that the inner bearing had been revolving around the crankshaft. To salvage the shaft, the bearing location diameter was further reduced and a hardened steel sleeve shrunk to the ground surface. The sleeve was then ground to suit the ID of a new bearing, and the unit was then reassembled. Testing was continued until October 13, 1976 without any further problems. The two combined runs were equivalent to two-years operation at 1000 rpm. The compression ratio above the piston was 1.87:1 with 40 psia of helium above the bellows.

A second series of bellows were installed and ran for 3.0×10^6 cycles before the inner bellows failed. Figure 8 shows the bellows and related components of the drive.

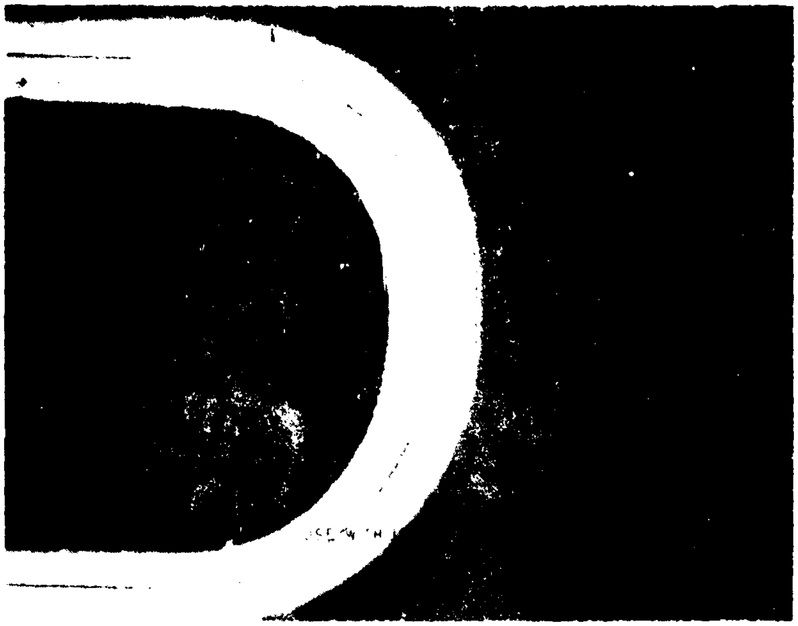

(a) Outer convolution

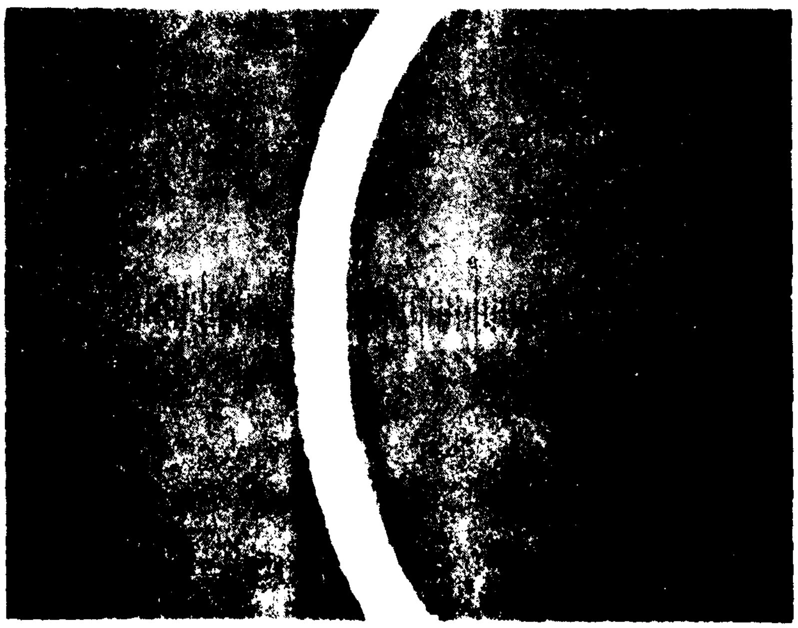

(b) Inner convolution

Figure 6: Sectional photomicrograph of bellows (Mag. 100X).

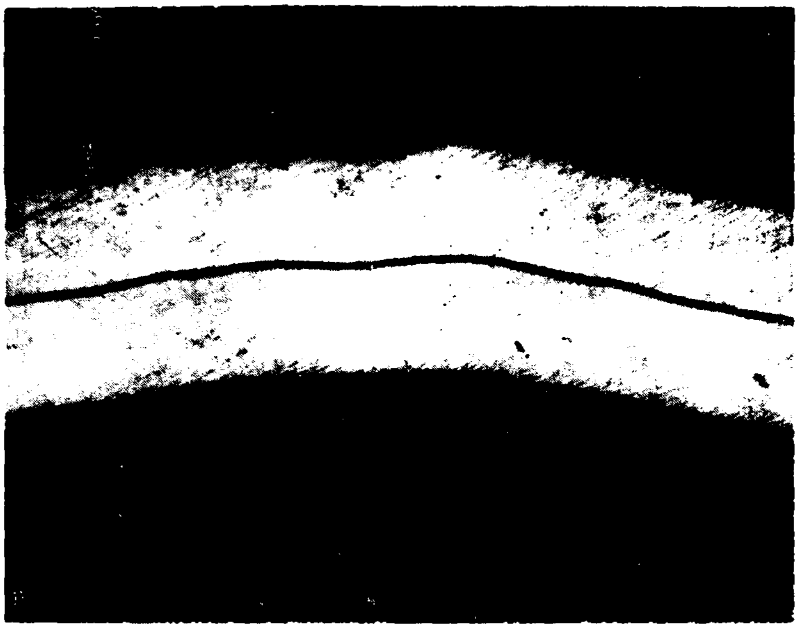

(a) Inner convolution (400X)

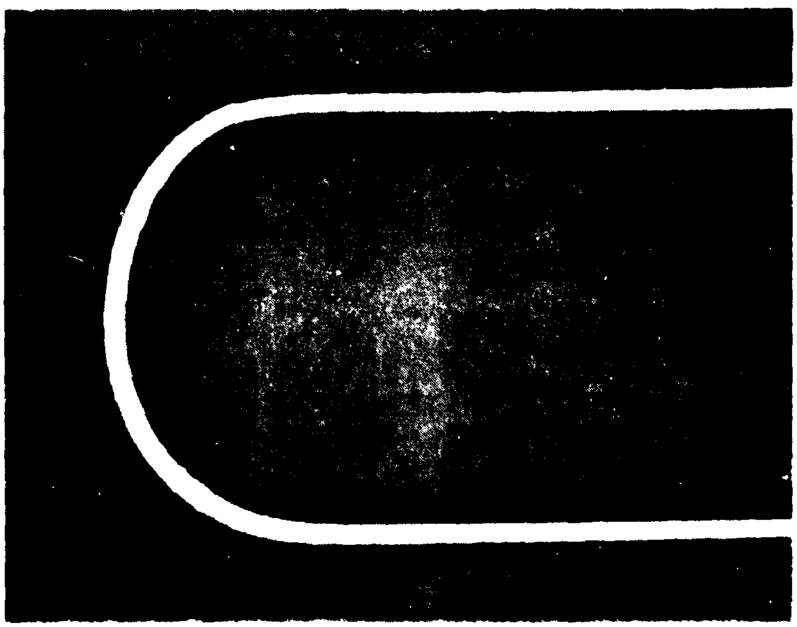

(b) Inner convolution (45X)

Figure 7: Sectional photomicrograph of bellows (Mag. 400X, 45X).

AD-A102 377 JOHNS HOPKINS UNIV LAUREL MD APPLIED PHYSICS LAB F/G 13/1
THE APL SATELLITE REFRIGERATOR PROGRAM.(U)
JUL 81 C S LEFFEL, R VON BRIESEN N00017-72-C-4401
UNCLASSIFIED JHU/APL/TG-1332 NL

2 OF 3
AD A
102377

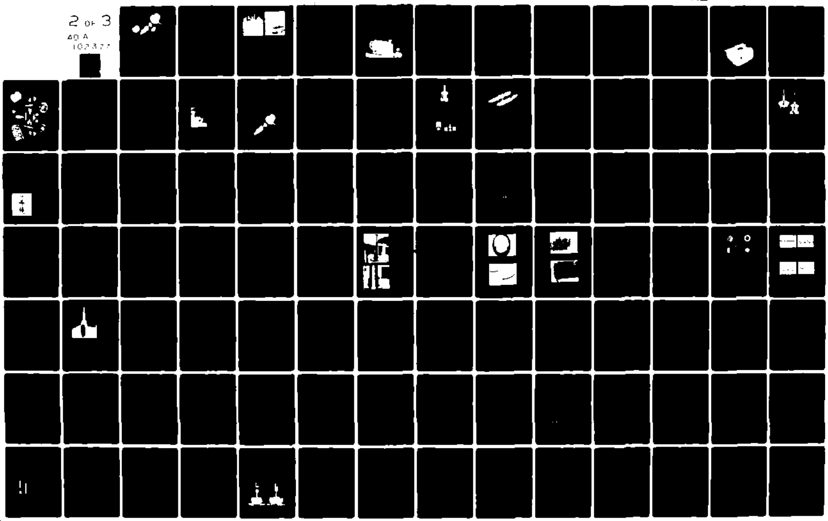

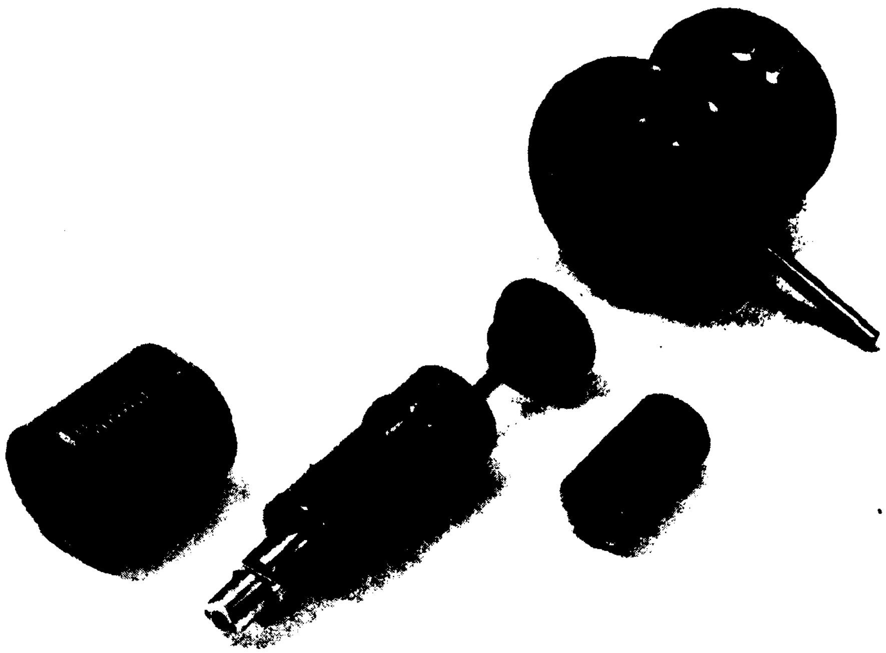

Figure 8: Bellows, piston and displacer rods with cylinder.

3.2.6 Lubrication

It became obvious that, in order to select reliable bellows for use in the refrigerator, a number of special test units would have to be constructed. Such testing would consume a great deal of time without any assurance that the total number of good bellows required would ever be achieved.

This situation was negated when an analysis of a low vapor pressure grease (Krytox 240AD) was conducted at JHU/APL. The results indicated that any outgassing of the grease due to elevated temperatures would have little or no effect on the performance of the refrigerators.

In support of the analysis conducted at JHU/APL, two types of Krytox grease were tested at PL. One was Krytox 240 AD; the other was Krytox 260 AC (made from Krytox 240 AD with 5% MoS_2 plus an inhibitor). Both types were subjected to 110°C for a period of two weeks; at the end of this time the Krytox 260 AC exhibited a separation of oil from the base grease, whereas the appearance of the Krytox 240 AD remained unchanged.

Due to the favorable results obtained by both investigations of the grease, a more realistic test was prompted in the form of a working unit. The test unit was the same one described in Par. 3.2.1. All bearings of the unit were packed with a 30% fill of the Krytox 240 AD in an effort to determine if the grease permeated to the cold region during operation. After 23 days of continuous running, the unit was stopped and dismantled. Examination of the second stage displacer showed an amount of Rulon debris from the seals and a small deposit of the grease. A contributing factor in the loss of grease from the bearings was that none of the bearing contained shields or retainers.

The fact that the bellows were rejected as part of the design did not eliminate them completely. It was felt that, if bellows of a better design with a more dependable life can be obtained, a longer lasting refrigerator would emerge. Should such bellows become available, the option of retrofitting them is still possible.

3.2.7 Cold Finger Conduction

Initial predicted heat conduction between the heat exchanger flange at 300°K and the 1st stage expansion flange at 210°K was 0.0049 W/K°. The predicted conductance between the 1st expansion stage at 140°K and the 2nd expansion stage at 77°K was 0.0012 W/K°. The predicted conductance between the 1st and 2nd expansion stage was 0.0017 W/K° with the temperatures at 210°K and 140°K. These predictions were based on projected values and on tests which indicated an error band of $< \pm$ 20%.

The experimental setup for verifying the analytical prediction of the cold-end thermal conductance is shown in Figure 9; a schematic of the experiment is shown in Figure 10. Figure 9 shows an actual cold end (including regenerator and displacer) of a refrigerator pressurized with helium and coupled to the

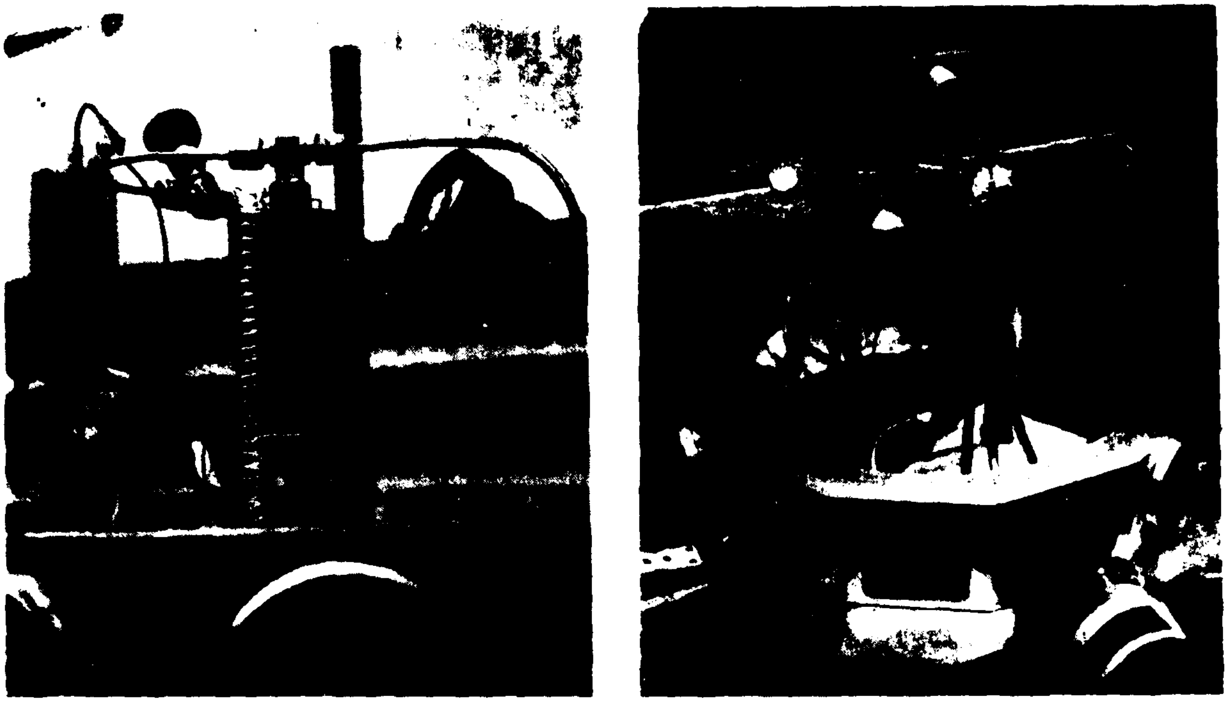

(a) (b)

Figure 9: Two views of apparatus for measuring thermal conductance.

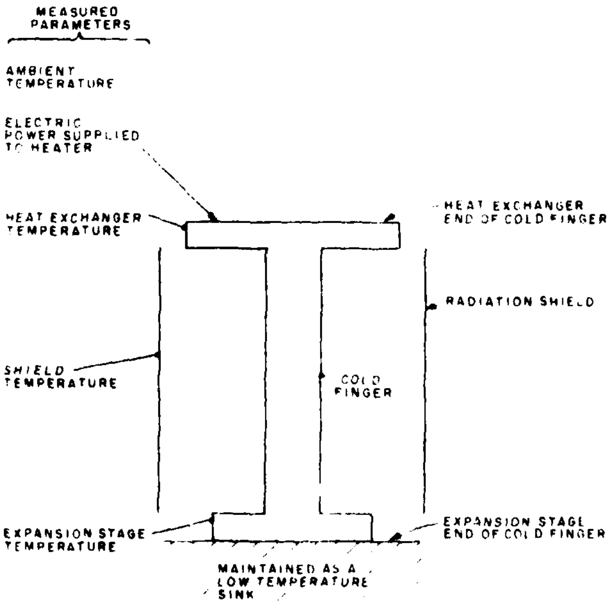

Figure 10: Schematic of experiment for measuring steady-state thermal conductance.

experimental setup -- all of which were installed in a vacuum chamber. Electric power was dissipated at the heat exchanger end. The expansion stage end was kept at a low temperature (usually at 77°K by circulating liquid nitrogen through it) and served as a low temperature sink. The high-conductivity radiation shield surrounding the finger was kept at a predetermined temperature by coupling it to the low temperature sink via heat-leak wires. Four temperatures were monitored: the ambient, the heat exchanger, the radiation shield, and the expansion stage flange.

Two types of steady-state tests were performed: one yielded a value of λ, thermal conductance, greater than the true value; the other yielded a lower value. In the first type, the temperature of the heat exchanger was kept higher than the ambient temperature. The temperature of the radiation shield around the cold finger was kept low enough to ensure a net transfer of heat energy out of the cold finger to the surrounding shield. Under these conditions, the measured electric power delivered to the heat exchanger would be sufficient to supply the losses from the heat exchanger to the ambient and from the cold finger to the shield. Therefore, the calculated value of the thermal conductance, defined below, will be greater than the true value.

$$\lambda = \frac{\text{electric power supplied to heat exchanger}}{\text{(heat exchanger temp.)} - \text{(expansion stage temp.)}}$$

In a similar manner, a value of λ less than the true value can be obtained. This is accomplished by maintaining the heat exchanger at a temperature lower than ambient and maintaining the radiation shield at a temperature high enough to insure a net trasfer of heat energy into the cold finger.

As mentioned, the experiment was refined until a band of $\pm$ 20% around the true λ was established. The test results were used to predict the thermal conductance of the cold end of the flight model, whose cold end is slightly different from that used in this experiment.

3.2.8 Piston Rings

To evaluate the potential of a piston ring of single-piece contruction, a glass-filled molybdenum disulfide Teflon Bal seal was installed in a conventional crank-throw refrigerator, but without a regenerator or coldfinger; in their place a pressure plate covered the cylinder with a duplicate compression volume above the piston head (Fig. 11).

To accumulate any significant data, the test unit was accelerated to 3500 rpm and was stopped after 2.278×10^9 cycles. To support these results, a similar ring was installed in the bellows tester. This piston ring accumulated 4.556×10^9 cycles or 2 years at 1000 rpm and still produced a compression ratio of 1.62:1. Examination of the ring suggested it still had a considerable amount of life.

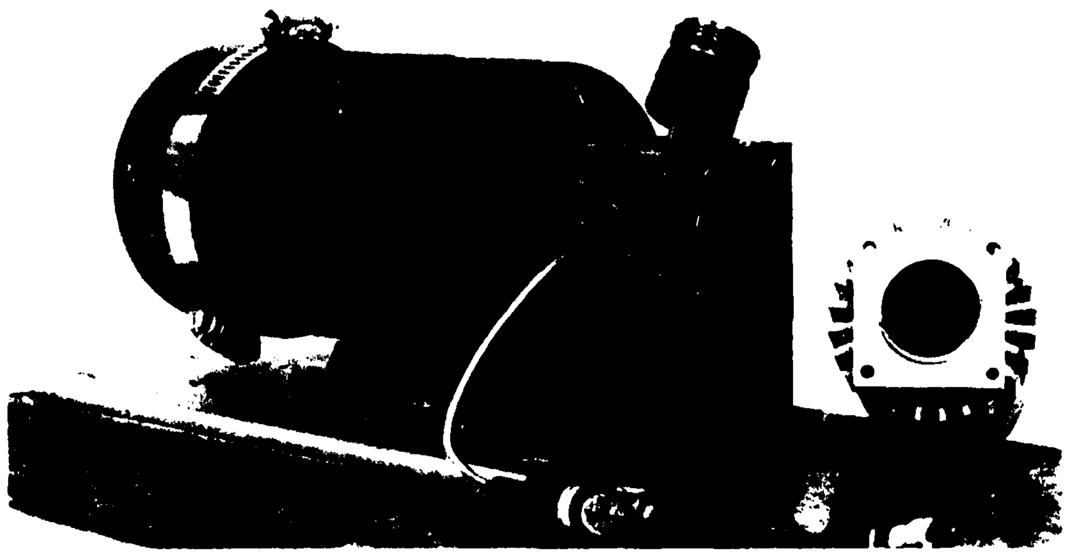

Figure 11: Drive and compressor used for testing piston ring and grease retention of bearings.

3.2.9 Displacer Seals

To ensure that gas is shuttled back and forth through the regenerators and not through the annulus netween the displacers and the cold finger, a seal is mounted on the lower section of each displacer. A Bal seal is mounted on the first stage displacer, while a solid Rulon band provides the sealing medium for the second stage.

A Bal seal was tested on the 2nd stage displacer, but testing showed that the seal froze when subjected to the 145°K cold production. This condition resulted in either the seal shrinking (allowing gas blow-by) or, more severely, expanding (scoring the inside of the cold finger).

3.3 Test Conclusions

The test results indicated:

- Brush-type dc motors were not recommended because of debris generated by brush wear.
- External motor mounting created gas leakage problems.

  Step-joint piston rings allowed excessive gas blow-by, resulting in compression loss.
- Heat-conducting materials affected performance efficiency.
- The reliabilty of flexible metal bellows was questionable.
- Ball bearings were not heavy enough for the life expectancy.
- Static balance of the moving parts was inadequate.
- A 2nd stage Bal-seal was not practical due to the seal freezing.

The above findings resulted in the following design changes:

- High-efficiency brushless dc motors with Hall-effect sensing devices were selected and mounted within the crankcase envelope.

- The step joint piston rings were replaced by single-piece glass-filled Teflon Bal-seals.

- Low conductivity materials were used wherever practical to increase efficiency.

- Flexible metal bellows were omitted from the final design (option is still available to retrofit bellows at any time).

- Ball bearings were increased in size to give longer life with higher reliability.

- A dynamic balance as well as a static balance was performed on the moving parts to reduce vibration (see Appendix C).

- A solid band of Fulon was fitted to replace the 2nd stage Bal seal.

The final design parameters are given in Tables 3 and 4.

TABLE 3: GENERAL DESIGN CHARACTERISTICS.

Item	Value
Input power	< 30 W
Cold production	0.3 W @ 77°K and 1.5 W @ [illegible]°K
Shaft speed	1000 rpm ± 200 rpm
Working fluid	Helium
Mean pressure	4.8 atm
Piston stroke	0.2198 in (7.5692 mm)
Swept volume	0.4425 in^3 (7.2525 cm^3)
Heat rejection temperature	20°F - 113°F
Thermodynamic phase (volume)	92.6°
Mechanical phase angle	74.46°
Displacer stroke	0.298 in. (7.5692 mm)

TABLE 4: COMPONENT DESIGN CHARACTERISTICS.

Item	Value
Number of regenerators	2
1st stage regenerator:	
Diameter	0.566 in. (14.376 mm)
Length	1.953 in. (49.6062 mm)
Filling factor	42%
Wire diameter	0.004 in. (0.1016 mm)
Displacer body thermal conductivity (NEMA G-7)	0.003 $W/cm^2/°K$
2nd stage regenerator:	
Diameter	0.3065 in. (7.7851 mm)
Length	1.277 in. (32.4358 mm)
Filling factor	42%
Wire diameter	0.0026 in. (0.0660 mm)
Displacer body thermal conductivity (2.5 Sn, 5 Al)	0.08 $W/cm^2/°K$
Pistons:	
Number	1
Diameter	1.375 in. (34.925 mm)
Rod diameter	1.156 in. (29.3624 mm)
Displacer rod diameter	0.157 in. (4.445 mm)

4. FABRICATION AND ASSEMBLY

All parts of the refrigerator, with the exception of the crankcase and the dc drive motors, were fabricated at Philips Laboratories. The crankcases are sand-cast magnesium produced by Control Casting Corp., Plainview, New York. The permanent magnet brushless dc motors were custom-built by Herbert C. Rotors, Plainview, New York. Each finished part was etched for identification and boxed with its mating components so that the parts of the various refrigerators could not be interchanged. The reason for separating each refrigerator's parts was because the moving parts of each mechanism were accurately weighed in preparation for dynamic balancing of the drive. By performing a dynamic balance of the moving parts, vibration of the operating refrigerator is virtually eliminated. Balancing procedures are given in Appendix C.

4.1 Materials

Because of its low density, magnesium was used for the crankcase and coverplates. The cylinder was constructed of 304 stainless steel with a Nitralloy liner hardened to Rc 64. The heat exchanger flange was machined from CRES 304, with an inner sleeve of hardened 440C steel. The thin sidewalls of the cold finger were made of titanium 5Al-2.5Sn, as was the second stage regenerator shell, because of the low thermal conductivity and strength of titanium. The 1st stage regenerator shell was constructed of woven-glass fabric silicone laminate because of the exceptionally low thermal conductivity.

Copper was used for the freezer cap on the second stage of the cold finger and for the flange of the 1st expansion stage.

The connecting links were made of AISI 416 stainless steel; the displacer rod was made from hardened 440C steel; the crankshafts and the extension displacer flex-rod wire were made from 416 stainless steel; and both yokes were made from 2024 aluminum.

Five ball bushings were incorporated into the refrigerator: two in tandem inside the piston rod to guide the displacer rod; two in parallel in the piston yoke to give support; and one in the lower crankcase housing to guide the extension displacer rod.

Beneath the 1st stage displacer is an extension displacer (referred to as the dummy displacer) made of 2024 aluminum which is screwed onto the displacer rod. Within the body of the extension displacer is a flexible support rod which deflects to compensate for any misalignment between the displacer rod and the two-stage displacer.

The 1st stage displacer is made of woven-glass fabric silicone laminate and filled with layers of phosphor bronze mesh. The 2nd-stage displacer is made of thin wall titanium, also with a fill of phosphor bronze mesh. Depending on the required cold production of the refrigerator, the size of the mesh and the fill factor of the displacer can be tailored to meet different requirements.

Two pressure sensors are mounted to the refrigerator. A *Kulite* pressure transducer is isolated inside the crankcase and secured to the right-hand stator clamp ring. The transducer is activated by 10 Vdc and rated for 100 psig with a maximum pressure of 200 psig. The second sensor is a strain gauge mounted externally on the buffer tank wall. The buffer tank is a cylinder capped at one end with a fill valve on the other. A section of the tank wall is reduced in thickness to 0.030", so that the strain gauge mounted on the thin wall responds to pressure variations that flex the wall. The inner volume of the tank is joined to the base of the cylinder by a short stainless steel tube, and provides extra dead volume beneath the piston head. The extra volume allows for metal bellows which can be added to the piston and displacer rods. The bellows, which can be retrofitted to the refrigerator, form a barrier between the crankcase volume and the working volume above the piston to prevent possible contaminants from reaching the regenerators.

All finished components of the refrigerator were ultrasonically cleaned using solvents prior to assembly. The assembly was performed within a laminar flow hood to maintain cleanliness of the parts. Each finished part was handled by personnel wearing lint-free gloves; every effort was made to eliminate dirt particles from the components.

4.2 Crankcase

The total weight of the refrigerator was not severely restricted; however, the use of steel or similarly heavy metal for the outer envelope would increase the weight of the refrigerator excessively. The crankcase and cover plates were formed of die cast magnesium, thereby holding the total weight at an acceptable level.

The rough casting cover plates were machined to size, and the "O" ring groove in each plate was polished. The crankcase casting (Fig. 12) was rough-machined with only the "O" ring

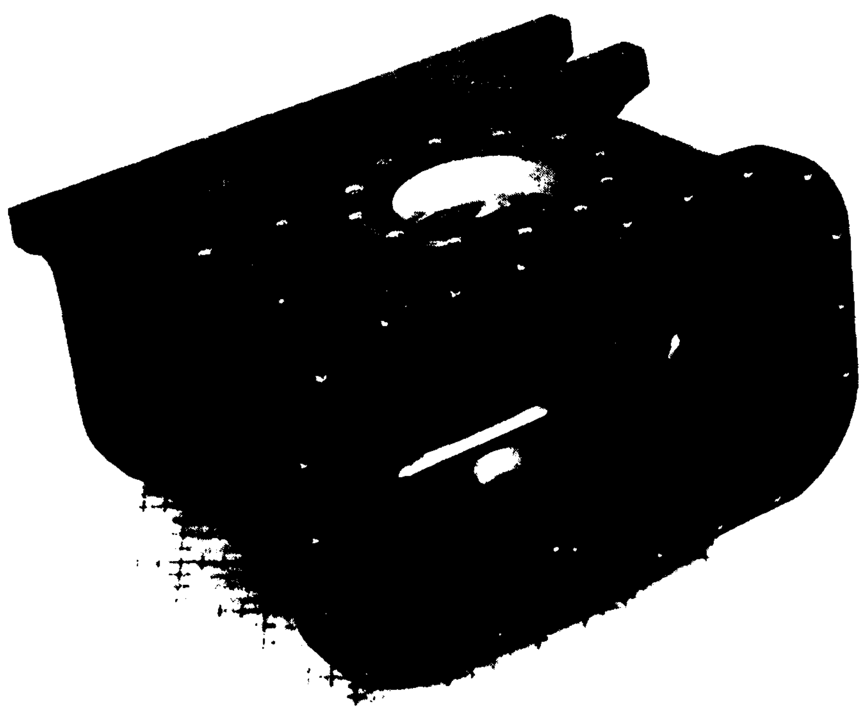

Figure 12: Crankcase casting.

grooves polished and reduced to their final dimensions. Since the uniform density of soft die cast materials cannot be guaranteed by most suppliers, the castings were impregnated with a sealant (Dow 17) to eliminate porosity.

Critical surfaces, such as those of the motor housings, the interfaces for the rhombic drive enclosure, and the cylinder were left unfinished so that any distortion of the casting during the impregnation treatment would not affect final machined sizes. These remaining unfinished surfaces required extremely close machining tolerances to ensure that mating components of the crankcase were located correctly (Fig. 13). The cumulative effect of any machining errors, outside the tolerances, could reach a point where correct internal alignment of the refrigerator is not possible.

The two dc motor stator windings are housed in the crankcase and secured by a locking collar. Each collar is fastened in place with four screws tightened into the crankcase inner face. Since all six crankcases were impregnated with sealant and machined to size consecutively, it was not apparent (initially) that a problem existed between the casting dimensions and the crankcase material available for machining. The depth of the screw holes was excessive; as a result, the tapping drill used for the holes broke through the castings wall. It was felt that the time required to manufacture new castings and to finish-machine the crankcase would prolong the delivery date.

To stay within the delivery schedule, an attempt was made to cover the breakthrough holes with a run of magnesium weld. The weld was not successful in sealing the hole, although the magnesium crankcase readily accepted the weld. A second attempt was made using threaded magnesium plugs (Fig. 14) coated with "Bondmaster" 777 epoxy and screwed down into the base of the screw hole. A stainless-steel, threaded stud was screwed

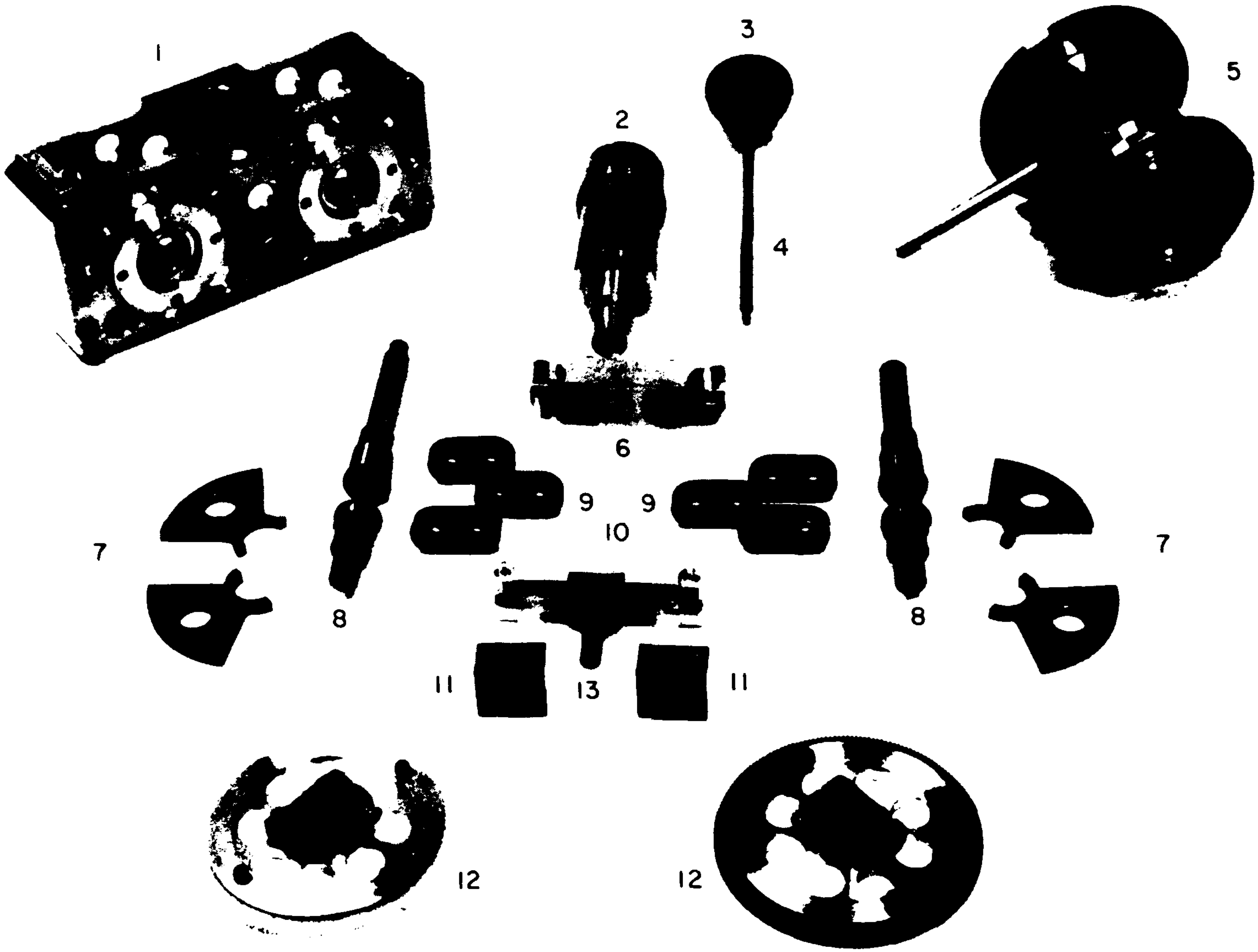

Figure 13: Crankcase components. (Sheet 1 of 2)

Parts List for Figure 13

Item No.	Part	Part No.
1	Rhombic drive	5941
2	Piston rod	5956
3	Piston	9342
4	Displacer rod	7517
5	Cylinder	5959
6	Piston yoke	7475
7	Counterweights	7524
8	Crankshafts	5952
9	Connecting rods	9343
10	Displacer yoke	7476
11	Displacer yoke weights	9369
12	Timing gears	9491
13	Extension displacer rod	9233
Not Shown	Cold finger assembly	5935
" "	Displacer/regenerator assembly	5933
" "	Crankcase	5304

(Sheet 2 of 2)

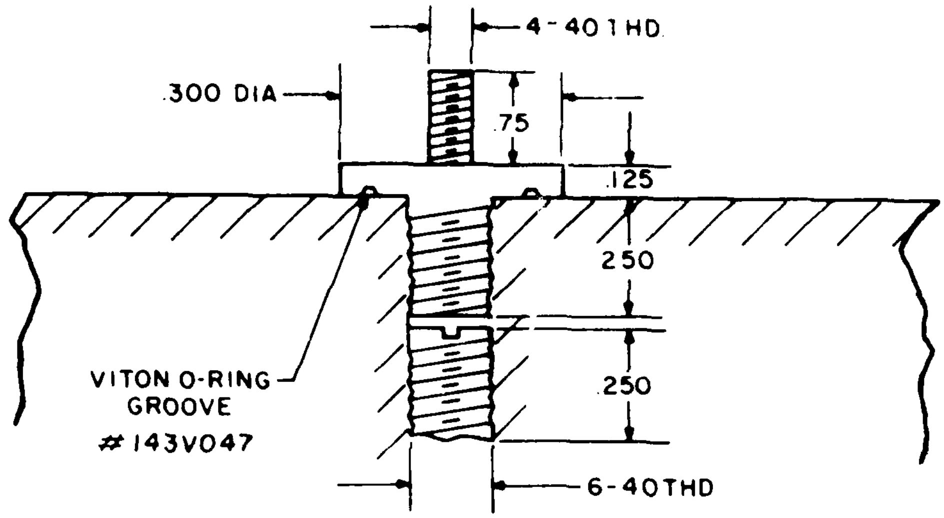

Figure 14: Crankcase plugs.

in behind the magnesium plug and secured with a high density epoxy produced by the 3M Company. The crankcase was inserted into an oven to bake cure the epoxy for 40 minutes at 250°F.

To check the effectiveness of the epoxied plugs, the open faces of the crankcase were covered and the crankcase pressurized to 90 psig with helium. The crankcase was then installed in an environmental chamber and the temperature cycled between - 30°F to + 180°F. The crankcase was then leak-checked using a mass spectrometer leak detector. With no evidence of a helium leak, each crankcase was repaired and checked using the method described.

4.3 Coverplates

The die-cast, magnesium, coverplates of refrigerator S/N 1 developed an excessive helium leak shortly after delivery of the refrigerator. Acceptance-level leak checking prior to

delivery indicated a leak-tight envelope. Microscopic examination of the coverplates suggested a progressive erosion of the surfaces (Fig. 15). This erosion was attributed to the methods used for sealant impregnation. The remaining coverplates, intended for use with subsequent refrigerators, showed identical deterioration, resulting in a number of plates being discarded. New coverplates were manufactured using solid plate magnesium. During the manufacture of the new plates, two refrigerators, S/N 2 and S/N 3, were delivered to JHU/APL with the die-cast plates fitted so that the refrigerators could be checked and instrumented. The intention was to retrofit the refrigerators with the new coverplates when they became available. This was accomplished some months later.

Figure 15: Erosion of crankcase coverplate.

The coverplates are secured to the crankcase with 4-40 cap head screws. The helium pressure within the crankcase is maintained by double "O" rings between each interface. Viton and polyurethane were selected as the "O" ring materials, with the Viton rings being used as compression seals and the polyurethane rings as slip seals. The polyurethane "O" rings were mounted on the flange grooves of the coverplates and an attempt made to

mount the plates to the crankcase. However, due to the ... durometer of the polyurethane, the inner lips of the "O" ring groove in the crankcase cracked. The polyurethane rings were replaced by neoprene rings and the plates installed without further problems. All polyurethane rings intended for use on the crankcase were subsequently replaced by neoprene rings and lightly coated with Krytox AD 240 grease. The compression "O" rings were assembled dry in all instances.

4.4 Piston Rod

The piston rod consists of two pieces screwed together and pinned, then TIG welded (Fig. 16). The upper section is stainless steel and locates on a shoulder of the lower aluminum body. The aluminum body is secured to the piston yoke by two screws inserted through clearance holes in the displacer yoke. The screws can only be inserted into the piston yoke through the

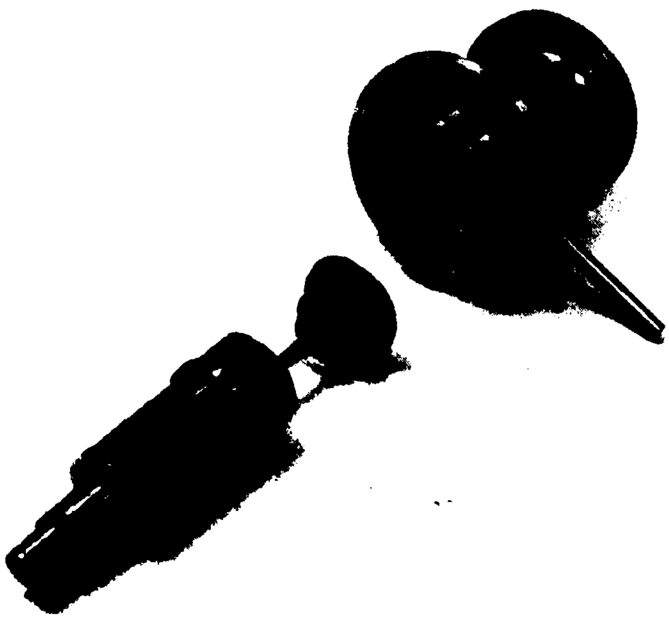

Figure 16: Piston and displacer rods with piston and cylinder.

base of the crankcase with the rhombic drive secured. The inner body of the aluminum base extends up into the steel rod body, and serves to house two linear ball bushings. An aluminum spacer separates the two ball bushings which guide the displacer rod.

4.5 Displacer Rod

The displacer rod is ground and polished hardened steel with a surface finish of < 5 μm. A thread at the top of the rod provides a location for the extension displacer, while a thread at the base of the rod provides a means of securing the rod within the displacer yoke.

During quenching of the rod after heat treatment, the threaded portions moved away from the center line of the rod. As a result of the top thread being bent, the mating extension displacer was at an angle. Straightening the thread was impractical due to the 55C Rockwell hardness of the rod. Some success was achieved in improving the alignment by counter boring the base of the extension displacer and inserting a steel sleeve to locate around the top shoulder of the rod. This action was accompanied by easing the thread on the rod and using an oversize tapping drill in the steel insert of the extension displacer. The result was a loose mating fit between threads which permitted the steel insert of displacer to force a good alignment between the rod and the displacer.

Since heat treatment of the displacer rod proved to be a problem, machining methods were reviewed and revised. The result being that when new rods were made, the threaded ends were left blank until the rods were hardened; the blank ends were then threaded.

4.6 Extension Displacer

The extension displacer (Fig. 17) is an aluminum body with a 4-40 thread in one end which screws onto the displacer rod. Fitting inside the body is a split guide sleeve through which the flex rod is located. The flex rod screws into the inside of the hole in the displacer body. The opposite end of the flex rod has a 10-32 thread to screw into the base of the 1st stage displacer.

4.7 Rhombic Enclosure

The rhombic drive is located within a frame independent from the crankcase. The frame is constructed of five parts: two main plates facing each other and each containing two SR8 bearings for the two crankshafts; two end plates separating the main plates (these four plates are aluminum); mounted across the top of the two face plates is a stainless steel plate containing two 1/4" dowel pins to guide the ball bushings in the piston yoke. The five parts are dowled and secured with pan head screws (Fig. 13, Item 1). The SR8 bearings of each faceplate are individually fitted to their respective housing and crankshafts.

4.8 Crankshafts

Each crankshaft is of two-part construction (Fig. 18). The two halves of a single shaft are coupled together at the eccentric. The eccentric extends from the face of one-half of the crankshaft and is inserted into a hole in the face of the other half of the crankshaft. Their coupled position is held by a stainless steel pin driven through the two mated pieces.

The crankshafts are rough machined in a lathe and then machined to size on a grinder. To enable each diameter of the shaft to be ground, a large flange is left at each end of the crankshaft. The center lines of each diameter are continued into the flanges

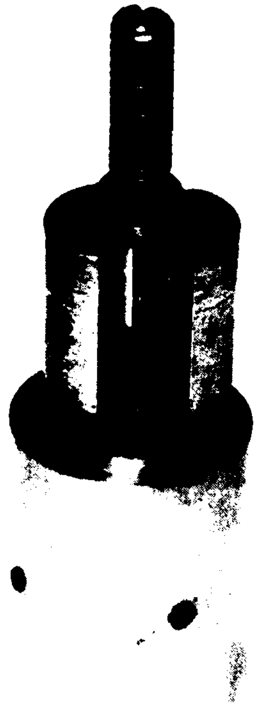

(a)

(b)

Figure 17: Extension displacer.

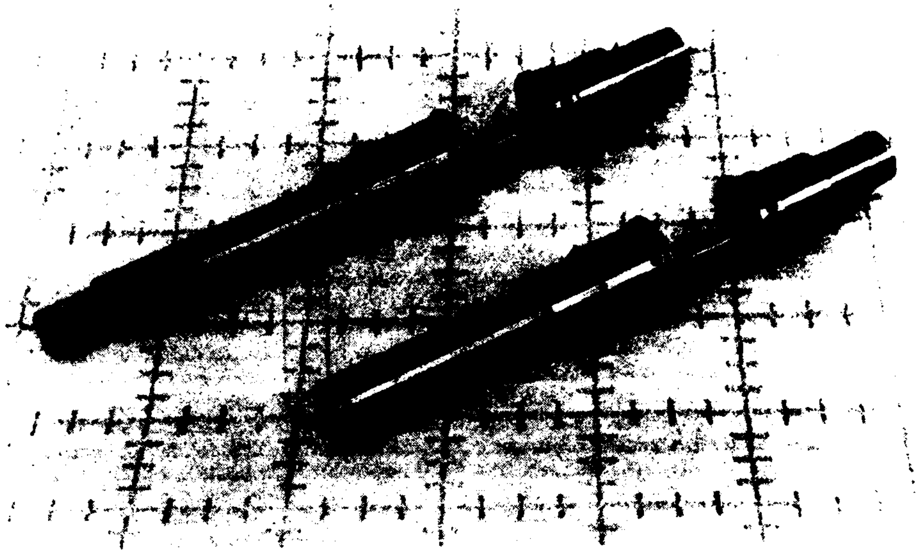

Figure 18: Crankshafts.

and center drilled. This enables the shafts to be set up between centers on a cylinder grinder and all diameters ground to a finished size. The flanges at the ends of the shafts are then removed, leaving the shafts the correct length.

The two crankshafts in the rhombic drive are of different lengths. The longer shaft extends to provide location for the commutation sensor disk. Both shafts have a keyway milled into the surface of the long ends to facilitate the magnetic rotors of the dc motor.

The rhombic drive is designed so that mass can be added to or subtracted from the displacer or piston masses to balance the drive and maintain a fixed center of gravity. As part of this balance, the crankshafts must also be dynamically balanced. The mass of the eccentric is counteracted by adding two copper counterweights, 180° out of phase to the eccentric. The counterweights are oversize to begin with; then mass is removed from the copper to effect the balance (see Appendix C).

Emphasis is placed on the machining accuracy of the crankshafts, since the eccentrics of a pair of mated shafts must be identical. Each shaft eccentric is the location for three SR3 bearings mounted in tandem, with each bearing separated by Teflon spacers. Three connecting rods are fitted onto the SR3 bearings on the crankshaft. The opposite end of each rod contains another SR3 bearing. The outer two rods on each shaft are coupled to the upper piston yoke by a wrist pin passing through the yoke and the SR3 bearings. The wrist pins are secured in position by set screws through the wall of the yoke. The remaining inner connecting rods are coupled to the lower displacer yoke in the same manner.

The symmetry of the rhombus depends on the machining accuracy of the parts. To achieve uniform position of the drive, the six connecting rods are clamped together in a common fixture on a jig borer. The bearing holes in all the connecting rods are bored together, so that the distance between hole centers are the same in each rod.

All ball bearings in the refrigerator are Class 7, with dust shields and synthetic ball retainers. Each bearing is loaded with a 30% fill of Krytox 240 AD grease. To insure that each bearing carries an equal uniform radial loading, the bearings are individually fitted to the crankshafts and wrist pins.

The two crankshafts are fitted through two SR8 bearings in one faceplate, and extend beyond the bearing faces to provide location for the two timing gears.

4.9 Timing Gears

Each gear consists of an aluminum hub which holds a gear ring, and an aluminum clamping ring which captures the gear ring against the hub. Four screws pass through the aluminum hub, through the gear ring, and tighten into the clamping ring. This prevents the gear ring from rotating within the confines of the

two hub parts. The face of the hub contains a split clamp which secures the gear to the crankshaft.

Two dissimilar materials were used for the gear rings, viz., Delrin AF and Teflon 610. This material combination results in lower friction and longer life of the mating gears.

The opposite ends of the crankshafts pass through the rear of the rhombic case and provide location for the two dc magnetic rotors. Each rotor is held on a shaft by a key and secured with a snap ring. The right hand crankshaft, when viewing the open crankcase from the rear, is the longer of the two. This shaft provides location for the magnetic timing disk of the motors.

4.10 Dispacer/Regenerator--1st Stage

The 1st stage displacer consists of: a stainless steel adapter to accommodate a glass-filled Bal seal, a stainles steel cap to contain the seal, a laminated woven-glass fabric silicone body to encase the phosphur bronze regenerator mesh, and a top cap of glass-filled fiber extending through the center of the mesh layers. The glass-filled body in the center of the mesh is screwed to the top thread of the flex-rod.

The use of woven-glass fabric for the regenerator shell and top cap reduces the heat losses down the displacer wall and through the top cap center body. The base of the center body is supported by a steel sleeve. Inside the base of the body is a helicoil into which the flex-rod of the extension displacer is screwed. The top face of the cap provides a seating for the 2nd stage displacer. The center of the cap is counter bored, and two 1/16" diameter dowel holes are drilled 180° apart on either side of the counter bore.

The regenerator mesh is selected by computing the heat capacity of the mesh for a selected working volume and consideration of the characteristics of the other materials in the working gas

area. Other inputs for the computer program include: thermal losses, flow losses, heat leaks, output temperature goals, and internal parameter variations.

The phospher-bronze mesh required is 110 x 110 with a wire diameter of 0.004" and a filling factor of 42% within the displacer. The number of layers of mesh required is calculated as follows:

where, N = number of mesh layers

ft = % fill factor of mesh

d = wire diameter

L = internal length of displacer

$$fg = \frac{\pi}{4\tau}\sqrt{1 + \frac{1}{\tau^2}}$$

τ = dimensionless mesh

$$\text{so} \quad \tau = \frac{\frac{1}{110}}{0.004} \qquad \text{Then } fg = \frac{\pi}{4\tau}(1.0925) = .3775$$

$$\text{Substituting:} \quad N = \frac{(.42)(1.953)}{(.008)(.3775)} = \frac{.82026}{.003} = 271.609$$

Since a compression factor is not considered in the equation (compressing the mesh to the required length for the displacer increases the mesh diameter and it must therefore be machined to suit the inside diameter of the displacer), an extra 10% of mesh must be added to the calculated number (N), making the number of mesh layers required as 299. The same equation applied to the 2nd stage regenerator results in being 345 layers of mesh required.

4.11 Displacer/Regenerator--2nd Stage

The 2nd stage displacer could not be designed to use the woven-glass fabric laminate due to the structural strength of the material being affected by the small diameter of the displacer shell. By selecting titanium alloy for the displacer body, the heat losses through the displacer wall were kept to an acceptable level. The titanium also provided a stronger envelope to contain the phospher bronze mesh. Both regenerators are cleaned by flushing liquid freon through the gas ports of each displacer.

4.12 Rhombic Alignment

The rhombic drive is a symmetric shape maintained by two timing gears mounted on the crankshafts. The timing gears govern the position of the shaft eccentrics, which in turn determine the parallel condition between the yokes and the rhombic enclosure. The two yokes are held parallel by the displacer rod (secured in the displacer yoke) and by the piston rod (secured in the piston yoke). The displacer rod is guided within the piston rod by two ball bushings mounted in tandem. Although the yokes are held parallel to each other by the rods, the yokes must be adjusted to ride parallel to the top surface of the rhombic enclosure. The instruction manual submitted under this program describes the alignment procedures for both the rhombic drive and the displacers.

4.13 Cold Finger

The cold finger (Fig. 19) consists of various metals furnace brazed together. The stainless-steel, heat-exchanger flange has a copper body brazed into the bore for heat transfer. Joining and extending above the copper insert is a titanium alloy sleeve. This sleeve forms the first expansion space for the 1st stage displacer. At the top of the sleeve is a copper flange to provide location for a radiation shield which extends up around

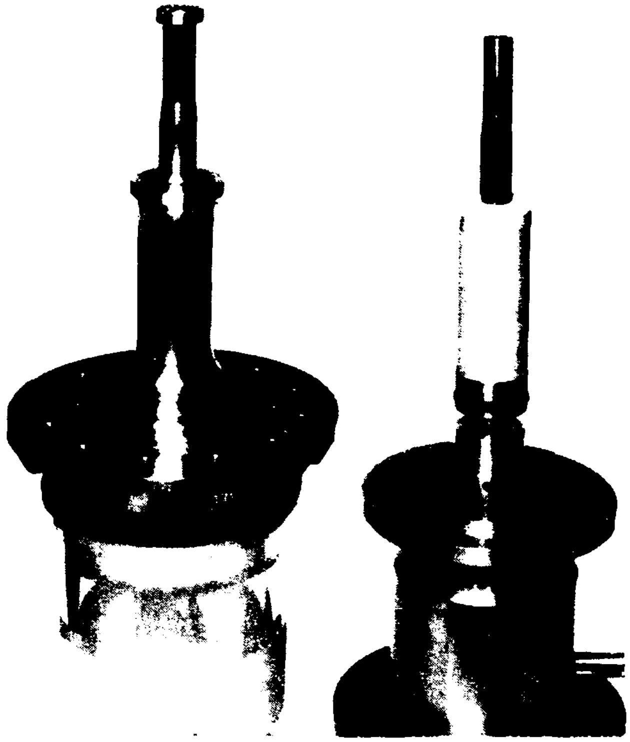

Figure 19: Cold finger and displacers.

the second stage of the cold finger. The second stage of the cold finger is also a titanium alloy sleeve which is furnace-brazed to a copper flange at the top of the 1st expansion stage. The top of the 2nd stage titanium shell is sealed with a brazed copper cap.

The inner ports of the cold finger are machined to within 0.002" of the finished sizes. A steel mandrel is used to hold each part in position during the brazing procedure. The inner dimensions of the finger are then honed and polished to a 11 micron-inch finish. To reduce the emissivity of the outer surfaces of the cold finger, a 2 μm layer of gold is deposited over the entire outer faces of the thin walls and copper flanges.

Before mounting the cold finger to the cylinder top, an exact measurement of the depths of the first and second stages of the

cold finger must be made. The depth measurements are compared to the height of the 1st and 2nd stage displacers when the displacer rod is at top dead center. The 1st stage displacer should have between 0.010" and 0.015" top clearance inside the finger while the 2nd stage displacer should have 0.004" to 0.008" top clearance. Height adjustment of the 1st stage displacer is accomplished by adding a spacer or removing material at the interface between the seal cap of the displacer and the top shoulder of the flex-rod. The height adjustment of the 2nd stage displacer is achieved by adding a spacer or removing material from the interface between the displacers.

4.14 Instrumentation

The refrigerator is required to produce 0.3 W and 1.5 W of power simultaneously. To simulate these power loads, three 1000 ohm ceramic heaters were mounted on an auxiliary copper plate clamped to the copper flange of the cold finger at the 1st expansion stage. A second auxiliary copper plate was secured to the copper cap on the second expansion stage of the cold finger. This second plate held a single 800 ohm ceramic heater (Fig. 20).

Figure 20: Cold finger with auxiliary heater plates.

The electrical leads coupled to the heaters were 0.010" in diameter, each wire having a free length of at least twelve inches. The wires were wound in coils within the covering vacuum dewar, and in close proximity to the cold finger. The two temperatures were monitored by chromel/alumel thermocouples mounted on each flange. Again the wires were at least twelve inches in length and coiled within the vacuum dewar. The thermocouple wires were 0.005" in diameter. The thermocouple and heater leads from the cold finger were fed through the wall of the vacuum dewar. The EMF outputs from the thermocouples were monitored by a millivolt potentiometer.

The total heat leak through all wires was calculated to be 0.004 W and was considered negligible in affecting the cold production of the refrigerator.

The two thermocouples were calibrated by immersing the cold finger in a bath of liquid nitrogen and reading the output EMF on the millivolt potentiometer. (LN_2 temperature of 77°K produces - 5.829 mV from a Chromel/Alumel thermocouple.) The calibration point of 77°K coincides with the temperature produced by the 2nd stage regenerator.

4.15 Motors

The refrigerator is driven by two counter-rotating brushless dc motors mounted in parallel. The motors were manufactured and tested by Herbert C. Roters Associates, Inc. (see Appendix D for efficiency curves). Each motor is designed to operate at an efficiency of over 73%, with an input voltage of between 26 - 30 Vdc under full load. Maximum applied torque during efficiency calibration did not exceed 40 in-oz at speeds between 860 and 1164 rpm.

The permanent-magnet armatures of the dc motors are driven by field coils which are switched externally in the electronics controller by Hall sensor signals picked off the magnetic disk

located on the crankshaft. Drive currents to the field coils, Hall sensor signals, and instrument signals are fed into ane out of the crankcase via leads connected to both sides of the glass-insulated feed-throughs.

Speed control is obtained by pulse-width modulation of the drive current at a frequency of 10 kHz. The pulse width is controlled by comparing a voltage proportional to rpm (generated from one of the commutating Hall sensors by a counter) to a fixed voltage.

The electronic controller was supplied by Herbert C. Roters Associates, Inc. with the motors. Evaluation testing of all refrigerators was performed using Roters' controller, under identical conditions.

An electronic controller supplied by JHU/APL was used only when the Roters' controller was returned to Roters for testing the remaining undelivered dc motors. Since the JHU/APL controller consumed slightly more power than the Roters controller, testing performed with the JHU/APL controller was repeated when the Roters' controller was returned to Philips Laboratories.

To obtain optimum motor performance, the input power to the right-hand motor is monitored with a digital ammeter, and the stator winding is rotated clockwise or counter-clockwise to indicate the least possible current requirement while achieving the correct direction of rotation. The clamp ring seated against the stator plates is then tightened to lock the stator in position.

The left-hand stator winding is inserted into the crankcase parallel with the right-hand stator, and secured by a clamping ring against the stator body. To obtain optimum performance. each motor is individually coupled to a power source and the input power monitored on a digital ammeter.

The right-hand motor is positioned first by slowly rotating the rotor within the housing to a point where minimum power is

required to drive the motor. The stator is then locked in position by tightening the clamp ring seated against the stator body. The motor leads are disconnected from the power sou‹ce, and the left-hand motor leads are coupled to the power source. The motor is energized with the same voltage as that for the right-hand motor, and monitored with a digital ammeter as before. The stator is rotated in the crankcase to a position that requires minimum current while the motor is energized. The clamp ring is lightly clamped to secure the stator. By adjusting each stator winding within the crankcase to draw minimum current, the motors can only be phased to within 15° of each other.

For a finer adjustment of the phasing, the generated waveform from each motor is displayed on an oscilloscope having a dual trace and two amplifiers, each amplifier having a double input. The left-hand motor circuit is tapped into with a probe connected to one of the oscilloscope amplifiers. The right-hand motor leads are connected to the second amplifier of the oscilloscope. When the left-hand motor is energized to run at 1000 rpm, the generated waveform will be displayed on the oscilloscope screen in the form of a sine wave. The right-hand motor is rotated by the timing gears mounted on the ends of the crankshafts. The rotation of the right-hand motor generates a waveform which is also displayed on the oscilloscope. An out-of-phase condition between motors is evident if one sine wave is not superimposed over the other. To bring both waves toegther, the left-hand stator winding in the crankcase is rotated and then relocked in position by the clamp ring. An advantage of using a single controller for all testing was that the test results could be cross checked from one refrigerator to the next.

The six Hall effect sensors are coupled to the electronic controller by different colored wires. Each wire is fed through the wall of the sensor ring and looped around the inside of the crankcase. The wires are then soldered to the feed-through terminal pins. The feed-throughs consist of two groups of nine

hermetically sealed pins. Each group is contained within a stainless steel housing. The housings locate in two holes in the top face at the rear of the crankcase and are held in position by 2-56 cap head screws. Each housing has two O-rings mounted in tandem around the body to form slip joint seals inside the crankcase.

The Hall sensors are energized by 5 Vdc via the commutation circuit; the motors are energized by 26-30 Vdc and are counter rotating. The electronic control circuit diagram is shown in Figure 21. Motor efficiency curve data is given in Appendix D.

4.16 Final Assembly Checks

Following motor alignment, the refrigerator was checked for power consumption at various stages of assembly. Typical power requirements of the refrigerator during evaluation testing are shown in Table 5.

TABLE 5

Speed rpm	dc Volts (V)	dc Current (A)	Power (Watts)	He Pressure (psig.)	Assembly Condition With Two Motors Driving
1000	28.0	0.17	4.76	0	Piston Head and Bal Seal
1000	28.0	0.40	11.2	0	Piston Head and Bal Seal and 1st Stage Displacer
1000	28.0	0.50	14.0	0	Complete Assembly
1000	28.0	0.85	23.8	56	Complete Assembly

The readings on the last line of the table were taken two minutes after starting the refrigerator. Power requirements for the refrigerator increase during the cooldown period, reaching a maximum of 30 W when the cold finger attains a temperature of 77°K at the top of the second stage. The cooldown period is influenced by the addition or reduction of mass on the cold-finger flanges. The change in mass on the cold finger will not affect the refrigerator's cold production.

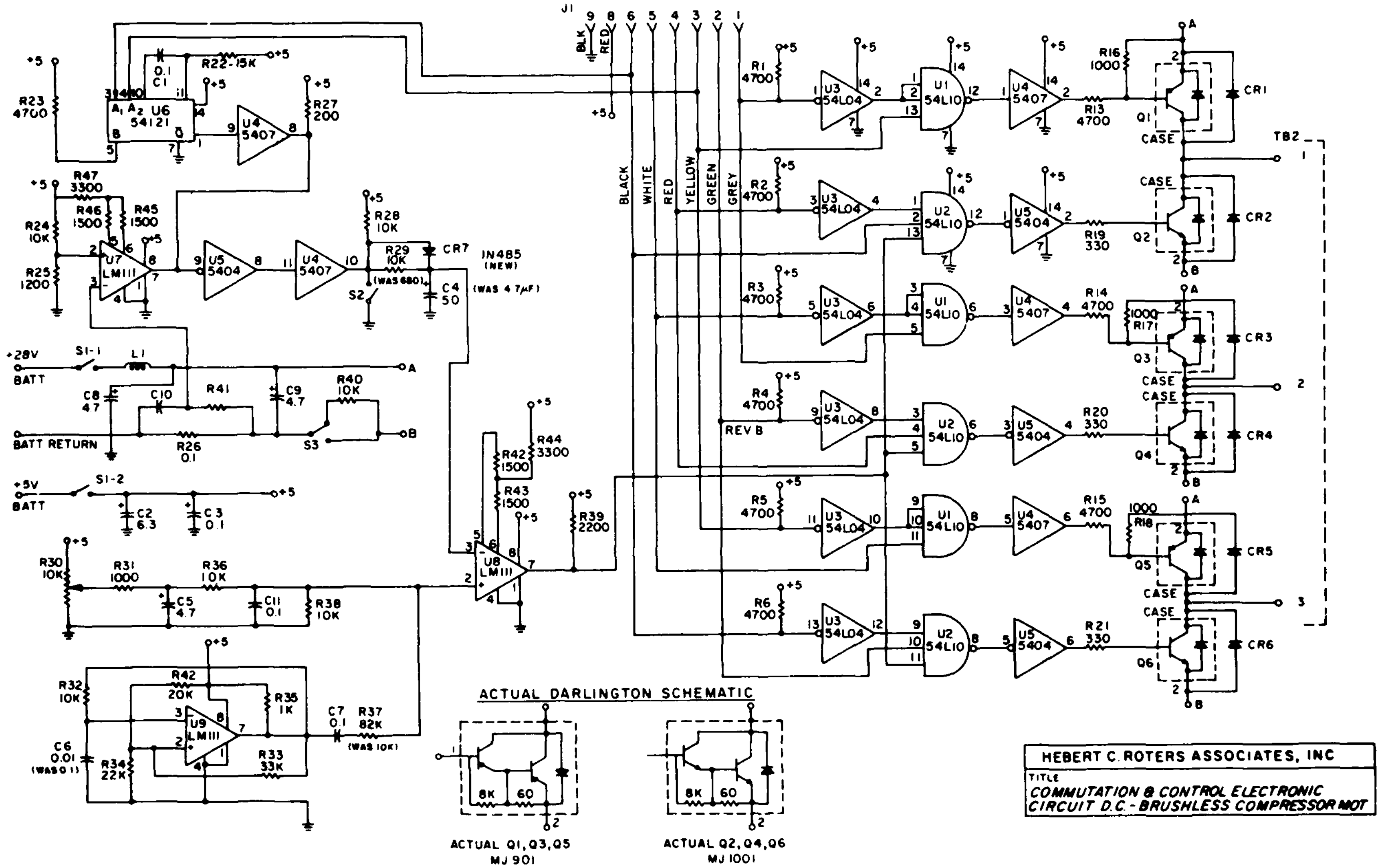

Figure 21: Schematic of drive control circuit.

5. CONTAMINATION REMOVAL METHODS

5.1 Bakeout and Purging

The refrigerator is pressurized to 70 psia of helium. To ensure that other gases such as oxygen, nitrogen, and carbon dioxide, are removed from the inside of the unit, helium is purged in and out of the cooler to remove these gases. Such action has proved successful to a point, but does not remove air which may be trapped within motor windings or porous materials. A more serious problem is the elimination of moisture from within a system. The removal of moisture and any remaining air can be accomplished by both baking and evacuating the system simultaneously; however, this method is somewhat restrictive, as some components in the cooler may be heat sensitive or may outgas and create further contamination problems. Therefore, the amount of heat applied to the refrigerator could be somewhat less than that required to vaporize any moisture. As a result, an applied temperature of 140°F combined with vacuum pumping is required over a period of days to remove the moisture.

Subsequent testing of refrigerators had indicated that the cold production remains constant for a longer period of time when a liquid nitrogen cold trap is used during purging. The helium purging procedures introduced were designed to prevent other gases from entering the system by freezing the unwanted gases inside copper coils immersed in liquid nitrogen.

Purging procedures previously used consisted of coupling a gas cylinder to the refrigerator and pressurizing to 10% above the operating pressure. The system would then be exhausted and pressurized continually for about two hours for a minimum of thirty cycles. The pressure would then be reduced to the required level and the refrigerator valve closed.

The method was improved by introducing an automatic purge system which was allowed to cycle for 24 hours. The system consisted of a timer controlling two solenoid valves. The refrigerator

was pressurized over a three minute period, held for three minutes, then exhausted over a three minute period. After the gas was exhausted, a one minute lapse occurred, before the cycle was repeated. A full single cycle was thus ten minutes.

A further improvement evolved when it became obvious that water vapor was not removed from the refrigerator using the previous methods. This was evident during disassembly of the engineering model at JHU/APL (see Section 8).

Initially, the first refrigerator was located on a hot plate and both inserted into a vacuum bell jar (Fig. 22). The temperature of the hot plate was raised to 180°F. (This temperature was later reduced to 140°F for subsequent units due to the sensitivity of the pressure transducer and strain gauge to high temperatures). The combination of heating and evacuating the system over a period of 5-7 days provided a relatively moisture-free internal condition of the refrigerator in preparation for purging. Pressure inside the bell jar reached 1.0×10^{-5} mm/Hg.

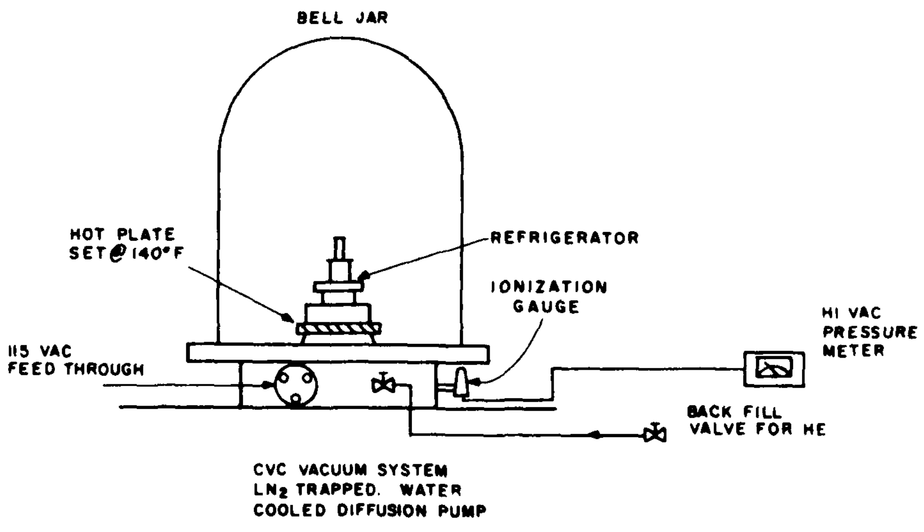

Figure 22: Setup for vacuum bakeout of refrigerator.

The unit was transferred from the bell jar to the bench for purging, with connection to the purge setup being done rapidly. The setup consisted of a sequence relay timer controlling two solenoid valves (S_1 and S_2), two copper coils of tubing, a series of hand-operated valves, and a hot plate for the refrigerator to rest on (Fig. 23). Helium from the supply cylinder was directed through the valve S, into a copper coil immersed in liquid nitrogen and into the refrigerator. The exhaust from the unit was actuated by S_1 closing and S_2 opening. The flow of gas was discharged through a second copper coil also immersed in liquid nitrogen, then via a throttle valve into a container of low vapor pressure diffusion oil. The hot plate maintained a temperature of 140°F.

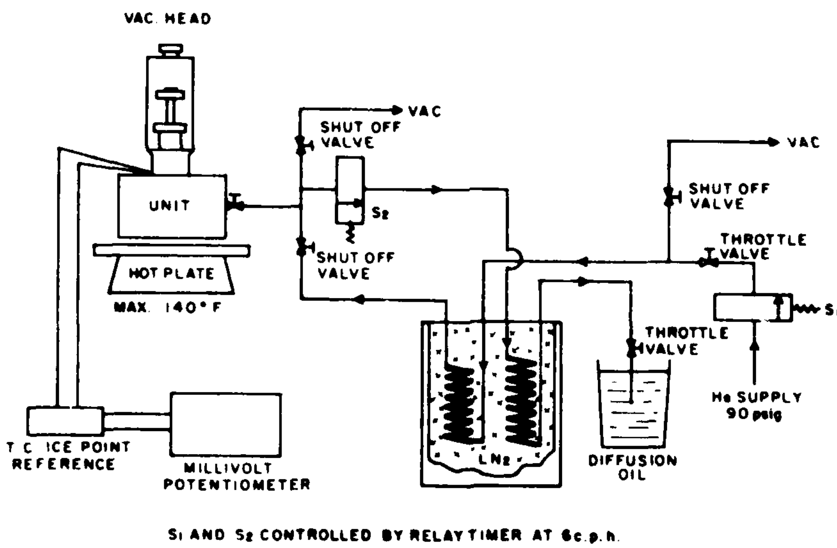

Figure 23: Schematic of setup for recharging and purging.

All lines of the purging system were purged 30 times at a pressure of 90 psia before opening the crankcase valve. This action eliminated all other gases from the system and prevent liquification or freezing within the immersed copper coils. Since equipment was not available to maintain a LN_2 level over the copper coils overnight, the automatic purging system was

de-energized each evening. The exhaust valve above the diffusion oil was closed and a vacuum pump connected to the shut-off valve nearest the unit. The vacuum dewar covering the cold finger was also evacuated so that the thin wall of the cold finger did not collapse during evacuation of the refrigerator. Each morning the shut-off valve to the vacuum system was closed, and the automatic purging system was reactivated. These procedures were repeated over several days after which the pressure was adjusted to 70 psia. The purging cycle was allowed to continue for an additional four hours to stabilize the pressure within the unit. The main shut-off valve on the refrigerator was closed after the pressurization cycle.

During the purging operation, the gas pressure was never allowed to exhaust completely before valve S_2 actuated; this was controlled by the throttle valve above the diffusion oil.

5.2 Leak Checking

Since the intended life of each refrigerator was designed to exceed 12 months, double O ring seals were incorporated in the design of each interface. These O rings were of two different materials with the purpose of minimizing the leak rate from any joint. To check the leak-rate, each refrigerator was individually placed inside a bell jar and coupled to a Veeco MS9 leak detector. By first calibrating the detector with a calibrated leak-rate cylinder giving a rate of 2.18×10^{-8} cc/sec, a check of each refrigerator was made. The maximum acceptable leak-rate was 4.5×10^{-5} Std. cc/sec.

6. PERFORMANCE TESTING

Each refrigerator was performance tested before delivery to JHU/APL. The tests were conducted at a constant temperature within an environmental chamber. The temperature of the heat exchanger flange was maintained at 113°F and monitored by a chromel/alumel thermocouple mounted on the heat exchanger flange.

The heat exchanger and vacuum dewar over the cold finger did not provide an efficient heat sink for the refrigerator; additional air-convection cooling was supplied by an electric fan directed at the heat exchanger. The fan, positioned at the opposite side of the thermocouple location, was later replaced by a water-cooled, copper conduction plate mounted to the heat exchanger flange.

The instrumentation used for each test was as follows:

TABLE 6

Qty.	Name	Mfgr.	Type or Part No.
5	DC Power Supply 0-30 V	Power Mate (or equiv.)	BP-40F
5	Digital Voltmeters 0-30 V	Data Precision	134
4	Digital Ammeters 0-2 A	Data Precision	134
1	Ice Point Reference	Kaye Inst.	K150-60
1	Millivolt Potentiometer	Leeds and Northrup	8686
1	Vacuum System	Veeco (or equiv.)	V-300
1	Pulse Counter	Fluke	1911A
3	Thermocouples	Omega	Chromel/Alumel
2	Ceramic Heater	MEPCO	1000 ohm
1	Oscilloscope	Tektronix	5103 N

Figure 24 is a block diagram of the test setup.

Before each test, the vacuum dewar was mounted over the cold finger and evacuated to a pressure of $< 1.0 \times 10^{-6}$ mm Hg. The power supplies for the sensors and drive motors were preset to 5 Vdc and 28 Vdc, respectively. To safeguard the circuit,

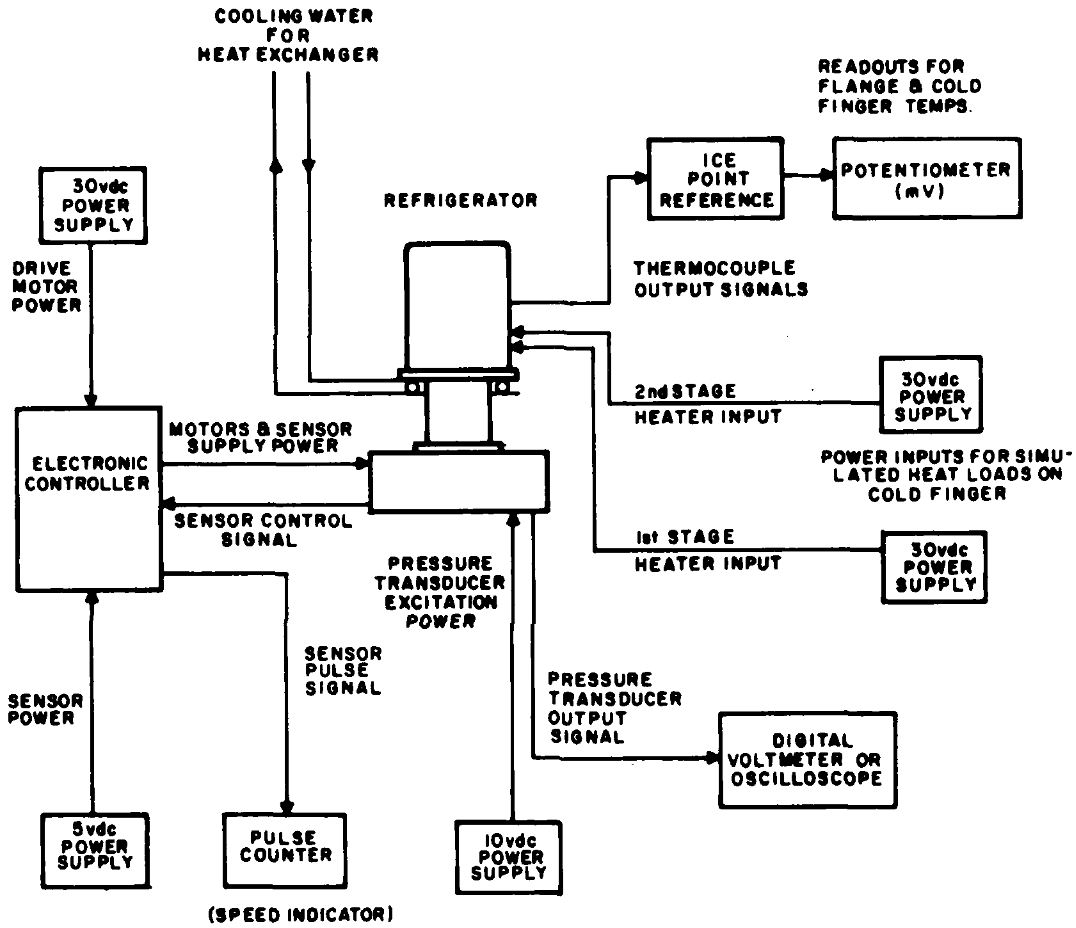

Figure 24: Block diagram of bench test setup.

the 5 Vdc supply was energized first and de-energized last. The main switch on the electronic controller was activated to start the refrigerator which was allowed to run for thirty (30) minutes before energizing the two heater power supplies. Power input to the heaters was adjusted to 1.5 W and 0.3 W for the simulated heat loads on the first and second stages of the cold finger. The output temperatures were monitored by thermocouples mounted on the first and second stage flanges of the cold finger. Temperature readings were shown in mV on a potentiometer and converted to degrees Kelvin. Heat rejection at the heat exchanger flange was maintained at 113°F by a supply of cooling water flowing through a copper tube mounted on a plate secured to the flange. Operating speed of the refrigerators was set at 1000 rpm and monitored by a pulse counter coupled into the sensor circuit.

The performance map supplied by JHU/APL for engineering model S/N 1 is shown in Figure 25; the performance maps for the remaining refrigerators (S/N 2-6) are shown in Figures 26 through 30.

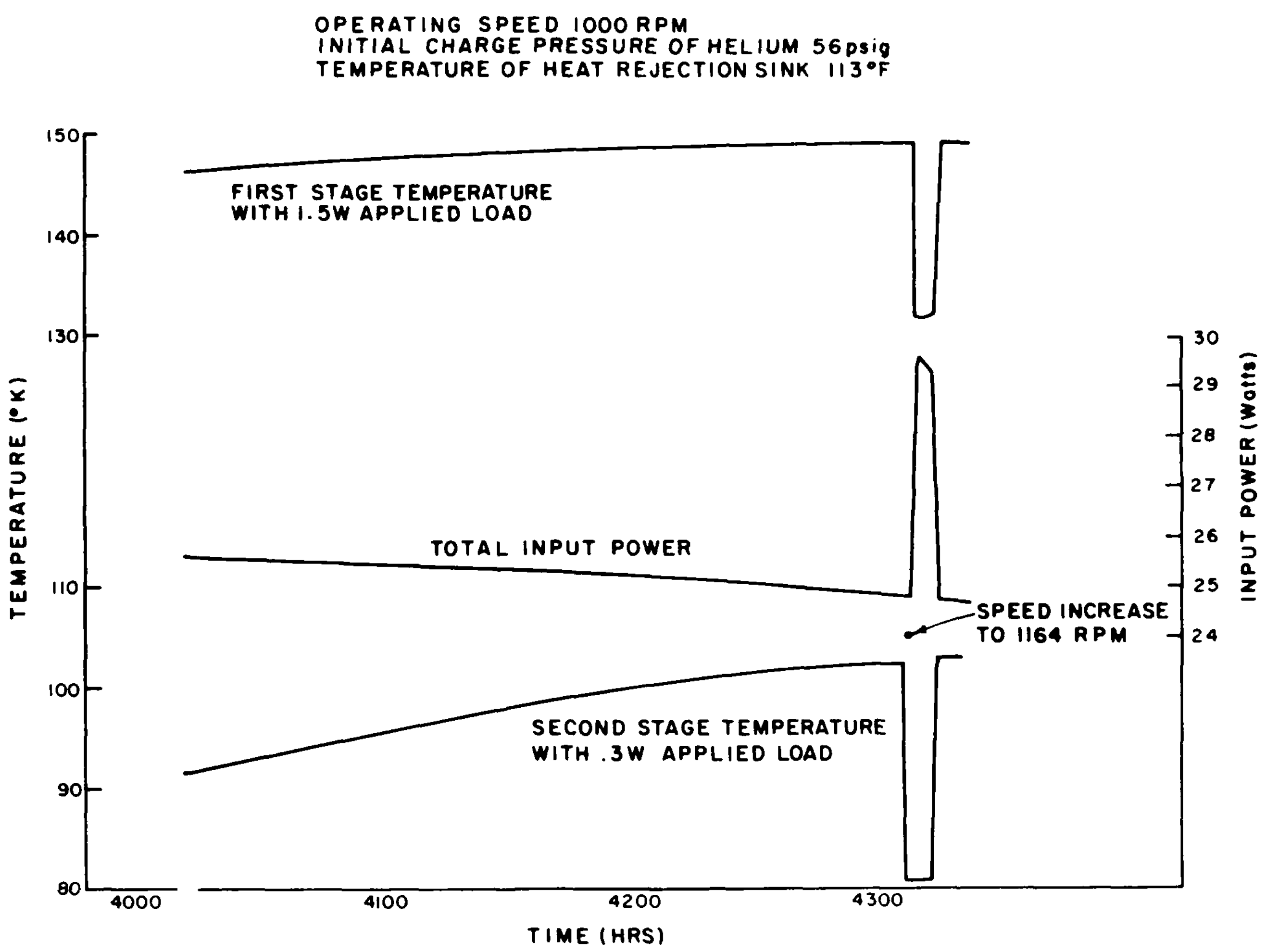

Figure 25: Performance map S/N 1.

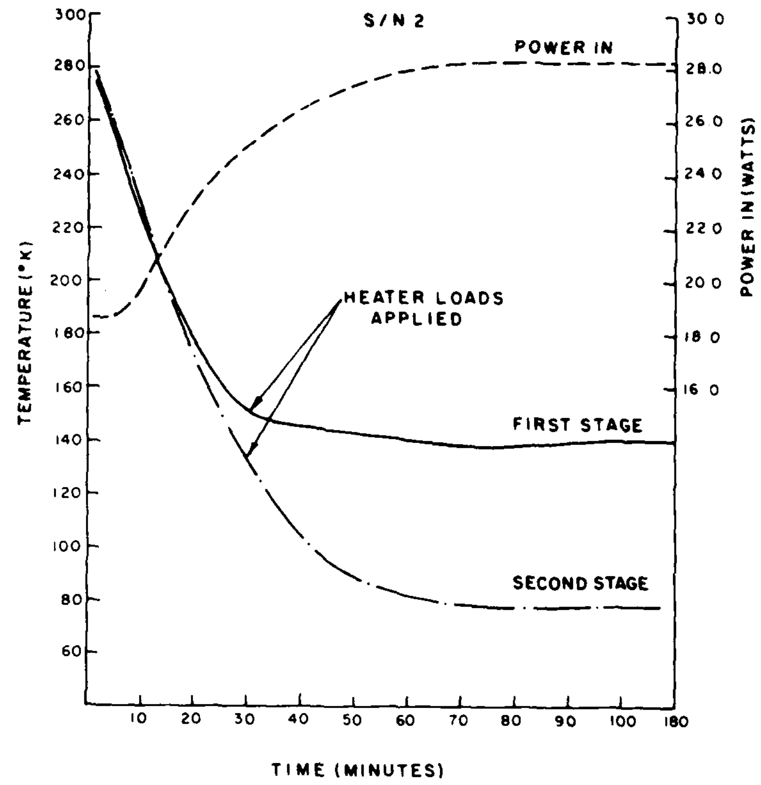

Pertinent Cooldown and Cold Production Data for S/N 2*

Time (Min)	1st. Stage °K	Load (W)	2nd Stage °K	Load (W)	P_{in} (W)	Heat Reject. Temp. (°F)
02	277	0	278	0	20.16	72
20	140	0	170	0	23.24	85
60	140	1.5	83	0.3	28.00	110
180	140	1.5	79	0.3	28.28	113

He charge pressure 56 psig
Speed 1000 rpm
Ambient 72°F

Figure 26: Performance map of S/N 2.

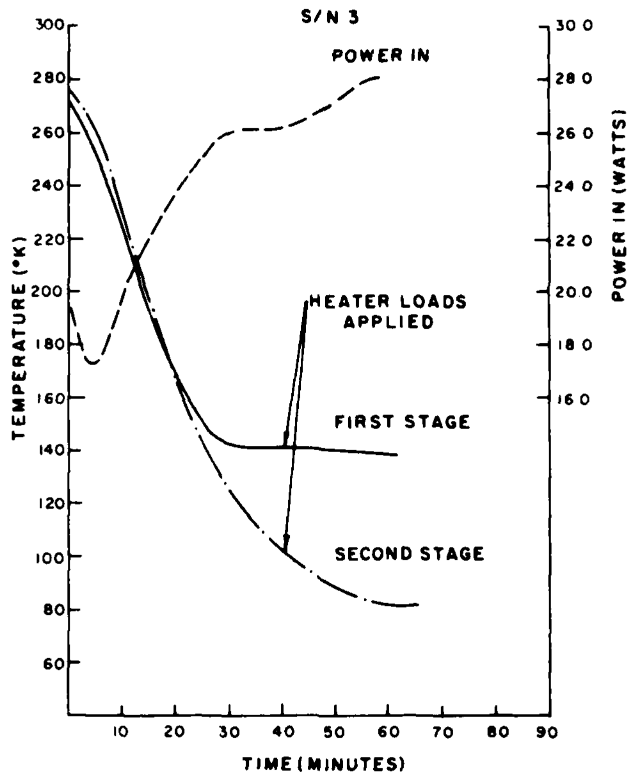

Pertinent Cooldown and Cold Production Data for S/N 3*

Time (Min)	1st. Stage °K	Load (W)	2nd Stage °K	Load (W)	P_{in} (W)	Heat Reject. Temp. (°F)
02	270	0	276	0	19.32	74
20	175	0	168	0	23.24	90
60	139	1.5	81	0.3	28.28	113

* He charge pressure	56 psig
Speed	1000 rpm
Ambient	72°F

Figure 27: Performance map S/N 3.

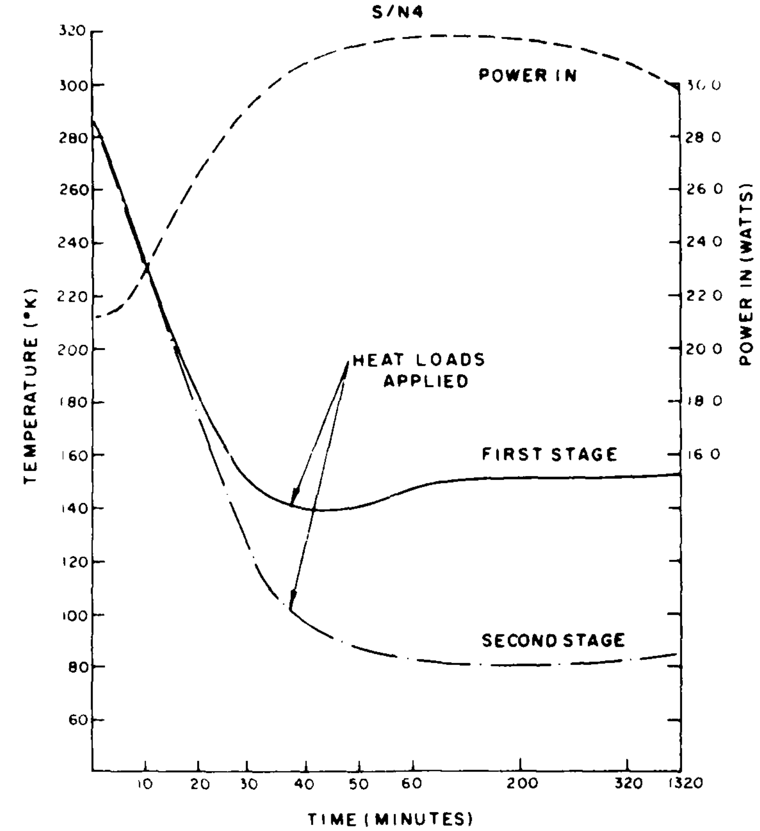

Pertinent Cooldown and Cold Production Data for S/N 4*

Time (Min)	1st Stage (°K)	Load (W)	2nd Stage (°K)	Load (W)	P_{in} (W)	Heat Reject. Temp. (°F)
02	280	0	283	0	21.28	--
20	183	0	171	0	26.60	--
60	144	1.5	81	0.3	31.64	113
300	147	1.5	80	0.3	30.8	113

* He charge pressure 56 psig
Speed 1000 rpm
Ambient 72°F
Leak Rate 3.4×10^{-5} cc/sec

Figure 28: Performance map S/N 4.

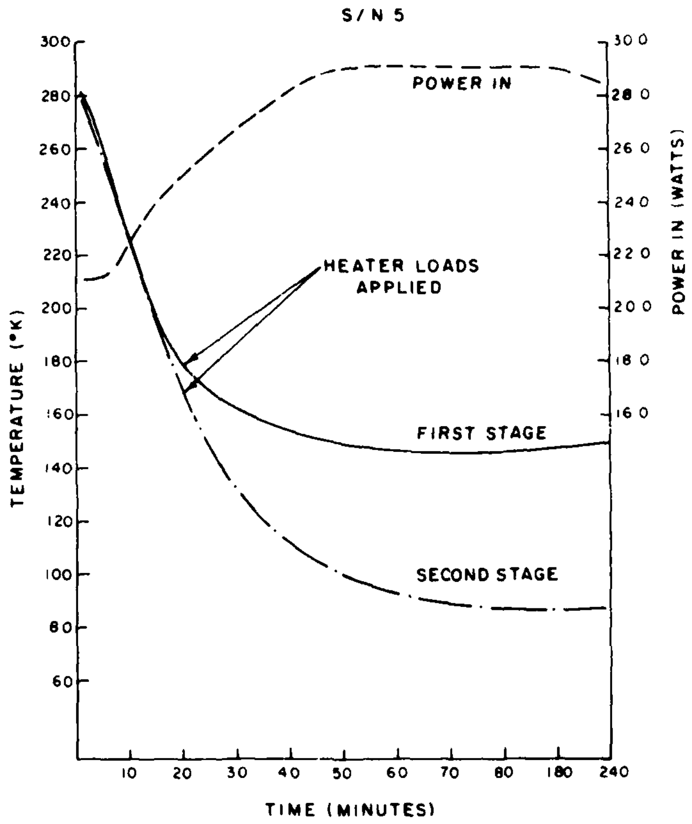

Pertinent Cooldown and Cold Production Data for S/N 5*

Time (Min)	1st Stage (°K)	Load (W)	2nd Stage (°K)	Load (W)	P_{in} (W)	Heat Reject. Temp. °F
02	280	0	278	0	21.28	--
20	179	0	170	0	25.20	95
60	149	1.5	100	0.3	29.96	121
180	147	1.5	81	0.3	28.84	113

* He charge pressure 56 psig
Speed 1000 rpm
Ambient 72°F

Figure 29: Performance map S/N 5.

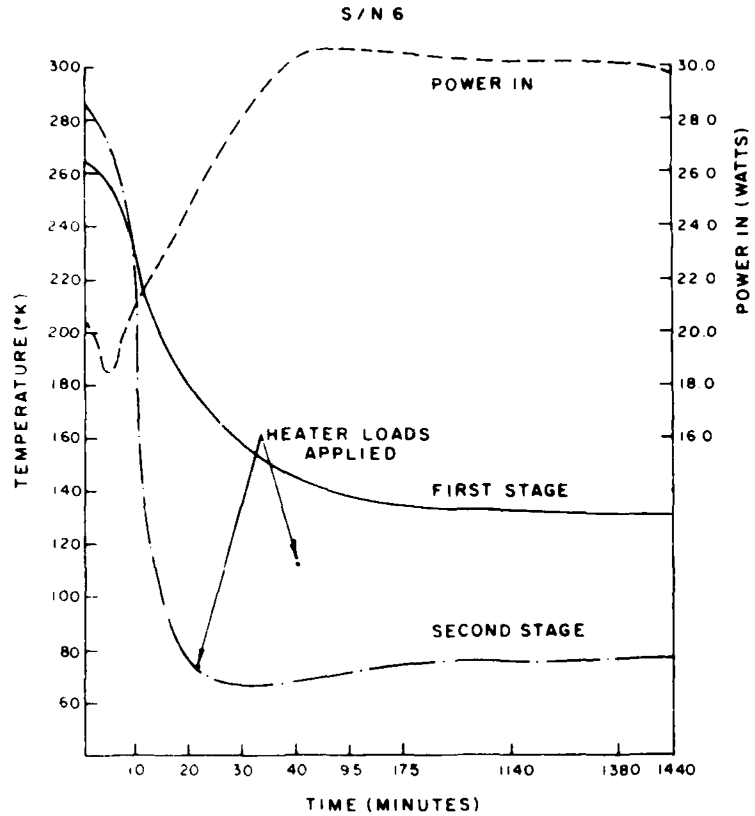

Pertinent Cooldown and Cold Production Data for S/N 6*

Time (Min)	1st Stage (°K)	Load (W)	2nd Stage (°K)	Load (W)	P_{in} (W)	Heat Reject. Temp. (°F)
2	278	0	280	0	26.04	--
120	128	1.5	77	0.3	29.96	113

* He pressure 62 psig
Speed 1000 rpm
Ambient 72°F
Leak Rate 3.174×10^{-5} cc/sec

Figure 30: Performance map S/N 6.

7. VIBRATION AND NOISE LEVEL TESTING

Three qualification tests were performed to determine: (1) the effect of vibration on the refrigerator, (2) how much displacement of the second-stage cold spot was generated by operation, (3) what was the acoustic noise level of the refrigerator while in operation.

The first test was conducted at JHU/APL using S/N 1 as the test subject. The refrigerator was subjected to random vibrations for a period of two minutes for each of the three axis.

The second and third tests were performed at Philips Laboratories using refrigerator S/N 4 as the test subject. Displacement of the cold spot was measured for each of the three axis.

Acoustic data was taken in a room about 25' x 25' x 10' with a 40 dB ambient. Using a General Radio sound level meter with a Type 1560-P5 microphone, measurements were taken at various distances from three feet to twenty feet.

7.1 Vibration Tests

Severe random vibration tests were conducted at JHU/APL on S/N 1 on Sept. 3, 1975 to determine if the refrigerator was capable of withstanding the vibrations which accompany the launching of satellite vehicles.

After one minute of random vibration at the acceptance level, a crack appeared at the base of the cold finger. This test was conducted 3 dB below the qualification power spectral density level (PSD) (i.e., 14.6 g rms) and for 1/2 the time duration. The observed fracture was a circumferential crack about 3/4 inch above the base of the cold-finger first stage (see Fig. 31).

Following the failure of the cold finger it was subjected to metallurgical examination after it was sectioned through the

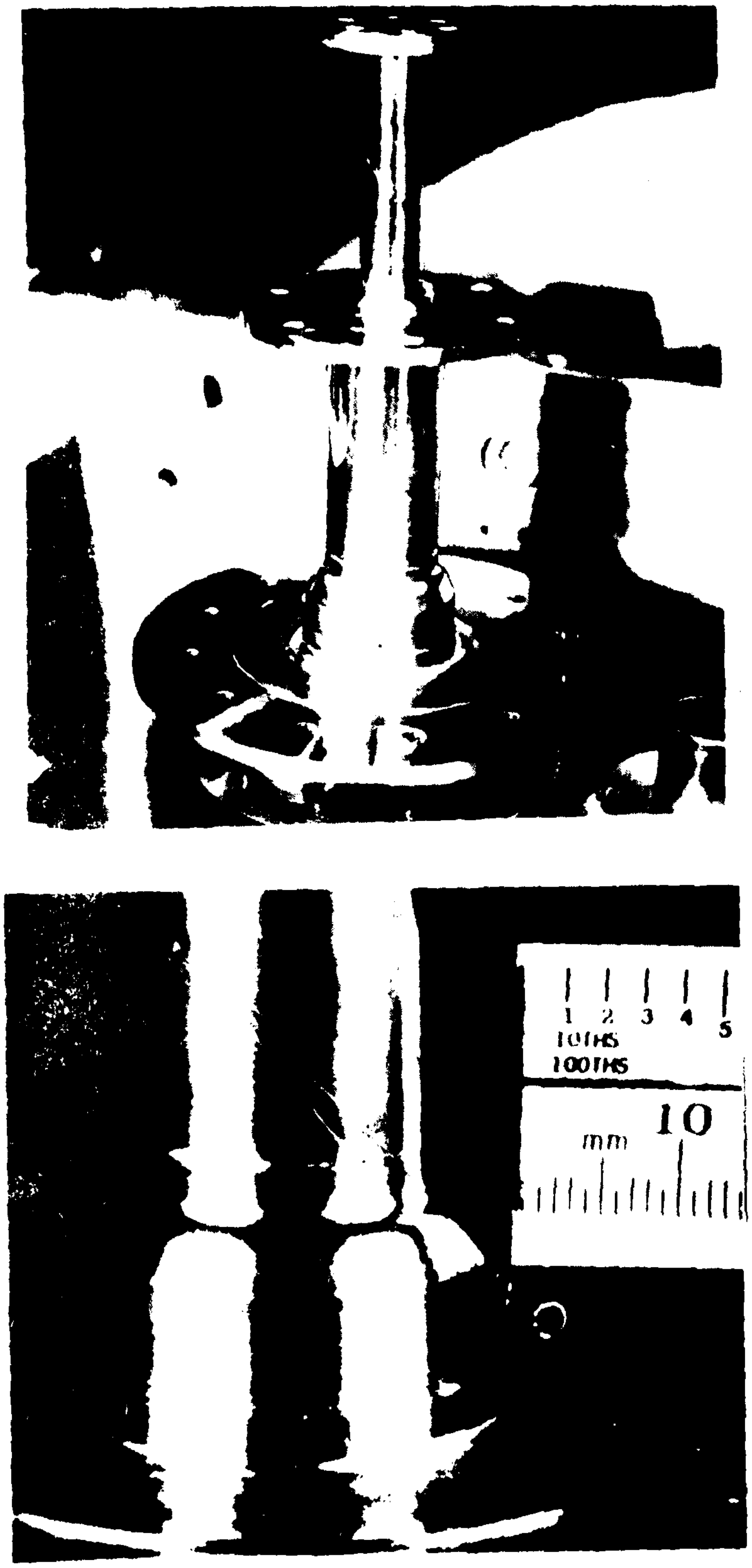

(a)

(b)

Figure 31: Fractured cold finger.

ruptured area as shown in Figure 32. The edges of the rupture are shown in Figure 32b at 30X and again in Figure 33 at 400X.

The examination did not indicate any microstructural abnormalities in the titanium alloy, and the microcracks immediately adjacent to the broken edges are believed to be a part of the microstructure rather than the cause of the failure.

Using refrigerator S/N 2, APL ran vibration surveys on Sept. 9, 1975. These surveys consisted of sweep sinusoidal vibration tests at 0.5 g input. For the first set of surveys, the control accelerometer was located in the same position as the flight acceptance random vibration tests. The resonance of the support fixture is 880 Hz. In addition to the 880 Hz fixture resonance, there are resonant frequencies of the cold finger at about 380 Hz and 1000 Hz. Later vibration surveys which decoupled the fixture verified an unloaded fixture resonance of 880 Hz and the cold finger cantilever modes at 380 Hz and 1000 Hz. The cantilever modes had gains of about 40.

A preliminary analysis of stress level at the base of the cold finger during the flight acceptance tests was inconclusive due to the close spacing between the 880 Hz fixture mode and the 1000 Hz cantilever mode.

If one assumes no amplification from the fixture, a bending stress of 49,000 psi can be generated by linearly summing a three-sigma response of the 380 Hz mode with a mean (=) response of the 1000 Hz mode. When extrapolated to qualification levels, bending stresses of 70,000 psi could result. The yield strength of the 5Al-2.5Sn titanium alloy is 117,000 psi. When one considers possible reduction in strength of the material due to fatigue, and also considers increase stresses due to stress concentration, the design becomes suspect. Philips had originally calculated a safety factor of about 3 for the titanium column at the qualification level, using a simple cantilever mode analysis.

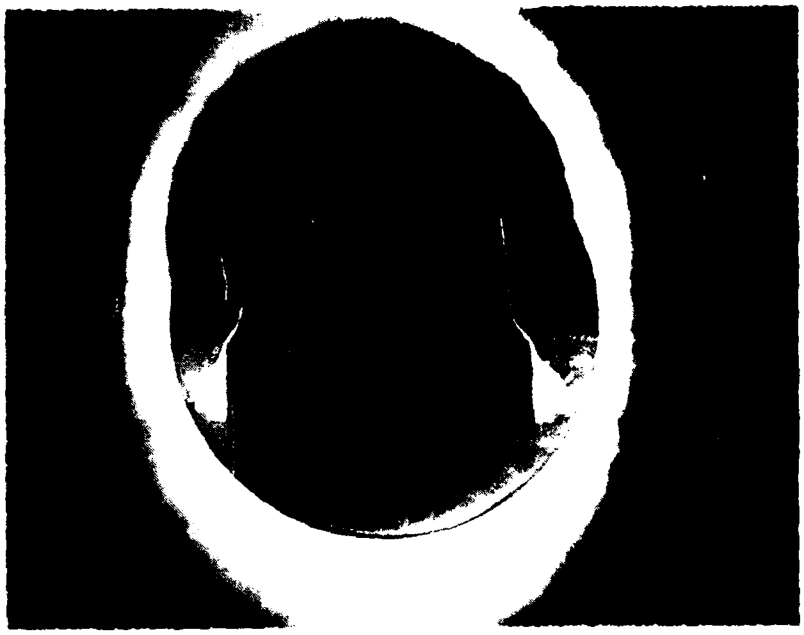

(a) Mag. 2X

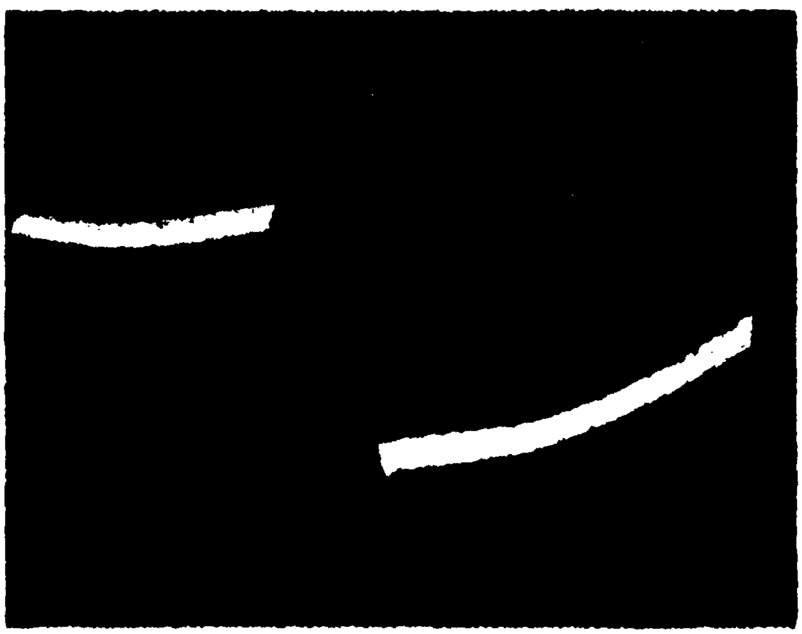

(b) Mag. 30X

Figure [illegible]2: Fractured cold finger (Mag. 2X, 30X).

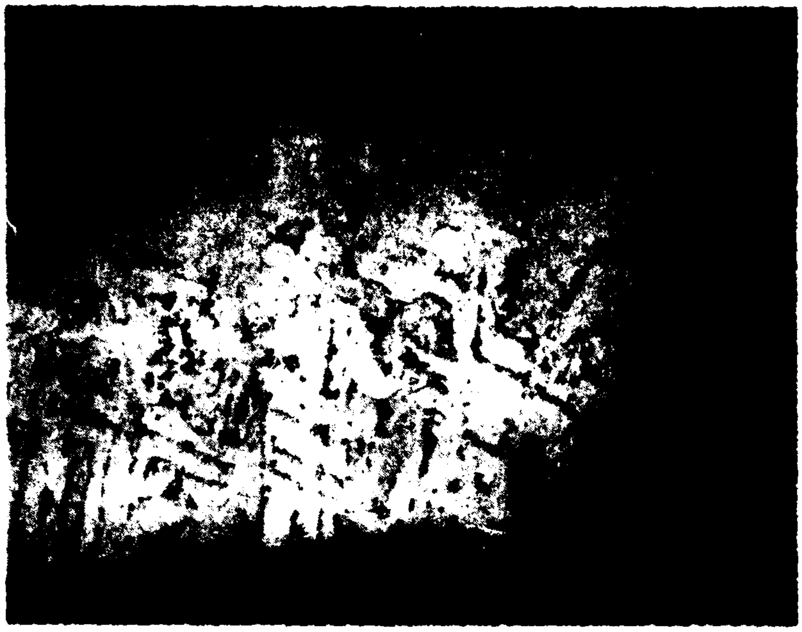

(a) View 1

(b) View 2

Figure 33: Fractured cold finger (Mag. 400X).

The random vibration environment that the cold finger of refrigerator S/N 2 survived is shown in Figure 34.

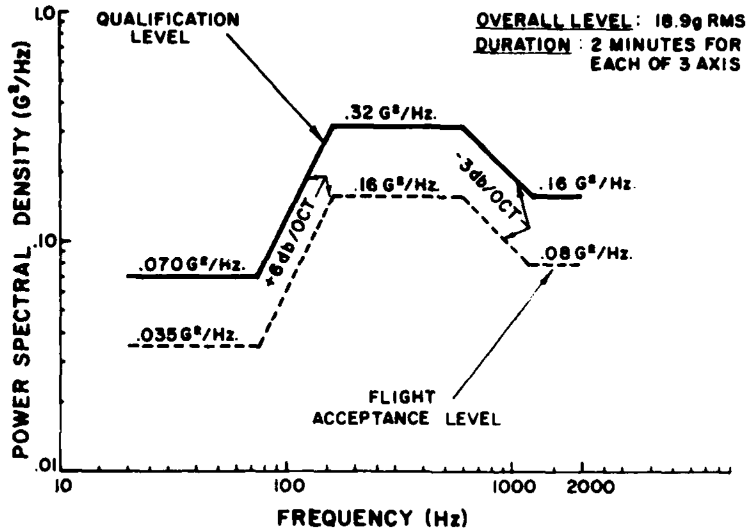

Figure 34: Random vibration input to S/N 2 cold finger.

7.2 Noise Level Measurements and Displacement

Vibration displacement measurements were conducted using S/N 4 as the test subject. The instrumentation consisted of a Bentley Nevada proximity probe mounted to within 0.005" of the top of the cold finger (y plane). Two other readings were taken at the periphery of the top flange of the cold finger. Direct readout was provided by coupling the proximeter output directly into an oscilloscope and measuring the amplitude of the y sine wave created by displacement. This test indicated movement greater than 0.005" in all directions. To verify these figures, the proximity probe was replaced by an accelerometer which indicated readings of between 0.000125" and 0.00015" with the unit running at 1000 rpm. Since both measurements were questionable, further tests were postponed until reliable instrumentation was available. This was later achieved by using a Fotonic sensor.

The noise level was measured by placing an operating unit in the center of a room which had a background noise level of 40 dB; readings were taken of the refrigerator at distances of 3, 5, 10, 15 and 20 ft (see Fig. 35).

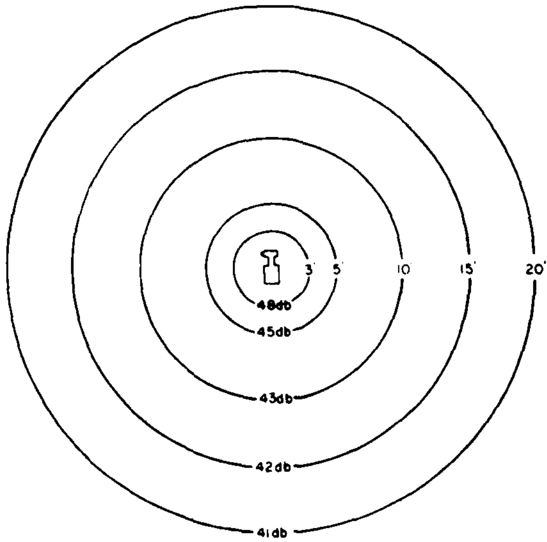

Figure 35: Schematic of noise levels for S/N 4.

Specifications allowed a maximum displacement of the cold finger of 0.0004" in any direction with the refrigerator in operation. To measure this displacement, a Fotonic sensor was mounted on an independent surface with the sensor probe suspended in close proximity to the top of the 2nd stage of the cold finger.

The instrument used, a product of MTI, had a flexible probe consisting of two sets of fiber optics jacketed together to form a single unit. One set of filaments transmited light from the Fotonic control unit to a target surface, i.e., in this case the topmost flange of the cold finger; the other set received the light reflected from the surface of the object and conducted it back to the control unit where it was converted to an electrical signal proportional to the amount of reflected light. Various patterns of transmit/receive filaments can be used for different applications (see Fig. 36).

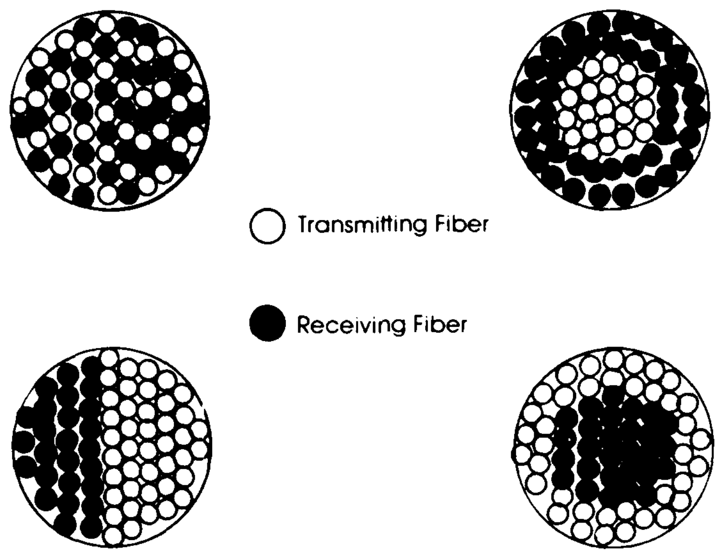

Figure 36: Fotonic sensor fibers.

To obtain a graphic record of the waveform produced by deflection, the rear output jack of the control unit was coupled to an oscilloscope while the fiber sensor was calibrated at a distance of 0.005" from the cold finger. The basic sensitivity of the probe was 1 in/mV. To determine erroneous readings, the first trace on the oscilloscope (Fig. 37) showed background noise without the unit running. Fiber distribution in the sensor probe is random placement, with the probe diameter 0.109" and each fiber diameter 0.0025".

The first measurement was taken off the top periphery of the cold finger (x plane), giving a displacement of 0.00016". Vertical displacement (y plane) showed 0.00032" and the front-to-rear movement (z plane) indicated 0.00016". Tests to determine how much of this displacement was due to movement of the unit, and how much was due to cold-finger pulsing from pressure variations within the cold finger were not conducted since the readings fell within specifications.

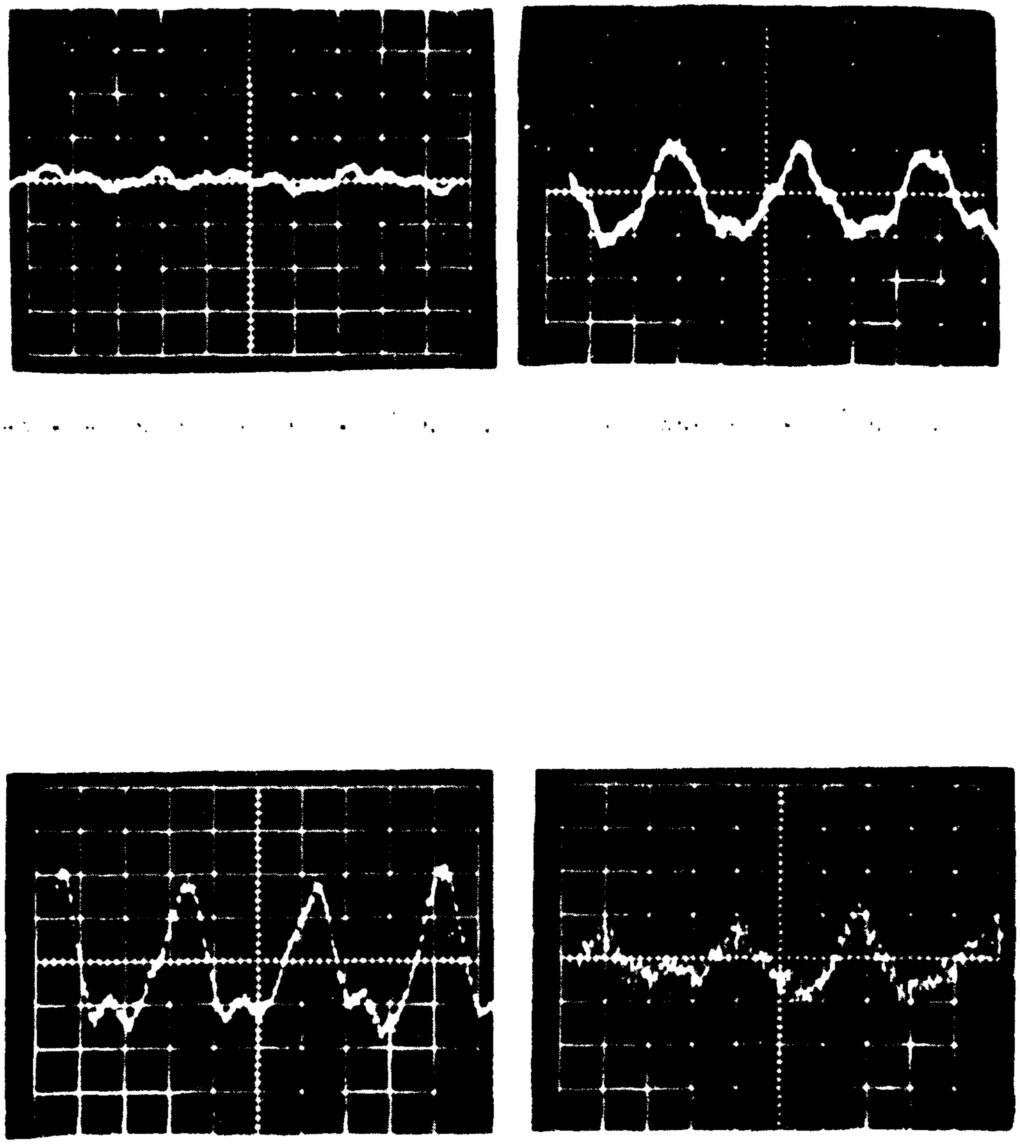

Figure 37: Vibration levels for S N 4.

8. PROBLEMS AND SOLUTIONS

The various problems, and their solutions, encountered during assembly and running-in of the refrigerators are summarized in the following paragraphs.

S/N 1

To establish a life expectancy of the refrigerator, this unit was supplied to JHU/APL for evaluation (Ref. JHU Progress Test Report for S/N 1 Performance QM-76-041, April 14, 1976). Initial testing gave no indication that major problems would arise after a short period (1000 hrs). After this time, a steady rise of both temperatures at the cold finger suggested a number of possibilities, viz., second-stage seal separation from the regenerator; failure of the displacer rod seal in the piston; collapse of the piston Bal-seal; collapse of the 1st stage regenerator Bal-seal; gear slippage on the crankshaft creating a timing problem or angular shift in the displacer rod in relation to the piston rod; contamination.

Examination of the displacers showed excessive debris had accumulated at the top of the first-stage displacer and further debris extended up the wall of the second stage displacer, with severe rubbing marks on the second stage seal (Fig. 38). To identify the source of the debris, samples were removed from the outer walls of the displacers (referred as Reg. Test #1) and also from inside the cold finger (referred as Finger Test #2). These samples along with the four known substances used within the refrigerator, i.e., Krytox grease, Rulon, Nema, Bal-seal, were submitted for infrared spectroscopy to Spectrochem Laboratories, Inc. of New Jersey. The results of testing the two unknown samples were: Reg. Test #1 was found to contain 33% by weight Rulon, 33% by weight Bal-seal, 34% by weight an ammonium compound. Finger Test #2 contained the Telfon from of the Bal-seal. It was concluded that frozen droplets of moisture were responsible for initiating the debris.

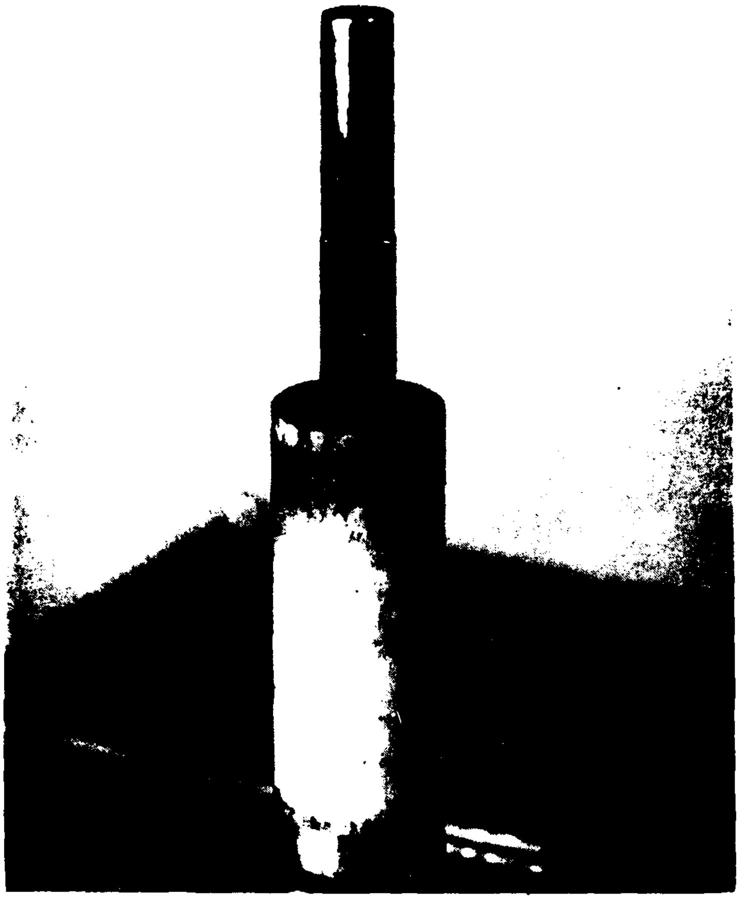

Figure 38: Displacers of S/N 1.

Extensive cleaning of both regenerators did not improve the poor performance of the second stage regenerator; this was subsequently replaced. Performance improved to an acceptable level whereby the unit was again put on life test at APL when a second performance failure occurred on July 28, 1976.

Since the unit was still producing cold in the cryogenic range, it seemed unlikely that moisture inside the unit would be the cause; however, upon removing the cold finger to expose the regenerators, droplets of moisture were observed on the regenerators and on the inner walls of the cold finger. The cause of this amount of moisture was attributed to high humidity in the assembly area when the unit was assembled. Consequently, further evaluation of purging procedures was necessary.

S/N 2

The random vibration tests conducted at JHU/APL on refrigerator S/N 1, and the subsequent effect on the cold finger, resulted in the reduction of the copper flanges on all remaining cold fingers. During machining of the cold finger flanges on S/N 2, the 2nd stage seal area in the cold finger relaxed slightly (estimated at about 0.0002"). This was sufficient to affect the fit of the 2nd stage displacer seal within the finger. A new seal was fitted to the regenerator and machined to suit the cold finger bore. The effect on the remaining cold fingers and displacer seals was negligible since the seals still required finish machining.

S/N 3

The first indication of problems with the displacer rods arose during the running-in period of the piston Bal seal. The piston and Bal seal were fitted to the piston rod, and the extension displacer had been screwed onto the displacer rod. The intended 24 hr running-in period was terminated when the thread holding the extension displacer sheared. Examination of the remaining displacer rods showed that, as a result of quenching the rods after heat treatment, the threads at each end of the rods bent away from the centerline of the rod. The problem was corrected by counter boring the base of the extension displacer and inserting a steel sleeve for locating the top shoulder of the displacer rod. To allow the sleeve bore and the rod shoulder to align correctly, the thread on the top of the displacer rod was eased.

S/N 4

The extension displacer was modified as with S/N 3. Testing of this refrigerator was halted when JHU/APL indicated that the performance of refrigerator S/N 1 was failing. Inspection of S/N 1 revealed moisture within the refrigerator. This discovery

prompted a review of the purging procedures with modifications to the purging hardware (see Section 5). The new purging procedure was applied to S/N 4 before restarting the test.

S/N 5

Alignment of the extension displacer with the displacer rod was again a problem as with S/N 3 and S/N 4. A steel sleeve was inserted in the base of the extension displacer to provide location for the displacer rod (see also S/N 6).

S/N 6

The alignment problem between the displacer rod and the extension displacer was eliminated with a displacer rod having ground threads. The threads were ground into the ends of the displacer rod after heat treatment of the rod.

As a result of the comparative ease of completing alignment between the displacer rod and the extension displacer in S/N 6, S/N 5 was retrofitted with a new rod with ground threads. The alignment between the displacer rod and the extension displacer in S/N 5 was accomplished without any trouble.

The location of the 1st stage displacer Bal-seal was machined to maximum tolerance. The result was excessive friction between the seal and the seal area inside the finger (an extra 8.5 W of input power was required). The seal-location diameter was reduced by 0.005", and input power fell below 28 W. Combined with the reduction of input power was a loss of performance. Thorough examination of component parts, including displacer X-ray, showed no evidence of a fault within construction. The working gas pressure of the refrigerator was increased to 76 psia, and performance returned to an acceptable level with a power requirement of 29.96 W for a cold production of 0.3 W at 77°K on the second stage of the cold finger.

The inside faces of both crankcase coverplates were covered with discs of "Corning Thirsty Vycor". The discs were to act as moisture collectors in a further effort to reduce any moisture which might affect the refrigerator performance. The effectiveness of the discs was uncertain, and when the pressure transducer within the crankcase failed and had to be replaced, the coverplates containing the discs were discarded and new plates (less the discs) were fitted to the crankcase.

9. CONCLUSIONS

The objective of this program to develop, fabricate and deliver six (6) long-life, maintenance-free, Stirling-cycle refrigerators was accomplished. Except for weight, which was exceeded by 1.8 lbs, all specifications were met or bettered. The engineering model at JHU/APL was successfully life-tested for one (1) year.

10. RECOMMENDATIONS

a. Avoid soft or potentially porous materials for the outer envelope. Reduce the number of interface joints which contain seals, and replace by welded seams.

b. Eliminate elastomer seals and replace with metal seal rings at interfaces where weld joints are impractical.

c. Reposition dc stator windings outside the crankcase to minimize potential contamination entrapment areas and to reduce the number of feed-throughs.

d. Modify the interfaces between displacers to eliminate alignment problems.

e. Investigate unsupported metal bellows for extending life expectancy of the refrigerator.

f. Further develop balancing procedures, with the possibility of using a more-sensitive dynamic balancing machine.

APPENDIX A

BASIC THEORY OF THE STIRLING-CYCLE REFRIGERATOR

In this section a brief outline of the basic principles of the Stirling cycle is presented.[1,2] From an elementary theory the general properties of the cycle will be derived with a discussion of the most important losses. It should be noted that the presentation is essentially taken from Part Two of reference 1. For a more extensive treatment of the subject reference should be made to the original paper[3].

Fundamental Cycle

In the ideal Stirling cycle, the cold is produced by the reversible expansion of a gas. The gas performs a closed cycle, during which it is alternately compressed at ambient temperature in a compression space and expanded at the desired low temperature in an expansion space, thereby reciprocating between these spaces through one connecting duct, wherein a regenerator provides for the heat exchange between the outgoing and the returning gas flow. Figure 1 shows stages in carrying out the ideal cycle.

In this diagram, A is a cylinder, closed by the piston B, and containing a nearly perfect gas. A second piston, the displacer C, divides the cylinder into two spaces, D at room temperature and E at the low temperature, connected by the annular passage F. This passage contains the regenerator G, a porous mass with a high heat capacity; the temperature in the passage is shown in the graph. The cycle, consisting of four phases, runs as follows:

I Compression in space D by the piston B; the heat of compression is discharged through the cooler H.

---

1 Dr. J. W. L. Köhler "The Gas Refrigerating Machine and Its Position in Cryogenic Technique," Progress in Cryogenics 2, 41-67 (1960) London, Heywood and Company Ltd.

2 A. Daniels, "Cryogenics for Electro-Optical Systems," Electro-Optical Systems Design, vol. 3, pp. 12-20, July 1971.

3 J. W. L. Köhler and C. O. Jonkers, Philips Tech Rev. 16 69-78, 105-115 (1954)

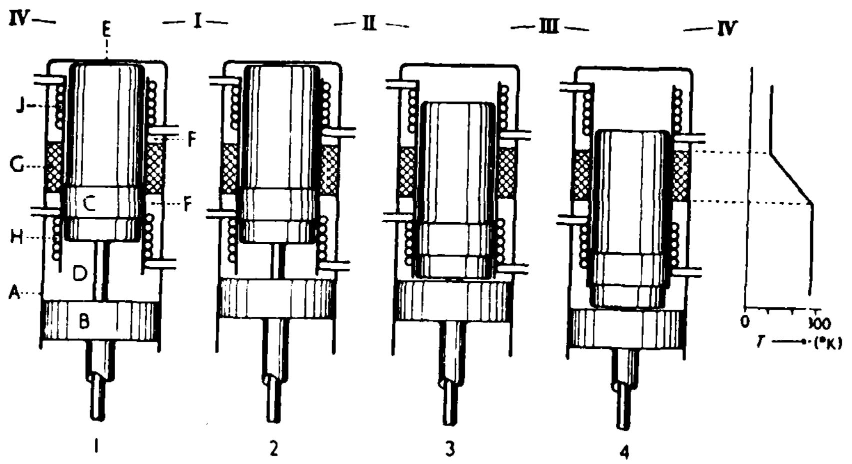

Figure 1. *The ideal Stirling cycle. The Figure shows the different positions 1–4, according to Figure 2. I–IV refer to the four phases of the cycle. The graph on the right shows the temperature distribution in the machine*

II Transfer of the gas through the regenerator to space E by movement of the displacer. The gas is reversibly cooled down in the regenerator, the heat of the gas being stored in the regenerator mass.

III Expansion in the cold space by the combined movement of the piston and the displacer; the cold produced is discharged through the freezer J, and utilized.

IV Return of the gas to space D; thereby the gas is reheated, the heat stored in the regenerator being restored to the gas.

With no regenerator present the gas flowing to the expansion space would arrive there at ambient temperature, whereas the returning gas would arrive in the compression space at the low temperature; this effect would cause such a tremendous cold loss that the whole process would become futile. In an ideal regenerator, a temperature gradient is established in the direction of the gas flow. This causes the gas to be cooled down reversibly, so that it arrives in the expansion space with the temperature prevailing there.

Figure 2 shows the p-V diagram of this schematic cycle, neglecting the dead space. It consists of two isotherms and two isochores; at T_C (compression temperature) the amount of heat Q_C is rejected, at T_E (expansion temperature) the amount of heat Q_E is absorbed.

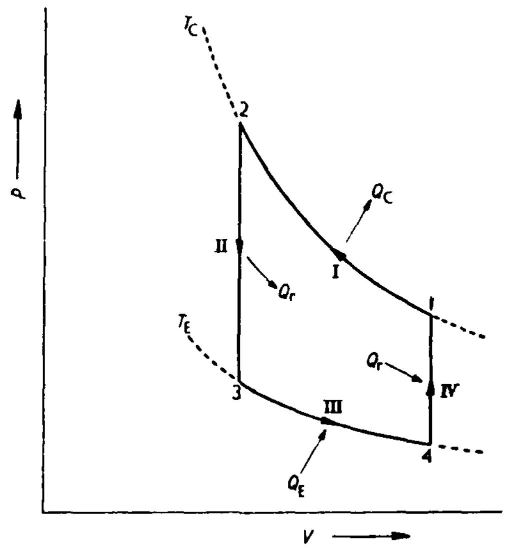

Figure 2. p–V *diagram of the ideal cycle between the temperatures* T_C *and* T_E*, where the amounts of heat* Q_C *and* Q_E *are discharged and absorbed, respectively. The heat* Q_r*, rejected in phase II, is stored in the regenerator and absorbed in phase IV*

Actually, the discontinuous movement of the pistons is difficult to achieve. In practice, the pistons are actuated by a crank mechanism and are thus moving harmonically; for the machine to act as a refrigerator, the expansion space E (Figure 1) has to lead in phase with respect to the compression space D. The harmonic motion and the volume of the heat exchangers (the so-called 'dead space') cause the four phases of the cycle to merge somewhat, so that they cannot be distinguished very well; the gas is not exclusively compressed in the compression space, but also in the expansion space, and the same holds for the expansion. It can be shown however that the difference in output between the discontinuous and the harmonic process is only a few percent.

The fundamental cycle is explained here with the help of the displacer machine. The reason is that actual machines are also of this type. It will be obvious, however, that the cycle may be described more generally by two synchronously changing volumes interconnected by a cooler, a regenerator, and a freezer, whereby the volume that is leading in phase becomes the expansion space wherein the cold is produced. Formulae for the pressure variation, the refrigerating capacity, and the shaft power for this general case will be given in the next section.

Performance of the Ideal (Isothermal) Cycle

In the ideal machine, the thermal contact in the heat exchangers is assumed to be perfect, so that the gas temperature there is equal to the temperature of the walls; the same temperature is supposed to prevail in the adjoining cylinders, which temperatures thus are constant with time. The regenerator is also assumed to be perfect, so that no regeneration loss occurs and the gas temperature there is also constant with time. The working fluid is supposed to be a nearly perfect gas; this condition can be met sufficiently by using hydrogen or helium in practice.

(1) Pressure variation. For the expansion space V_E (temperature T_E) and the compression space V_C (temperature T_C) we write

$$\left.\begin{aligned} V_E &= \frac{1}{2} V_0(1 + \cos\alpha) \\ V_C &= \frac{1}{2} wV_0[1 + \cos(\alpha-\phi)] \end{aligned}\right\} \qquad (1)$$

where V_0 is the maximum volume of the expansion space, w the ratio of the swept volumes of the compression and the expansion space, and ϕ the phase difference between these spaces; the crank angle α (= 0 for $V_E = V_{max}$) changes linearly with time ($\alpha = \omega t$). The volumes of the freezer, the regenerator, and the cooler, which form the connecting channel (the dead space), will be indicated by V_S with the corresponding temperature T_S. The variation of the pressure p with time (or α) now follows from the condition that the mass of the system as a whole is constant:

$$\frac{M}{R}p\left[\frac{V_E}{T_E}+\frac{V_C}{T_C}+\sum\frac{V_s}{T_s}\right] = \text{constant} = C.\frac{M}{R}\frac{V_0}{2T_C}$$

where M is the molecular weight of the gas, R is the gas constant, and C is a constant. After introduction of V_E and V_C from equation (1) and of the symbols

$$\tau = \frac{T_C}{T_E}, \quad \text{the temperature ratio}$$

and

$$s = \sum\frac{V_s}{V_0}.\frac{T_C}{T_s}, \quad \text{the total dead space}$$

(reduced to the swept volume of the expansion space V_0 and normalized to the temperature of the compression space T_C), this reduces to

$$\frac{C}{p} = \tau\cos\alpha + w\cos(\alpha-\phi)+\tau+w+2s$$

This expression is easily transformed into

$$\frac{C}{p} = A\cos(\alpha-\theta)+B = B[1+\delta\cos(\alpha-\theta)]$$

with the abbreviations

$$A = \sqrt{(\tau^2+w^2+2\tau w\cos\phi)}; \qquad B = \tau+w+2s$$

$$\frac{A}{B} = \delta; \qquad \tan\theta = \frac{w\sin\phi}{\tau+w\cos\phi}$$

The constant A may be interpreted as two times the total change of volume, while B equals two times the mean total volume, both reduced to V_o and normalized to T_C. For the pressure p we thus find

$$p = \frac{C}{B}\frac{1}{1+\delta\cos(\alpha-\theta)}$$

which may be written more conveniently

$$p = \frac{p_{max}(1-\delta)}{1+\delta\cos(\alpha-\theta)} = \frac{p_{min}(1+\delta)}{1+\delta\cos(\alpha-\theta)} \tag{2}$$

with the introduction of p_{max} and p_{min} for the maximum and minimum values of the pressure during the cycle.

Expression (2) shows that the pressure variation with time is not purely harmonic. In practice, the deviation of harmonic behaviour is rather small however (the function is symmetrical with respect to p_{max} and p_{min}, which points are 180° apart), as the value of δ seldom exceeds 0.4. This means that the pressure ratio of this type of machine

$$\frac{p_{max}}{p_{min}} = \frac{1+\delta}{1-\delta}$$

is about 2, a remarkably low value compared with what is normal in refrigerating apparatus. The presence of the phase angle θ shows that the pressure variation is not in phase with the variation of the expansion or the compression space; it is easily checked that its phase is intermediate between that of these spaces ($\theta \to \phi$ for $\tau \to 0$). It will be found, for this reason, heat is absorbed in the expansion space and liberated in the compression space. For later reference, given here is the expression for the mean pressure p_m, deduced by integrating the pressure with respect to the crank angle α:

$$p_m = p_{max}\sqrt{\left(\frac{1-\delta}{1+\delta}\right)} \tag{3}$$

(2) Heat absorption in cylinders. The heat absorbed per cycle in the expansion space (Q_E) and in the compression space (Q_C, a negative quantity) is given by

$$Q_E = \oint p\, dV_E, \quad Q_C = \oint p\, dV_C$$

That these expressions, which are normally used for spaces with a constant gas content, may also be used in the case where gas enters and leaves the space can be proved by an involved thermodynamic reasoning which is omitted here. It is easily seen that the value of the integrals depends only on the components of p which have the same phase as dV_E and dV_C; this means that $0 < \theta < \phi$ if the machine has to operate as a refrigerator. Evaluation of the integrals leads to

$$\left.\begin{aligned} Q_E &= \frac{\pi}{a} V_0 p_m \frac{w \sin\phi}{B} \\ Q_C &= -\tau Q_E \end{aligned}\right\} \qquad \ldots(4)$$

with $a = 1 + \sqrt{(1-\delta^2)} \simeq 2$

For practical use, equation (4) may be transformed into q_E, the heat absorbed per second (or the refrigerating capacity) by inserting n, the number of revolutions per minute. If V_0 is expressed in cm^3, p_m in kg cm^{-2}, and q_E in watts, it is found that

$$q_E = \frac{5 \cdot 136}{a} V_0 p_m \frac{n}{1000} \frac{w \sin\phi}{B} \quad \text{(in watts)} \qquad \ldots(4a)$$

Expression (4a) shows that, besides with V_0 and n, the output is proportional to p_m and inversely proportional to the function B, which was defined as the mean reduced and normalized volume. The consequences of the dependence on the mean pressure and the temperature ratio (τ is also contained in s), which constitutes one of the features of the process, will be discussed at more length later. According to expression (4a) an increase of the dead space s reduces the output, as could be expected. A discussion on the influence of the design constants w and ϕ would be very elaborate and lengthy and is therefore outside the scope of this report; their choise depends largely on the losses of the process.

(3) Shaft power and efficiency. For the work W needed to drive the machine one may write

$$W = -Q_E - Q_C$$

Thus

$$W = (\tau - 1)Q_E = \frac{\pi}{a}(\tau - 1) V_0 p_m \frac{w \sin\phi}{B} \qquad \ldots(5)$$

Using equation (5) the efficiency of the cycle is

$$\eta = \frac{Q_E}{W} = \frac{1}{\tau - 1} = \frac{T_E}{T_C - T_E} \qquad \ldots(6)$$

The efficiency of the ideal cycle thus equals that of the Carnot cycle; this is obvious as the cycle is completely reversible.

Although in actual machines the performance is reduced by losses, to be discussed in the next section, the ideal cycle has to be considered as the reference process, because most essential facts can be deduced from it.

Before closing this section two remarks on the representation of the process will be made. The first remark concerns the representation in a thermodynamic diagram (e.g., p vs V, T vs S, etc.). These diagrams always relate to a fixed quantity of the working fluid, which has to be in internal equilibrium (equal p and T throughout); this quantity is passed through a number of thermodynamic states and (at least in a closed system) is returned ultimately to its initial state, so that a cycle is described. Looking at the Stirling process, it is found that, in so far as cyclic behaviour is concerned, nothing abnormal is at hand. However, the system is not homogeneous at all, as different parts of it have a different temperature. As a consequence, different gas particles describe completely different cycles between different temperatures; to mention only two extreme examples, some particles are reciprocating between the compression space and a point in the cooler, while other particles are reciprocating between a point in the freezer and the expansion space. That, because of this situation, normal diagrams have lost their value is shown by the fact that one would have to draw an infinite number of diagrams for the diverse particles with different cycles, which obviously leads

nowhere. The only diagram which still has some sense is the p-V diagram, as the system is homogeneous in p. But in such a diagram one is not allowed to draw isotherms or adiabates, as these lines have lost their meaning. To avoid this difficulty when drawing Figure 2, the dead space was assumed to be zero; in that case isotherms may be drawn, since only then the gas is at thermal equilibrium during the compression and the expansion. When the adiabatic losses are discussed in the next section, this subject will have to be returned to. The second remark concerns the description of the cycle in a schematic form. The transfer of the gas from the compression space to the expansion space and vice versa is performed with constant volume of the gas; this is the simplest representation, as the transfer can be effected by the movement of the displacer only. But this way of transfer is only one example of a multitude of possibilities which exhibit the common property that regeneration is possible. As another example consider transfer at constant pressure, which way of transfer approximates the harmonic cycle much better. The only reason why this manner of transfer is not used to explain the cycle is that it can only be accomplished by simultaneous movement of the piston and the displacer, which obviously is more complicated. This point is stressed because at many places in literature the transfer with constant volume is considered to be one of the main characteristics of the Stirling cycle, to contrast it with the cycle of Claude (with separate compressor and expander), where the transfer is performed at constant pressure. As explained, this view does not correctly locate the distinction between the two cycles, the real difference being that in the Stirling cycle the gas is reciprocating through one connecting duct, wherein the heat exchange is brought about by regeneration, whereas in the Claude cycle the connecting circuit consists of a counter-flow heat exchanger (with two channels). Apart from the restriction contained in the first remark the Stirling cycle thus closely resembles the Claude cycle thermodynamically.

The Actual Cycle

As stated already, the actual cycle differs from the ideal one by the occurrence of losses. For a fuller discussion on this subject reference is made to the original paper[2], here only the most characteristic effects will be treated.

The losses can affect the process in two different ways, viz., by increasing the shaft power and by decreasing the refrigerating capacity; the smaller the ideal values of these quantities, the more pronounced will be the relative effect. Figure 3 illustrates that increase of the shaft power exerts the greatest influence at high refrigerating temperatures, while decrease of the output creates the most adverse effects at low temperatures. In this way a temperature range arises, the "optimum working range", wherein the actual efficiency differs least from the ideal one (i.e., where the figure of merit is highest). This range may be shifted both to higher and to lower temperatures by suitable design; moreover, its limits greatly depend on present and future technological possibilities.

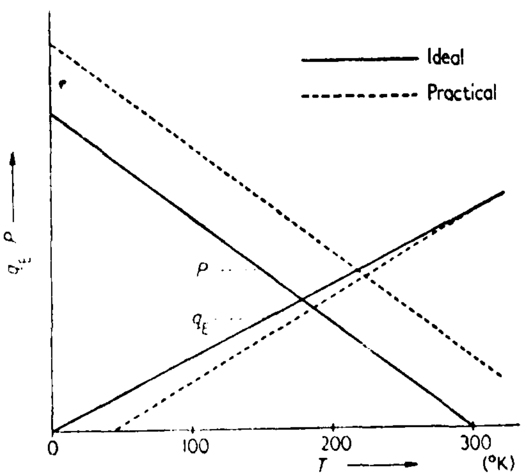

Figure 3. *Graphs of the shaft power P and the refrigerating capacity q_E as a function of temperature. The full lines apply to the ideal process, the dotted lines to an actual machine with losses*

The increase in shaft power is mainly due to three causes, namely, the mechanical loss of the drive, the flow loss (that is, the power needed to force the gas through the narrow connecting circuit) and the adiabatic loss. The first two losses need no further comment, but the adiabatic loss will be discussed at greater length. In the ideal isothermal process it was assumed that the temperature in the cylinders is constant with time. This means that the thermal contact between the gas and the wall in the cylinder spaces is assumed to be so perfect that these walls can be employed as well to establish the contact between the gas and the surroundings, that is, to serve as cooler and freezer. In this case, separate heat exchangers are of no use and must be omitted; this ideal machine thus consists of the two cylinders and the regenerator and is therefore referred to as the "three-element machine".

Actually, the separate heat exchangers are introduced because the thermal contact between the gas and the cylinder walls is always so poor that insufficient heat exchange with the surroundings can be established through these walls; for this case the name "five-element machine" is used. As a consequence, the temperature of the gas in the cylinders changes nearly adiabatically with time. This adiabatic behavior has only a minor influence on the efficiency (it would be too involved to give the full explanation here; it is based on the fact that these processes occur in both cylinders with the same phase, so that the temperature ratio is independent of time), but in this case the heat (or the cold) must be transported from the cylinders to the heat exchangers. This transport can only be effected by the reciprocating gas which performs it by assuming different temperatures when flowing in opposite directions, with the result that the mean temperature in each cylinder deviates from that in the adjoining heat exchanger. Figure 4 shows schematically the temperature distribution in the machine. It will be observed that the mean temperature in the expansion cylinder is lower than that of the freezer and that the mean temperature in the compression cylinder is higher than that of the cooler. This means that the ratio of the cylinder temperatures is higher than that of the temperatures of the

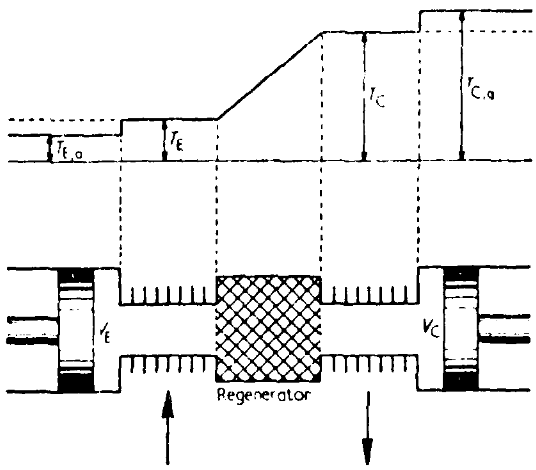

Figure 4. *Temperature distribution in the adiabatic 'five-element machine'. The contact with the surroundings is effectuated by the cooler and the freezer. The mean temperature in the compression space* $T_{C,a}$ *is higher than the cooler temperature* T_C *as heat must be transported from the cylinder to the cooler; by the same argument the mean temperature in the expansion space* $T_{E,a}$ *is lower than that of the freezer* T_E.

heat exchangers, which causes an increase in shaft power. Strictly speaking, the expression "adiabatic loss" is therefore misleading and should be replaced by "transport loss". It is adhered to though, because ultimately the adiabatic behavior is the fundamental cause that has necessitated the introduction of separate heat exchangers. Because the value of the temperature ratio τ is larger in the adiabatic than in the isothermal case, one would expect also a decrease in refrigerating capacity; this influence is very small, however, as the larger value of τ is nearly compensated by a decrease of the quantity B, the mean relative volume of the working circuit, which quantity has another form in the adiabatic case.

In the above discussion the use of the expressions "adiabatic compression" or "expansion has been intentionally avoided. The reason is that the gas is compressed and expanded everywhere in the working space; its behavior during these processes, however, depends largely on the condition of heat transfer prevailing in the various sections of the volume. While in the cylinders the gas temperatures change nearly adiabatically, this is not the case in the connecting circuit;

in the regenerator, for example, the heat transfer is so high, that the behavior is practically isothermal. Thus, while the actual Stirling process is certainly not isothermal, it would be incorrect to call it adiabatic. This situation thus furnishes still another example for the previously made remark that thermodynamic diagrams are of little value for this process.

The decrease of the refrigerating capacity is mainly due to two effects, the flow loss and the insulation loss. Again no comment is made on the flow loss. Also the insulation (and conduction) loss proper needs no discussion. There exists another loss, however, that acts as an insulation loss as well which has the utmost importance for the quality of the process. This loss, caused by the non-ideal behavior of the renerator, will now be discussed.

It is obvious that in the Stirling process ideal regeneration is possible in principle as the same amount of gas passes the regenerator in both directions with the same temperature difference, so that the amount of heat rejected and absorbed by the gas for both directions of flow is the same, since the specific heat is independent of pressure (which is practically the case for nearly perfect gases). The following argument shows the extreme importance of a small departure from ideality of the regenerator, caused by non-ideal heat transfer. In the regenerator a quantity of heat Q_r must be absorbed and rejected in each cycle. Owing to imperfections, this amount is reduced to $\eta_r Q_r$, where η_r is the efficiency of the regenerator. This means that only part of the available heat is transferred to the regenerator. The rest, that is $(1-\eta_r)Q_r$, is carried along with the gas through the regenerator, so that the gas arrives too hot in the expansion space. This remainder, ΔQ_r thus constitutes the regeneration loss. As this loss must be made up from the cold produced Q_E, it must be compared with this quantity. Calculations show that

$$\frac{\Delta Q_r}{Q_E} = C_r(1-\eta_r)\frac{T_C - T_E}{T_E} \qquad \ldots(7)$$

The constant C_r depends mainly on the compression ratio; its value is approximately 10. For example, take T_C = 300°K, T_E = 75°K, and the regeneration loss $1-\eta_r$= 1%; then

$$\frac{\Delta Q_r}{Q_E} = 10 \times 1 \times 3 = 30 \text{ per cent}$$

Thus each percent of regeneration loss involves a loss of 30 per cent in refrigerating power; below 30°K this figure even increases to greater than 90 percent, meaning that at such temperatures the entire cold production is consumed by the regenerator. It is thus no exaggeration to call the regenerator the heart of the machine.

The regenerator used in actual gas refrigerating machines consists of a mass of fine metal wire, forming a light felt-like substance. With this type of material, efficiencies of 99 per cent and higher can be obtained; the thermal conductivity of the material is very low.

This section will be ended with a short discussion on the problem of how to minimize the total sum of the losses; this problem is very involved indeed, so that only a very broad outline can be given. As an example, the regenerator will be considered. The losses of the regenerator make themselves felt in three different ways, viz., the regeneration loss (reducing the cooling power), the flow loss, and the dead space (this is not a real loss as the shaft power is also decreased; it exerts its influence through the other losses, as these increase relatively). The regeneration loss can be reduced by making a longer regnerator; this, however, increases the flow loss and the dead space. One may also give the regenerator a larger cross-section; this reduces the flow loss and somewhat the regeneration loss, but increases the dead space. Thus it is possible to find optimum dimensions for the regenerator. The same hold for the freezer and the cooler, where the regeneration loss is replaced by the loss due to insufficient heat transfer. Moreover, the losses are governed by the choice of the values of w and ϕ. Finally, the

outside of the cooler and the freezer must be made optimal. Thus a very large number of design parameters are to be fixed such that the total result gives an optimum condition; it will be obvious that a lot of experience is needed to find the right solution quickly. This is compensated by the fact that once a system of calculation is worked out, it holds for any size of machine.

APPENDIX B

IMPROVEMENTS TO THE BASIC STIRLING-CYCLE: EXPANSION STAGING

EXPANSION STAGING FOR REGENERATIVE CYCLES

Regenerative type refrigeration cycles, e.g., Vuilleumier (VM) and Stirling, produce cold by the reversible expansion of an ideal gas. The number of expansion stages and their geometry have a significant effect on the efficiency with which the required cold can be produced. The design aspects of single and multiple expansion refrigerators are discussed below.

1. Single Expansion

The characteristics of the VM and Stirling cycles are normally described by depicting one expansion space of the refrigerator (Ref. 1). The configuration of a typical VM or Stirling cycle "cold cylinder", i.e., expansion space, displacer, and regenerator, is shown in Figure 1. In principle, ideal regeneration

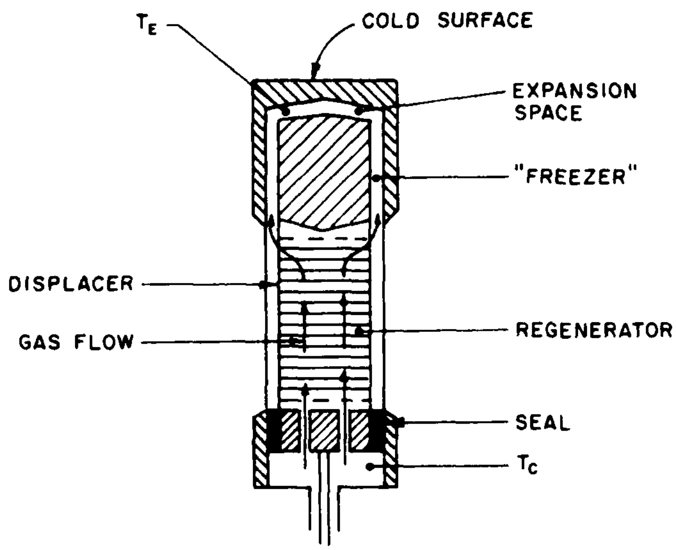

Figure 1: Typical Single Expansion Configuration

is possible in both cycles, since the same quantity of gas flows through the regenerator in both directions, with the same temperature difference, i.e., $T_C - T_E$. The amount of heat rejected and absorbed by the gas for both directions of flow is the same, since the specific heat for nearly perfect gases is essentially independent of pressure.

In actual practice, the regeneration is not ideal, i.e., there is a small departure from the ideal caused by imperfect heat transfer. In a typical regenerator, a quantity of heat Q_r must be absorbed and rejected during each cycle. Due to various imperfections, this amount is reduced to $\eta_r Q_r$, where η_r is the efficiency of the regenerator. This means of course that not all of the available heat is transferred to the regenerator. The rest, that is $(1-\eta_r)Q_r$, is carried along with the gas through the regenerator, so that the temperature of the gas flowing into the expansion space is somewhat above that desired. This remainder, which we will designate as ΔQ_r, constitutes the regeneration loss. Since this loss must be made up from the refrigeration produced Q_E, it should be compared with Q_E. Calculations show that:

$$\frac{\Delta Q_r}{Q_E} = C_r(1 - \eta_r)\,\frac{T_C - T_E}{T_E} \qquad (1)$$

The constant C_r depends mainly on the compression ratio in the refrigerator; for small units, its value is approximately 10. For example, if $T_C = 300°K$, $T_E = 75°K$, and the regeneration loss $1-\eta_r = 1\%$, we find:

$$\frac{\Delta Q_r}{Q_E} = 30\%$$

This means that a 1% loss in regeneration involves a 30% loss in refrigeration. It is therefore clear that for efficient operation, the regeneration loss in a VM or Stirling unit has to be minimized.

In practice, refrigerators having only a single expansion chamber are referred to as "single expansion" units.

2. Possible Improvements

Equation (1) for the relative regeneration loss suggests two possible methods for improving the refrigeration process: decreasing the value of C_r, and increasing the value of η_r.

The way to decrease C_r would be to increase the compression ratio since C_r depends mainly on this ratio. At present, no practical configurations exist to achieve this in either the VM or Stirling cycles.

The value of η_r, about 99% in typical regenerative refrigerators, can be increased somewhat. Regenerators with efficiencies of 99.5% and higher have been made. However, since a regenerator with such high efficiencies normally has very high flow losses, lower refrigerator efficiency will result.

3. Double Expansion

To avoid the disadvantages cited above, Philips, in 1963, modified the conventional single expansion system (Ref. 2). The modification consisted of thermally staging a number of expansion processes in as many expansion spaces. The method is somewhat analogous to the Keesom cascade process, except that no separate thermodynamic cycles are used, since the complete cycle is performed in one closed system. This modified cycle has been referred to as the "double expansion" cycle.

In this method the expansion is performed in two expansion spaces, each at a different temperature. The spaces are connected in series, with regenerators in the interconnecting passages. The displacer used in the single expansion machine has been adapted to the double expansion process, as shown in Figure 2. The additional, intermediate expansion space M_M is obtained by "stepping" the diameter of the displacer. By virtue of this stepped displacer, volume variations of the two expansion spaces (E and M) are in phase. The advantage of this type of construction is that the pressure difference across the seal between the expansion spaces is small, as in the conventional design.

As a result of the additional expansion space, the refrigerator produces cold at two different temperatures, whereas in the conventional process cold production takes place at only one temperature. The resultant advantages are discussed in Paragraph 4.

The following discussion shows how this system reduces the influence of the regeneration loss. Assume that a mass of

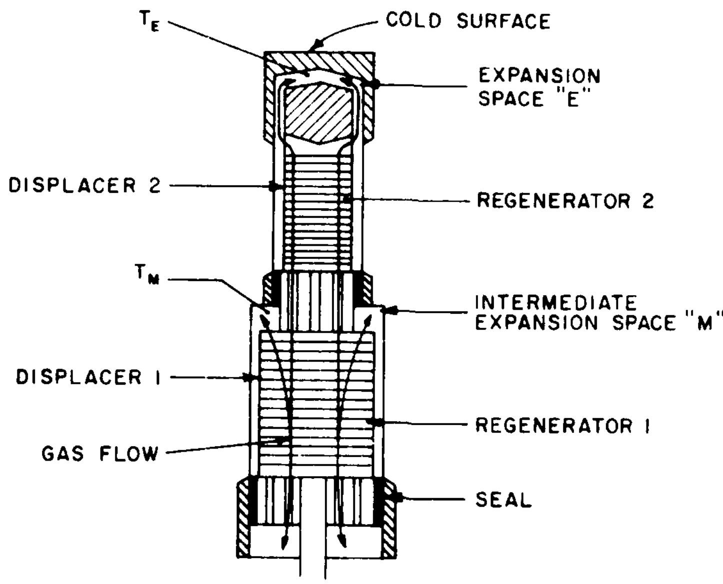

Figure 2: Typical double expansion configuration

working gas m_M is expanded in the intermediate expansion space at a temperature T_M, and that a mass of working gas m_E is expanded in the top expansion space at a temperature T_E - both gases expanding from a pressure p_1 to a pressure p_2. The ideal cold productions in the expansion spaces are:

$$Q_M = m_M R T_M \ln(p_1/p_2)$$

$$Q_E = m_E R T_E \ln(p_1/p_2)$$

The mass flowing through regenerator 1 between room temperature and the intermediate temperature now is $m_M + m_E$, and the mass flowing through regenerator 2 between the intermediate space and the expansion space is m_E. The regeneration losses for these regenerators are:

$$\Delta Q_{r1} = (m_M + m_E)\ C_p(1 - \eta_{r1})(T_C - T_M)$$

$$\Delta Q_{r2} = m_E C_p(1 - \eta_{r2})(T_M - T_E)$$

Hence, the relative regeneration losses are:

$$\frac{\Delta Q_{r1}}{Q_M} = \frac{m_M + m_E}{m_M} C_r(1 - \eta_{r1})(\frac{T_C - T_M}{T_M}) \qquad (2)$$

$$\frac{\Delta Q_{r2}}{Q_E} = C_r(1 - \eta_{r2})(\frac{T_M - T_E}{T_E})$$

It should be noted that C_r again has the same value if P_1/P_2 has the same value, i.e., about 10.

Now $\Delta Q_{r2}/Q_E$ is small, because T_M is of the order of 140°K, and T_M-T_E is therefore less than T_C-T_E, the quantity that occurred in Equation (1). The consequence is that little of the cold production in the top expansion space is lost, thereby resulting in a relatively large increase in net cold production. When the refrigerator of interest needs cold at one level only, no net production Q_M is needed, and it is permissible for $\Delta Q_{r1}/Q_M$ to be of the order of unity. Taking the efficiency of regenerator 1 to be 98%, it follows from Equation (2) that:

$$\frac{\Delta Q_{r1}}{Q_M} = 0.2\ \frac{m_M + m_E}{m_M}$$

Hence, $(m_M + m_E)/m_M$ can have a value of about 5. This means that in a refrigerator using a double expansion configuration only a mass of about one-fifth of the total mass flowing through the first regenerator needs to be expanded in the intermediate space; this causes only a relatively small increase in the compression work.

4. <u>Applications</u>

It is evident from the foregoing that given the same conditions, i.e., cold production at a given operating temperature, the double expansion configuration is more efficient. There is, however, additional complexity, viz., two regenerators instead of one. It should be noted that an intermediate temperature level in the double expansion configuration offers significant advantages in some cases. For instance, in certain applications where radiation shielding is desirable, the shield can be cooled at the intermediate temperature level. The required refrigeration can of course be produced more efficiently at this level.

Both the single and double expansion configurations have been incorporated in many operational systems. Figure 3 shows, for comparison, single and double-expansion displacer-regenerators of a VM refrigerator producing 1 W at 77°K. The construction is similar in both cases.

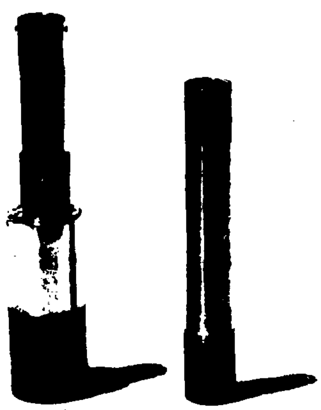

Figure 3: Single and double expansion displacer-regenerators of a VM refrigerator producing 1 W at 77°K.

... -expansion concept has been extended one step further, ...le-expansion Stirling cycle configuration (Ref. 3). ... temperatures as low as 7.2°K, with only one cycle, ...ained. A triple-expansion VM refrigerator is ... development for a spaceborne application (Ref. 4).

5. References

(1) A. Daniels, "Cryogenics for Electro-Optical Systems," Electro-Optical Systems Design, vol. 3, pp. 12-20, July 1971.

(2) G. Prast, "A Philips Gas Refrigerating Machine for 20°K," Cryogenics, vol. 3, pp. 156-160, September 1963.

(3) A. Daniels and F.K. du Pré, "Triple-Expansion Stirling Cycle Refrigerator," Advances in Cryogenic Engineering, vol. 16, pp. 178-184, June 1970.

(4) G.K. Pitcher, "Development of Spacecraft Vuilleumier Cryogenic Refrigerators," AFFDL TR-71-147, Part I, Contract F33615-61-C-1024, December 1971.

APPENDIX C

IMPROVEMENTS TO THE BASIC STIRLING-CYCLE REFRIGERATOR:
PHILIPS RHOMBIC DRIVE

RHOMBIC DRIVE

1. DESCRIPTION

The rhombic drive comprises twin cranks and con-rod mechanisms, identical in design and offset from the cent al axis of the engine; the cranks which rotate in opposite directions may e coupled by two gear wheels. The gear wheels may be removed if sufficient linear guidance is used to insure that the reciprocating members are constrained to execute only linear motion.

Figure 1 is a schematic diagram of a typical rhombic-drive Stirling or VM machine. Fixed to the power piston 1 by way of piston rod 2 is a yoke 3. One end of the yoke is linked by con-rod 4 to crank 5, the other end by con-rod 4' to crank 5'. The displacer piston is actuated by a precisely similar arrangement: the displacer-piston rod 7, which passes through the hollow rod 2, has fixed to it a yoke 8 which is linked to cranks 5 and 5' by con-rods 9 and 9', respectively. If 9 and 9' are given the same length as 4 and 4', the two pairs of con-rods will form a rhombus, only the angles of which vary when the system is in motion; it is for that reason that the name "rhombic drive" was adopted. Gear wheels 10-10' ensure exact symmetry of the system at all times. Ideally, no power is transmitted through the gears, which only act to synchronize the drive motion.

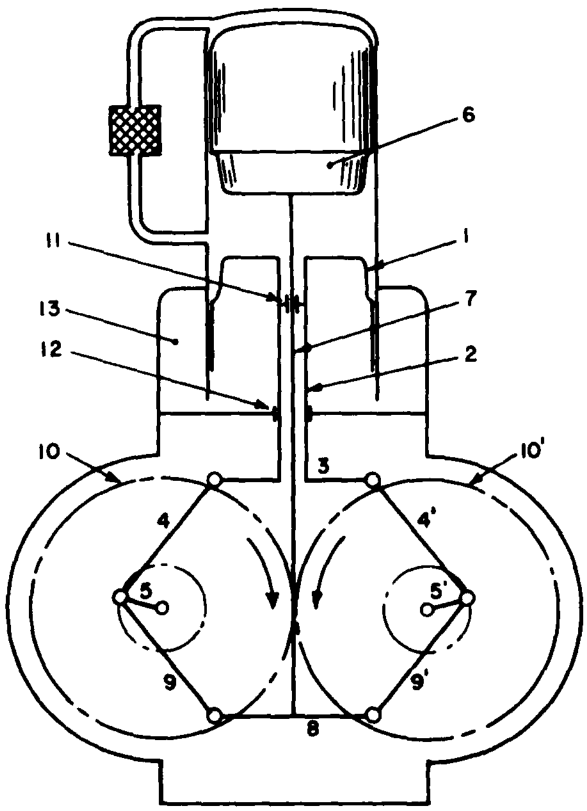

Figure 1: Schematic diagram of rhombic drive mechanism.

The symmetry of the system and the coaxial arrangement of the piston and the displacer rods permit the design of a simple crankcase structure. The displacer rod seal 11 is inside the hollow piston rod. With the aid of a seal on the piston rod (12 in Fig. 1), a compartively small cylindrical chamber 13 under the piston can be formed, separate from the crankcase; this "buffer space" can be filled with gas at the desired buffer pressure. The success of this arrangement depends essentially on the fact that the piston rod is subject to no lateral thrust, since the horizontal components of the forces exerted by each pair of con-rods are in the ideal case exactly balanced at each yoke. That they do so, and that frictional losses are low as a consequence, has the further advantage of enhancing the mechanical efficiency of the system. The minimum permissible volume of the buffer space is determined only by the range within which it is desired to limit the pressure variations inside the chamber.

Figure 2 shows an actual rhombic drive mechanism. Its motion is illustrated by having the mechanism in two different positions.

The piston and the displacer movements resulting from the rhombic drive are displayed graphically in Figure 3. It will be seen that if the direction of rotation is as indicated in Figure 1, the volume variation of the expansion space V_E will have a phase lead with respect to that of the

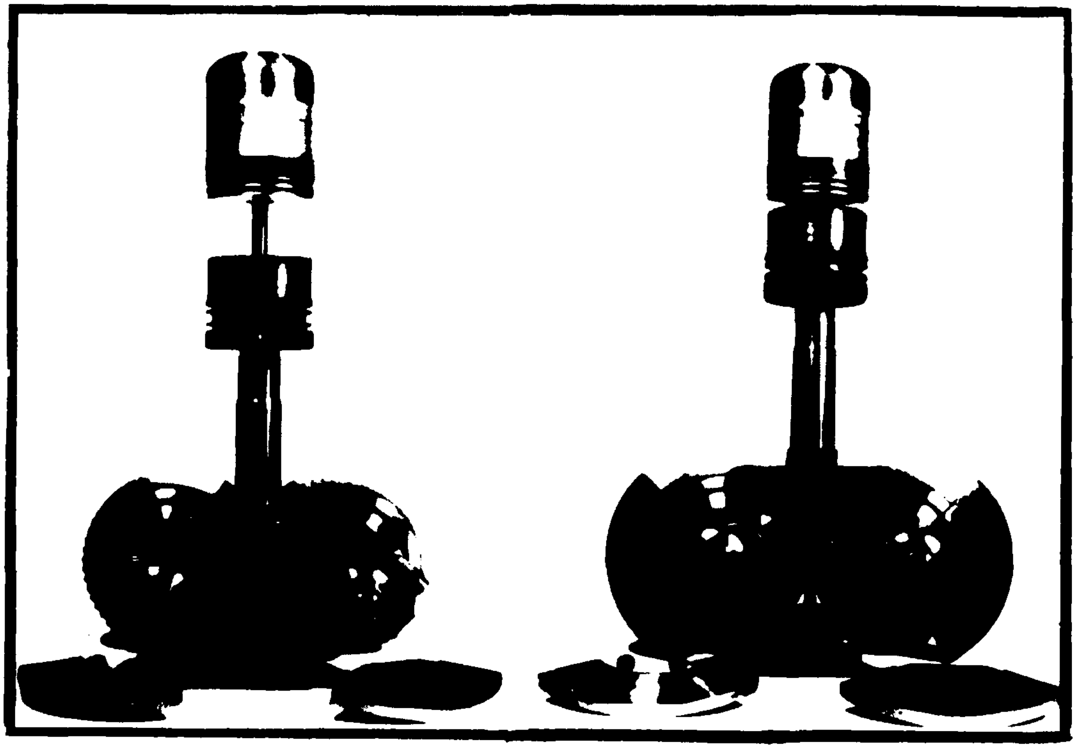

Figure 2: Model of an actual rhombic drive mechanism, in two positions.

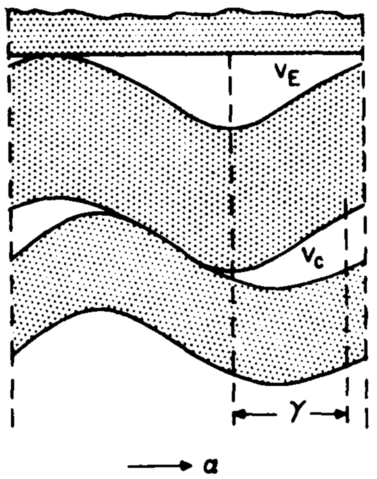

Figure 3: Curves showing displacements undergone by piston and displacer in a rhombic drive system.

V_E = expansion volume
V_C = compresior volume
γ = phase lead of V_E relative to V_C
α = crank angle

compression space V_c, as required. Although the piston and displacer do move in simple harmonic motion, the kinematics are very close to those of the classical Stirling cycle. This might seem surprising, since the use of the rhombic drive may appear to have restricted the freedom of choice with regard to parameters w and γ (the amplitude ratio and relative phase of the variations in volumes V_E and V_c), which are important in the design of a Stirling machine. However, a more exact analysis of the rhombic drive shows that it is in fact possible to vary these parameters over a relatively wide range; this can be done by altering the offset of the crankshaft, the radius of the cranks, the lengths of the con-rods, and the ratio of the piston and displacer diameter.

2. BALANCING OF DRIVE MECHANISM

The rhombic drive has the important property, especially for spaceborne applications, of permitting an engine or cooler with only one cylinder to be completely balanced both for the forces due to the inertia of the moving parts, and for the moments of these forces -- "complete" in the sense that the fundamentals and all the higher harmonics are balanced. This can be demonstrated for the simple case where the con-rods are of equal length (as in Fig. 1).

The configuration is given in Figure 4. By symmetry it is clear that the sum of all inertial forces acting horizontally is zero at any given instant. The same applies to all inertial-force moments about an axis perpendicular to the plane of the figure. Hence, all one need consider are the inertial forces acting in the vertical direction. The circular motion of each crankpin T-T' can be resolved into a vertical and a horizontal component. The vertical movements that the piston and the displacer make as a result of the horizontal movement of the crankpins are equal and opposite because the con-rods are of equal length (symmetrical deformation of the "rhombus"). Hence, if the masses of the piston and the displacer (including the rods etc., attached to them) are made equal, then the sum of the vertical inertial forces corresponding to horizontal crankpin movement is always zero. There remains the vertical movements of the piston and the displacer

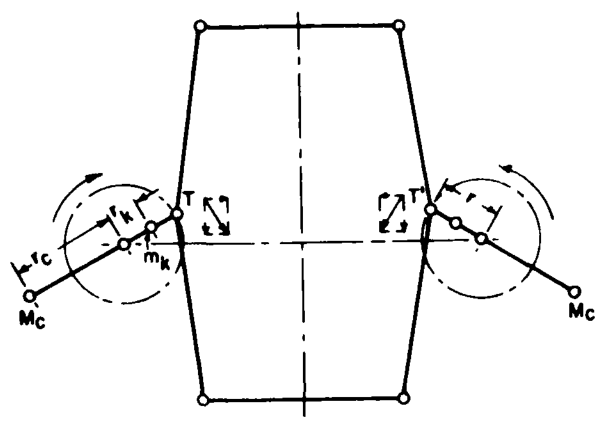

Figure 4: Configuration of rhombic drive with equal yoke length.

as a result of the vertical component of the crankpin movement. These movements are exactly equal and, moreover, identical with the vertical movement of the crankpins. One can therefore imagine the moving mass of the two pistons, $M_P + M_D$ (including the con-rods), as localized in the crankpins, $1/2(M_P + M_D)$ in each. By means of two counterweights M_c mounted opposite each crankpin at a suitable radius r_c, vertical inertial forces can be created which exactly balance those of $(M_P + M_D)$ -- and this is true even if the rotation of the crankshafts is not exactly uniform. In fact, the mass and offset of each counterweight are chosen such that the latter also serves to balance the crank and other eccentrically positioned moving parts. If M_k is the effective mass of all these parts, and r_k the distance of their center of gravity from the crankshaft axis, the condition for balancing is as follows:

$$r_c M_c = 1/2 r(M_P + M_D) + r_k M_k \tag{1}$$

The configuration of Figure 4 is a special case of a more general form of the rhombic drive. One can obtain the more general form by abandoning the restriction that the pairs of connecting rods have to be equal in length, and by allowing each displacer con-rod to hinge not on the crankpin but about an arbitrary fixed point on the piston con-rod (see Fig. 5). In

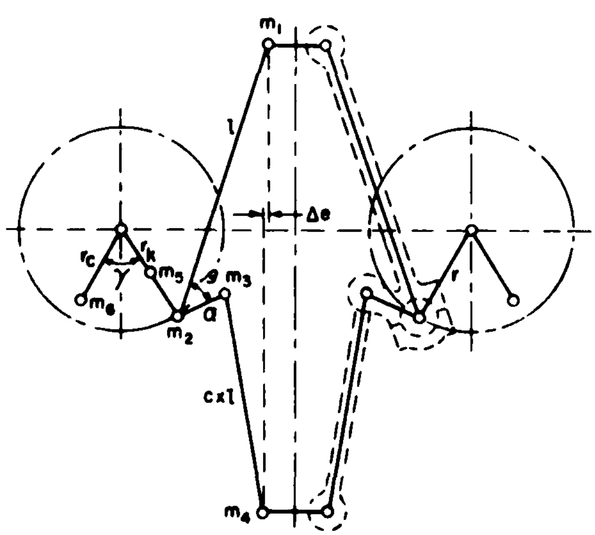

Figure 5: General form of the rhombic drive.

this general form, which design considerations may render more attractive than the special one of Figure 4, the piston and the displacer rods continue to move coaxially without the presence of any lateral thrust. This means that the expedient of the buffer chamber with gas under pressure can again be applied without complications. Moreover, it can be shown that the inertial forces of the moving parts of the general form of this drive mechanism can be completely balanced as before, provided certain conditions are fulfilled. These conditions will be stated here without proof. For balancing to be possible, the parameters of the mechanism as indicated in Figure 5 must satisy the equations:

$$\Delta e = 0,$$

$$c = \sqrt{1-2\frac{a}{\ell}\cos\beta+\left(\frac{a}{\ell}\right)^2},$$

$$m_1-m_4+\frac{a}{\ell}(m_3+2m_4)\cos\beta = 0.$$

The net inertial force can then be completely balanced by fitting counterweights whose positions and masses, respectively, are given by:

$$\gamma = \pi-\tan^{-1}\frac{\frac{a}{\ell}(m_3 + 2m_4)\sin\beta}{m_1 + m_2 + m_3 + m_4 + \frac{rk}{r} m_5} \qquad (2)$$

and

$$m_6 = \frac{r}{r_c}\sqrt{(m_1 + m_2 + m_3 + m_4 + \frac{rk}{r} m_5)^2 + \{\frac{a}{\ell}(m_3+2m_4)\sin\beta\}^2} \qquad (3)$$

It will be seen that when a is zero, as in the special case first discussed, these conditions transform into the simple ones given earlier.

This configuration lends itself to the use of two motors or flywheels (one on each shaft) rotating in opposite directions; as a result, it is possible to balance the reaction torques on the crankcase as well.

3. EFFECTING A BALANCE OF THE SPECIAL FORM OF RHOMBIC DRIVE

As discussed previously, the 1st balancing condition that must be satisfied is that the sum of the vertical inertial forces corresponding to the horizontal component of the crankpin movement be always zero. This condition means that the piston mass and a fraction of its associated con-rod mass must equal the displacer mass and a fraction of its associated con-rod mass. Since the mechanism is symmetrical, this condition can be expressed for half of the rhombus:

$$1/2\ Lm_p + A_{pc}\ m_{pc} = 1/2\ Lm_d + A_{dc}\ m_{dc} \qquad (4)$$

where, m_p = mass of piston

m_{pc} = mass of piston con-rod

m_d = mass of displacer

m_{dc} = mass of displacer con-rod

L = length of con-rod

For the special form of the rhombic drive:

$A_{dc} = A_{pc}$ = distance between center of gravity (cg) of con-rod and center of crankpin hole in con-rod.

The values of the masses can be accurately determined, as can the value of L. The value of A_{pc} can in most cases also be accurately determined so the 1st balance condition can be accurately satisfied. This is usually accomplished by adding mass to the piston or the displacer yokes.

The 2nd balancing condition to be satisfied is that the sum of the vertical inertial forces corresponding to the vertical component of the crankpin movement be always zero. As discussed previously, this can be accomplished by fixing counterweights opposite the crankpins. This as expressed in Equation (1) is:

$$r_c m_c = 1/2\ r\ (m_p + m_d) + r_k m,$$

which can be written to show the mass of the con-rods and crankpin separately:

$$r_c m_c = r \left[m_{pc} + m_{dc} + 1/2\ (m_p + m_d) \right] + r_{cr} m_{cr} \qquad (5)$$

where, r_{cr} = r (the crank radius) and m_{cr} refers to the crank mass, or where r_{cr} = distance from crankshaft centerline to crankshaft cg, and m_{cr} = total mass of crankshaft.

From the 1st balancing condition, all the terms within the large brackets are known. At this point one or more of three available techniques are used, depending on the quality of balance desired.

A crude static balance may be obtained by repeatedly suspending the crankshaft-counterweight assembly from a pin point on one of the shaft cheecks until the shaft centerline is vertical. The distance between the pin point and the shaft centerline multiplied by the mass of the crankshaft-counterweight assembly is equal to $(r_c m_c - r_{cr} m_{cr})$ in the above equation. This must equal r times the known quantity in the brackets for the 2nd balancing condition to be satisified. This is usually accomplished by removing mass from the counterweights.

A more accurate balance can be achieved if a bob weight with mass equal to the quantity in brackets is first attached to the crank-throw pin so its cg is at the center of the pin, then each entire crankshaft-counterweight-bob weight assembly is dynamically balanced. Timing gears, flywheels, motor rotors, etc., can also be included in this assembly.

Some shortcomings of this technique are that the cg's of the con-rods might not be accurately known and also that the resultant forces from piston, displacer and con-rods and/or the bob weights representing them might not be located at the center of the crankpins. These would cause unbalanced forces and/or moments. To correct this situation, a dynamic balance of the assembled rhombic-driven machine can be performed. Constrained maily by the limitations of state of the art balancing machines, a complete static and 1st harmonic dynamic balance can be achieved.

The pivoted-cradle balancing technique is used twice, one to correct unbalance forces in the transverse direction and then in the vertical direction. By first measuring the unbalance in the transverse direction and adding or subtracting adequate mass in two balancing planes on one crankshaft (see Fig. 6), the transverse unbalance can be minimized. Generally, there will still be a vertical unbalance which can be corrected by measuring in the vertical direction and adding or subtracting equal mass in a symmetrical way on both crankshafts (see Fig. 6). The vertical correction must, of course, also be performed in two planes.

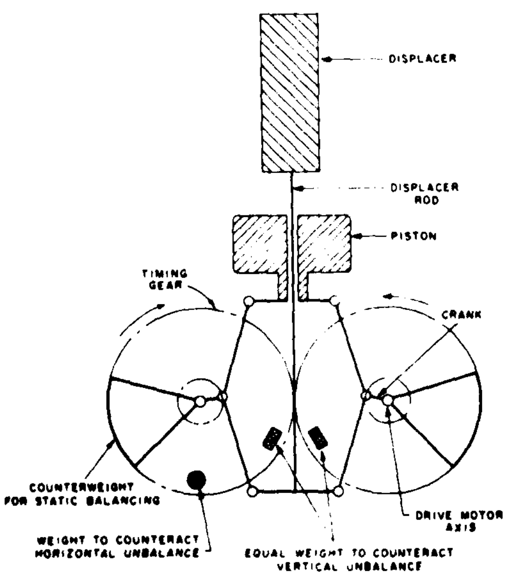

Figure 6: Rhombic drive mechanism with static and dynamic balancing weights shown in one correction plane.

APPENDIX D

MOTOR CHARACTERISTICS

MOTOR CHARACTERISTICS
BRUSHLESS D-C MOTORS FOR RHOMBIC DRIVE REFRIGERATOR
PHILIPS LABORATORIES **P.O. #334133**
28 Volts Supply Input, 25° C Ambient
Herbert C. Roters Associates, Inc. **December 1974**

Two motors, electrically in parallel, mechanically in tandem.
Armature input from B-3212 Commutation Electronic Circuit
(no pulse modulation of d-c input)
Power input and efficiency does not include 91 mA at 5 V
for the commutation circuit drive input

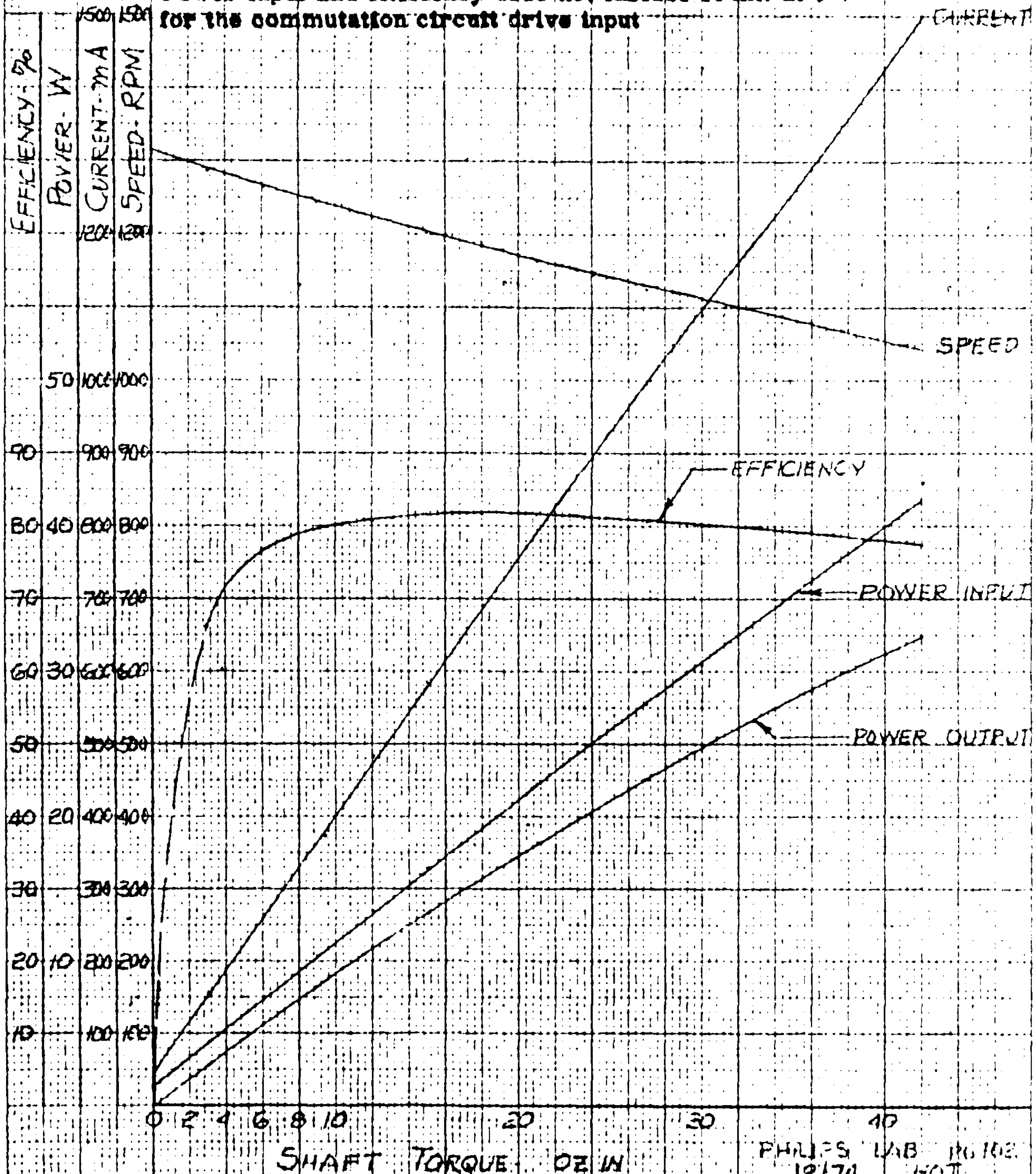

MOTOR CHARACTERISTICS

BRUSHLESS D-C MOTORS FOR RHOMBIC DRIVE REFRIGERATOR

PHILIPS LABORATORIES **P.O. #334133**

26 Volts Supply Input, 23° C Ambient

Herbert C. Roters Associates, Inc. **December 1974**

Two motors, electrically in parallel, mechanically in tandem.
Armature input from H-3212 Commutation Electronic Circuit
(no pulse modulation of d-c input)
Power input and efficiency does not include 91 mA at 5 V
for the commutation circuit drive input.

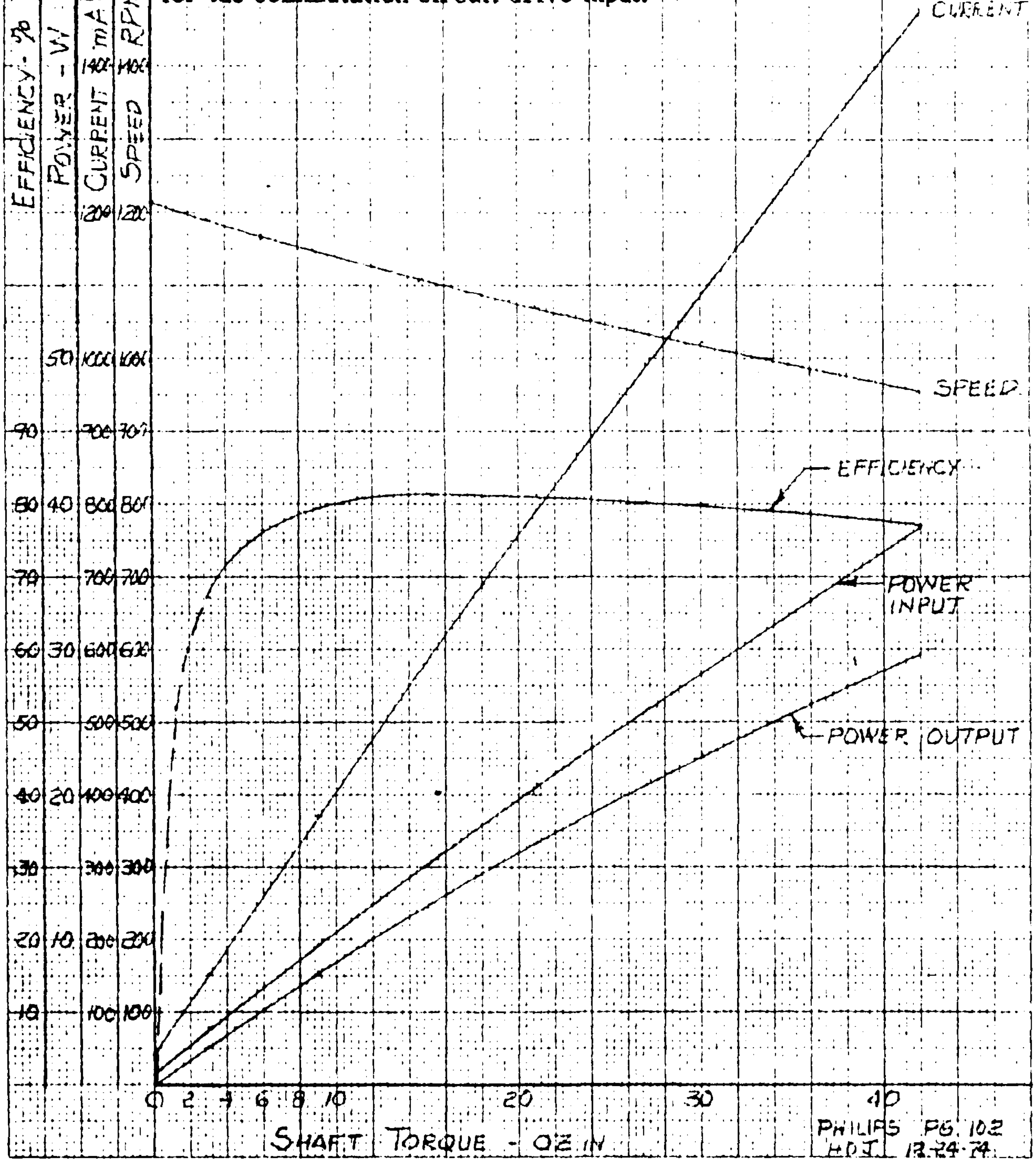

M-2657

MOTOR CHARACTERISTICS
BRUSHLESS D-C MOTORS FOR RHOMBIC DRIVE REFRIGERATOR
PHILIPS LABORATORIES P.O. #334133
30 Volts Supply Input, 23° C Ambient
Herbert C. Roters Associates, Inc. December 1974

Two motors, electrically in parallel, mechanically in tandem.
Armature input from B-3212 Commutation Electronic Circuit
(no pulse modulation of d-c input)
Power input and efficiency does not include 91 mA at 5 V
for the commutation circuit drive input.

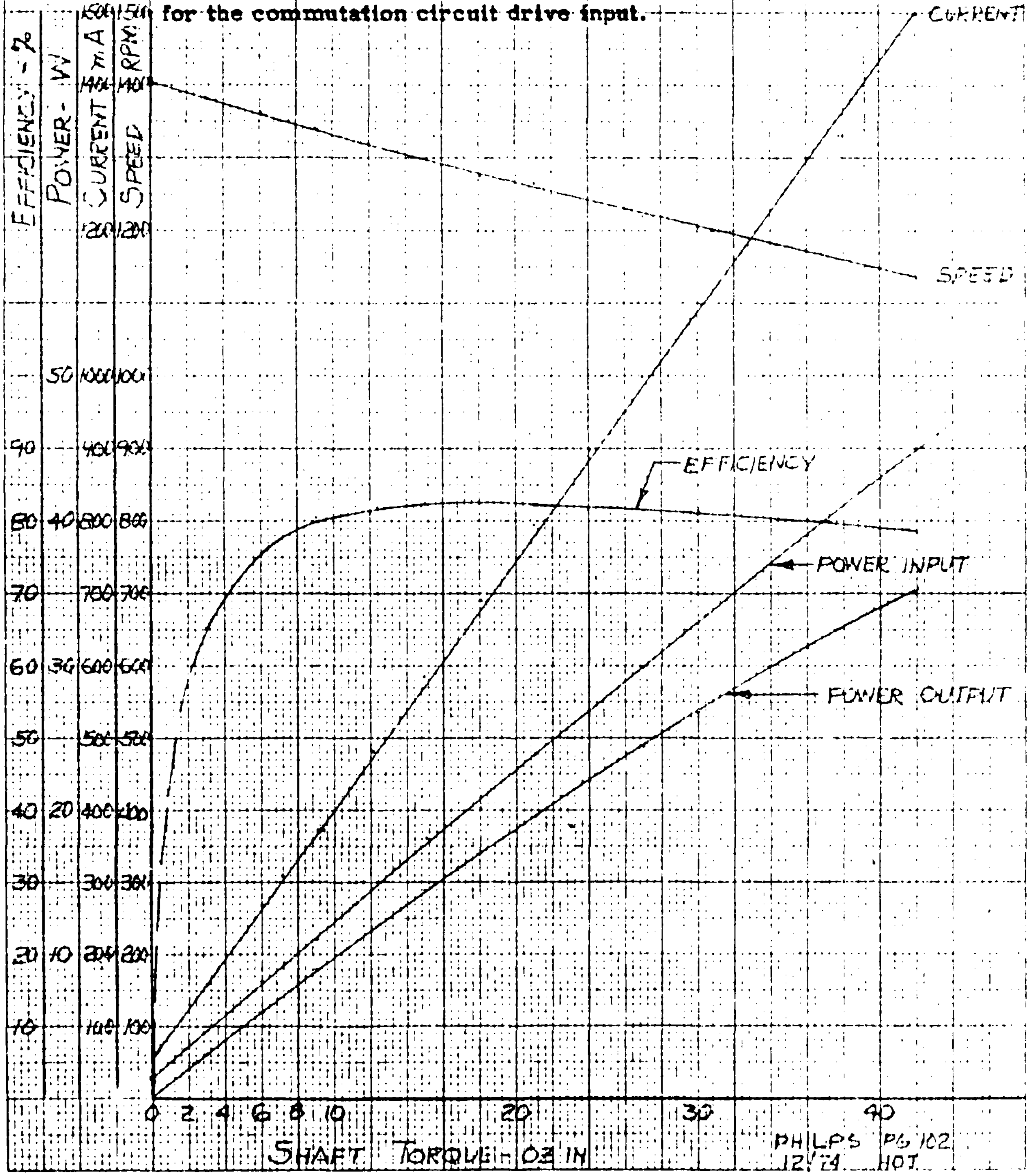

M-2658

AD-A102 377 JOHNS HOPKINS UNIV LAUREL MD APPLIED PHYSICS LAB F/G 13/1
THE APL SATELLITE REFRIGERATOR PROGRAM.(U)
JUL 81 C S LEFFEL, R VON BRIESEN N00017-72-C-4401
UNCLASSIFIED JHU/APL/TG-1332 NL

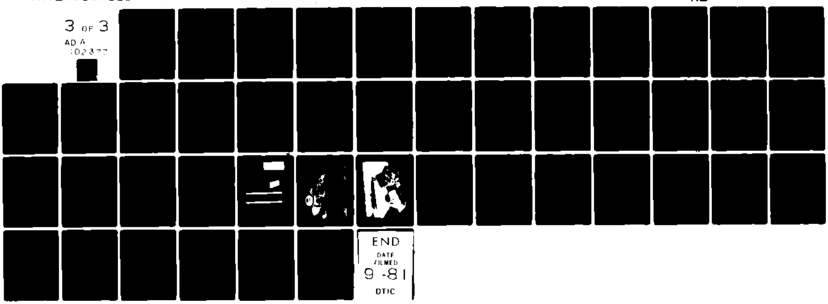

NO-LOAD MOTOR CHARACTERISTICS

BRUSHLESS D-C MOTORS FOR RHOMBIC DRIVE REFRIGERATOR

PHILIPS LABORATORIES P.O. #334133

23° C Ambient

Herbert C. Roters Associates, Inc. December 1974

Two motors operating individually or in electrical parallel and mechanical tandem with the field poles on the same shaft.
Curves for current and power input are almost exactly similar.
Electrical armature input from B-3212 Commutation Electronic Circuit (no pulse modulation of d-c input).
Power input does not include 91 mA at 5 V for the commutation circuit drive input.

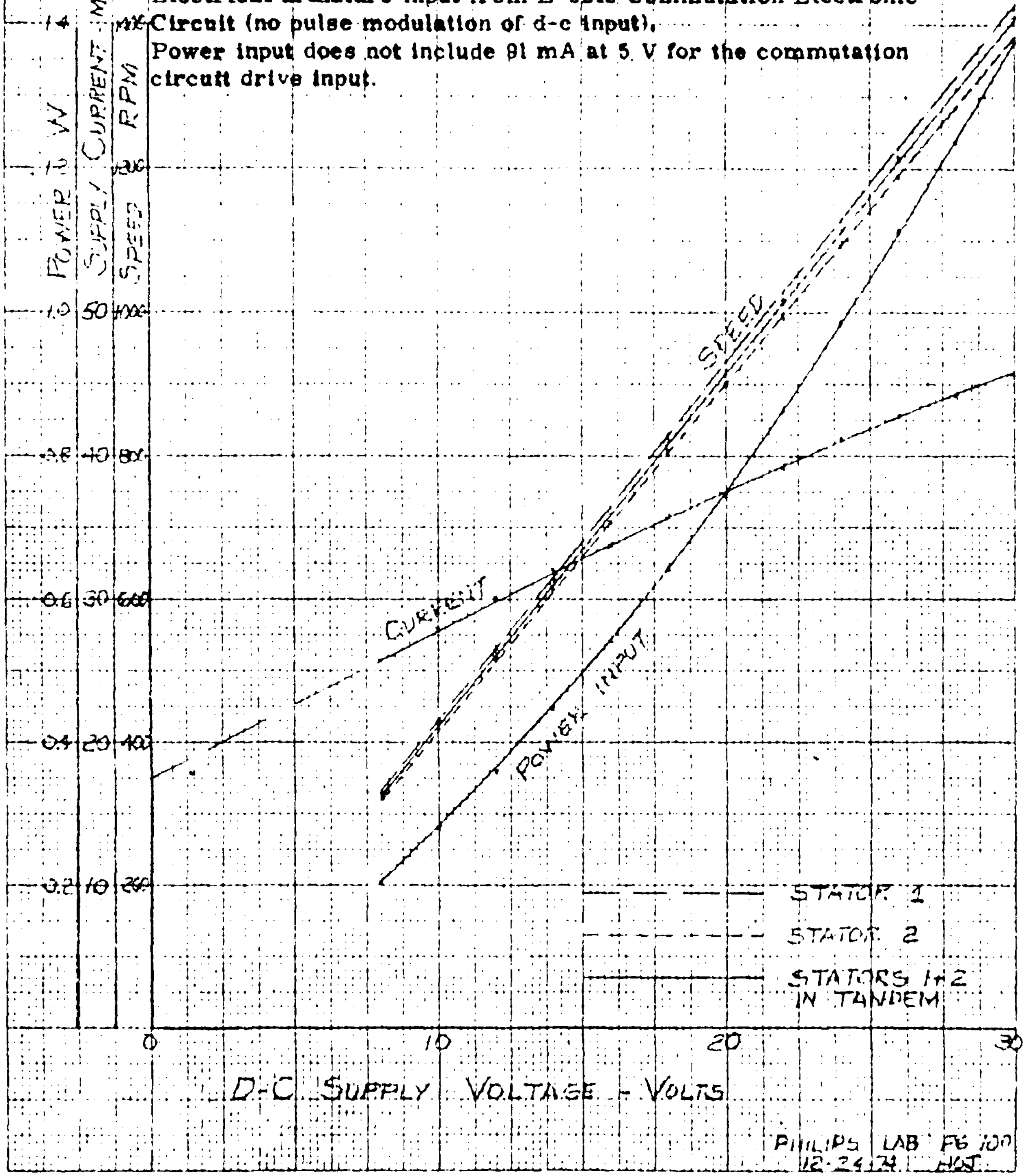

M-2659

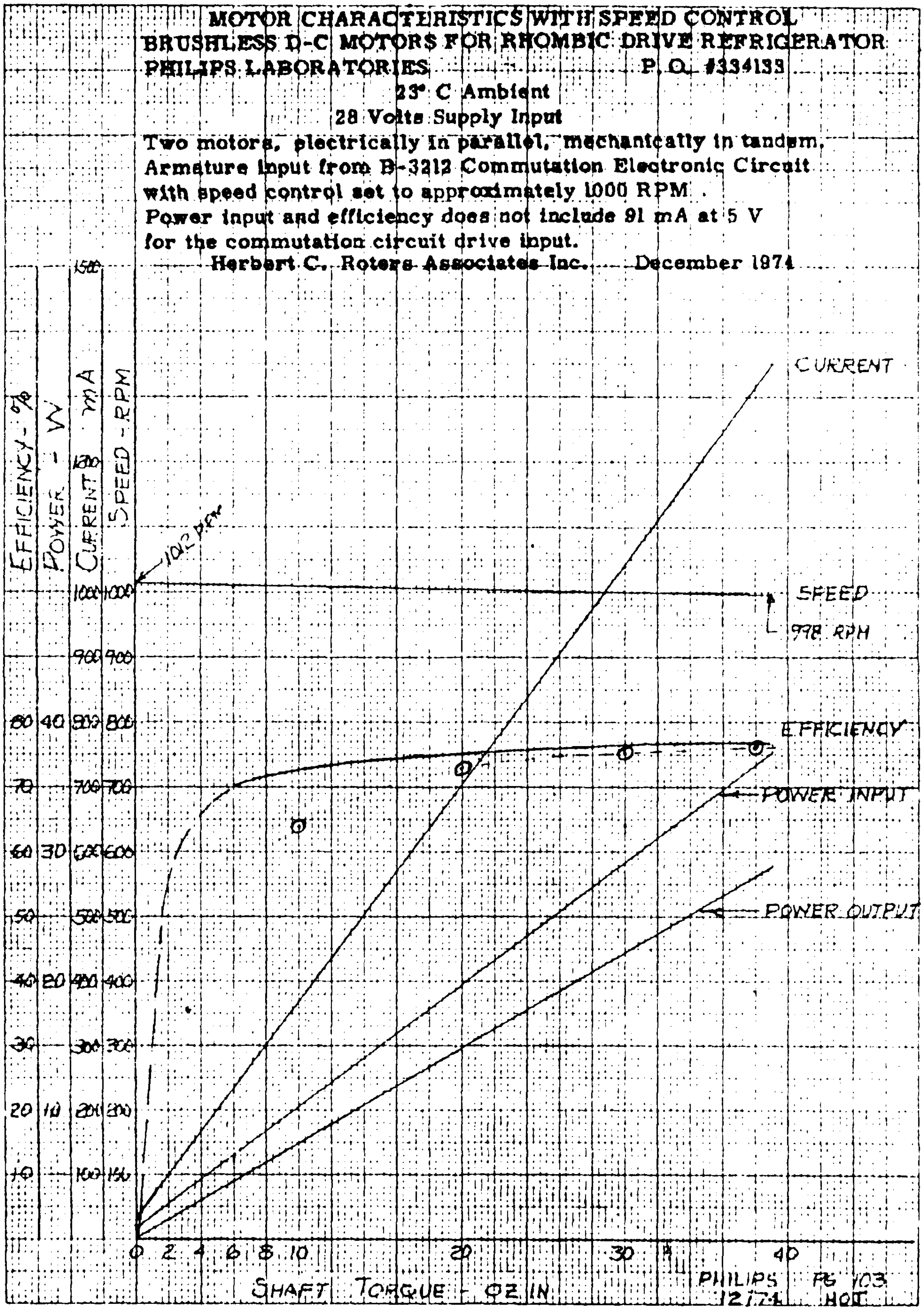
MOTOR CHARACTERISTICS WITH SPEED CONTROL
BRUSHLESS D-C MOTORS FOR RHOMBIC DRIVE REFRIGERATOR
PHILIPS LABORATORIES P.O. #334133
23° C Ambient
28 Volts Supply Input
Two motors, electrically in parallel, mechanically in tandem.
Armature input from B-3212 Commutation Electronic Circuit
with speed control set to approximately 1000 RPM.
Power input and efficiency does not include 91 mA at 5 V
for the commutation circuit drive input.
Herbert C. Roters Associates Inc. December 1974
EFFICIENCY - %
POWER - W
CURRENT mA
SPEED - RPM
1012 RPM
CURRENT
SPEED
998 RPM
EFFICIENCY
POWER INPUT
POWER OUTPUT
SHAFT TORQUE - OZ IN
PHILIPS
12774
PG 103
HOT

MOTOR CHARACTERISTICS WITH SPEED CONTROL
BRUSHLESS D-C MOTORS FOR RHOMBIC DRIVE REFRIGERATOR
PHILIPS LABORATORIES P.O. #334138
28 Volts Supply Input; 23° C Ambient

Two motors, electrically in parallel, mechanically in tandem.
Armature input from B-3212 Commutation Electronic Circuit
with speed control set to approximately 1000 RPM. See M-2660.
Power input and efficiency do not include 91 mA at 5 V
for the commutation circuit drive input.
Herbert C. Roters Associates, Inc. December 1974

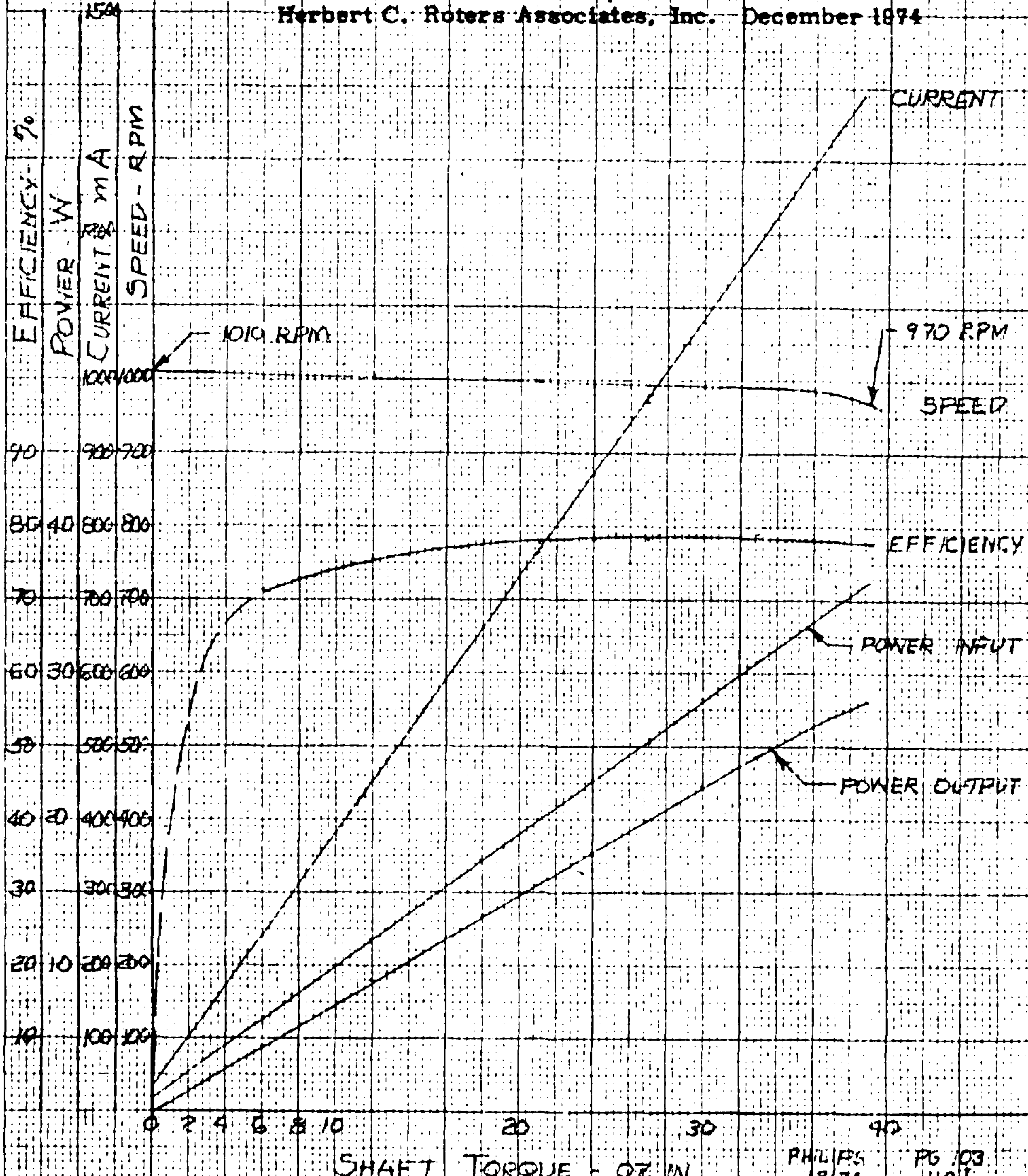

M-2661

MOTOR CHARACTERISTICS WITH SPEED CONTROL
BRUSHLESS D-C MOTORS FOR RHOMBIC DRIVE REFRIGERATOR
PHILIPS LABORATORIES P.O. #334133
30 Volts Supply Input; 23° C Ambient

Two motors, electrically in parallel, mechanically in tandem. Armature input from B-3212 Commutation Electronic Circuit with speed control set to approximately 1000 RPM. See M-2660 Power Input and efficiency do not include 91 mA at 5 V for the commutation circuit drive input.

Herbert C. Roters Associates, Inc. December 1974

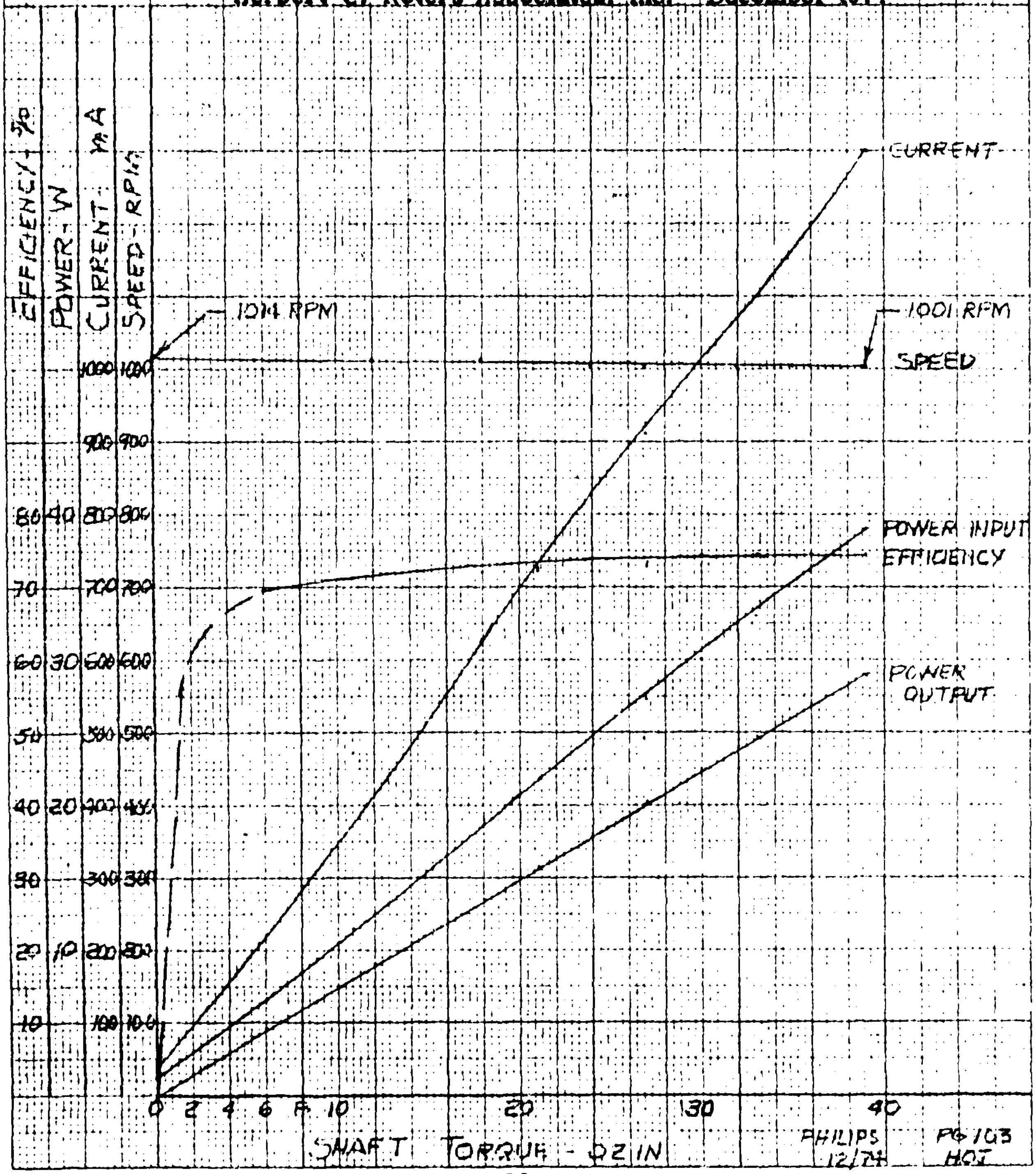

M-2662

MOTOR SPEED CONTROL CHARACTERISTICS
BRUSHLESS D-C MOTORS FOR RHOMBIC DRIVE REFRIGERATOR
PHILIPS LABORATORIES P. O. #334133
23° C Ambient
Herbert C. Roters Associates, Inc. December 1974

Two motors, electrically in parallel, mechanically in tandem. Armature input from B-3212 Commutation Electronic Circuit with speed control set to approximately 1000 RPM. See M-2660 to M-2662

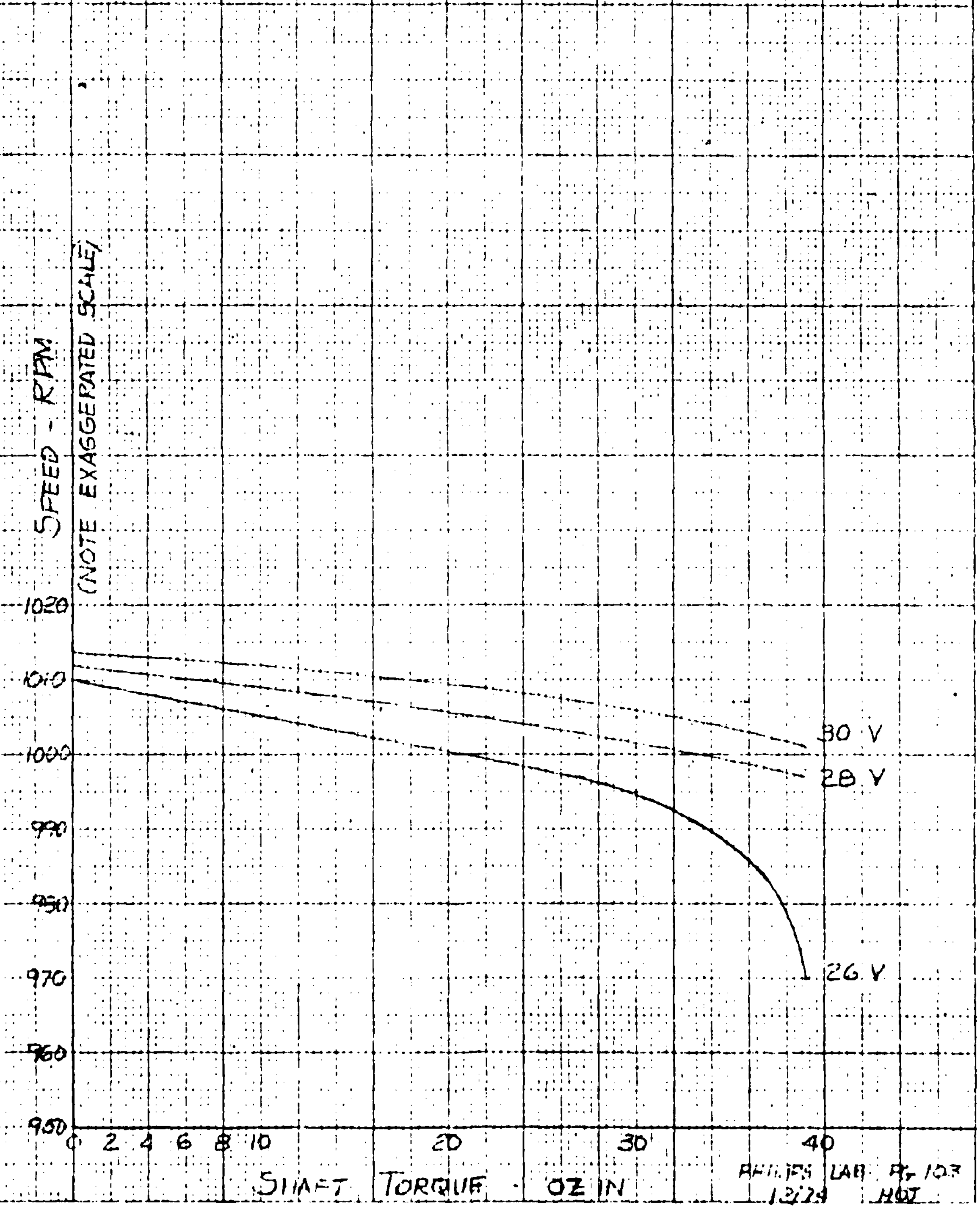

M-2663

APPENDIX II

Appendix II, on the following pages, is a reproduction of the JHU/APL internal report that describes the motor control and telemetry circuits developed for the Stirling cycle refrigerator.

THE JOHNS HOPKINS UNIVERSITY
APPLIED PHYSICS LABORATORY
LAUREL, MARYLAND

EEO-78-10
June 4, 1979

TO: B. D. Kellam

FROM: G. S. Keys

SUBJECT: Description of Motor Control and TM Circuits for the Cryogenic Cooler Program

Introduction

A Sterling Cycle Refrigerator has been developed by Philips Laboratory in conjunction with A.P.L. The purpose of this refrigerator is to cool the detector of a Gamma Ray Spectrometer developed by Lockheed Palo Alto Research Laboratory.

A.P.L. was responsible for the design of the control circuitry for the Motor Drive and the T. M. Interface between the refrigerator and the Lockheed T. M. System.

The following memo describes in detail the Motor Control and T. M. Circuits.

Four of the refrigerators were launched on a satellite during February 1979 and are performing as expected.

Gary S. Keys

Gary S. Keys

GSK/mrh

Distribution:

RTEllis
BDKellam
SDAhlbrand
JWFollin, Jr.
CSLeffel (2)
RVonBreisen
RLee
HLee
GSKeys (3)
File
Archives

Table of Contents

VII. Figures

VIII. Drawings

I. ELECTRONICS PACKAGE

A. General Description

The circuitry contained in the Electronics Box located on the refrigerator is made up of two sections, the first being the speed control for the motor and the second is conditioning circuits for the various sensors located on the refrigerator. This circuit supplies the signals to the Lockheed TM System. The block diagram (figure 1) shows a more detailed breakdown of the circuits in the electronics box. The following is a brief description of each block.

Motor Hall Sensors Provide a logic level output coincident to the position of the Motor Rotor. Six sensors are used.

Sensor Integrater Comprised of a one-shot that is triggered by two of the Hall sensors. The output is a fixed pulse width with the repetition rate determined by the repetition rate of the Hall sensors. The pulse is then integrated into a DC voltage. Voltage amplitude is then equal to repetition rate of Hall sensors which is equal to RPM of motor.

Speed Comparator Compares a DC level set by the Speed Select Circuit with the integrated DC voltage from the motor and develops a varying pulse width modulation signal for the motor drive.

Speed Select Controlled by external relays and is used to develop the DC reference voltage to control the RPM of the motor.

Start-up Current Limit Controls the drive capability of the stator drive transistors to limit the initial start current to 300% of the run current. This circuit remains energized for a predetermined time.

150% Current Limit Limits the current to the motor to 150% of the run current in all conditions except when the motor is first energized. This current limiting is accomplished by forcing the pulse width modulation from the speed comparator to 0%, therefore turning the motor drive off.

Motor Drive Logic Combines the outputs of the Hall sensors and the pulse width modulation from the speed comparator to provide drive to the motor drive transistors. This circuit controls which phase of the motor will be supplied current and for what percentage of the time.

Motor Drive Transistor These are Darlington Complementary Pairs for each motor phase, one for sourcing current and one for sinking current.

DC-DC Converter This is a commercial converter that produces the 5 volts necessary for operating the logic, from 28 volts. Standard converter built with screened parts. Mil-Electronics Mod XD324.

TM Regulator This is a linear DC regulator which develops 15 volts from the TM 28 volt buss for the TM buffers and 5 and 10 volt references for the TM sensors.

TM Buffers Convert the DC levels for the TM sensors to a zero to five volt level compatible with the Lockheed TM system.

II. DC MOTOR AND SPEED CONTROL

A. General Description

The motor used in the refrigerator is a specially designed high efficiency brushless DC motor. The motor is designed and built by Roters Associates. It is configured as a six pole permanent magnet rotor with a three phase Delta connected stator winding. The phases of the stator are energized in a sequence determined by the position of the rotor. The position of the rotor poles is precisely determined by a commutation circuit comprised of six Hall sensors. The precise switching of the stator phases provides the maximum efficiency of the motor.

The actual motor configuration in the refrigerator is two of these motors operating in parallel, mechanically turning in opposite directions. Both motors share the stator drive circuits and the Hall sensor commutation circuits.

The speed control circuit incorporated into the commutation and drive circuits will keep the motor operating at a constant speed with variations in mechanical load on the motor shaft. This keeps the overall efficiency of the motor high.

The speed control circuitry operates on a pulse width modulation drive to the stator phases. The speed control performs two functions, the first being to decode the Hall sensor signals to determine the position of the rotor so the appropriate phase of the stator can be energized. The second is to develop the modulation signal for the stator drive circuits to control the speed of the motor.

The modulation signal is derived by integrating two Hall sensor signals to determine the speed of the motor. This voltage is then compared to a pre-set voltage that is related to a set motor speed, increasing or decreasing the pulse width of a 10 kHz signal that is applied to all of the stator drive circuits. The wider the pulse the longer the motor is energized, thus causing it to gain speed. The opposite is true for a narrower pulse width.

If the speed control is disabled, modulation set at 100%, then the motor speed will be determined by the motor supply voltage and the mechanical load.

A more detailed description of the motor and speed control is contained in Sections III and IV.

III. MOTOR DESCRIPTION

A. Design Specifications

The specifications as set by the refrigerator design which determined the design of the motor are that the RPM should be controlled to 1000 and be capable of delivering 34 inch ounces of torque.

The efficiency of the motor under these conditions should be 75%, deliver 15 watts to motor shaft and consume 20 watts.

The motor must also be capable of delivering a starting torque of 300% nominal for 1 second and 200% for 10 seconds, also deliver 150% of nominal indefinitely. The main goal besides meeting these mechanical specifications was to produce a very efficient motor. Refer to figure 6 for motor performance curves.

B. Motor Configuration

Referring to figure 2, the motor is configured with a 6-pole permanent magnet rotor consisting of alternating north, south pole samarium cobalt magnets.

The stator winding consists of three phases connected in a Delta configuration (figure 3). Each phase consists of six coils in series equally spaced mechanically with three coils per pole.

The commutation circuit consists of the six Hall sensor circuits spaced as shown in figure 2. The Hall sensors are turned on by the South pole and off by the North pole of the rotor magnets. The alternate North, South pole configuration gives a more precise on/off switching of the Hall sensors for less rotation of the rotor.

C. Motor Operation (refer to figure 4)

The operation of the motor depends upon switching the current to the proper motor phase and in a set direction depending upon the configuration of the Hall sensors that are energized. The three connections to the Delta stator windings can be either a source or sink of the stator current.

A rotation of 120° mechanical of the rotor will produce a complete electrical rotation (360°) of the Hall sensors. The combination of the Hall sensors (figure 4) determines the current flow through the legs of the Delta winding.

The precise turn-on of the Hall sensors aligns the rotor poles with the coils in the stator windings. This precise turn-on and current switching provides maximum efficiency.

As can be seen from figure 4, there is a factor of three difference between the mechanical rotation of the motor and the electrical rotation (switching of the current through the stator winding).

A different Hall sensor is energized every 20°M (60°E) and as can be seen by referring to the logic diagrams on figure 4, the direction of the current flow through the three legs of the Delta stator will change with the turn-on of the next Hall sensor.

The turn-on must be precise but the on duration can be between 150° and 180° electrical.

IV. DETAILED CIRCUIT DESCRIPTION (Drawings #5114-2401, 5114-2301)

A. Sensor Integrator

This circuit consists of a one-shot (U1) and inverters contained in U2 and U4 and an RC network consisting of R41, R42 and C8.

The one-shot which has a fixed time of 2.7 Msec is triggered by the leading edge of Hall sensors three and six, a negative going transition (off = high level). The "on" time of the one-shot will remain constant but the rate that it is triggered is determined by the speed of the motor. The one-shot pulse is applied to the integrator as a +5 volt level (R41, CR11, C8). The higher repetition rate causes the pulse to be present at the integrator more frequently, developing a higher DC voltage at the integrator capacitor C8. A slower motor speed causes the integrator to discharge for longer periods of time (time between one-shot pulses longer) through R42 and U2-6 which sets at ground level when the one-shot is not active.

The integrator DC voltage is then representative of the motor RPM and is used in the speed comparison circuit (U10) and also goes to the TM circuit as a calibrated RPM voltage.

B. Speed Select and Pulse Modulation

This section of the speed control circuitry consists of a voltage divider made up of a resistor divider (R35 through R40) a voltage comparator (U10) and 10 kHz oscillator (U11).

The speed select which utilizes the voltage divider generates three DC voltages used as reference voltages for the voltage comparator U10). These voltages are equal to voltages developed from the integrator when the motor is operating at the desired RPM settings of 850, 1000 and 1150 RPM. The reference voltages for the RPM settings are selected by combining the terminals E7, E8, E9 and E10. The nominal running RPM is obtained with all the terminals open. The low RPM (850) is obtained by connecting E9 and E10 lowering the reference voltage and the high RPM (1150) by connecting E7 and E8.

The voltage comparator combines the integrator voltage, reference voltage and a 10 kHz sawtooth signal from U11 to form the pulse modulation signal to control the motor speed.

The sawtooth 10 kHz is generated by the square wave oscillator (U11) and is integrated by C10. This signal is then summed with the reference voltage on pin 2 of U10. The amplitude of the sawtooth signal is determined by the voltage divider of R50 and R44. Refer to figure 5 (voltage comparator signal). The voltage comparator output U10-9 will normally set at +5 volts if the two

inputs are not equal. When the inputs are equal the output goes to a 0 volt level. When the inputs are equal and the 10 kHz signal is added to the reference voltage, the excursion above and below the reference voltage will cause the output of the comparator to turn on and off at the rate of the 10 kHz signal. The on and off times will be equal.

Since the sawtooth signal and the reference are fixed, the integrator voltage will cause the output on/off time of U10 to vary. When the integrator voltage rises in amplitude due to an increase in motor RPM then a condition exists as shown in figure 5a where the integrator voltage is above the reference voltage and the sawtooth signal equals the integrator voltage for only a short time during one cycle, causing the output of U10 to be at +5 V (off) for a short time compared with 0 V (on) time. The 5 volt level is equal to 100% modulation (motor energized) and the 0 volt level is zero modulation (motor off).

The example in 'a' energizes the motor for a shorter time thus causing the motor to reduce speed. The opposite example is shown in figure 5b, the motor slows so the modulation is increased. When operating at normal speed the modulation should be 50%.

This 10 kHz modulation signal is connected to the logic circuit that controls the transistors that drive the motor phases.

C. Motor Drive Logic

This section of the speed control is made up of circuits U3 through U6 and the associated diodes and transistors.

The inputs to this section are the six Hall sensor signals. The Hall sensor outputs are ground level "true" signals so they are inverted by U3 before being combined in the Nand gates U4 and U5. The combination of the sensor signals provides the voltage source and current sink control signals for the drive transistors on the three phases of the motor.

Referring to the logic circuits associated with Hall sensor #1 (U4-12), the combination of sensor #1 true (U4-12), high level, and U4-13 high indicating a false from Hall sensor #3 causes U4-14 to go low. This is inverted by U6-6. The positive level on the base of Q1 will cause Q1 to conduct reducing the voltage level on E19. Referring to drawing 5114-2301 it can be seen that this voltage level on E19, which is the base of Q1, causes Q1 to conduct applying +28 volts to E16, which connects to phase one of the motor, the emitter of Q1 is connected to +28 V. This sequence develops the +28 volt source for phase one of the motor. There must now be a sink for the motor current. Referring to drawing 5114-2401, a combination of Hall sensor 6 ON (U5-9) high and sensor 2 OFF (U5-12) high and the 10 kHz modulation signal will cause E24 to vary from 0 to +5 volts at the 10 kHz rate. This signal at the base of Q6 (5114-2301) will cause Q6 to conduct at the 10 kHz rate, sinking current from phase three of the motor. Therefore, under this set of conditions, current flows from phase one to phase three.

The combination of the sensor signals is shown in figure 4. The zener diodes CR1 through CR6 provide protection for the logic circuits by limiting any pick-up on the sensor lines to the supply voltage and to a negative .6 volts. The diodes CR-7, 8 and 9 protect the inverters (U6) from any negative transient signal.

The transistors Q1 and Q2 are used to switch the +28 volts since this voltage is unregulated and could exceed the rating of logic inverters U6.

D. Motor Current Limit

There are two protective modes of limiting the amount of current the motor can draw. One is during the initial power-on sequence and the second is during the normal running of the refrigerator.

The power-on current limit is initiated by the five volt power integrating the RC network of R31 and C5. When the threshold of U9 is exceeded a pulse is generated by U9 which resets U8-13 which turns off Q2 on the output of U2-12. This inhibits all of the motor drive source transistors. The resetting of U8-13 will cause U8-9 to set. This in turn forces the speed control integrator to zero volts (U2-10 low) forcing 100% modulation. U8-9 is also used to drive relay K-1 (5114-2301). This relay has two sets of contacts, the first set K1-B1 and B2 shorts R34 (5114-2401) to ground pre-setting U8-13 which in turn causes Q1 and Q2 to be enabled, allowing one of the motor phases to be energized thus starting the motor.

The second set of contacts of K1 switch in R1 (1.0 ohm resistor) in the emitter legs of the current sinking motor drive transistors. If the current through R1 reaches 3.3 amps the voltage across R1, 3.3 volts, will cause the drive transistors to turn off, thus limiting the current to this value.

The one-shot (U9) is set for an ON time of approximately 1.0 sec. This is sufficient time for the refrigerator to start. At the end of this time U8-9 is clocked to a reset state and relay K1 is de-energized, removing the current limiting resistor R1.

The second form of current limit is to protect the cooler during normal running. This is accomplished by measuring the current through a .1 ohm resistor (5114-2301). The voltage is conditioned with an op-amp in the TM circuitry and applied to a comparator (U7) on the speed control board (5114-2401). The reference voltage is equal to maximum current allowed during normal running, 150% of nominal (1.8A). When the voltage on U7-3 exceeds the reference (U7-2), the comparator output goes low forcing the input to the integrator to maximum causing the modulation to go to zero shutting the motor off. When the current falls below the maximum the comparator resets, allowing the motor to run.

E. Motor Drive Transistors

These transistors are Darlingtons and there is a complementary pair for each phase of the motor. Referring to drawing 5114-2301 it can be seen that the emitters of the PNP transistors are connected to +28 volts and are the voltage source transistors. The emitters of the NPN transistors are connected to the +28 volt return and are the current sinking transistors. The collectors of the complementary pairs are tied together and connect to the three phases of the motor. The drive signals come from the speed control board. The diodes CR1-CR6 provide a current path for the inductive voltage when the particular phase is de-energized.

F. Power Conditioning

There are two voltages associated with the motor drive and control, +28 V and +5 V.

The +28 volts supplied by an external source passes through the LC (L1, C1 and C2) network on 5114-2301 before being distributed to the motor. This filter is to provide a smoothing of the 28 volt current drawn from the source so the reflected ripple of the motor current variations caused by the varying load of the cooler and the 10 kHz modulation will not be seen by the voltage source.

The internal +5 volts for the logic is provided by a DC-DC converter which is powered by the +28 volt input. The specifications of the converter are shown in figure 7.

V. T.M. SIGNAL CONDITIONING CIRCUITS

A. General

This section is contained on two boards (A1, A2) of the electronics package.

The function of this section is to supply reference voltages to the various sensors and to condition the signal output of the sensors to be compatible with an external recording or TM system.

This section is powered by 28 V DC.

B. Voltage Regulator (Drawing 5114-2201)

The 28 volt DC input to the TM section is regulated by a 15 volt zener (CR1) to supply power to the operational amplifiers used as the TM buffers (U1 on A1 and A2). U2 on board A2 is powered by the 5 volt converter because the signal from this circuit must function when the TM circuit is powered down. The 15 volts is further regulated by Q1, a stable 5 volt regulator. This voltage is used as the reference voltage by the temperature sensor and the helium volume pressure transducer. The 5 volts is also multiplied by two to produce the 10 volt reference for the crankcase pressure transducer.

C. TM Buffers (Drawing 5114-2201 for A2 and 5114-2101 for A1)

There are five buffers that condition three sensor signals and two motor operating conditions. All the TM signal outputs are set to produce a 0 to +5 volt signal for the maximum range of the function it is monitoring.

1. Temperature Sensor

This circuit is located on A1 and consists of an operational amp (U1) with a gain of 4.83- The resistor (R3) sets a constant current of 10 uamps through the thermister.

2. Volume Pressure

This buffer is also located on A1 and consists of a bridge amplifier with a gain of 50. The volume pressure transducer is a strain gauge bridge with a 0 to 100 MV full scale output using a 5 volt DC reference.

3. Crankcase Pressure

This is a bridge amplifier also located on A1. The gain of this circuit is 100. The crankcase pressure transducer is a strain gauge bridge that has a 0 to 37.5 MV full scale signal using a 10 volt DC reference voltage.

4. Motor Speed

This buffer is a non-inverting amplifier with a gain of 1.3. The input is derived from the motor speed control board. The monitor voltage is the integrated voltage of the motor Hall sensor which is representative of the RPM of the motor.

5. Motor Current

This buffer is located on board A2 and consists of U1 which is the TM buffer and U2 which is the current monitor for the speed control circuitry.

The input voltage for this circuit is obtained by measuring the voltage drop across a .1 ohm resistor in the 28 volt return line of the motor power. The voltage to the TM buffer is filtered by the RC combination of R13 and C9. The gain of this buffer is 20.

The current monitor buffer is not as heavily filtered, so it will respond to faster current changes. This voltage is then amplified by U2 (gain = 9.25). The voltage from this circuit is the input to the motor speed current limiting circuitry.

VI. INTERFACE

A. Electronics Package to Cooler

This interface is accomplished through two separate routes. The first is the connection to the motor, which is situated in the sealed crankcase. The electrical interface to the motor is through two 9 pin feed-through connectors. The wiring between the feed-through and the electronics is hard wired solder connections.

The feed-throughs as shown on drawings 5114-2051, 5114-2001, contain all the Hall sensor signals, power to the Hall sensors, the three motor drive lines, and the reference voltage and signal for the crankcase pressure transducer.

Mechanically, the electronics box has a cutout area for the feed-throughs and the box bolts to the cooler with the feed-through protruding into the box. A service loop in the connecting wires allows physical separation of the two units.

The second interface is through connector J3. This connector contains the signals and reference voltage for the thermister and the volume pressure transducer. These sensors are located on the exterior of the cooler.

The thermister is attached to the cold flange and the volume pressure transducer, which is a bridge with four strain gauge elements, is wrapped around the buffer tank. The compensating resistors for the bridge are located on a terminal board attached to the top of the crankcase.

B. Electronics Package to External Systems (Drawings 5114-0001 and 5114-2001)

This interface is accomplished through connectors J1 and J2. J1 contains the power and control signals for the motor speed control. This consists of a +28 volt and 28 volt return line and two lines each for speed controls 2 and 3. Speed 2 is the low RPM setting and speed 3 is the high. The selection of the different speeds is accomplished by connecting the two designated lines for the desired speed. When speed 2 is being used, the lines for speed 3 should be open; when the lines for both speed 2 and 3 are open, the motor will run at the nominal RPM. The RPM for the nominal (speed 1) is 1000, speed 2 is 850 and speed 3 is no speed control; thus, the RPM will vary with the cooler load and power supply voltage.

There is one additional line used in J1. This contains the +5 volt reference voltage used in the TM circuits. This function is labeled APL TEST and is used during bench test of the cooler.

J2 is the TM connector. Included in this connector are the five buffered TM signals used to determine the status of the cooler. These signals are low impedance signals capable of driving a maximum load of 2.0 K ohms.

There is a +28 volt power and return for the TM circuits. Internal to the electronics box, this power is separate from the 28 volt power to the motor control circuits.

The remaining signals labeled APL TEST, are Hall sensor #1, converter +5 volt power and return, and +10 volt reference.

The Hall sensor signal is a T^2L output and is used to directly measure the RPM of the motor.

The +5 volt power is the output of the DC-DC converter used to power the motor control circuitry.

The 10 volt reference is the reference used in conjunction with the TM sensors.

When monitoring any of the signals, or supplying power and control signals to the functions contained in J1 and J2, it is necessary to use the return lines associated with that particular function. As an example, use the signal return of J2 for monitoring any functions associated with the speed control.

In any test or operational setup refrain from having any of the 28 volt return current flowing external through the converter +5 volt return line or the TM signal return line.

EDO-78-10

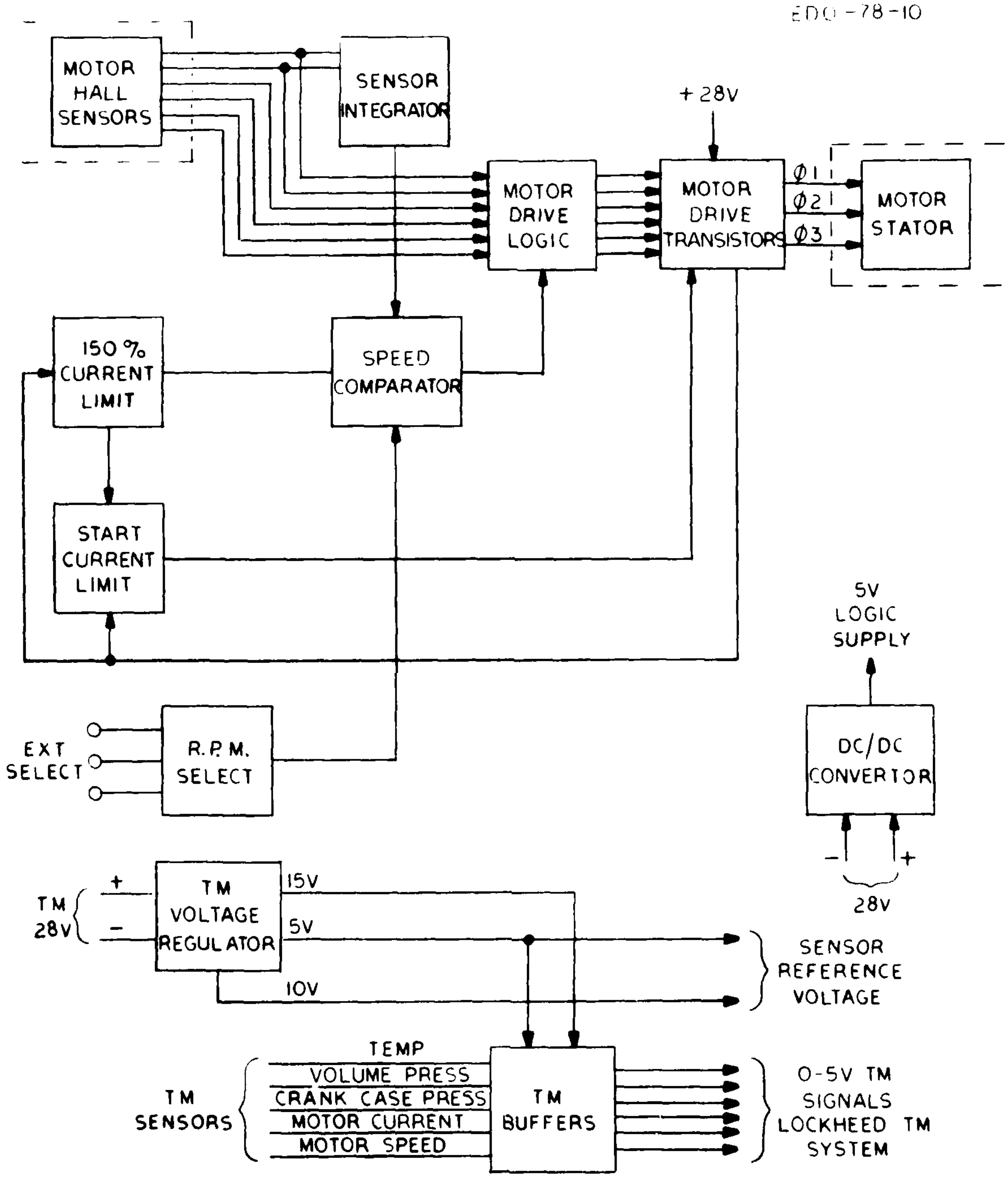

SATELLITE COOLER
SPEED CONTROL & TM CIRCUIT
FIG 1

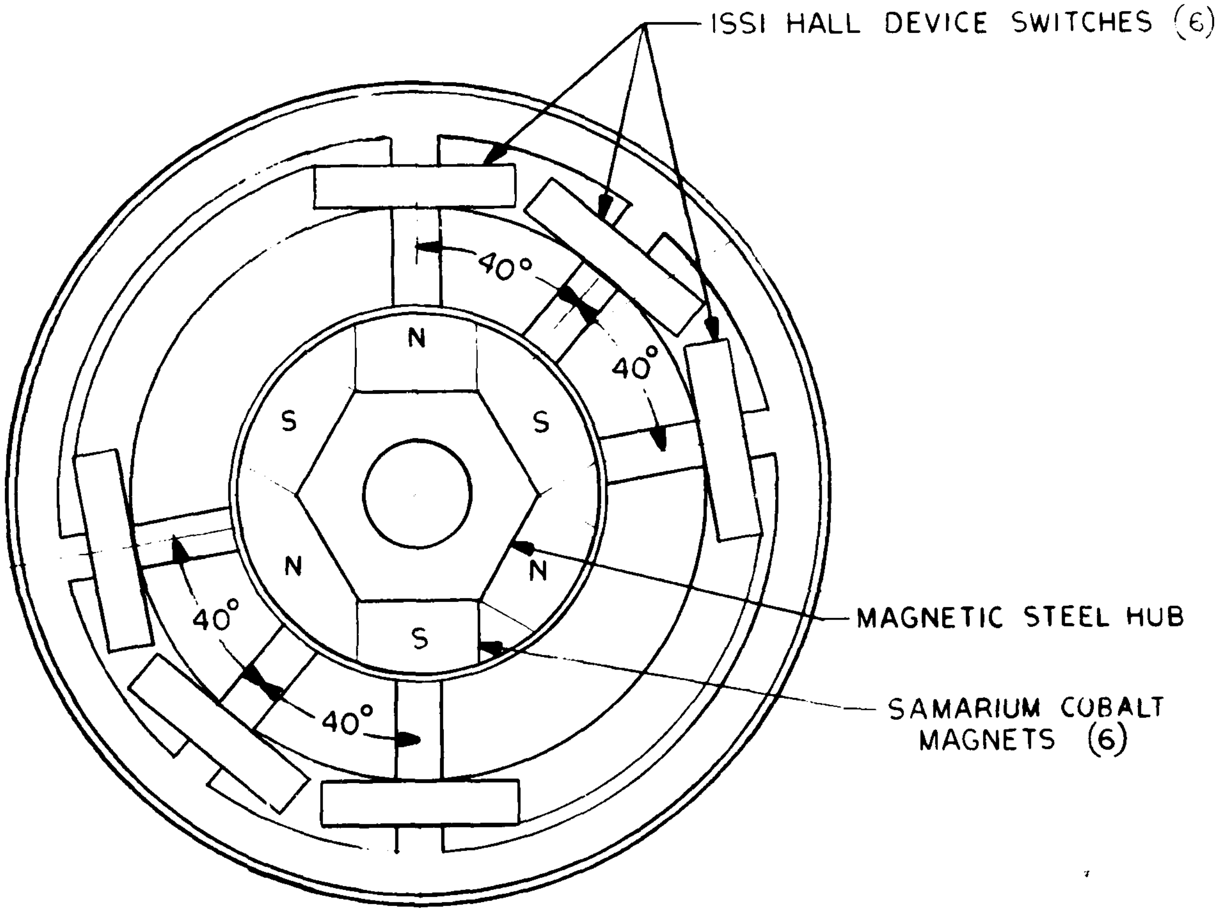

COMMUTATION SENSOR COMPRESSOR MOTOR

FIG 2

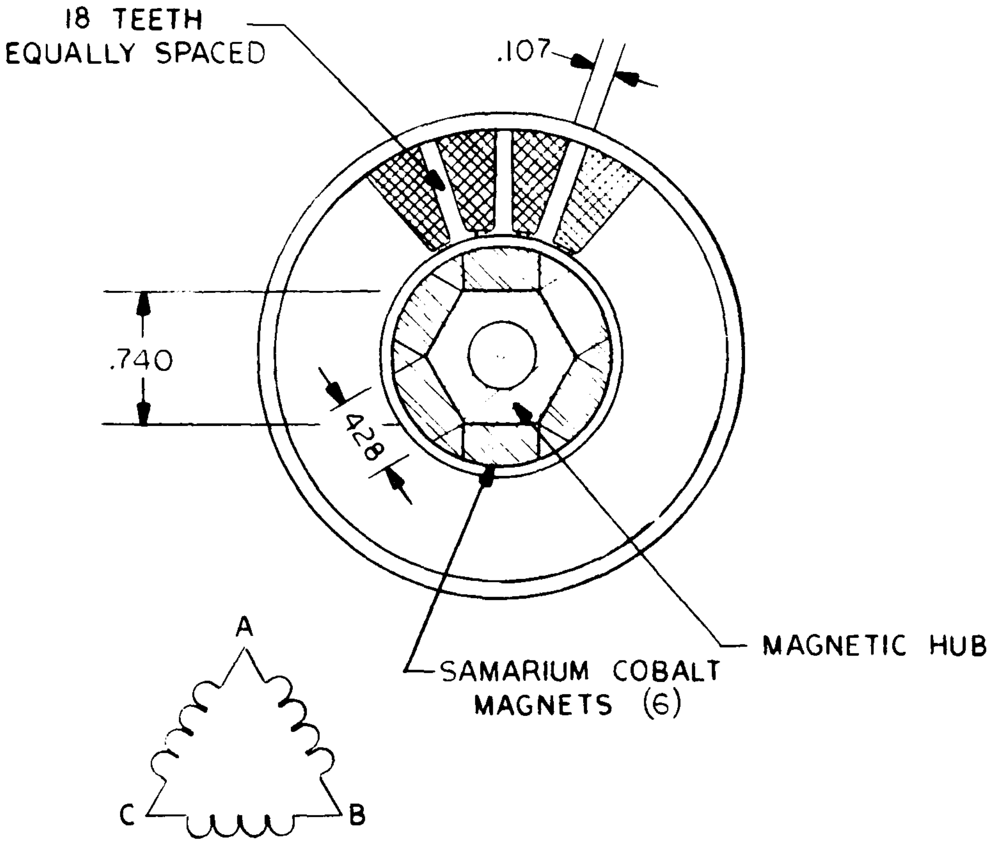

WINDING

6 COILS IN SERIES PER PHASE, 7.03 Ω @ 20°C PER MOTOR

TWO POINT INPUT TO DELTA, 4.69 Ω @ 20°C PER MOTOR

COMPRESSOR MOTOR OUTLINES

FIG 3

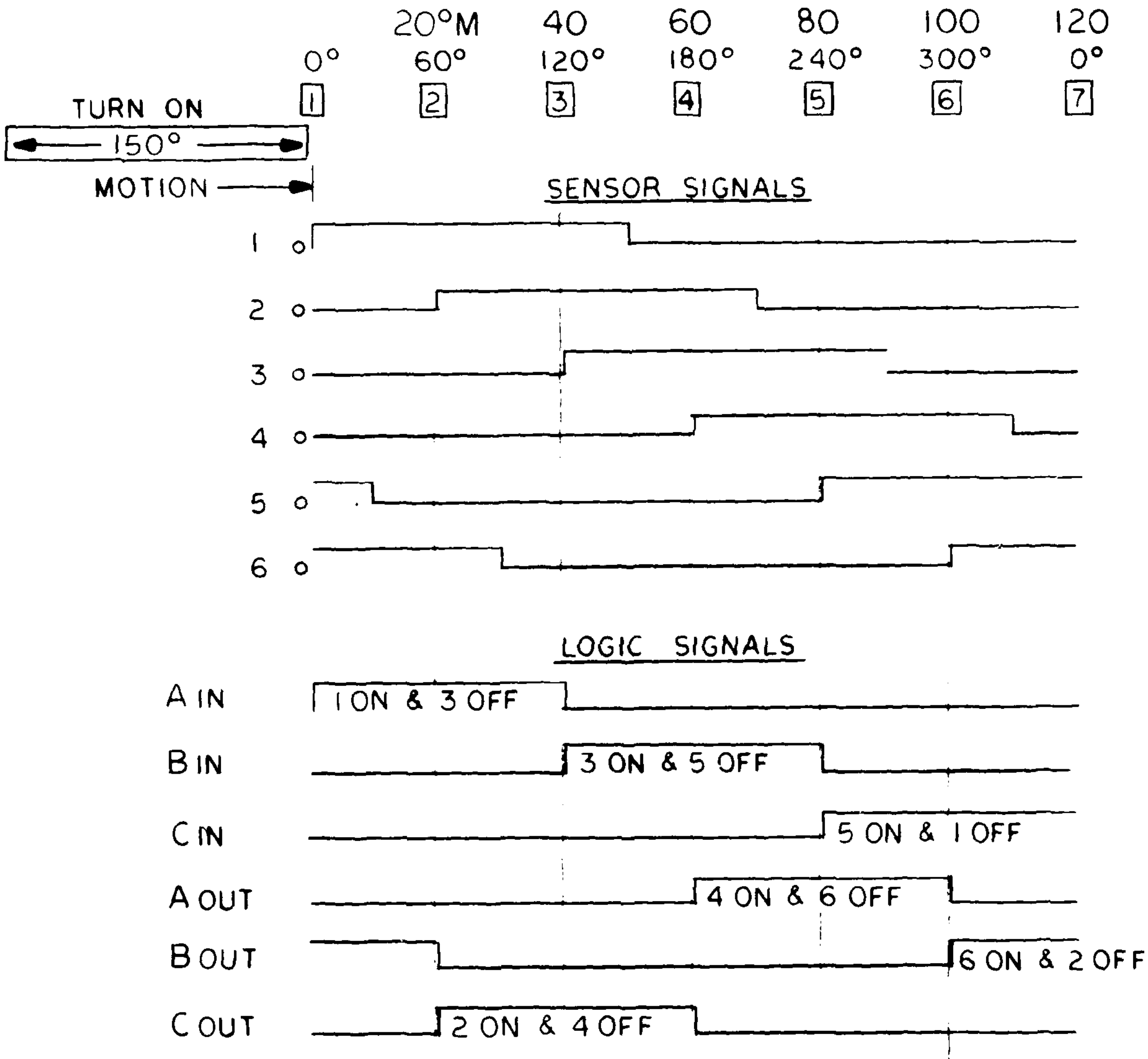

MOTOR ARMATURE

ANGLE ° M	ANGLE °E	+	−
0 – 20	0°– 60°	A	B
20 – 40	60°–120°	A	C
40 – 60	120°–180°	B	C
60 – 80	180°–240°	B	A
80 – 100	240°–300°	C	A
100 – 120	300°–380°	C	B

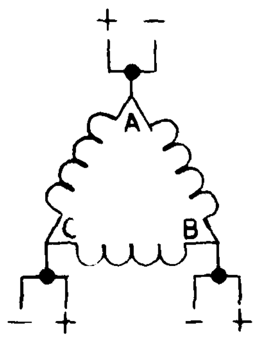

COMMUTATION SIGNALS
SENSOR, LOGIC AND ARMATURE

FIG. 4

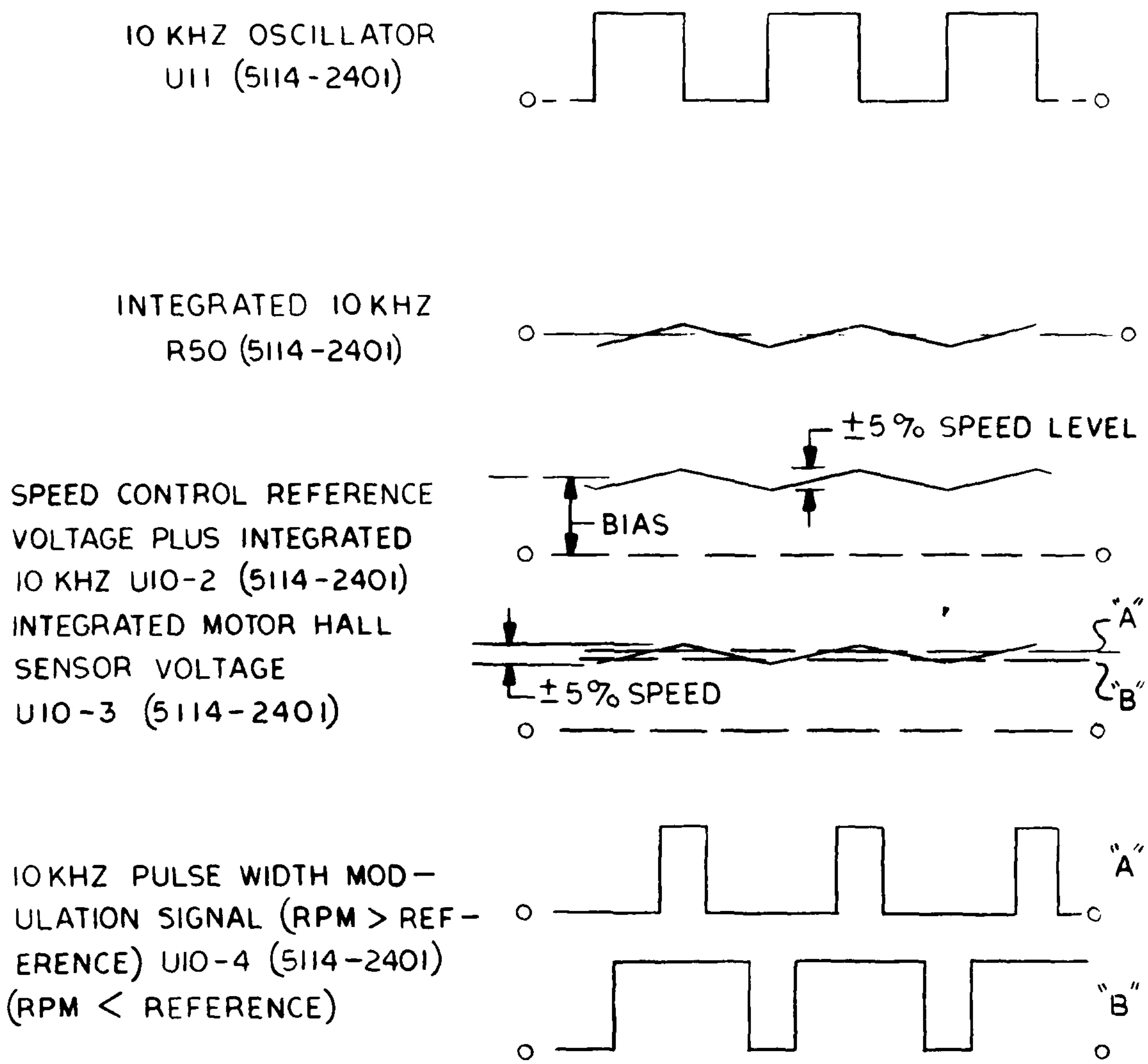

PULSE WIDTH CURRENT MODULATION
SPEED CONTROL

FIG. 5

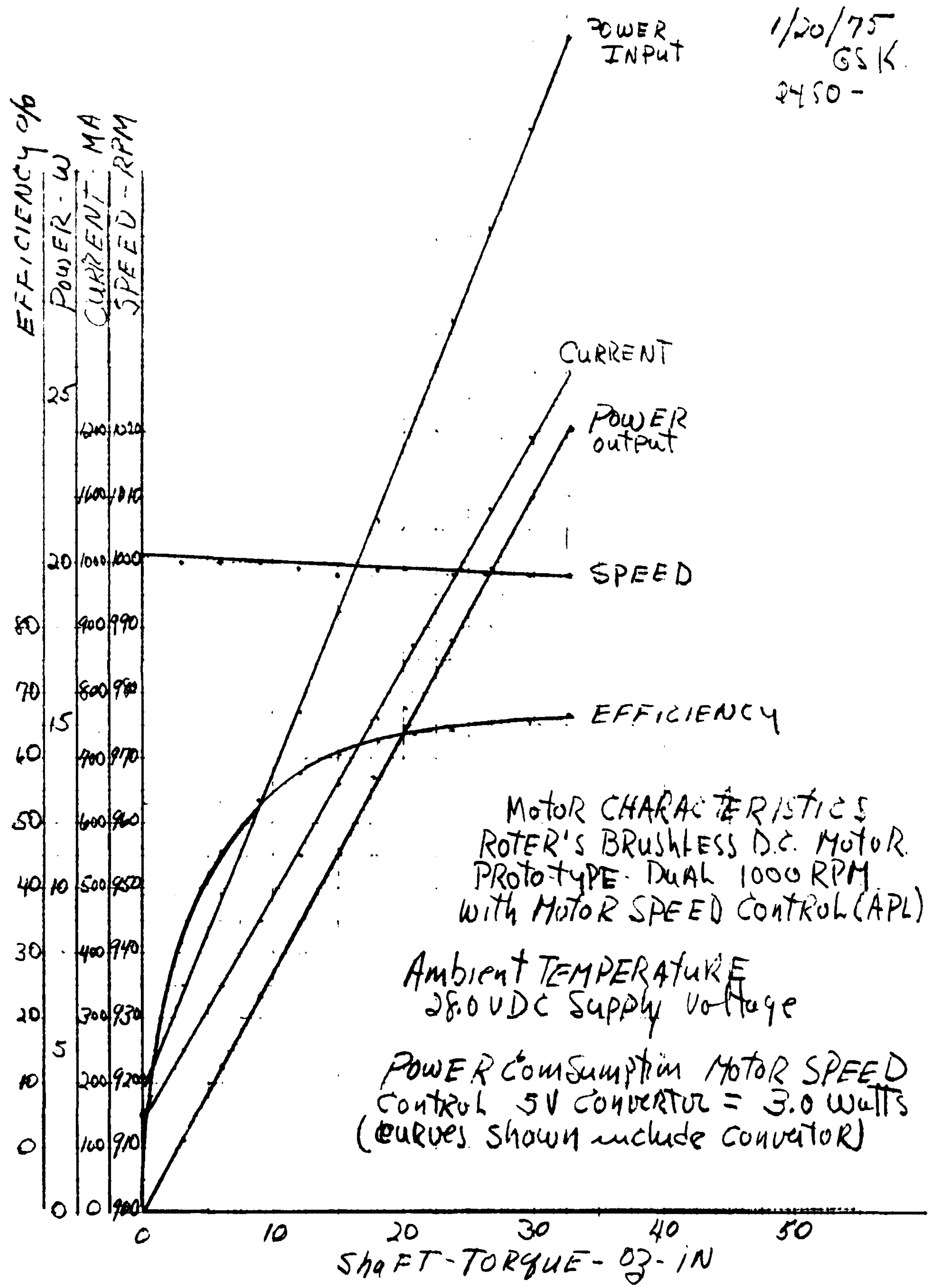
1/20/75
GSK
2450-
POWER INPUT
CURRENT
POWER output
SPEED
EFFICIENCY
EFFICIENCY %
POWER - W
CURRENT - MA
SPEED - RPM
Motor CHARACTERISTICS
ROTER'S BRUSHLESS D.C. MOTOR
Prototype - Dual 1000 RPM
with Motor SPEED Control (APL)
Ambient TEMPERATURE
28.0 VDC Supply Voltage
POWER Consumption Motor SPEED
Control 5V Convertor = 3.0 Watts
(curves shown include Convertor)
SHAFT-TORQUE - OZ-IN

FIG 6A

1/20/75
GSK
Q450-

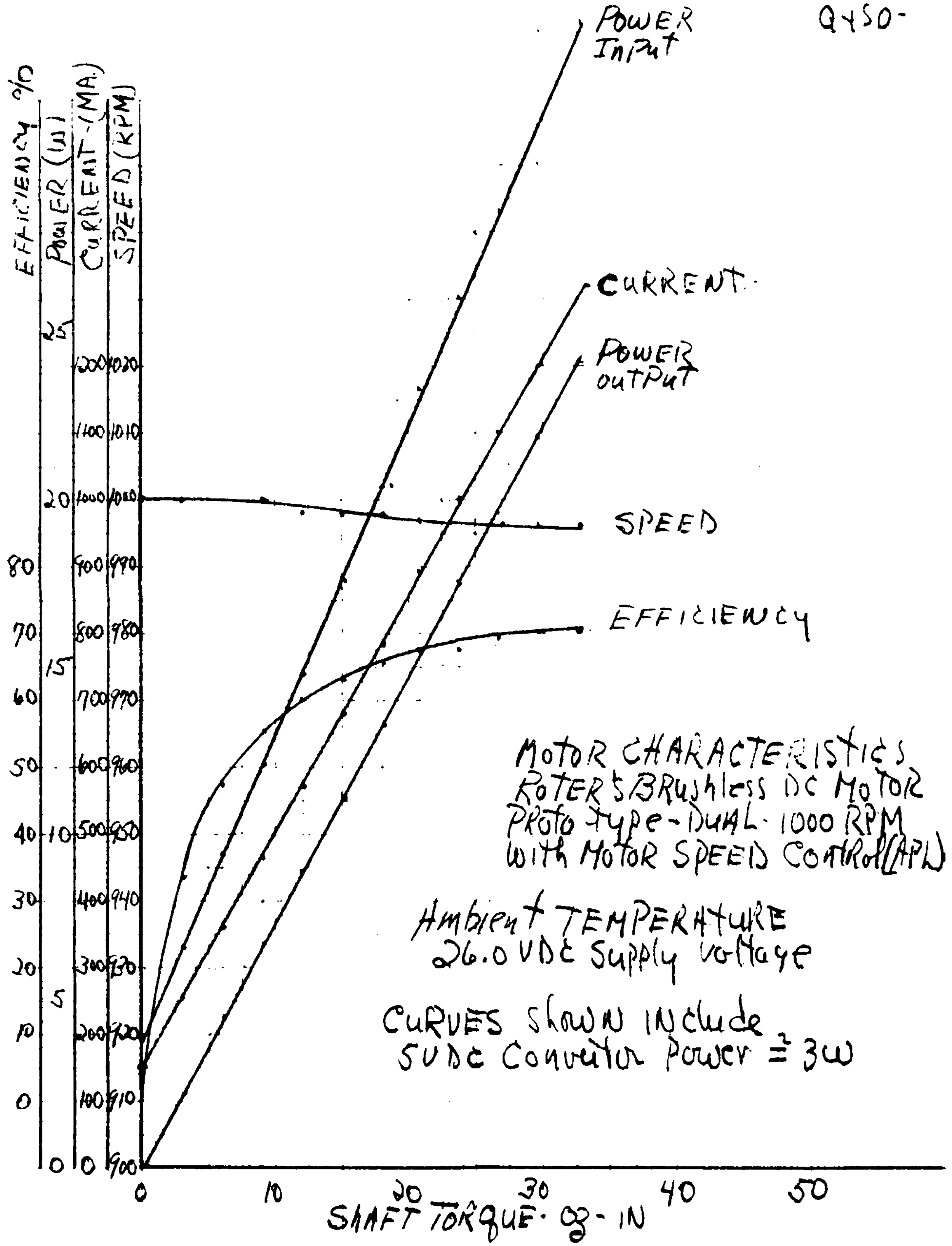

FIG 6B

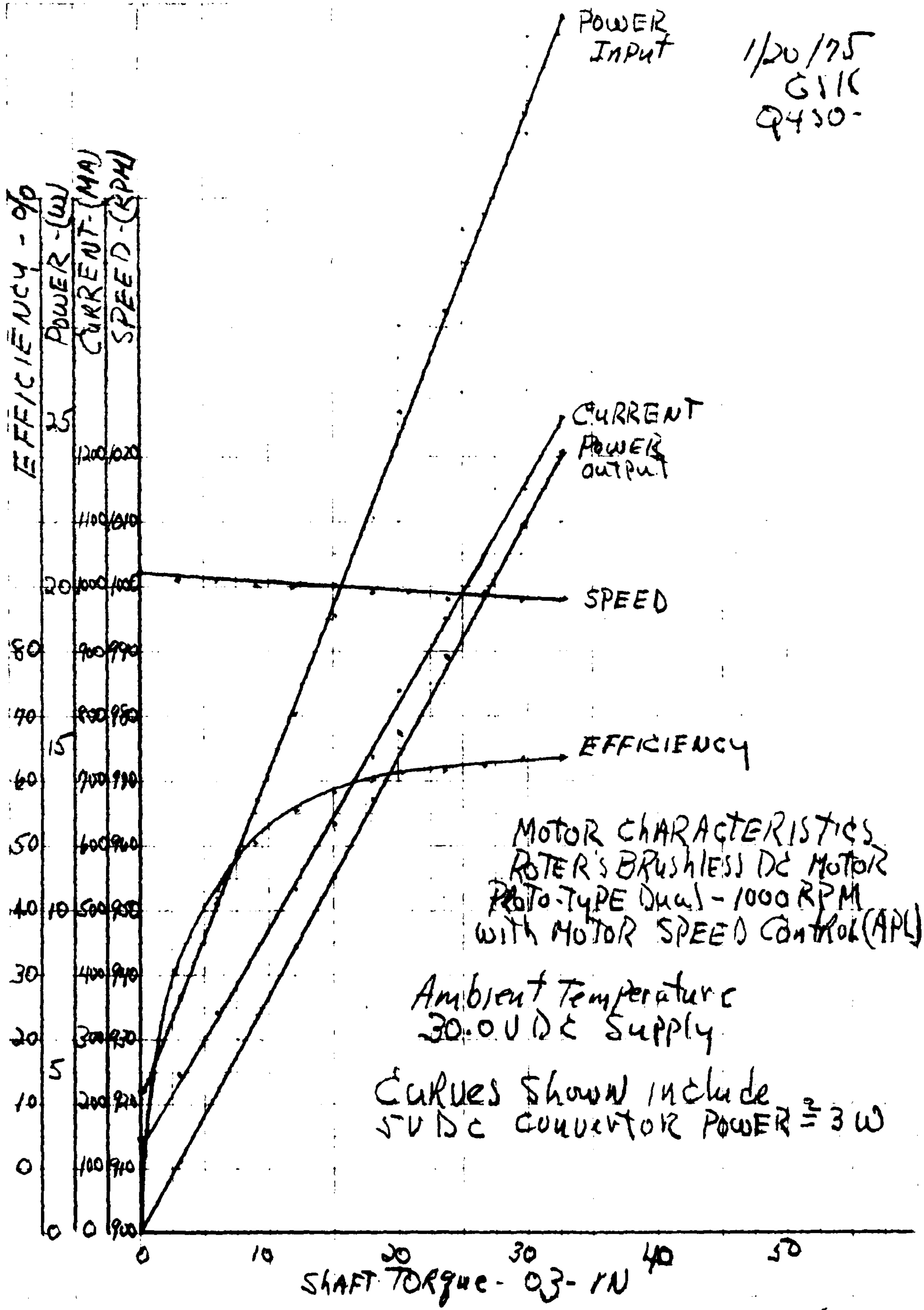
1/20/75
GJK
Q430-
POWER INPUT
CURRENT
POWER OUTPUT
SPEED
EFFICIENCY
EFFICIENCY - %
POWER - (W)
CURRENT - (MA)
SPEED - (RPM)
MOTOR CHARACTERISTICS
ROTER'S BRUSHLESS DC MOTOR
PROTO-TYPE DUAL - 1000 RPM
WITH MOTOR SPEED CONTROL (APL)
Ambient Temperature
30.0 VDC Supply
Curves shown include
5 VDC Converter Power ≈ 3 W
SHAFT TORQUE - OZ - IN

FIG 6C

THE JOHNS HOPKINS UNIVERSITY
APPLIED PHYSICS LABORATORY
LAUREL, MARYLAND

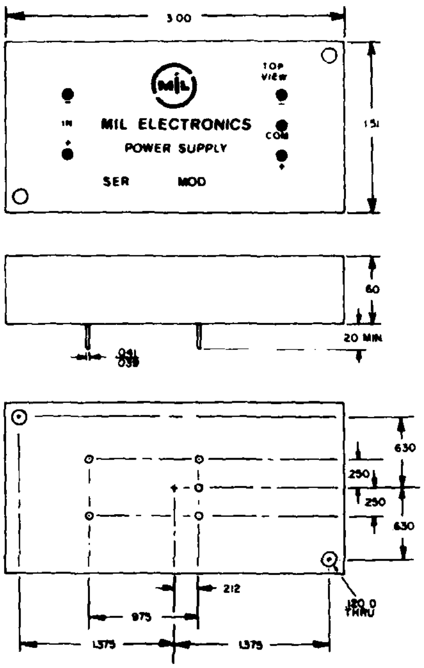

CENTER OUTPUT TERMINAL INSTALLED BUT NOT CONNECTED ON SINGLE OUTPUT MODELS.

13

SERIES D

- 3 WATTS OF ISOLATED OUTPUT POWER
- SINGLE OR DUAL OUTPUTS
- HIGHLY REGULATED
- SEALED METAL CLOSURE
- CURRENT LIMITING

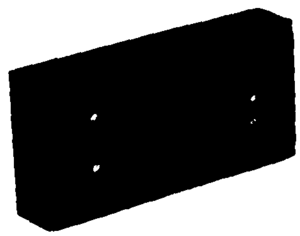

ELECTRICAL SPECIFICATIONS

Regulation for Input	± .05%	Efficiency (Typical)	50%
Regulation for Load (zero to full)	± .2%	Reverse Polarity	100 Volts*
Output Ripple	1% pp†	Input Over Voltage	[illegible]
Temp Stability	less than .01%/°C	Isolation (Input-Output-Case)	250 Volts
Temp (Operating Case)	-55 to +100 C	Current limiting	[illegible] +20% Max
Temp (Storage)	-55 to +1?0°C		

PHYSICAL SPECIFICATIONS

Weight	92 gms	Mounting	Two thru holes
Acceleration	45 G's	Terminals	Printed circuit pins
Shock	50 G's	Case Finish	Aluminum, gold alodine
Vibration	20 G's	Volume	2.7 cubic inches
Altitude	see level to space	Semiconductors	All silicon
Thermal Shock	MIL STD 810/503	Encapsulation	100%

FIG 7

*Reverse polarity not applicable to 5 volt input models
† 0 to 500 KHz bandwidth

Except for dual output units below 14 volts

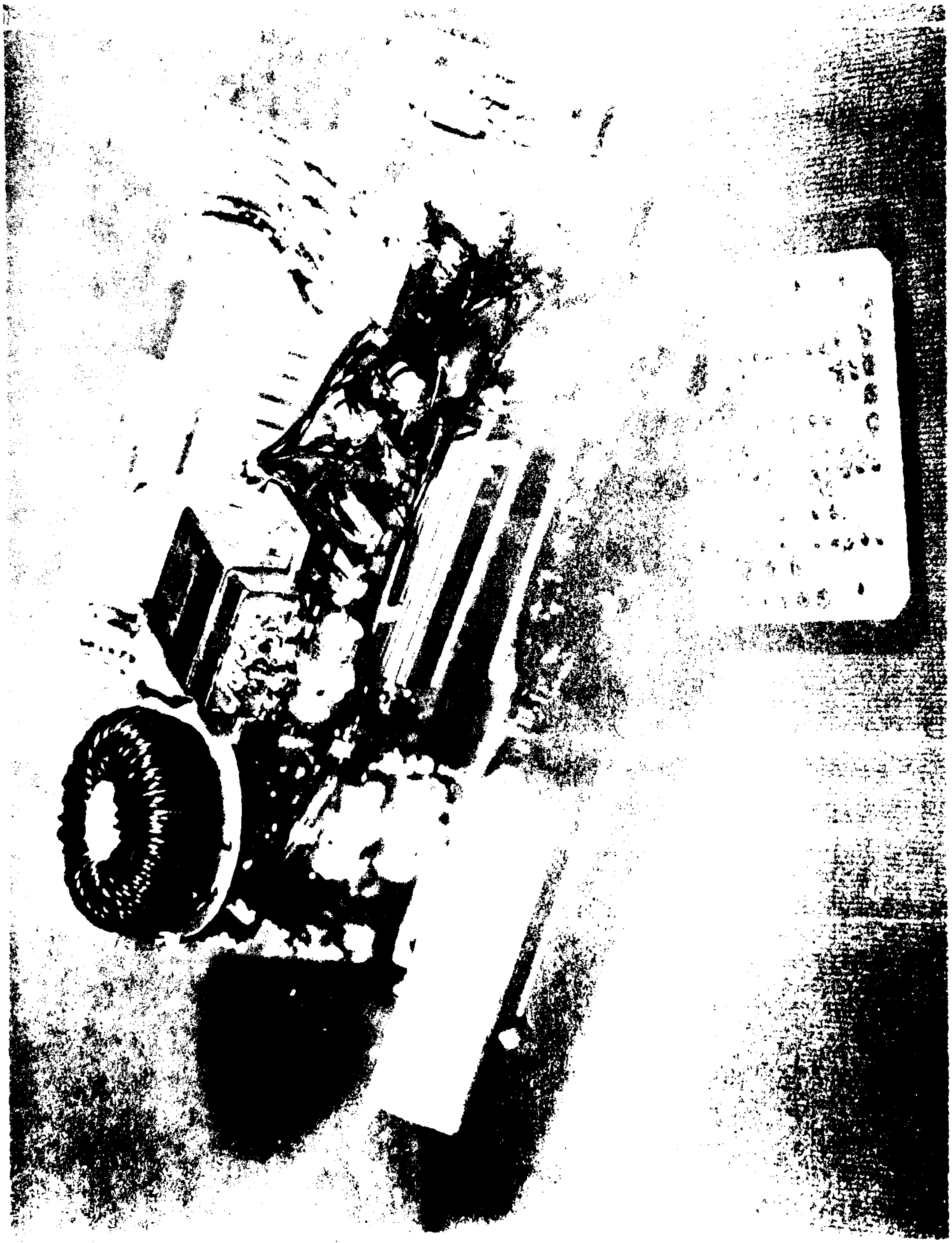

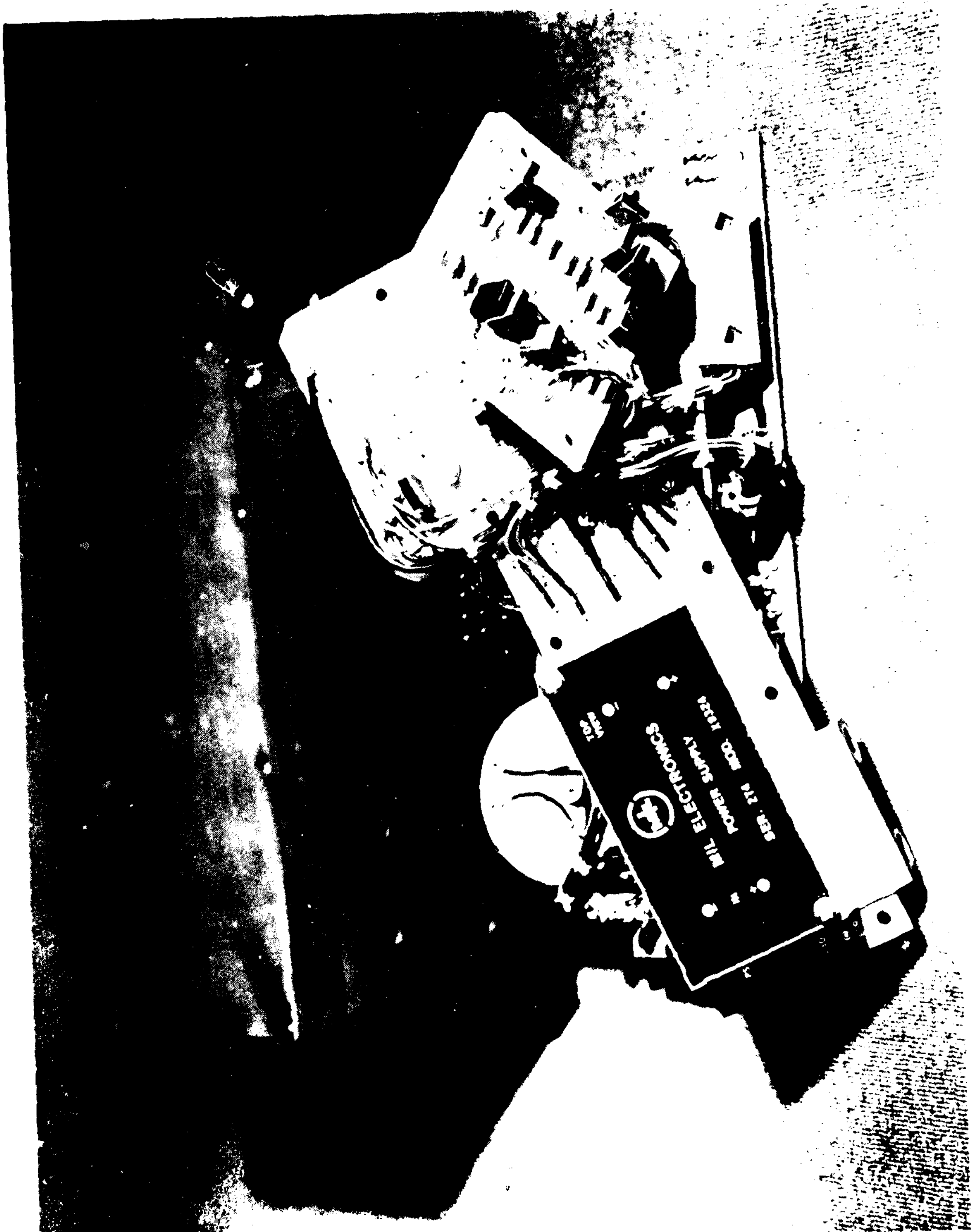
MIL ELECTRONICS
POWER SUPPLY

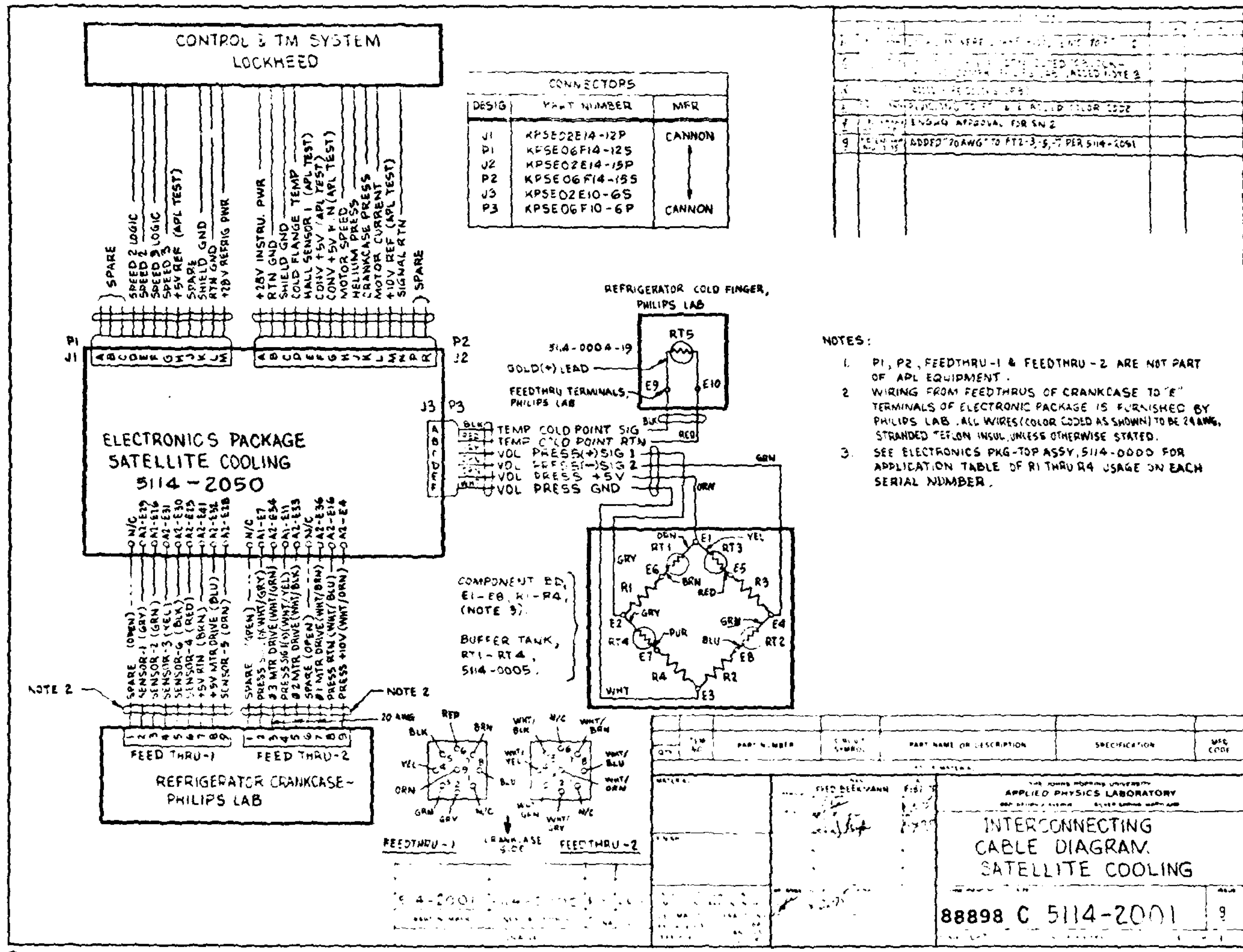
CONTROL & TM SYSTEM
LOCKHEED
CONNECTORS
DESIG | PART NUMBER | MFR
J1 KPSE02E14-12P CANNON
P1 KPSE06F14-12S
J2 KPSE02E14-19P
P2 KPSE06F14-19S
J3 KPSE02E10-6S
P3 KPSE06F10-6P CANNON
SPARE
SPEED 2 LOGIC
SPEED 2
SPEED 3 LOGIC
SPEED 3
+5V REF (APL TEST)
SPARE
SHIELD GND
RTN GND
+28V REFRIG PWR
+28V INSTRU. PWR
RTN GND
SHIELD GND
COLD FLANGE TEMP
HALL SENSOR 1 (APL TEST)
CONV +5V (APL TEST)
CONV +5V RTN (APL TEST)
MOTOR SPEED
HELIUM PRESS
CRANKCASE PRESS
MOTOR CURRENT
+10V REF (APL TEST)
SIGNAL RTN
SPARE
P1
J1
P2
J2
J3
P3
ELECTRONICS PACKAGE
SATELLITE COOLING
5114-2050
REFRIGERATOR COLD FINGER, PHILIPS LAB
RT5
5114-0004-19
GOLD(+) LEAD
FEEDTHRU TERMINALS, PHILIPS LAB
E9
E10
TEMP COLD POINT SIG
TEMP COLD POINT RTN
VOL PRESS(+)SIG 1
VOL PRESS(-)SIG 2
VOL PRESS +5V
VOL PRESS GND
COMPONENT BD, E1-E8, R1-R4, (NOTE 3)
BUFFER TANK, RT1-RT4, 5114-0005
NOTES:
1. P1, P2, FEEDTHRU-1 & FEEDTHRU-2 ARE NOT PART OF APL EQUIPMENT.
2. WIRING FROM FEEDTHRUS OF CRANKCASE TO "E" TERMINALS OF ELECTRONIC PACKAGE IS FURNISHED BY PHILIPS LAB. ALL WIRES (COLOR CODED AS SHOWN) TO BE 24 AWG, STRANDED TEFLON INSUL. UNLESS OTHERWISE STATED.
3. SEE ELECTRONICS PKG-TOP ASSY, 5114-0000 FOR APPLICATION TABLE OF R1 THRU R4 USAGE ON EACH SERIAL NUMBER.
SPARE (OPEN)
SENSOR-1 (GRY)
SENSOR-2 (GRN)
SENSOR-3 (YEL)
SENSOR-6 (BLK)
SENSOR-4 (RED)
+5V RTN (BRN)
+5V MTR DRIVE (BLU)
SENSOR-5 (ORN)
SPARE (OPEN)
PRESS (WHT/GRY)
#3 MTR DRIVE (WHT/GRN)
PRESS SIG(+)(WHT/YEL)
#2 MTR DRIVE (WHT/BLK)
SPARE (OPEN)
#1 MTR DRIVE (WHT/BRN)
PRESS RTN (WHT/BLU)
PRESS +10V (WHT/ORN)
NOTE 2
20 AWG
FEED THRU-1
FEED THRU-2
REFRIGERATOR CRANKCASE - PHILIPS LAB
FEEDTHRU-1
CRANKCASE SIDE
FEEDTHRU-2
ADDED "20 AWG" TO FT2-3,5,7 PER 5114-2051
APPLIED PHYSICS LABORATORY
INTERCONNECTING
CABLE DIAGRAM
SATELLITE COOLING
88898 C 5114-2001 9
5114-2001

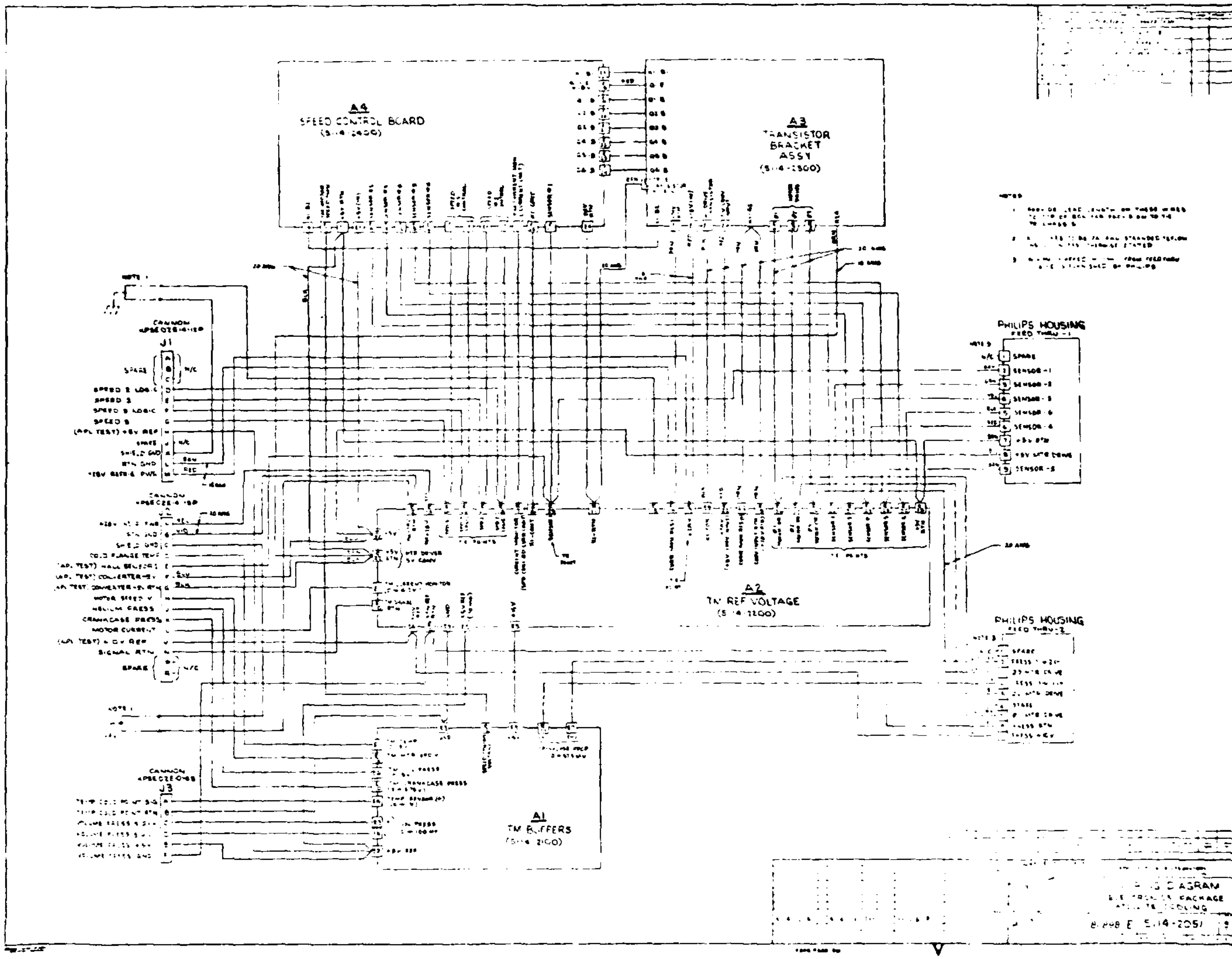

A4
SPEED CONTROL BOARD
A3
TRANSISTOR
BRACKET
ASSY
(5-14-2300)
A2
TM REF VOLTAGE
A1
TM BUFFERS
PHILIPS HOUSING
PHILIPS HOUSING
CANNON
J1
J3
SPARE
SPEED 5
MOTOR SPEED
HELIUM PRESS
CRANKCASE PRESS
MOTOR CURRENT
SIGNAL RTN
SENSOR-1
SENSOR-2
SENSOR-3
SENSOR-6
SENSOR-4
SENSOR-5
+5V RTN

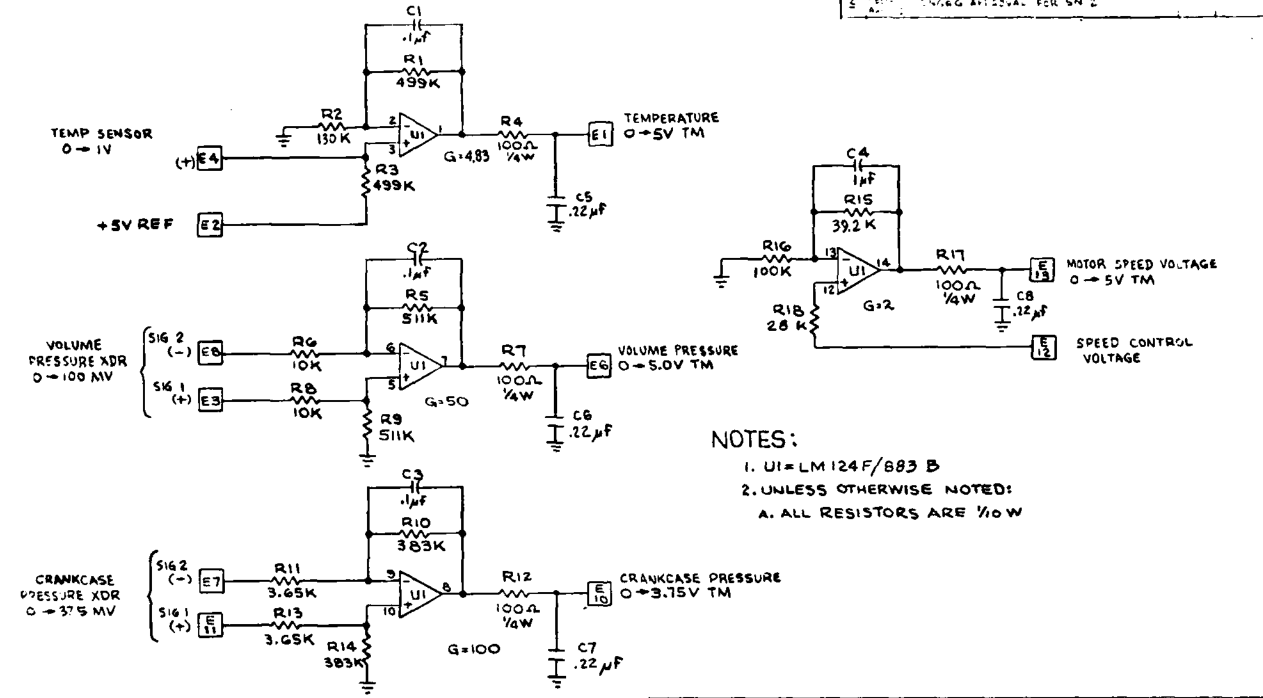

NOTES:

1. U1 = LM 124F/883 B
2. UNLESS OTHERWISE NOTED:
   A. ALL RESISTORS ARE 1/10 W

I.C. DATA			
SYM	DEVICE	Vcc	GND
U1	LM 24	4	11

REVISIONS TO AGREE WITH S/N 1 CHANGES

ENGRG APPROVAL FOR SN 2

QTY	ITEM NO	PART NUMBER	CIRCUIT SYMBOL	PART NAME OR DESCRIPTION	SPECIFICATION	MFG CODE

5114-2101	5114-2100	REF	GRUP
PART NUMBER	NEXT ASSY		
USAGE			

ROUCHARD 3-12-75

THE JOHNS HOPKINS UNIVERSITY
APPLIED PHYSICS LABORATORY

SCHEMATIC
TM BUFFERS - BOARD A1
ELECT PACKAGE SATELLITE COOLING

88898 C 5114-2101

5114-2101

FORMFEED 301

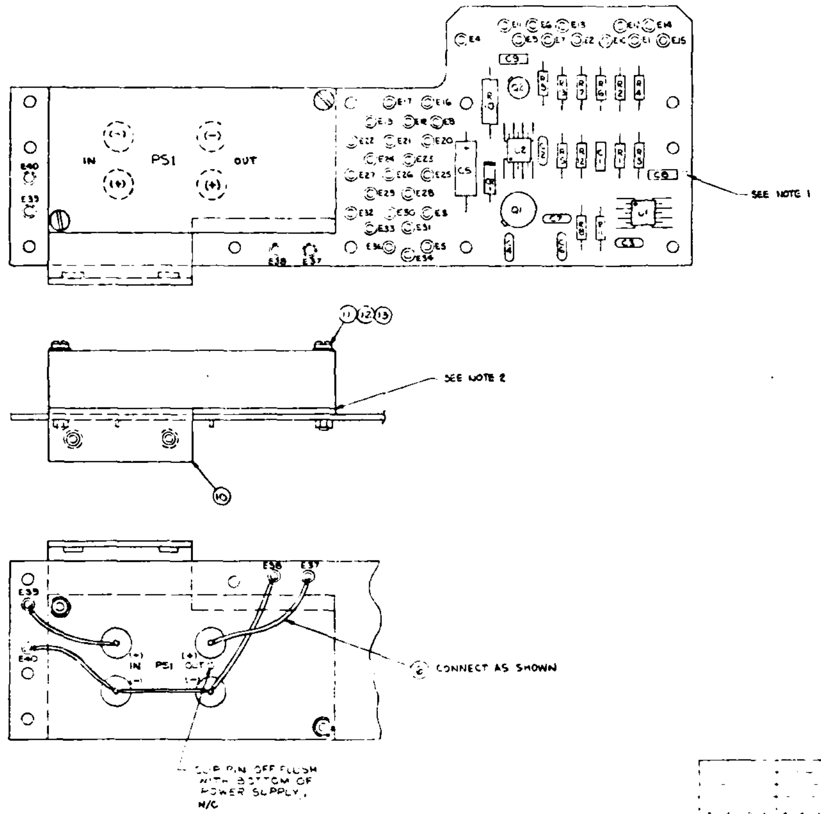

NOTES:

1. MARK LATEST REVISION ISSUE LETTER OF THIS ASSEMBLY 5114-2200 ... 1/8 INCH HIGH CHARACTERS IN APPROXIMATE POSITION FOR ITEM (6).
2. SPREAD HEAT SINK COMPOUND ITEM (?) BETWEEN BRKT, ITEM (?) & PS1.
3. AFTER ALL ELECTRICAL TESTS HAVE BEEN SATISFACTORILY ACCOMPLISHED CONFORMAL COAT BOTH SIDES OF ASSEMBLED BOARD PER (6).

2	MS15795-803	WASHER FLAT #4	
2	HWA2...	WASHER #4 ...	RAYNAR 5623
	...	SCREW ...	
	...	HEAT SINK	
	...	SOLDER	
	...	CONFORMAL COATING	
	...	SCHEMATIC DIAGRAM	

NOTE 3

APPLIED PHYSICS LABORATORY

ASSY, TM BUFFERS (A2), ELECTRONICS PACKAGE, SATELLITE ...

88898 D 5114-2200

5114-2200 [11]

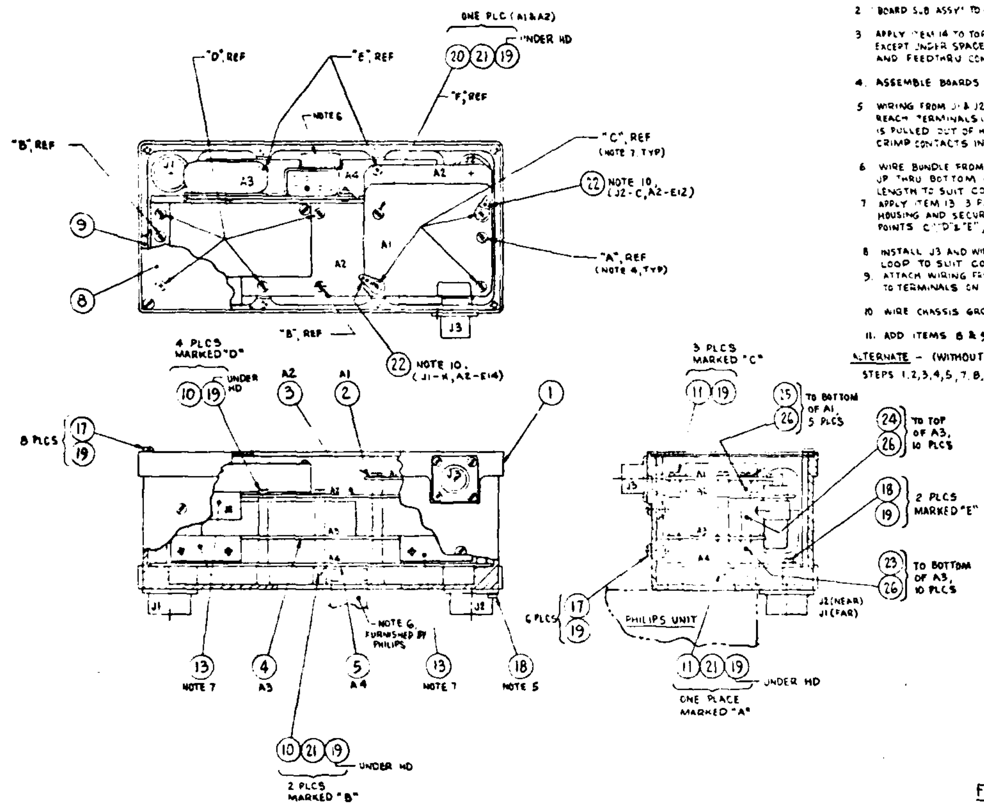

NOTES:

ORDER OF ASSEMBLY – (MOUNTING TO PHILIPS HOUSING)

1. WIRE INTERCONNECTIONS BETWEEN BOARDS A1, A2, A3 AND A4, OUT OF HOUSING, BOARDS TO BE IN FAN-OUT POSITION FROM THE J3 SIDE
2. "BOARD SUB ASSY" TO PASS ELECTRICAL TEST BY ENGRG GROUP
3. APPLY ITEM 14 TO TOP & BOTTOM OF BOARDS A1 A2 A3 & A4, EXCEPT UNDER SPACER LOCATIONS & TERMINALS FOR J1, J2, J3 AND FEEDTHRU CONNECTIONS.
4. ASSEMBLE BOARDS A1 A2, A3 & A4 AT POINTS "A", "B" & "F".
5. WIRING FROM J1 & J2 TO BE A LOOP OF SUFFICIENT LENGTH TO REACH TERMINALS (NOTE 9) ON A1 WHEN "BOARD SUB-ASSY" IS PULLED OUT OF HOUSING FOR TEST CHECK. INSERT CRIMP CONTACTS INTO REAR OF CONNECTORS.
6. WIRE BUNDLE FROM "PHILIPS" FEEDTHRUS -1 & -2 TO COME UP THRU BOTTOM HOLE AND LAY IN POSITION SHOWN (NOTE 9). LENGTH TO SUIT CONDITION OF NOTE 5
7. APPLY ITEM 13 3 PLACES THEN INSERT "BOARD SUB ASSY" INTO HOUSING AND SECURE WITH THRU SCREWS AT POINTS "C", "D" & "E", AND HEATSINK HARDWARE.
8. INSTALL J3 AND WIRING TO TERMINALS ON A1. LENGTH OF LOOP TO SUIT CONDITION OF NOTE 5.
9. ATTACH WIRING FROM J1-J2 AND "PHILIPS" FEEDTHRUS -1 & -2 TO TERMINALS ON A1 & A2. (LENGTH – SEE NOTES 5 & 6).
10. WIRE CHASSIS GROUND USING ITEM 22, 2 PLCS.
11. ADD ITEMS 8 & 9.

ALTERNATE – (WITHOUT PHILIPS HOUSING)

STEPS 1,2,3,4,5,7,8,9 (EXCEPT FEEDTHRUS), 10 & 11.

TABLE "A"

	AWG	COLOR		AWG	COLOR
1	24	WHT	7	20	RED
2	24	BLK	8	20	YEL
3	24	RED	9	20	ORN
4	24	BLU	10	20	VIO
5	20	BRN	11	18	RED
6	20	BLK	12	18	BRN

FLIGHT

APPLIED PHYSICS LABORATORY

ELECTRONICS PACKAGE ASSEMBLY SATELLITE COOLING

88898 D 5114-2050

5114-2050

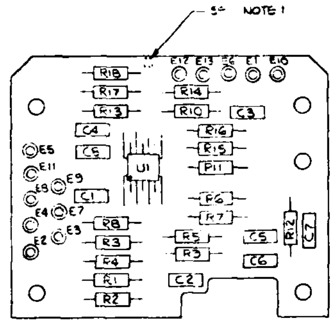

NOTES:

1. MARK LATEST REVISION ISSUE LETTER OF THIS ASSEMBLY 5114-2100, IN 1/8 INCH HIGH CHARACTERS IN APPROXIMATE POSITION SHOWN PER ⑤
2. AFTER ALL ELECTRICAL TESTS HAVE BEEN SATISFACTORILY ACCOMPLISHED, CONFORMAL COAT BOTH SIDES OF ASSEMBLED BOARD PER ④

5114-2100

REQD	ITEM NO	PART NUMBER	CIRCUIT SYMBOL	PART NAME OR DESCRIPTION	SPECIFICATION	MFG CODE
REF	5	7205-3323		MARKING PROCEDURE		
REF	4	7205-8963		CONFORMAL COATING		
1	3	5114-2103		BOARD BASIC		
REF	2	5114-2102		LIST ELEC PARTS		
REF	1	5114-2101		SCHEMATIC DIAGRAM		

Note 2

B LONG 3/26/75

THE JOHNS HOPKINS UNIVERSITY
APPLIED PHYSICS LABORATORY

ASSY TM BUFFERS (A1) ELECTRONICS PACKAGE SATELLITE COOLING

88898 C 5114-2100 A

5114-2100 5114-2100

FORMFEED 301

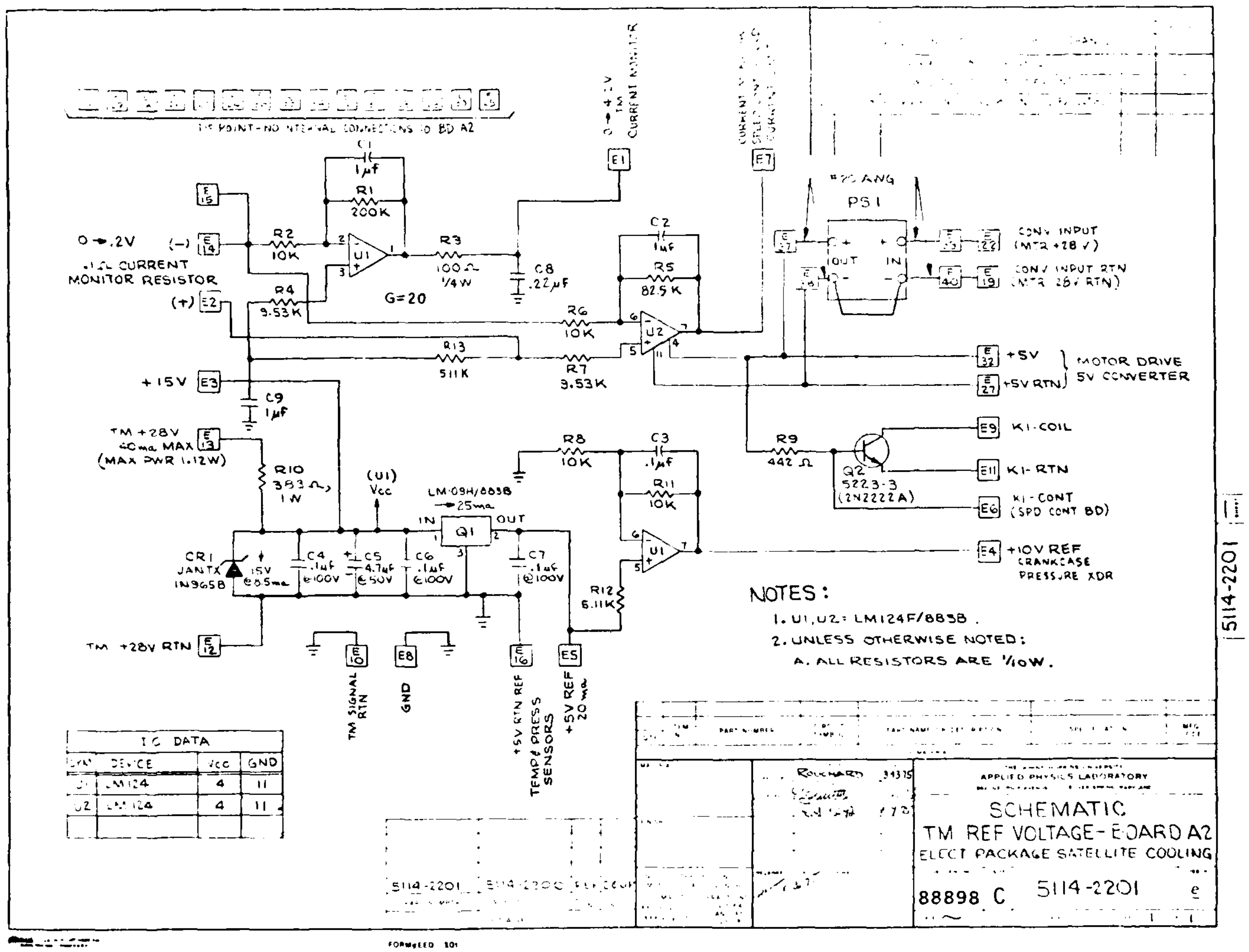
TIE POINT-NO INTERNAL CONNECTIONS TO BD A2
0 → .2V (−) E14
.1Ω CURRENT MONITOR RESISTOR
(+) E2
+15V E3
TM +28V 40ma MAX (MAX PWR 1.12W) E13
TM +28V RTN E12
R1 200K
C1 1μf
R2 10K
R3 100Ω 1/4W
R4 9.53K
U1
G=20
C8 .22μf
0 → 4.2V TM CURRENT MONITOR E1
E7
R5 82.5K
C2 1μf
R6 10K
R7 9.53K
R13 511K
U2
C9 1μf
R10 383Ω 1W
CR1 JANTX 1N965B 15V @8.5ma
C4 .1μf @100V
C5 4.7μf @50V
C6 .1μf @100V
(U1) Vcc
LM109H/883B → 25ma
IN Q1 OUT
C7 .1μf @100V
R8 10K
C3 .1μf
R11 10K
R12 6.11K
#20 AWG
PS1
CONV INPUT (MTR +28V)
CONV INPUT RTN (MTR 28V RTN)
+5V
+5V RTN
MOTOR DRIVE 5V CONVERTER
R9 442Ω
Q2 5223-3 (2N2222A)
E9 K1-COIL
E11 K1-RTN
E6 K1-CONT (SPD CONT BD)
E4 +10V REF CRANKCASE PRESSURE XDR
E10 TM SIGNAL RTN
E8 GND
E16 +5V RTN REF
TEMP & PRESS SENSORS
E5 +5V REF 20ma
NOTES:
1. U1, U2: LM124F/883B.
2. UNLESS OTHERWISE NOTED:
A. ALL RESISTORS ARE 1/10W.
IC DATA
SYM | DEVICE | Vcc | GND
U1 | LM124 | 4 | 11
U2 | LM124 | 4 | 11
APPLIED PHYSICS LABORATORY
SCHEMATIC
TM REF VOLTAGE-BOARD A2
ELECT PACKAGE SATELLITE COOLING
88898 C 5114-2201
5114-2201
FORMFEED 101

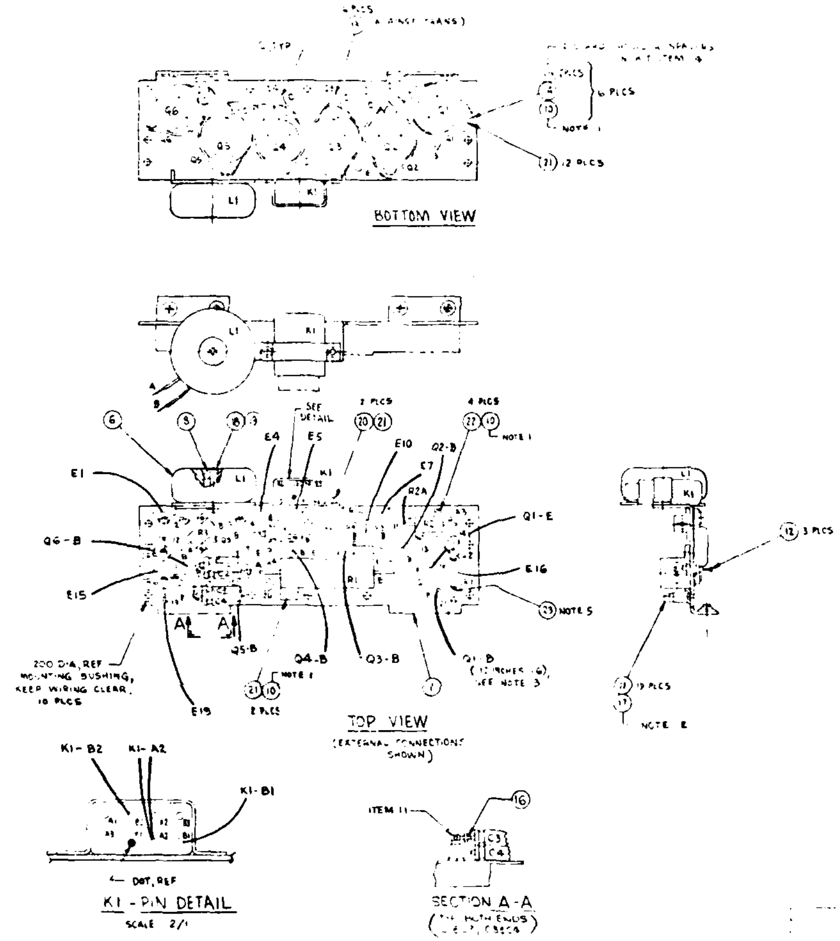

NOTES:

1. APPLY HEAT SINK COMPOUND ITEM 10 TO R1 R2 R3 AND BETWEEN MICA WASHER (ITEM 4) & BRACKET ITEM 1 ON Q1 THRU Q6
2. APPLY SEALANT, ITEM 17 AT ASSEMBLY AS REQUIRED
3. EXTERNAL WIRING CONNECTIONS PER ITEMS 2 & 4 FOR TEST PURPOSES AND INTERCONNECTIONS WITH CARDS A2 & A4
4. SIZE & COLOR OF WIRE ITEM 6 TO BE: 8 AWG RED, 24 AWG RED, 8 AWG BRN, 24 AWG GRN, 8 AWG WHT, 20 AWG WHT & 24 AWG WHITE
5. USE TUBING ITEM 25 ON COMPONENT LEADS OF CR1 ... ETC

TRANSISTOR BRACKET ASSY - A3
... PACKAGE

88898 D ... 4-2300

5114-2300

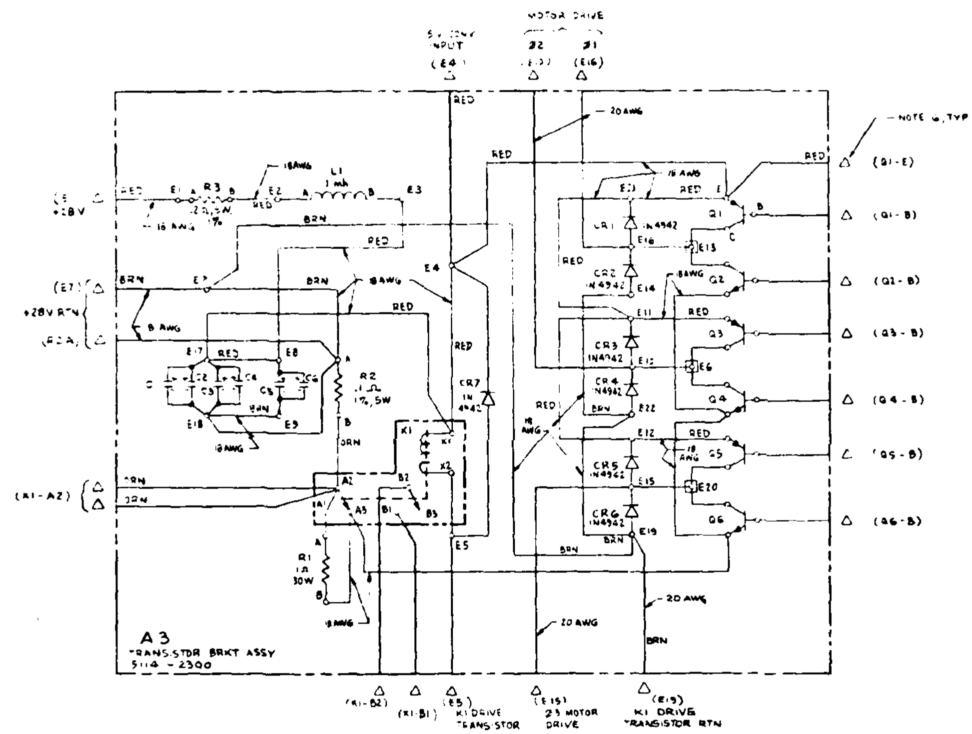

NOTES:

1. Q1, Q3 & Q5 ARE MOTOROLA, MJ 901.
2. Q2, Q4 & Q6 ARE MOTOROLA MJ 1001.
3. K1 IS BABLOCK, BR 9X-30002-26V.
4. FEEDTHRU TERMINALS E6, E13, E20.
5. ALL WIRES #24 AWG STRANDED TEFLON INSUL, UNLESS OTHERWISE STATED.
6. △ INDICATES WIRE LENGTH OF 12 INCHES (SEE 5114-2053 FOR TERMINATION OF WIRE RUNS).
7. C1 THRU C6 ARE 160μF @ 50V CAPACITORS.

5114-2301

APPLIED PHYSICS LABORATORY

SCHEMATIC
TRANSISTOR BRACKET ASSY A3

88898 D 5114-2301

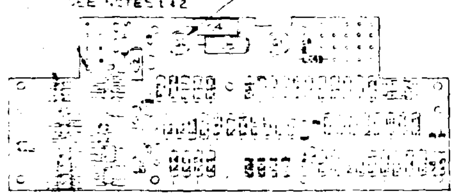

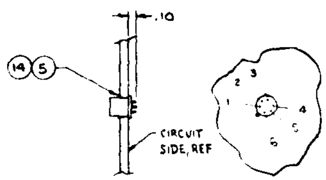

DETAIL A
(TYP 2 PLACES)

NOTES:
1. MARK SERIAL NO. IN 1/8 INCH HIGH CHARACTERS IN APPROXIMATE POSITION SHOWN PER ⑨
2. MARK LATEST REVISION ISSUE LETTER OF THIS ASSEMBLY 5114-2400 IN 1/8 INCH HIGH CHARACTERS IN APPROXIMATE POSITION SHOWN PER ⑨
3. USING 14 & 15 PERFORM POINT TO POINT WELDING OPERATION PER ⑩ & ⑪
4. MOUNT ALL COMPONENTS AS SHOWN BY WELDING SAME TO BUTTON AND FEED-THRU PINS PROVIDED IN ③
5. AFTER ALL ELECTRICAL TESTS HAVE BEEN SATISFACTORILY ACCOMPLISHED CONFORMAL COAT BOTH SIDES OF ASSEMBLED BOARD PER ⑧

REQ'D	ITEM NO.	PART NUMBER		PART NAME OR DESCRIPTION	SPECIFICATION	
A/R	15			WIRE TEFLON INSUL	#26AWG NICKEL ALY 99	17217
REF	4	7205-3975		PROC FOR A-[illegible] CEMENT		
REF	3	SOR-7-[illegible]		[illegible] AND [illegible] STD		
REF	2	7232-2059		TEST PROCESS		
REF	11	7205-3927		WELDING SPEC		
REF	10	7205-3935		PT TO PT SPEC		
REF	9	7205-[illegible]		MARKING PROCEDURE		
REF	8	7205-3923		CONFORMAL [illegible]		
REF	7	7205-[illegible]		FAB PROCEDURE MULTILAYER BD		
A/R	6			WIRE TEFLON INSUL	#[illegible] AWG NICKEL ALY 99	17217
A/R	5	3[illegible]		[illegible] CATALYST		A622
REF	4	5114-2404		LIST WIRE RUNNING		
	3	5114-2403		BOARD BASIC		
	2	5114-2402		LIST ELEC PARTS		
REF		5114-2401		SCHEMATIC DIAGRAM		

SEE NOTE 5

B. LONG

THE JOHNS HOPKINS UNIVERSITY
APPLIED PHYSICS LABORATORY

ASSY SPEED CONTROLLED -A4
ELECTRONICS PACKAGE
SATELLITE COOLING

88898 C 5114-2400

5114-2400

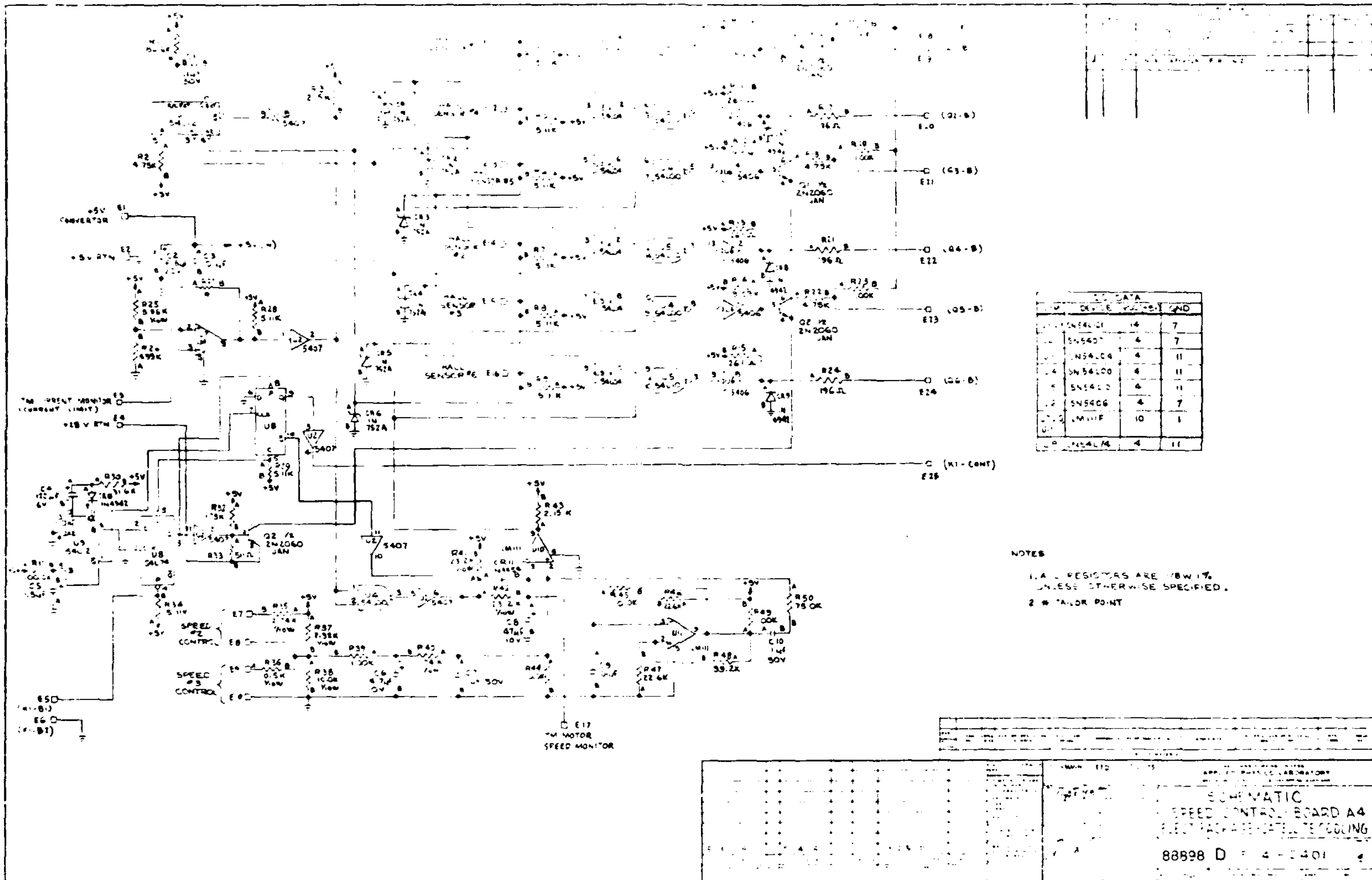

DEVICE	+5V	GND
SN54L01	14	7
SN5407	4	7
SN54L04	4	11
SN54L00	4	11
SN5412	4	11
SN5406	4	7
LM111F	10	1
SN54L14	4	11

INITIAL DISTRIBUTION EXTERNAL TO THE APPLIED PHYSICS LABORATORY*

The work reported in TG 1332 was done under Contract N00017-72-C-4401. This work was related to Task Q4S0, which is supported by DARPA.

ORGANIZATION	LOCATION	ATTENTION	No. of Copies
DEPARTMENT OF DEFENSE			
DARPA	Washington, DC	Director's Office	1
		Deputy Dir. of Res., Dr. C. F. Romney	1
		Program Management Office	1
		Strategic Technology Office	1
		Tactical Technology Office	1
		NMRO	3
		Dr. E. C. Levinthal	1
		Col. George Bulin	1
		Library	1
DTIC	Alexandria, VA		12
Institute for Defense Analysis	Arlington, VA		1
UnderSecretary of Defense for Research and Engineering	Washington, DC	C^3 and Intelligence,	1
		Research & Advanced Technology	1
		Strategic and Space Systems	1
		Tactical Warfare Programs	1
DEPARTMENT OF THE NAVY			
Asst. Sec. for the Navy (Res., Eng. & Sys.)	Washington, DC		1
CNO	Washington, DC	OP-03EG	1
CNM	Washington, DC	NMAT-03	1
NRL	Washington, DC	2627	1
NAVAIRSYSCOM	Washington, DC	AIR-53661	1
NAVSEASYSCOM	Washington, DC	SEA-09G3	1
NAVELEXSYSCOM	Washington, DC		1
NAVPRO	Laurel, MD		2
Office of Naval Research	Arlington, VA	Dr. J. B. Herzig	1
		Gracen Joiner, Code 464	1
DEPARTMENT OF THE ARMY			
Asst. Secretary of the Army (R&D)	Washington, DC		1
Army Night Vision and Electro-Optics Laboratory	Ft. Belvoir, VA		1
DEPARTMENT OF THE AIR FORCE			
AF Technical Applications Center	Patrick AFB, FL	TFS/J. L. Shrum	1
AFWAL/FIEE, AF Wright Aeronautical Labs.	Wright Patterson AFB, OH	Capt. Paul Wren	1
		James Chenowith	1
GOVERNMENT AGENCIES			
Central Intelligence Agency	Washington, DC	CSR/ADD/Std. Dist.	1
NASA/GSFC	Greenbelt, MD	Max Gasser, CODE 713	1
CONTRACTORS			
General Research Corp.	McLean, VA	Doc. Control	1
Institute for Defense Analyses	Arlington, VA	Library	1
MIT/Lincoln Labs.	Lexington, MA	Library	1
		M. J. Lewis	1
MITRE Corp.	Bedford, MA	Doc. Control Center	1
RAND Corp.	Santa Monica, CA	Library	1
Riverside Research Inst.	Arlington, VA	R. E. Huffman	1
		Andre DeVilliers	1
Sanford Research Inst.	Menlo Park, CA	Doc. Library	1
Aerospace Corp.	Los Angeles, CA	Dr. Otto Ledford	1
		Dr. A. L. Johnson	1

Requests for copies of this report from DoD activities and contractors should be directed to DDC, Cameron Station, Alexandria, Virginia 22314 using DDC Form 1 and, if necessary, DDC Form 55.

*Initial distribution of this document within the Applied Physics Laboratory has been made in accordance with a list on file in the APL Technical Publications Group.

INITIAL DISTRIBUTION EXTERNAL TO THE APPLIED PHYSICS LABORATORY*

ORGANIZATION	LOCATION	ATTENTION	No. of Copies
Analytic Decisions, Inc. (ADI)	Lawndale, CA	James Cunningham	1
Analytic Decisions, Inc. (ADI)	Arlington, VA	Al Eckert	1
Los Alamos National Laboratory	Los Alamos, NM	Mail Sta. 5000	1
Lockheed Palo Alto Res. Laboratory	Palo Alto, CA	William Imhoff	1
		Dr. Joe Ragan	1
		Larry Naes	1
Philips Laboratories	Briarcliff Manor, NY	Alexander Daniels	1
		Eric Lindale	1

*Initial distribution of this document within the Applied Physics Laboratory has been made in accordance with a list on file in the APL Technical Publications Group.

N